The optimisations of a biohybrid scaffold from Poly(Glycerol Sebacate) Methacrylate polymer

Thesis submitted for the degree of Doctor of Philosophy at the University of Sheffield

Jeerawan Thanarak

180280353

Department of Materials Science and Engineering

May 2023

Acknowledgement

This is a very long journey of course. It started off with excitement, fill with the eager to learn and finish with proud (or a relief that I can get this thing done at last). There is also a road full of anxiety, loneliness and frustrating. However, this is the largest class I have registered to, and I am proud that I got this opportunity.

First, I would like to thank my supervisors. Dr.Nicola Green, the person I would take as my role model for being a good supervisor once I get back to Thailand. Thank you so much for driving me, push me and support me through thick and thin. I could not do this without you. Dr. Dana Damian, thank you so much for helping me all along and support me throughout all crises. And last but not least, Prof. Frederik Claeyssens, thank you for your support since my MSc. You gave me as much support I can get throughout these years.

Secondly, I would like to thank the Royal Thai Government for giving me this opportunity. Their funding allows me to work on this MSc and PhD. I would like to also express my gratitude to the Royal Thai Embassy for taking care of me throughout these years.

I would like to thank all of my friends. Their supports get rid of the loneliness in my heart. It makes me feel relief and drive me toward the end of the journey. I might have a chance to travel abroad, but this is the first time ever for studying abroad. The language, the field, the cultures, those things I am not familiar with. Without these good friends, I don't think I can get to this stage.

To my family, thank you so much for believing in me. Dad, mom and my sister who always checking in on me. I must say, you believe in me more than I believe in myself, and it does help. To my grandmom who passed away during my last few months of dissertation.

I promised you I would finish this and bring the MSc and PhD certificate to you. Just want to let you know that I still keep that promise. I will show you the certificates as soon as I get them. You are still proud of me, right? And the person I must mention, Keaw, you keep me sane and on track. Without you, I might end up in a hospital waiting for mental treatment. Thank you so very much for driving me to the finish line.

Throughout these 6 years in Sheffield (including MSc), I have learnt a lot. Covid-19 pandemic happened. I had to go back to Thailand and couldn't come back here for half a year because of it. This virus attacked me 2 times, especially the last one which happened to be during the last week of my writing up. These lessons turned me to a stronger person. I wouldn't say it was easy. It's everything opposite to 'easy'. This will be my last degree of course, but if you ask me would I do it again if I could turn back time? I would, even though I know it's going to be soooo hard on me.

Declaration

Unless otherwise specified, all of the work presented in this document is my own work.

I declare that no part of this thesis has been accepted, or is currently being submitted, for any degree or diploma or certificate or any other qualification in this University or elsewhere

Abstract

Collagen, the primary protein in the human body, plays a critical role in fabricating extracellular matrix (ECM)-based scaffolds for treating damaged soft tissues. This study focuses on the creation of polyglycerol (sebacate)-methacrylate (PGS-M) scaffolds to promote the proliferation of human dermal fibroblasts (HDFs) and encourage collagen production. The PGS-M scaffolds boast the advantageous properties of PGS combined with the polyHIPEs structure, including biocompatibility, biodegradability, porosity, and interconnectivity, which have been employed in various cell cultivation studies. The objectives of this research are to optimise a mechanical stimulation protocol to enhance the rate of HDF proliferation, collagen synthesis, and tissue architecture on PGS-M scaffolds, as well as to establish effective sterilisation methods to ensure sterility and improve cell attachment. To this end, a state-of-the-art robotic bioreactor equipped with position and force sensing capabilities and a feedback mechanism was built. Additionally, various decellularisation techniques were assessed for PGS-M scaffolds. The findings reveal that lower displacement and shorter resting times during mechanical stimulation facilitate increased cell proliferation, while higher displacement and longer resting times promote collagen production. Moreover, the freeze and thaw technique was identified as the appropriate approach for decellularising cultured PGS-M scaffolds. Notably, the successful application of force sensing capability in the in-house robotic bioreactor further enriches the scope of this study. This research enhances the understanding of the optimal conditions for stimulating collagen synthesis and cell proliferation on PGS-M scaffolds, thus contributing to the potential of these scaffolds for tissue engineering applications.

Table of Contents

Lists of Figures

List of Tables

List of Abbreviations

µm	micrometre
2D	two-dimensional structure
3D	three-dimensional structure
AU	Absorbance unit
CD marker	A cluster of differentiation marker
CFs	Cardiac Fibroblasts
CF_4	Carbon tetrafluoride
CH_3COOH	Acetic acid
CHO	Chinese hamster ovary cells
CinA	Cinnamate group
DAPI	4′,6-diamidino-2-phenylindole
DCM	Dichloromethane
DMEM	Dulbecco's Modified Eagle Medium
DNA	Deoxyribonucleic acid
DSA	Drop Shape Analysis
E	Emulsion technique
ECM	Extracellular matrix
EDTA	Ethylenediaminetetraacetic acid
ERK1/2	The extracellular signal-regulated kinase 1/2
EVG	Elastin van Gieson stain
FDA	Food and Drug Administration

FTIR	Fourier transform infrared
GAGs	Glycosaminoglycans
H_2O	water
H_2O_2	Hydrogen peroxide
HCl	Hydrochloric acid
HDFs	Human dermal fibroblasts
HEPES	4-(2-hydroxyethyl)-1-piperazineethanesulfonic acid
HIPE	High Internal Phase Emulsion
IHC	Immunohistochemistry
IMS	Industrial Methylated Spirits
ISO17665	Specifies requirements for the development, validation and routine control of a moist heat sterilisation process for medical devices.
M	Molar
MAA	Methacrylic anhydride
MMPs	Matrix metalloproteinases
mRNA	messenger ribonucleic acid
MPa	Megapascal unit
MTT	3-(4,5-Dimethylthiazol-2-yl)-2,5-Diphenyltetrazolium Bromide
N	Newton
NH_4OH	Ammonium Hydroxide
O_2	Oxygen
OH	Hydroxide group
PBS	Phosphate buffered saline

PCL	Polycaprolactone
PEO	poly(ethylene oxide)
PET	Polyethylene terephthalate
PGS	Poly(glycerol sebacate)
PGS-M	Poly(glycerol sebacate) methacrylate
PGSM-50	50% Poly(glycerol sebacate) methacrylate scaffold
PGSM-80	80% Poly(glycerol sebacate) methacrylate scaffold
PLA	Polylactic acid
PLGA	Poly(lactic-co-glycolic acid)
PMMA	Poly(methyl methacrylate)
RNA	Ribonucleic acid
S	Sugar-leaching technique
SD	Standard deviation
SDS	sodium dodecyl sulfate
SEM	Scanning electron microscope
SMCs	Smooth muscle cells
TCP	Tissue culture plastic
TEA	Trimethylamine
TGF	Transforming growth factor
UK	United Kingdom
UTS	Ultimate tensile strength
UV	Ultraviolet

Chapter 1 – Introduction and aims

A bio-friendly scaffold holds significant importance in the field of tissue engineering, as it facilitates the self-repair of tissues across wounded areas. Currently, two primary types of scaffolds in the field: natural (or biological) and synthetic scaffolds. The natural scaffold, sourced from living organisms, offers the advantage of structural similarity to the target wounded tissue. However, it comes with inherent risks of disease transmission and limited availability. Additionally, autografts, involving scaffold retrieval from the patient's body, may necessitate additional surgical procedures.

On the other hand, synthetic scaffolds, being a prominent biomaterial, may not perfectly mimic the target tissue's structure. Nevertheless, they offer the advantage of eliminating disease transmission risk and can be tailored to meet specific application requirements due to the abundance of available polymers in the market. Furthermore, their off-the-shelf availability addresses supply constraints.

To address the structural disparities of synthetic scaffolds, the concept of a biohybrid scaffold emerges. By incorporating biological components into the synthetic scaffold, a biohybrid scaffold can be developed. This involves cultivating cells on the biodegradable synthetic scaffold, enabling cellular incorporation, growth, and secretion of biological components, such as the extracellular matrix (ECM), into the scaffold structure. Consequently, the synthetic scaffold takes on characteristics more closely resembling the target tissue, transforming into a biohybrid scaffold.

Although various forms of synthetic biomaterials exist, users have the flexibility to select the most suitable one for their specific intended purpose. For this study, human dermal fibroblasts (HDFs) were chosen as the primary cells, given their crucial role in collagen

production, which is the most abundant protein in the extracellular matrix (ECM). Among the available options, poly(glycerol sebacate)-methacrylate (PGS-M) was selected as the material of choice due to its biocompatibility and porosity, along with its desirable biodegradability and physical properties. In order to maximise the formation of ECM, particularly collagen, and achieve optimal cell proliferation rates, it is important to establish an appropriate mechanical regimen.

Chapter 2 – Backgrounds and Literature Review

2.1 Biomaterials and Tissue engineering

Tissue Engineering represents a multidisciplinary field dedicated to the exploration and advancement of biocompatible materials to facilitate the repair and regeneration of damaged human tissues. Originating in the 1980s, this revolutionary concept amalgamates various principles, including biomaterials and cell biology, with the ultimate aim of constructing scaffolds that can effectively treat patients. In the medical realm, tissue engineering has proven instrumental in wound healing and tissue replacement procedures, encompassing applications such as skin grafts, cartilages, bones, trachea, and esophagus. Furthermore, ongoing research endeavours seek to develop complex tissues like the heart, liver, and lungs for therapeutic use.[1, 2].

To produce a functional scaffold for therapeutic purposes, cells are seeded onto the designated scaffold and cultivated in a nutrient-rich environment. Subsequently, the cells generate an extracellular matrix (ECM), the significance of which in terms of cell support and signaling will be further explored in Chapter 2.3.2.3. The resulting scaffold is then implanted into the target tissue of interest [1]. While tissue engineering presents promising advantages in replacing damaged tissues within the human body, certain limitations necessitate further research and resolution. Key areas of focus include tracking the differentiation pathways of stem cells, achieving vascularization in engineered tissue, and minimizing unnecessary surgery in articular cartilage repair. Efforts in addressing these challenges hold significant potential in advancing the field and maximizing the impact of tissue engineering in clinical applications [3-5].

2.2 Biomaterials

2.2.1 Choices of biomaterials

As highlighted in Chapter 2.1, biomaterials play such a crucial role in enabling the process of tissue repair and replacement [6, 7]. In tissue engineering applications, two primary types of biomaterials are categorised: naturally derived and synthetic scaffolds (Figure 2.1). The classification of these biomaterials is based on their origin. Naturally derived scaffolds, acquired from living organisms, are renowned for their structural similarity to the target wounded area. Examples of such scaffolds include skin grafts, bone grafts, and Porcine Small Intestinal Submucosa. However, these naturally derived biomaterials suffer from limitations such as restricted availability and the potential risk of disease transmission from the donor source [8-10]. Moreover, naturally derived biomaterials can be categorized into three main groups: autografts, allografts, and xenografts, depending on the source of the scaffold. Autografts are derived from the patient's own healthy tissue, ensuring compatibility. Allografts involve the collection of scaffolds from suitable donors [11, 12]. Conversely, xenografts refer to materials sourced from different species [13].

Ceramics, including zirconia, alumina, and hydroxyapatite, are also widely employed in orthopaedics and dental applications, boasting corrosion resistance and suitable mechanical properties for bone and dental implantation. Furthermore, ceramics are available in various forms, ranging from bioinert to bioactive. Nevertheless, they suffer from drawbacks like fragility, low sinterability, and limited ductility [19-21].

Composite biomaterials, another prominent category, consist of two or more components combined into a single material. These composites find versatile use in diverse tissue engineering applications, including bone, vascular, and neural contexts. Various techniques, such as incorporating bioactive substances into biodegradable scaffolds, are employed to fabricate composite materials. One key advantage of these composite biomaterials is the synergistic combination of the strengths of their constituent components [22, 23]. However, these materials require further development, as they may also exhibit some of the drawbacks of their individual constituents [24, 25].

Polymer biomaterials, widely favoured in tissue engineering, offer multiple options tailored to specific applications. The adjustable physical properties of these biomaterials make them highly versatile. Additionally, they can be designed as bioactive, biodegradable, or biocompatible materials, rendering them suitable for various tissue-engineered applications. Examples of polymeric biomaterials include polyglycolic acid (PGA), polystyrene, and polycaprolactone (PCL) [26]. However, the use of polymeric biomaterials inside living organisms carries the potential risk of toxicity [14, 25, 27, 28].

Another main type of biomaterial is synthetic biomaterial. This group of synthetic biomaterials includes metallic, ceramic, composite and polymeric scaffolds. This synthetic scaffold is well-known for its wide range of choices and designable properties [14-16]. Metallic scaffolds, such as steel and titanium alloys, find extensive use in orthopaedics, dental, and stent applications due to their inherent strength and shape memory properties. However, their integration with host tissue may be compromised, leading to inadequate interconnectivity, inflammation, and necrosis [17, 18]. Ceramic materials are well-established components in orthopaedic and dental applications. Examples of ceramics

employed in tissue engineering include zirconia, alumina, and hydroxyapatite. The advantages of these materials lie in their corrosion resistance and mechanical properties, which render them suitable for bone and dental implantation. Ceramics also exist in diverse characterisations including bioinert and bioactive variants. Nevertheless, ceramics have drawbacks such as fragility, limited sinterability, and reduced ductility. [19-21]. Composite biomaterials represent another significant category within the range of biomaterials. The designation 'composites' pertains to the integration of two or more components within a singular biomaterial. Such composite biomaterials find utility across diverse tissue engineering domains, spanning bone, vascular, and neural applications. A multitude of techniques exist for fabricating composite materials, one of which involves the amalgamation of bioactive agents with biodegradable scaffolds. A key advantage offered by these composite biomaterials is their capacity to amalgamate the strengths of two distinct components into a unified entity [22, 23]. Nevertheless, the refinement of this material remains ongoing, as it inherits certain limitations from its sourced components [24, 25]. Polymers constitute another pivotal class of biomaterials highly regarded in tissue engineering. A diverse array of polymeric biomaterials is accessible for selection, contingent on the intended application. The advantage of these biomaterials lies in their tuneable physical properties. Additionally, polymeric biomaterials manifest an assortment of bio-relevant characteristics, encompassing bioactive, biodegradable, and biocompatible attributes, rendering them applicable across various tissue-engineering scenarios. Noteworthy examples of polymeric biomaterials comprise polyglycolic acid (PGA), polystyrene, and polycaprolactone (PCL) [26]. Nonetheless, it's important to

acknowledge that the utilisation of polymeric biomaterials within living organisms entails potential risks of toxicity [14, 25, 27, 28].

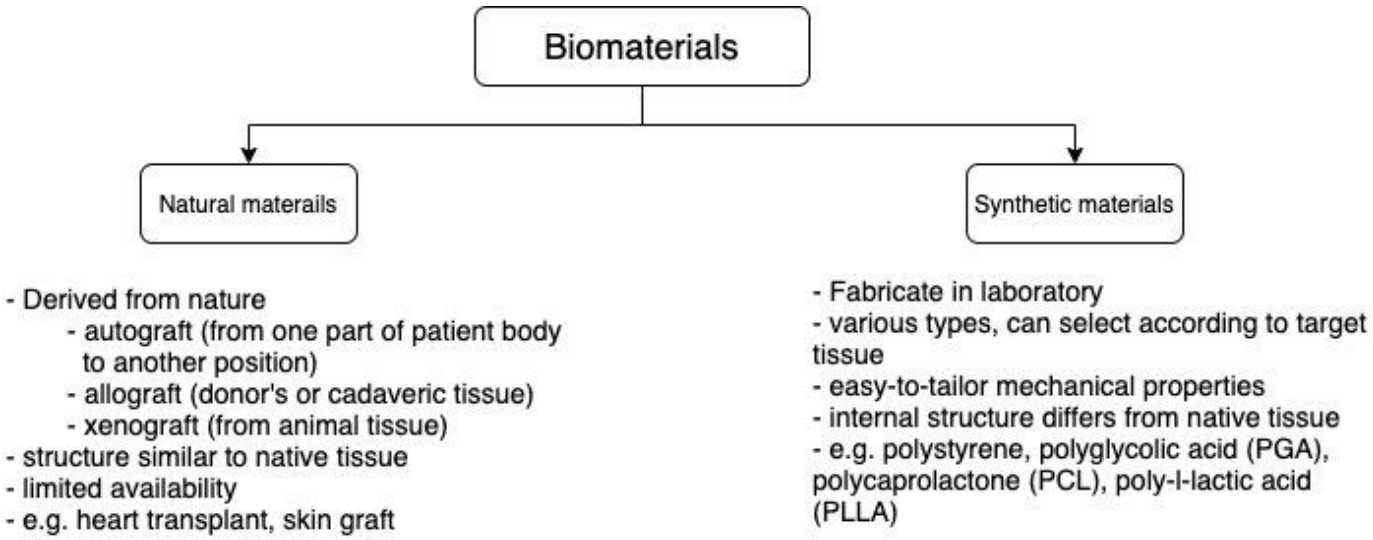

Figure 2.1 - the diagram of types of biomaterials which are commonly used in medicine.

Polymeric biomaterials have gained widespread popularity among scientists due to their extensive range of options tailor-made for specific applications. A notable instance is Poly(glycerol sebacate) or PGS, conceived in 2002, which promptly found utility in engineered soft tissues. The adoption of PGS was motivated by its notable biocompatibility, cost-effectiveness, tuneable mechanical characteristics, and rapid degradation kinetics [29-31]. The versatility of PGS extends to membrane construction for various contexts, such as cardiac tissue regeneration [32, 33] and nerve guide conduits for repairing peripheral nerves [34, 35]. Furthermore, its application in targeted antibiotic distribution for enhanced drug delivery has been explored [36]. Although the PGS polymer holds potential for advancing soft tissue engineering, it is not exempt from limitations, particularly concerning its manufacturing process. The synthesis of PGS polymer entails polycondensation, which demands elevated temperatures and vacuum

conditions to achieve optimal crosslinking. To tackle this challenge, a promising avenue emerges through the integration of photocurable chemical groups into PGS. Zhu et al. [37] demonstrated the viability of incorporating a cinnamate (CinA) group, enabling PGS polymer to undergo photocuring devoid of supplementary photoinitiators. The advantageous attributes of PGS-CinA, including its ability to facilitate cell adhesion and proliferation, as well as its biodegradability through hydrolysis, are indeed promising. However, it's noteworthy that photocrosslinking necessitates prolonged exposure to ultraviolet light.

Pashneh-Tala et al. [38] introduced the methacrylate group as an alternative approach for conferring photocurability to PGS. The incorporation of methacrylate groups facilitates crosslinking of PGS in the presence of a photoinitiator, requiring a shorter exposure time, as determined in their study. The degree of methacrylation can be tailored to meet specific requirements. PGS-methacrylate (PGS-M) holds diverse applications due to its biodegradability, biocompatibility, and ease of synthesis. By modulating the methacrylation concentration, precise adjustments to mechanical properties can be achieved. Furthermore, PGS-M polymer stimulates growth, adhesion, and extracellular matrix formation across various cell types [39]. Demonstrating commendable biocompatibility and support for cell proliferation, the PGS-M material lends itself to diverse fabrication techniques for enhancing tissue engineering scaffolds [38-40].

2.2.2 Fabrication techniques

A multitude of methods exists for creating scaffolds tailored for tissue engineering applications. Among the various synthetic biomaterials, polymeric biomaterials stand out due to their versatility in fabrication. Notable techniques include templating, emulsion, electrospinning, and 3D printing. Each method possesses distinct prerequisites that align with specific polymers [14]. Table 2.1 provides a concise overview of the merits and drawbacks of these techniques when applied to polymers for soft tissue engineering. Additionally, Table 2.1 showcases examples of scaffolds producible through these diverse fabrication approaches.

Fabrication techniques	Examples	Pros	Cons
Templating	Hydrogel [41, 42], PGS-M [40], PLGA[43]	- provides 2 phases: continuous and oily phase - controlled pore size - controlled overall size, geometry and orientation - enhanced mechanical properties	- uncontrollable homogeneous distribution - limited solvent can be used to create micro-structure
Emulsion	PGS-M scaffold[39], poly(ethylene oxide) (PEO), gelatin methacryloyl [44], PCL [45]	- Tunable pore sizes - tunable mechanical properties - can be used with various polymer	- strength and pore seize are proportional related and may not be able to tune one without interfering another - sensitive when change a parameter during fabrication
Electrospinning	PLGA [46], PEO [47], and PCL [48]	- able to fabricate fibres in nano scale - may be able to mimic the microstructure of the target tissue - highly reproducible when carefully control the parameters -can be incorporate with other techniques	- pore sizes are reduced - take time to produce
bioprinting	Alginate, Gelatin, Collagen, PCL [14, 49]	- high accuracy and reproducibility - can be used with other techniques - tunable mechanical properties - tunable pore size and surface roughness	- the cost is high - lack of optimisation in the process - the need to use a specific ink in stereolithography which limits the density of cells

Table 2.1 – the table summarises the pros and cons of each fabrication techniques that can be used to fabricates bio-friendly scaffolds.

As detailed in Table 2.1, most techniques offer researchers the flexibility to fine-tune both mechanical properties and pore size. However, the specific details of each technique

necessitate tailored optimisation based on the distinct biomaterials and intended applications. The selection of scaffold fabrication techniques for each polymer must be carefully delineated in accordance with the target applications and material characteristics. Notably, when considering metallic and ceramic biomaterials for bone and joint replacements, the chosen technique should augment strength and durability [50-52]. Moreover, Pashneh-Tala et al. [38, 40] have presented two distinct fabrication approaches for the PGS-M polymer, each yielding scaffolds with varying mechanical strengths. This underscores the importance of method optimisation for individual materials. In essence, the choice of fabrication method should be meticulously tailored to the unique attributes of each biomaterial.

2.2.3 Physical properties

2.2.3.1 surface property in relationship with cell attachment

In contemporary technological applications and materials science, the contact angle emerges as a crucial thermodynamic parameter, serving as a marker for the wettability of solid surfaces. This parameter assumes significance when evaluating biomaterials for specific research purposes [53, 54]. In the realm of biomaterials and tissue engineering, comprehending the interactions between these biomaterials and biological tissues at the cellular level holds paramount importance for the development of biomedical devices, artificial organs, and biosensors. Surface attributes of artificial materials, encompassing wettability, roughness, surface charge, and chemical functionalities, exert a profound influence on cellular adhesion to these surfaces [55]. Concerning the surface wettability of synthetic materials, cells exhibit notable adherence to polymer surfaces possessing

intermediate surface wettability, often characterized by water contact angles ranging from 40 to 70°. This specific range of water contact angle degrees corresponds to the hydrophilic nature of the material surface [56].

A comparative analysis of various sterilisation methods has also been documented as a means to modify biomaterials, with discernible impacts on surface characteristics. Among these methods, plasma treatment has garnered increasing attention due to its promising influence on surface hydrophilicity, an aspect that will be revisited in Chapter 4. Notably, this treatment fosters enhanced cell adhesion [57-60]. A notable advantage of plasma treatment is its operation at low temperatures [61-63], rendering it particularly advantageous for temperature-sensitive polymers. Interestingly, Farr et al. [64] conducted a comparison between two sterilisation techniques applied to PGS-M polymer: autoclaving, which necessitates elevated temperatures, and Ar plasma treatment. The findings indicated that plasma treatment bolstered cell activities and heightened hydrophilicity, thus promoting cell adhesion. However, an important caveat remains: a comprehensive comparison across diverse fabrication techniques from both cellular and tensile strength perspectives is yet to be undertaken.

2.2.3.2 Mechanical properties

Comprehending the mechanical properties of biomaterials assumes paramount significance during the design of tissue substitutes. This imperative arises from the need to ensure that the mechanical stimulation imparted by tissue-engineered scaffolds aligns with that of the native tissue, a pivotal criterion in achieving successful outcomes [65]. Notably, the elasticity and viscoelasticity of biomaterials stand out as intriguing properties,

and consequently, feature prominently in literature pertaining to the exploration of materials for soft tissue engineering applications [65-67].

The maximum stress a material can endure before experiencing stretching or pulling is referred to as its ultimate tensile strength (UTS). This UTS holds significance in soft tissue-related applications due to its association with elasticity [68]. The determination of a material's ultimate tensile strength involves dividing its cross-sectional area by the applied stress. This UTS is precisely calculated at the point of scaffold rupture, representing the ultimate tensile strength achieved during mechanical testing [69, 70].

Many materials showcase a linear elastic behaviour, signifying that they undergo temporary deformation when subjected to forces but return to their initial shape upon force cessation. This elastic response of materials is typically maintained until a specific juncture, termed the "yield point," where all deformations remain reversible upon unloading. However, beyond this yield point, ductile materials undergo plastic deformation. In instances of plastic deformation, the sample fails to regain its original shape and dimensions even upon the removal of the load or stress [70].

By plotting the graph, the x-axis corresponds to strain, while the y-axis represents stress. The linear segment extending from the origin to the juncture where the graph transitions into a curved line signifies the proportional limit stress. This juncture denotes the point at which the material sustains the force without undergoing any alteration in form. The ultimate tensile strength (UTS) is represented by the curved section of the graph, where the material remains intact while initiating deformation. This delineates the force that the material can endure prior to rupture or fracture.

2.3 Cells, their locations and functions

2.3.1 Basic of cells

A cell, encased within a membrane, is the fundamental self-contained unit that encompasses and comprises essential life molecules. In various instances, such as with bacteria and yeast, a solitary cell embodies the entirety of the organism. As cells diversify, they assume specialized roles. Collaborating with other types of specialized cells, they lay the foundation for intricate multicellular organisms. Notably, mycoplasmas, an exceedingly minute bacterial type, harbour the smallest known cells, with certain spherical ones measuring as diminutive as 0.2 μm in diameter. In contrast, human cells span approximately 20 μm in diameter, signifying a weight 400,000 times greater than a solitary mycoplasma. In the context of human development, constructing an entire human being necessitates more than 30,000,000,000,000 cells [71].

When considering the cells within the human body, they can be categorized into distinct types based on their functions and locations. This classification subsequently gives rise to the formation of organs composed of these grouped cells. For instance, nerve cells comprise the nervous system, chondrocytes contribute to cartilage, epithelial cells are present in the skin, and muscle cells constitute muscles. Alternatively, cells can also be classified based on their functional roles. Conductive cells, for example, facilitate the transmission of electrical impulses. Connective cells serve to link other cells to tissues, while supportive cells play a pivotal role in facilitating connections between two distinct cell types. This intricate classification system underscores the diversity and specialization of cells within the human body [72, 73].

2.3.2 Fibroblasts

2.3.2.1 Background

Fibroblasts play a dual role in the biological milieu. Beyond their role in establishing the extracellular matrix (ECM)-enriched microenvironment surrounding cells, fibroblasts also contribute to the dissemination of certain signalling macromolecules into the extracellular space. Notably, fibroblasts exhibit a remarkable responsiveness to diverse mechanical forces. This dynamic responsiveness prompts alterations in cellular signalling pathways, thereby orchestrating ECM production and influencing interactions with other cells. In essence, fibroblasts emerge as pivotal orchestrators within this intricate cellular landscape, bridging the gap between ECM modulation and intercellular communication [74, 75].

Fibroblasts serve a dual role, not only contributing to the provision of an ECM-rich environment for surrounding cells but also assuming responsibility for the transmission of signalling macromolecules into the extracellular space. Remarkably responsive to a range of mechanical forces, fibroblasts wield the ability to modulate cellular signalling pathways, thereby influencing both ECM production and intercellular communication. This unique capacity positions fibroblasts as pivotal regulators, adept at orchestrating the interplay between ECM dynamics and cellular responses [76].

2.3. 2.2 Extracellular matrix production

The extracellular matrix (ECM) stands as a tissue-specific macromolecular construct vital for maintaining normal organ function and furnishing physical support to tissues. This intricate ECM, tailored to each tissue type, constitutes the non-cellular component of

tissues, with its composition intricately adjusted according to the specific tissue and prevailing physiological conditions [77]. Beyond its structural role, the ECM holds paramount importance as it imparts critical spatial and contextual cues that profoundly shape cellular phenotypes [72, 77]. Comprising constituents such as collagen, elastin, fibrin, proteoglycans, and glycosaminoglycans (GAGs), the ECM assumes additional roles in processes like wound healing and fibrosis, both of which are modulated by fibroblasts [76, 78].

2.3.2.3 Mechanotransduction

The cytoskeleton surrounding the cells enables them to detect external stimuli. Upon seeding the cells on the scaffold, the stimulation was conveyed from the scaffold to the cytoskeleton, causing alterations in the cells' size and shape. The production and translation of mRNA from the nucleus contribute to the reinforcement of the ECM [18-21]. Figure 2.2 (top) illustrates the process of cells sensing stimuli and the resulting effects at the cellular level. As depicted in the diagram, the stimulus is detected by the cytoskeleton, and the signal is subsequently transmitted into the cell, prompting the release of signals and genes. The adjacent cells can also perceive the stimulation through integrin connections (Figure 2.2 bottom). This mechanism enables cells to communicate with one another and respond appropriately to mechanical stimuli. Gene expression resulting from cell stimulation varies depending on the cell type and the orientation of the regimen. Subsequently, cells respond and engage in specific cellular activities in accordance with the expressed genes [79].

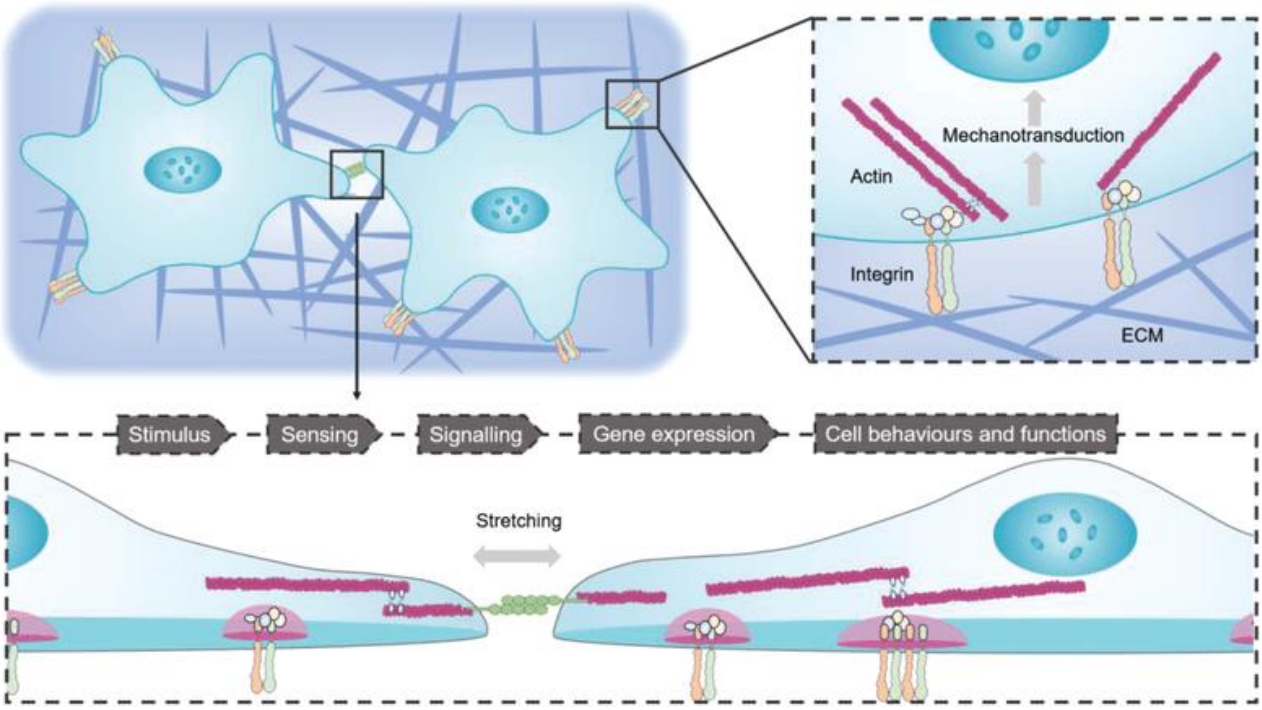

Figure 2.2 – the diagram demonstrates (top) the mechanotransduction of the cell explaining how cell senses the external stimuli and (bottom) cell to cell communication.
*This Figure **'Schematic diagram of Mechanotransduction'** was reprinted from Sun et al. [79], Creative Commons CC BY 4.0 DEED licensed.*

Fibroblasts constitute the most prevalent type of mechanoresponsive cells and are characterized by a notable degree of heterogeneity. The mechanotransduction mechanisms, through which cells convert mechanical signals into cellular biological events like the gene expression of extracellular matrix components, undergo alteration in response to mechanical loads applied to tissues. Once the cell perceives these loads, the signal is transmitted into the cells, consequently inducing various components, including collagen [80]. This process assumes significance in the context of wound healing. It has been documented that mechanical stimuli exert an impact on the cellular environment, subsequently leading to modifications in wound healing and fibrosis. Mechanotransduction indeed assumes a pivotal role in extracellular matrix production and brings about changes in the signalling pathway at the cellular level [81].

2.4 effects of different mechanical stimulations

As previously described in Chapter 2.3, mechanical stimulation exerts an influence on cell signalling, consequently influencing cell behaviours and activities. However, the precise effects of each regimen on various markers remain uncertain. Therefore, the optimisation of a suitable regimen for specific cells and applications becomes imperative. As illustrated within Table 2.2, an array of variables underwent scrutiny to ascertain the impact of the mechanical regimen on the pace of cell proliferation and the forging of collagen. Mechanical stimulation yields a propitious influence over cell proliferation and collagen generation. The outcomes of my master's degree research [82] indicate that incremental stimulation surfaces as the quintessential protocol for attaining utmost collagen production, mirroring the findings disclosed by Schmidt et al. [83]. Divergent patterns within the mechanical regimen confer distinctive ramifications upon the tiers of ERK1/2 and p38. ERK1/2 engages within an array of cellular processes, encompassing cell migration, cell proliferation, and the transcription of proteins, whereas p38 is instrumental in the transmutation of stimuli into cellular responses, notably in inflammation [84, 85], and p38 is instrumental in the transmutation of stimuli into cellular responses, notably in inflammation . Through the quelling of p38 expression, the augmentation of ERK1/2 expression materializes, thereby ushering forth an escalation in collagen synthesis [83, 86]. Given the aspiration for the efficacious proliferation of cells, the cyclic strain emerges as a preeminent regimen for inducing the rate of cell proliferation [30, 65]. Intriguingly, an observable phenomenon is that by subjecting cells to persistent stress for a fleeting interval each day, the multiplication rate of cells becomes invigorated. My conjecture posits that the optimal mechanical regimen should encompass a satisfactory

interlude of repose for cells to undergo mitosis, whilst simultaneously inciting the augmentation of collagen synthesis.

Authors	Cells	Methods	Focusing and Results
Ugolini et al [87]	Cardiac fibroblasts (CFs)	- Apply pathological condition (limited O_2) - 2% and 8% continuous strain	- To learn how CFs respond to damage - Hypoxia and 2% strain promoted inflammatory and fibrotic remodelling in CFs - Individual stimulation increased cell proliferation and collagen production
Ugolini et al [88]	Cardiac fibroblasts	- Apply pathological environment (limited O_2) - 2% and 8% continuous strain for 24 and 72 hrs	- To determine the effect of strain on cell markers, cell proliferation, and cell alignment - 2% strain enhanced the proliferation rate
Manuyakorn et al [89]	Bronchial fibroblasts	- Apply continuous strain in pathological condition, by using the cells from 6 normal patients and 11 asthmatic (non- smoking) patients	- To study the orientation and collagen/proteoglycan production. - No significant difference in decorin mRNA expression. - After 48 hours with strain, there was a considerable rise in collagen types I and II in asthmatic cells.
Schmidt et al [83]	Dermal fibroblasts	- Apply the continuous, intermittent, incremental strain - Increase the resting time for up to 6 h	- To observe ERK1⁄2, p38 and collagen production in response to stimulation. - ERK1⁄2 could reactivate fully after 6 h of rest - Incremental strain was the optimal condition for collagen synthesis.
Blaauboer et al [90]	Myofibroblasts from lung	- Apply cyclic mechanical strain - Applying TGFβ1, also known as the transforming growth factor β1	- To investigate the influence of mechanical strain and $TGF\beta_1$ on the differentiation of fibroblasts - Cyclic stimulation inhibited cell differentiation but $TGF\beta_1$ stimulated cell differentiation
Eastwood et al [91]	Dermal fibroblasts	- Apply mechanical stimulations	- To visualise the cellular morphology - Aligned perpendicular to the force direction (2D) - Aligned perpendicular to the force direction (3D) - There is no alignment 24 hours after loading
Syedain et al [92]	Dermal fibroblasts	- Implement uniaxial tensile strain on pulsed flow-stretch bioreactor, non-invasively observe	- To monitor the stiffness and mechanical quality of the grafts - No difference in graft stiffness - Constantly stimulated grafts exhibited superior mechanical and biological properties - The cells in the pulsed flow grafts produced 150% more collagen than those in the constant flow grafts
Lohberger et al [93]	Degenerative rotator cuff fibroblasts (9 patients)	- Apply the intermittent strain (10s strain followed by 30s rest) for 7 and 14 days.	- To assess a variety of CD markers, mRNA expressions of MMPs, and collagen production - The expression of CDs and MMPs confirmed the phenotype of RC fibroblasts. - Mechanical stress had a favourable influence on collagen synthesis.
Brunelli et al [94]	Human embryonic mesodermal progenitor cells (hES-MPs)	- Apply daily burst compression to the cells and compare early and late stage stimulation after four weeks of cell culture.	- Stimulation the cells at an earlier stage increased the rate of cell proliferation and inhibited mineralization, whereas stimulating the cells at a later stage had the opposite effect.

Table 2.2 - the Table of papers showing effects of mechanical regimes on cell activities.

or achieving the utmost quality in the biohybrid scaffold, the refinement of both mechanical stimulation and decellularisation stands as a necessity. Mechanical stimulation stands poised to amplify cell proliferation and ECM production throughout the course of 3D cell cultivation. On a parallel note, the imperative of decellularisation materialises due to the requisite removal of immunogenic constituents before integration into the recipient's physique [95]. The optimisation of the decellularisation process will pivot upon the extraction of immunogenic constituents from the cellular matrix while concurrently conserving the ECM production that permeates the biohybrid scaffolds.

2.5 Aims and Objectives

Having meticulously reviewed relevant articles encompassing cell options, biomaterials, and assorted facets, this thesis has been meticulously crafted to delve into and ascertain the most fitting methodology for crafting a hybrid scaffold reliant on extracellular matrix (ECM) for soft tissue applications. This undertaking centres upon the utilisation of PGS-M polymer, with the cultivation of human dermal fibroblasts (HDFs) serving as a pivotal element. An additional focal point is the identification of the optimal mechanical stimulation to augment cell proliferation and collagen synthesis from HDFs in an in vitro context.

This overarching goal will be achieved through the following objectives:

1. Optimise the sterilisation technique for PGS-M scaffolds.
2. Optimise and choose the most appropriate fabrication technique of PGS-M scaffolds for the best possible outcome of 3D cell culture.
3. Optimise the colorimetric assays to accurately test the cell metabolic rate, cell number and collagen production from HDFs that culture on PGS-M scaffolds.

4. Optimise the most appropriate decellularisation technique for cultured PGS-M scaffolds.
5. Observe and understand the effects of different mechanical stimulations on cultured PGS-M scaffolds.
6. Invent the inhouse robotic bioreactor according to the desired functions.

Chapter 3 - Methodology

3.1 Biomaterial synthesis and characterisation

3.1.1 PGS-M polymer synthesis

The polymer synthesis adhered to the methodology outlined by Pashneh-Tala et al. [38]. In its initial formulation, the polymer existed as PGS; subsequently, integration of the methacrylate group was effectuated to enable polymerization under ultraviolet light exposure. Unless explicitly specified, all materials were procured from Sigma-Aldrich, UK. To initiate the reaction, a mixture of sebacic acid and glycerol in a 1:1 molar ratio was introduced into a 500 mL three-neck flask (as depicted in Figure 3.1a). The concoction was stirred for a duration of 24 hours at 120°C, accompanied by the circulation of nitrogen gas within a fume hood. Throughout this reaction, one of the flask's three necks was deliberately left open to facilitate gas exchange. In the course of polycondensation, the nitrogen pressure was adjusted to 12 psi, while maintaining a flow rate of 1 meter per second. A temperature of 240°C along with a stirring speed of 150 rpm were designated for the hotplate, while the thermometer was set at 120°C. This temperature was upheld by immersing the system in a glass bath containing mineral oil (as illustrated in Figure 3.1b), and a magnetic stirrer (depicted in Figure 3.1c) was employed. This arrangement ensured the temperature of 120°C prevailed consistently throughout the reaction. Following the 24-hour polycondensation phase, water emerged as a by-product within the confines of the three-neck flask. The subsequent 24 hours were allocated to the removal of water. During this step, the polymer persisted within the same three-necked flask. While one neck of the flask was connected to a vacuum source, the other necks remained

sealed. The oil bath and magnetic stirrer were maintained at 120°C and 150 rpm, respectively, mirroring the conditions from the preceding phase. The culmination of these two procedures yielded a PGS prepolymer.

To create PGS-M polymer, PGS prepolymer was first diluted in dichloromethane (Fisher Scientific, UK) at a ratio of 1:4 (w/v). After complete dissolution, the reaction was cooled to 0 degrees Celsius in the dark. Using the same three-necked flask, the mineral oil was transferred to a bucket during this phase. Ice and aluminium foil were utilised to create 0°C atmosphere within a fume cupboard (Figure 3.2). The prepolymer was then blended with Triethylamine (TEA) at a ratio of 1:1 (mol/mol hydroxy group of PGS) and 4-methoxyphenol (MeHQ) at a concentration of 1 mg/ g hydroxy group of PGS. Methacrylate Anhydride (MAA), the chemical that controls the amount of methacrylation, was added overnight, drop-by-drop, via one neck of the three-neck flask using a dropping funnel, after the additional components had completely dissolved. The mass of MAA required was determined using the mass of PGS prepolymer and the specified percentage of PGS-M. The concentration of MAA was 0.5 and 0.8 mol/ mol of PGS prepolymer hydroxyl group for 50% and 80% PGS-M polymer. The reaction was set for 24 hours in a dark area under a fume hood. The polymer was subsequently rinsed 4 times with 30 mM hydrochloric acid (HCl). The PGS-M polymer was transferred into a separating funnel, mixed with 30mM HCl, agitated until thoroughly combined, and then left in a fume cupboard for the washing stage. After a specific interval, the layer separating the HCl and PGS-M polymer subsequently developed (usually overnight for the first cycle, then a few hours for the second and third cycle).

To effectuate the polymer washing process, the HCl solution employed in each cycle was withdrawn from the funnel, and fresh HCl solution was introduced in its stead. For the purpose of eliminating the water by-product subsequent to the removal of HCl from the prior cycle, $CaCl_2$ was harnessed. Ultimately, rotary evaporation was conducted at 0°C to extract dichloromethane (DCM) until the attainment of the PGS-M polymer, characterized by a viscosity akin to that of honey.

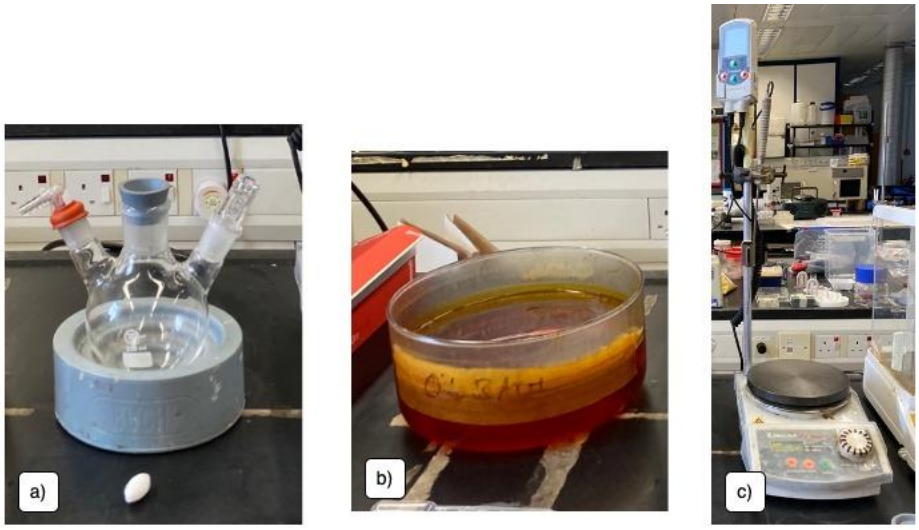

Figure 3.1 – a) three-neck flask, b) mineral glass in oil bath so called oil bath, c) hot plate with magnetic stirrer and temperature sensor.

Figure 3.2 – The set-up for methacrylation step where an ice bucket, a dropping funnel, and a sheet of foil were set on the plate to set up a 0°C environment at 350 rpm in dark.

3.1.2 Scaffold Fabrication

The creation of PGS-M scaffolds involved the implementation of two distinct methodologies: the emulsion process and the sugar-leaching technique.

3.1.2.1 Emulsion technique

The scaffolds were crafted following the formulation outlined by Pashneh Tala et al. for the emulsion technique [38]. A composition of 500 mg PGS-M polymer was amalgamated with toluene (at a ratio of 1:1, weight-to-weight), HypermerTM B246 (in a proportion of 10:1, weight-to-weight), and a blend of diphenyl (2,4,6-trimethylbenzoyl) phosphine oxide and 2-hydroxy-2-methylpropiophenone (constituting 25% of the weight of PGS-M), referred to as a photoinitiator. This amalgamation was stirred at a rate of 350 rpm. Following 5 minutes of agitation, 4 mL of deionized water (dH2O) was gradually introduced at a controlled rate of approximately 1 mL per minute, while the magnetic

stirrer plate continued operation for an additional 5 minutes. The resultant emulsion was subsequently transferred into a silicone mould, with dimensions measuring 30 mm by 10 mm by 2 mm (thickness). To solidify the emulsion, OmniCure Series 1000 was employed to subject it to ultraviolet (UV) light curing for 5 minutes per side (as depicted in Figure 3.3). Subsequent to the curing process, the scaffolds underwent a sequence of four methanol washes followed by four dH_2O washes.

Figure 3.3 – OmniCure Series 1000, for curing the PGS-M scaffolds.

3.1.2.2 Sugar-leaching technique

The sugar icing underwent filtration in accordance with the method devised by Pashneh et al. [40], with the specific intent of acquiring a precise range of sugar particles apt for scaffold construction. The range of sugar particles employed in this study comprised a blend of sizes, specifically 50–100mm and 38–50mm, each in equal proportions.

To engineer the sieve apparatus, an arrangement of filters characterized by progressively diminishing pore sizes was employed. The filters, ranging in sizes of 100mm, 50mm, and 38mm, were systematically layered from the uppermost to the lowermost segment of the

machine. Each filter exclusively retained particles of the predetermined and larger sizes, consequently implying that particles captured by the 100mm filter possessed dimensions equal to or surpassing 100mm.

In implementing the sugar-leaching technique, PGS-M polymer was intricately combined with the meticulously sieved sugar particles as previously described. Prior to the UV curing procedure, which entailed an exposure of 5 minutes per side, an incorporation of 1% (by weight relative to PGS-M polymer) of diphenyl(2,4,6-trimethylbenzoyl) phosphine oxide/2-hydroxy-2-methylpropiophenone (in a 50/50 blend) was administered and meticulously blended. Subsequently, the scaffolds were subjected to a sequential regimen of rinsing, encompassing four washes with deionized water (dH_2O), four methanol washes, followed again by four dH_2O washes. The samples of PGS-M scaffolds were illustrated in Figure 3.4.

Figure 3.4 – PGS-M scaffolds after being washed and cured.

3.1.3 Scaffold Sterilisation

3.1.3.1 Autoclave

A steam steriliser, commonly referred to as an autoclave, serves as a viable technique for rendering healthcare-associated materials and items sterile. The autoclave parameters were configured to achieve conditions of 120°C, 1 psi pressure, and a duration of 20 minutes. In order to effectuate the sterilisation of PGS-M scaffolds, the scaffolds were immersed in deionized water (dH_2O) within a 500mL Duran bottle. While ensuring an outlet for air within the container, the bottle cap was slightly loosened. Following the sterilisation process, the bags and bottles encompassing the autoclaved items remained securely sealed until the commencement of the experimental setup. At that juncture, the canisters were unsealed within a class 2 biosafety cabinet, thus mitigating the risk of contamination.

Every piece of equipment that came into contact with cells and cell medium, comprising Ebers chambers, was methodically enclosed within autoclavable bags and subsequently subjected to the same sterilisation procedure.

3.1.3.2 Plasma treatment

Before undergoing plasma sterilisation, the PGS-M scaffolds underwent a freeze-drying procedure spanning 24 hours. Freeze-drying, a dehydration process executed at low temperatures, involved immersing samples in deionized water (dH_2O) and leaving them at a temperature of -80°C overnight. The internal liquid within the scaffolds was eliminated without undergoing evaporation. This was achieved by swiftly reducing the pressure while maintaining the low temperature [96]. This technique proved instrumental in safeguarding the scaffold's pore structure. Following freeze-drying, the PGS-M scaffolds underwent

sterilisation via a low-pressure Ar and O_2 plasma treatment within the Zepto chamber (as illustrated in Figure 3.4) situated at the SORBY facility. The pressure was subsequently brought down to 0.2 mbar before initiating the treatment. Each side of the scaffolds was subjected to plasma treatment for a duration of 10 minutes. Post-plasma sterilisation, the scaffolds were conserved in sterile phosphate-buffered saline (PBS) until readiness for integration with cells. The containers enclosing the treated scaffolds were solely unsealed within a class 2 biosafety cabinet to uphold sterility. The container lid was opened exclusively when it was imperative to extract material, and aside from such instances, the lid remained securely shut.

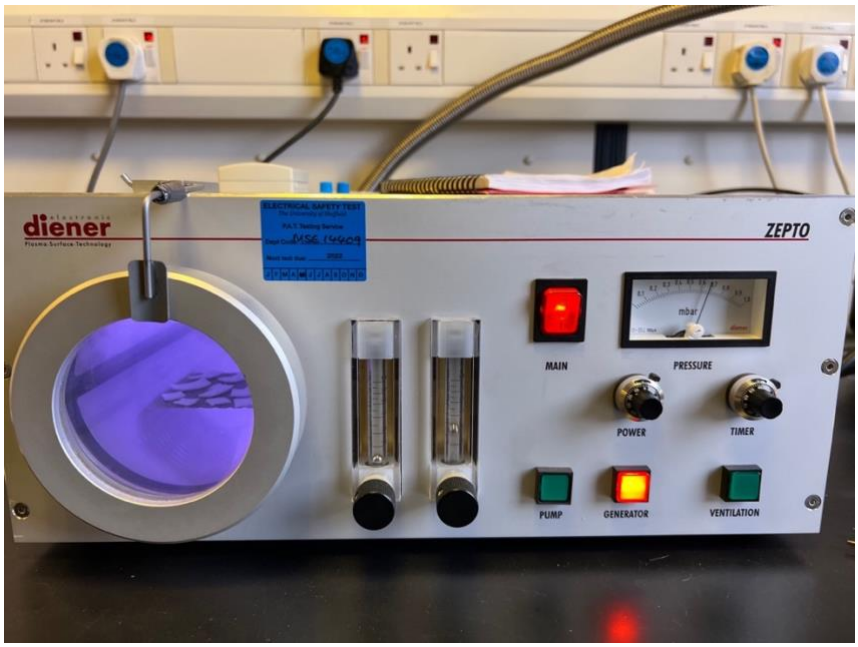

Figure 3.5 – Zepto chamber used in plasma treatment process.

3.1.4 Scaffold Characterisation

3.1.4.1 Mechanical Properties

The determination of the Young's modulus of PGS-M scaffolds was facilitated using the Mecmesin mechanical testing equipment (as depicted in Figure 3.5), located in S20

within the Kroto Research Institute. In this process, every scaffold underwent tension testing via a 250 N force sensor, with a displacement rate of 6 mm/min, until fracture occurred. The equipment's software autonomously computed the data for ultimate tensile strength, expressed in megapascals (MPa), based on the dimensions of length, width, and thickness inherent to each scaffold.

The measurements of length, width, and thickness for each individual sample were taken utilising a digital calliper.

Figure 3.6 –Mecmesin mechanical testing machine and 250N force sensor that were used to determine the ultimate tensile strength of the material.

Since the scaffolds were consistently stored in dH_2O, they were momentarily situated on a paper towel to absorb any excess moisture. Utilising a hexagonal screwdriver, the 250N force sensor was securely affixed in place after being properly positioned. Subsequently,

both grips were affixed; the first grip was directly attached to the force sensor, while the second was fastened to the base. All necessary connections between the tester and the computer were established. Once a scaffold was suitably held, the operator adjusted the upper grip until the scaffold stood upright without collapsing, a depiction of which is presented in Figure 3.6. The testing was then initiated via the computer interface after inputting the pre-measured parameters. Manual selection of the starting and breaking points was carried out, and this data was subsequently utilised to compute the ultimate tensile strength.

Figure 3.7 – The upper grasp was used to draw the scaffolding until it stayed in an upright posture. At this point, the scaffold was not yet dismantled. This was the condition before to beginning the experiment.

3.1.4.2 Contact angle

Water contact angle assessment was performed on freeze-dried, unseeded PGS-M scaffolds utilising the Drop Shape Analysis (DSA) apparatus. In this procedure, a precise volume of 5 µL of water was introduced onto each scaffold via syringe. Employing the KRÜSS DSA 100 equipment, the water contact angle exhibited by the water droplet upon the scaffold's surface was promptly quantified. Concurrently with each water droplet

measurement, a corresponding photograph was captured. The resultant data was derived from averaging three measurements acquired from two distinct samples (N=2, n=3), culminating in the presentation of the reported results.

3.1.4.3 Scaffold wettability

Due to pandemic-related equipment restrictions, an alternative approach was adopted to assess surface wettability. In this modified procedure, a volume of 5 µL of water containing red dye was vertically dispensed onto the freeze-dried PGS-M scaffold. This method aimed to acquire relevant data using minimal resources and a non-specialized apparatus. A digital camera was enlisted to document the water absorption process, concurrently serving as a timer to ascertain the duration required for each scaffold to absorb the water. Subsequently, the period (in seconds) spanning between the initiation of water droplet placement onto the surface and its complete absorption was quantified. For each category, three distinct samples were evaluated (N=3).

3.1.4.4 Scanning Electron Microscopy (SEM)

FEI Inspect F (FEI Co. XL-30 design TLD, USA) was employed for sample imaging purposes. To prepare the samples for imaging, a procedure involving submersion in liquid nitrogen was carried out, followed by snapping the samples in half. This meticulous process was implemented to preserve the intricate pore structure intrinsic to the scaffolds. The acquisition of all scanning electron microscopy (SEM) images was performed by Dr. Nicholas Farr.

3.1.4.5 Pore size analysis

Pore size analysis was conducted by Dr. Nicholas Farr using the ImageJ program. In summary, the SEM images were converted to binary and adjusted until the pores were distinctly distinguishable from the background. After setting the scale according to the scale displayed in the image, a line was drawn between two edges of a pore. This process was repeated for multiple pores to calculate the average pore size of each scaffold.

3.1.4.6 Fourier-transform infrared (FTIR) spectroscopy

A Fourier Transformed Infrared (FTIR) analysis was conducted using a Thermo Scientific Nicolet 380 FT-IR Spectrometer (depicted in Figure 3.7). Prior to the commencement of the experiment, the scaffolds were submerged in phosphate-buffered saline (PBS) and subsequently extracted. Subsequently, the scaffolds were placed on a paper towel for a brief period to facilitate the absorption of any residual moisture. The temperature of the sample plate was maintained at 25°C. Spectra were recorded within the range of 4000 to 800 cm^-1, with particular emphasis on the fingerprint region spanning from 1800 to 1000 cm^-1. For each category, three measurements were taken from two distinct samples (N=2, n=3). The entire FTIR analysis was overseen by Dr. Nicholas Farr.

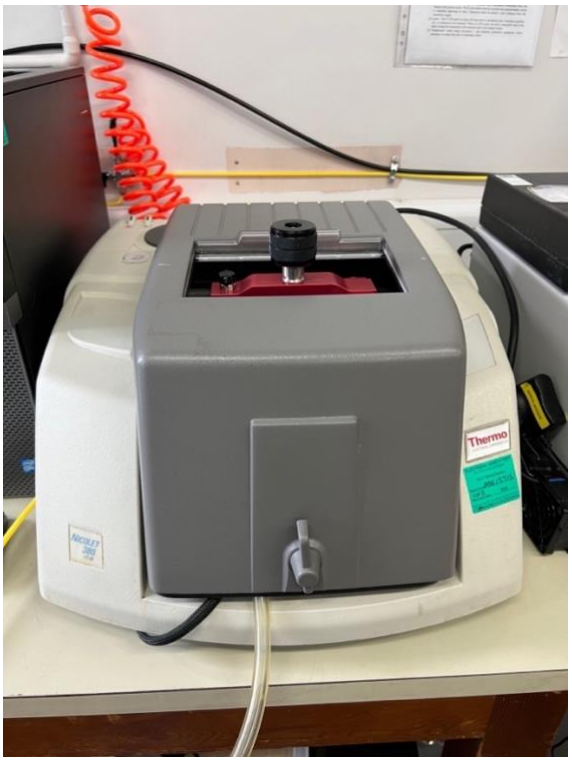

Figure 3.8 – Thermo Scientific Nicolet 380 FT-IR Spectrometer, the device used to determine FTIR spectra.

3.2 Tissue Engineering

3.2.1 Cell culture

Human dermal fibroblasts were sourced from surplus skin tissue, having obtained informed consent and ethical approval from patients undergoing breast reductions or abdominoplasties (UREC Committee Approval reference 15/YH/0177 and 21/NE/0115). The growth of HDFs took place within Dulbecco's Modified Eagle's Medium (DMEM), supplemented with foetal bovine serum in a 10:1 (v/v) ratio, along with 0.002 M glutamine and 100 g/ml streptomycin during the course of cell culture. In the subsequent sections of this thesis, this specific medium is consistently referred to as Complete DMEM. During passages 0 to 3, a period in which cutaneous keratinocytes might still be present within

the culture flask, exclusively Complete DMEM was employed for the purpose of cell culture. An evaluation of cell morphology through light microscopy established that all cells persisting in culture beyond this initial phase were unequivocally identified as fibroblasts. The harvesting of HDFs transpired using a trypsin/EDTA solution within passages 4 and 12. Every week, specifically on Mondays, Wednesdays, and Fridays, during each passage, a complete replacement of the medium was carried out using Complete DMEM. The cell cultivation process was maintained at a temperature of 37°C within a humidified environment, with the presence of 5% CO_2.

In instances where CO_2 was unavailable, HEPES buffer was utilised. The HEPES powder, obtained from Sigma Aldrich, was dissolved in phosphate-buffered saline (PBS) to generate a 1 mM HEPES solution. This solution was subsequently subjected to filtration to eliminate any potential pathogens. The HEPES buffer solution, integrated into complete DMEM, was freshly prepared at varying concentrations of 10 mM, 15 mM, 20 mM, and 25 mM, immediately prior to the medium switch. Throughout the experiment, a total volume of 3 mL of the prepared medium was dispensed into each well of a 6-well plate and subsequently placed within the designated incubator. Notably, this study did not encompass cell growth. On the same days allocated for cell culture activities, the medium was replaced as part of the experimental process. Following a week of incubation, pH measurements were conducted to assess any alterations.3.2.2 Cell passaging.

To detach HDFs from a T75 flask, a trypsin/EDTA solution was employed. Cells were passaged once they had covered approximately 75 to 90% of the flask's surface area. The process began by fully aspirating the DMEM from the flask. Subsequently, the flask was rinsed with PBS to ensure the removal of any residual Complete DMEM. Following

the removal of PBS, 2 mL of trypsin/EDTA was introduced, and the flask was then incubated for an approximate duration of 7 minutes. In cases where required, gentle physical agitation was applied to facilitate the detachment of cells.

To halt the trypsin/EDTA activity, the flask was refilled with 3 mL of Complete DMEM. The cell suspension was then transferred from the flask to a 20 mL centrifuge tube, and centrifugation was carried out to eliminate the trypsin/EDTA solution. The Relative Centrifugal Force (RCF) set for this centrifugation step was 154 g. The cell pellet was subsequently resuspended in 3 mL of fresh Complete DMEM to generate a new cell suspension.

For the subsequent culturing, 1 mL of the resuspended cell solution was apportioned into each fresh T75 flask. Additionally, 10 mL of fresh Complete DMEM was supplemented in each flask to ensure adequate nutrient supply for the cells. It is noteworthy that a single HDF flask could be passaged into three additional flasks.

Throughout each passage, the passage number was incremented by one to denote the cells' advancing age.

3.2.3 Cell seeding

To initiate a new series of experiments, the separation and transfer of HDFs from the flask to the designated platform, which could be either tissue culture plastic (TCP) or scaffolds, were necessary. Cell detachment from the flask was achieved using a trypsin/EDTA solution, as detailed in section 3.2.2. Subsequent to obtaining the cell suspension, a haemocytometer was employed to determine the cell count. For the purposes of this thesis, except during assay optimisation, a count of 1x105 cells was allocated to each

TCP well within a 6-well plate or to each scaffold (measuring 30 mm in length, 10 mm in width, and 2 mm in depth).

The designated cell concentration was meticulously calculated to ensure the desired cell quantity could be accommodated within a minimal volume of liquid, typically ranging from 200-250 µL. For seeding cells onto a 2D surface, the cell suspension was directly dispensed onto the surface, and fresh Complete DMEM was subsequently added. Meanwhile, for seeding cells onto the scaffold, a 1mm-diameter metal ring was employed to contain and position the cells on the scaffold, ensuring their retention. It is crucial for the ring's diameter to be smaller than that of the scaffold. Initially, the ring was placed on the scaffold surface, and Complete DMEM was added around the ring's exterior. This step helped ascertain proper alignment of the ring onto the scaffold. In cases where the ring wasn't completely seated on the scaffold, the introduced medium would work to establish equilibrium between the liquid inside and outside the ring.

Subsequent to this, the cell suspension was introduced within the confines of the ring, marking the initiation of the experiment (referred to as day 0), allowing the cells time to adhere to the scaffold surface.

3.2.4 Quantitative analysis of cell activity

3.2.4.1 Resazurin metabolic activity assay

The Resazurin assay serves the purpose of quantifying a cell's metabolic rate, which in turn reflects its activity and viability. To prepare a 10 mg/mL stock solution of resazurin, 1 g of resazurin sodium salt was dissolved in 100 ml of sterile PBS. Subsequently, the

resazurin active solution was formulated by diluting this stock with fresh Complete DMEM at either a 1:100 or 1:50 (v/v) ratio, depending on the specific experimental conditions.

In the staining process, the plates were positioned on a rocker within an incubator to facilitate uniform staining. By default, the incubation period lasted for 4 hours, unless explicitly specified otherwise. Following the completion of incubation, 3 aliquots of 200 µL each were transferred from every well to a 96-well plate. For every reading, the resazurin active solution was also included to serve as a reference for the stain's colour.

Using a fluorescence plate reader (Biotek FLx800), the fluorescence was measured at a wavelength of 530 nm for excitation and 590 nm for emission. This enabled the assessment of the Resazurin assay's outcomes.

3.2.4.2 Picogreen DNA quantification

The Picogreen assay serves as an indicator for cell proliferation by providing information about cell concentration and cell number based on the quantification of DNA present in the culture. To initiate the assay, the cells underwent lysis utilising a solution composed of 1% Triton-x in 1x TE buffer, followed by subjecting them to five cycles of the freeze-thaw technique. The DNA standard curve was established by diluting a 50x stock in 1x TE buffer to achieve a concentration of 2 µg/mL. For the assay procedure, a picogreen working solution was first prepared. This involved diluting a 200x Picogreen stock with 1x TE buffer to attain a 1x concentration. In line with the samples, triplicates of 100 µL aliquots were transferred to a 96-well plate, and these aliquots were then mixed with 100 µL of the prepared picogreen working solution. Subsequently, fluorescence

measurements were taken using excitation at 480 nm and emission at 520 nm to ascertain the results.

The λDNA concentration was employed as a reference for the DNA concentration, forming the basis for the generation of a standard curve. To establish a working solution with a concentration of 2 µg/mL, the 50x stock was appropriately diluted utilising 1x TE buffer. This working DNA solution was further diluted with 1x TE buffer to achieve the final concentrations for the standard curve, which included 0, 0.005, 0.01, 0.05, 0.1, 0.5, 1.0, and 2.0 µg/mL.

For the determination of the fluorescence of the standard curve, 100 µL of each final concentration was aliquoted in duplicate into a 96-well plate. Subsequently, these aliquots were mixed thoroughly with 100 µL of the picogreen working reagent. The fluorescence readings were then acquired and recorded using a Biotek FLx800 fluorescent plate reader. This facilitated the generation of accurate results for subsequent analysis and interpretation.

3.2.4.3 Sirius red collagen assay

Picrosirius red reagent was made by dissolving direct red 80 in picric acid until a 1 mg/ml solution was obtained. To stain the ECM production with the sirius red assay, the cells must be treated with a formalin solution containing 3.7% formaldehyde for 30 minutes. After fixing the cells, samples were wrapped in aluminium foil and rocked at room temperature for at least 18 hours. Unless specified otherwise, the samples were then rinsed with 0.5M HCl acid until there was no excess colour coming out from the sample. After washing the samples, a solution of 0.2 M NaOH in methanol was employed to

remove the colour. Absorbance at 530 nm was measured with a plate reader (Biotek ELx800).

3.2.5 Lightsheet z1 imaging

Fluorescence dye was employed as a method to capture images of the scaffolds. The process involved immersing the samples in a solution of 0.1% Triton-X in PBS for a duration of one hour. Subsequently, the samples were subjected to staining using DAPI and Phalloidin FITC for another hour, conducted in a light-free environment. For both staining solutions, a concentration of 1:1000 (v/v) was prepared in PBS. The scaffolds were then stored in PBS at 4°C, shielded from light, until they were prepared for imaging. To facilitate sample preparation, a mixture of 1% low-melt agarose in PBS was utilised to secure the samples within glass capillaries of size 4 (with an inner diameter of 2.15mm). The procedure involved melting the 1% low-melt agarose at 75°C, followed by adding approximately 2 mL of the melted agarose onto a petri dish. A dissected sample of about 2mm was placed onto the area where the agarose was deposited. This step encapsulated the sample within the agarose gel, rendering it ready for placement into the capillary. The plunger associated with the capillary was then employed to carefully position the sample within the capillary.

Once the sample was positioned appropriately to enable imaging, the Zeiss Z1 light sheet microscope was utilised to observe the samples at a magnification of 10x, using both green and blue channels. The light intensity setting used for this process was 30. The Zen software was employed for both image control and processing, utilising the Maximum

Intensity Projection profile during image processing. This comprehensive methodology facilitated the acquisition of detailed and informative images for analysis and study.

3.2.6 Histology

Histology is a valuable technique that enables researchers to apply different stains to sample sections, resulting in images that highlight various elements based on the specific stain used. In this thesis, the paraffin embedding method was adopted for sample preparation. It's important to note that unless otherwise specified, the chemical reagents were sourced from Sigma Aldrich, a well-known supplier of laboratory substances and equipment. This approach allows for the careful preparation and examination of tissue samples, contributing to a deeper understanding of the underlying structures and components within the samples.

3.2.6.1 Sample preparation

The sample processing for histology involved a series of meticulous steps to prepare the tissue sections for staining and examination. Initially, the samples were fixed by being incubated overnight in a solution of 3.7% formaldehyde. Following this, a tissue processor was employed to carry out the subsequent steps, which included dehydration, clearing, and infiltration.

During the dehydration phase, the samples were subjected to a series of treatments with varying concentrations of industrial methylated spirit (IMS). This process involved two cycles of 70% IMS for 1 hour each, followed by 80%, 85%, 90%, and 95% IMS for 1.5 hours per cycle. Subsequently, two cycles of 100% IMS for 1.5 hours each were employed to ensure thorough dehydration.

To enhance the clarity of the samples, two cycles of xylene were used to replace the IMS, with each cycle lasting 1.5 hours. After achieving suitable clarity, the infiltration step commenced, during which paraffin wax was introduced into the samples. The samples were placed in a wax-filled container for 2 hours, and this process was repeated twice to ensure proper wax infiltration.

For the creation of wax blocks, the samples were mounted with metal blocks and cassettes. Paraffin wax was used to fill the mould and create the block, which was then allowed to cool on a cold surface. This mounting process was facilitated by the Epredia HistoStar machine, which provided the necessary cold surface.

Once the wax blocks were properly formed, they were taken out from the moulds and stored at room temperature until they were ready for sectioning. To generate thin sections for examination, a microtome (Leica RM2145) was used to cut sections with a thickness of 10 µm. These sections were then transferred to a warm water bath, placed onto glass slides, and allowed to dry overnight before subsequent staining and analysis could be performed.

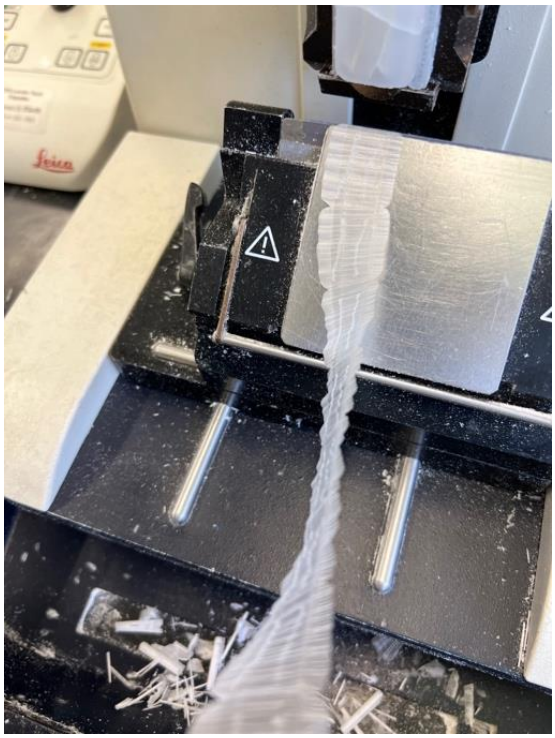

Figure 3.9 – The 10 µm thick ribbon created by sectioning the sample using a microtome.

3.2.6.2 Haematoxylin and eosin stain (H&E)

Haematoxylin and eosin are the two constituents of H&E histology staining. Haematoxylin imparts a purplish-blue colour to cell nuclei, whilst eosin imparts a pink colour to the extracellular matrix and cytoplasm. Different structures display a variety of shades, tones, and combinations of these colours.

The slides were deparaffinized and hydrated to enable staining with H&E. Subsequently, the slides were immersed in Haematoxylin Gill No.1 (Merck) for 1 minute and 30 seconds. Following this step, the slides were cleaned using deionized water, and then stained with Eosin Y solution (Merck) for five minutes. The slides were rehydrated afterwards. Finally, the slides were mounted (as previously described) after undergoing examination under a microscope.

3.2.6.3 Elastin Verhoeff-van Gieson (EVG) staining

The Elastic Stain Kit from Abcam UK was used to highlight the elastin fibres within the connective tissue. This method involves two stains interacting with the specimens. Acid fuchsin and Picric acid were used for double staining, which stains collagen fibres and muscle fibres. The staining procedure closely adhered to the manufacturer's instructions for the staining kit.

The stain included in the kit was pre-prepared and ready for use. The slides were deparaffinized using xylene and then hydrated using 100% methanol, followed by 70% methanol and distilled water, before staining. Subsequently, the slides were immersed in a working solution of the Elastin stain. After a 15-minute incubation, the sections were washed under running water to remove any excess stain. The slides were then repeatedly immersed in a differentiating solution about 15 to 20 times and washed under running water. Next, the slices were dipped into Sodium Thiosulfate Solution for one minute, followed by rinsing under running water. A 2 to 5-minute staining with Van Gieson's Solution was carried out. Afterward, the slides were rinsed twice with 95% alcohol and subsequently dehydrated with pure alcohol. To confirm the success of the staining process, the samples were examined under a light microscope. For mounting, a drop of DPX mounting medium was applied to the slide with caution, ensuring no air bubbles formed. The coverslip was carefully positioned on the slide to prevent the formation of air bubbles. This process was carried out within a fume cupboard at all times. After allowing the DPX mounting medium to dry for approximately 15 minutes, the slide was moved outside the fume cupboard and left on the benchtop to dry overnight. Following this, the slide was stored in a suitable container.

3.2.6.7 Immunohistochemistry (IHC)

Ki67 and DAPI were employed as IHC stains in this study, with all reagents supplied by Abcam, UK. The process commenced with deparaffinization and rehydration of the slides using xylene and methanol. Following a PBS wash, antigen retrieval was performed through heat treatment. The slides were heated in a microwave for eight minutes using sodium citrate along with 0.05% Tween. Subsequently, the slides were rinsed with PBS and permeabilized at room temperature for 20 minutes with 0.5% Tween 20.

The next step involved washing the slides once more, this time with PBS containing 0.025% Triton-X, followed by a 30-minute incubation in Protein Block. After this, the slides were rinsed again with PBS containing 0.025% Triton-X and were left to incubate overnight with 200 µL of anti-Ki-67 rabbit primary antibody per sample. The primary antibody was diluted to a concentration of 1:500 (v/v) in the Protein Block solution, which itself was prepared at a 1:100 (v/v) ratio with 0.025% Triton-X in PBS.

For subsequent steps, the material was stained with anti-rabbit AlexaFluor 647 Donkey antibody at a dilution of 1:200 (v/v) in the Protein Block solution. This secondary antibody was incubated at room temperature for one hour. The slides were then exposed to 1 µg/mL DAPI at room temperature for 30 minutes. Following this, the slides were mounted using DPX mounting medium, in accordance with the previously described method.

3.2.5 Statistical Analysis

All the results obtained from the plate reader were recorded in the Microsoft Excel program. For the 3D cell culture experiments, the control group consisted of static 3D cell

cultures on unstimulated PGS-M scaffolds. In the case of 2D cell culture, cells were cultured on tissue culture plastic (TCP) to serve as a reference for cell conditions.

To obtain accurate data, background readings were subtracted from the actual results. The background data were generated from blank, unseeded PGS-M scaffolds subjected to the same conditions as the experimental seeded scaffolds. When appropriate, the information was presented in graphs as percentages along with the corresponding standard deviation (SD).

To statistically evaluate quantitative data, including cell metabolism, cell count, and collagen production, unless stated otherwise, all data was assessed by using One-way ANOVA statistical approach. This was employed as the framework, with a significance level set at $P < 0.05$ to denote significant differences in the results. Prism software was utilised for performing the statistical analysis. In rare cases where sample per group was less than three samples, T-Test was employed as the statistical analysis between two different groups.

Chapter 4 - Optimisation of PGS-M scaffolds for in vitro culture

PGS is a widely utilised biomaterial in the realm of biomaterials, particularly for crafting ECM-based hybrid scaffolds due to its biocompatibility. However, the conventional fabrication process for this material demands elevated temperatures and extended durations [31]. In order to modify the production process, a methacrylate group is incorporated into the prepolymer, resulting in the formation of PGS-M polymer. This adaptation enables the creation of scaffolds under ambient conditions, simplifying the fabrication process. The methacrylation of PGS was developed in-house and was documented in two seminal papers authored by Singh et al. [97] and Pashneh-Tala et al. [38]. Despite the progress, this remains a relatively novel material that necessitates further refinement in both its application and characterization as a scaffold material. Various cell culture assays were employed to assess the material, and the outcomes were compared against the established 2D cell culture standard curve on tissue culture plastic (TCP).

4.1 Optimisation of sterilisation techniques

PGS is a straightforward polymer synthesized from glycerol and sebacic acid. It incorporates ester bonds within its polymer backbone, enabling covalent crosslinking to form a network structure, resulting in an elastomeric material. This process, known as curing, typically involves the application of heat. However, the introduction of the methacrylate group allows the polymer to be crosslinked using ultraviolet (UV) light

exposure. This modification simplifies and accelerates the curing of PGS-M scaffolds. Instead of subjecting scaffolds to prolonged high-temperature conditions, PGS-M can be cured within a matter of minutes by exposing it to a UV lamp [39].

Biomaterials and medical devices must undergo sterilisation before use to prevent microbial contamination, including bacterial presence [98]. The choice of sterilisation method depends on the properties of the biomaterial. Some well-established sterilisation methods approved by the FDA include radiation, ethylene oxide gas, hydrogen peroxide, and steam [99]. Among these, steam sterilisation, commonly referred to as autoclaving, is an FDA-approved method as well as recognized by ISO 17665 [100]. Given that the PGS-M scaffolds were initially sterilised using an autoclave, this technique was optimised and compared with alternative methods. Initially, the ultimate tensile strength of the scaffold was assessed to gauge its suitability for mechanical stimulation. To explore alternative surface disinfection methods that do not rely on heat, plasma treatment in a vacuum chamber was employed. Various exposure times of argon (Ar) plasma treatment were tested in comparison with the autoclave, taking into account different aspects. To facilitate successful plasma treatment, a dry scaffold was necessary. Consequently, the scaffold underwent freeze-drying before plasma treatment. Ar plasma treatment was favoured due to its capability not only to disinfect the scaffold surface but also to reduce the water contact angle on the material's surface[57].

Previous research employed a scaffold with 50% methacrylate content (PGSM-50) as the primary template for in vitro cell culture [39]. However, this current study identified a significant risk of scaffold rupture during mechanical stimulation. Consequently, the 80% methacrylate PGS-M scaffold (PGSM-80) was also evaluated. This scaffold contains a

higher proportion of methacrylate groups (as described in Chapter 3) and was introduced as an alternative template for in vitro cell culture, offering greater crosslinking and, thus, a higher Young's modulus. Additionally, various exposure times of Ar plasma treatment were applied to understand their impact on mechanical properties and surface wettability, both of which can influence cell attachment. Emulsion templating was utilised to create PGS-M scaffolds with varying stiffness levels.

To evaluate the effectiveness of different sterilisation methods, freshly manufactured untreated PGS-M scaffolds were compared with autoclaved scaffolds and those treated with Ar plasma for 4 and 10 minutes. However, it's important to note that plasma treatment is not currently categorized as a sterilisation method; it is considered a disinfection method [101]. The ultimate tensile strength was assessed using the procedure outlined in section 3.1.4. As shown in Figure 4.1A, the ultimate tensile strength of Ar plasma-treated PGSM-50 scaffolds following both 4 and 10 minutes of treatment was 5 to 6 times higher compared to untreated and autoclaved PGSM-50 scaffolds. For PGSM-80 (Figure 4.1(B)), the ultimate tensile strength of the Ar plasma-treated scaffold, regardless of the exposure period, was approximately 1.5 times greater than that of untreated and autoclaved PGSM-80 scaffolds. This indicates that disinfecting PGS-M scaffolds using Ar plasma treatment enhances their ultimate tensile strength compared to autoclaving.

Farr et al. [64] provide insight into the effect of Ar plasma treatment on PGS-M polymer, which could explain these findings. According to their research, Ar plasma treatment alters the surface chemistry of the polymer in contrast to autoclaved samples. This treatment promotes further crosslinking of the polymer's surface, resulting in a densely cross-linked surface layer that imparts qualities such as insolubility, high-temperature

stability, chemical resistance, and mechanical robustness [102, 103]. The use of Ar plasma for surface treatment on highly porous PGS-M polyHIPE scaffolds is also supported by their analysis, consistently treating the high surface area materials.

When assessing both percentages collectively, it became clear that the PGSM-80 scaffold possessed greater stiffness compared to PGSM-50. This conclusion was drawn from the fact that the PGSM-80 scaffold displayed an ultimate tensile strength that was 5 times higher than that of the PGSM-50 scaffold. This observation substantiates the notion that an increased proportion of methacrylate groups within the polymer corresponds to an elevated ultimate tensile strength in the scaffold.

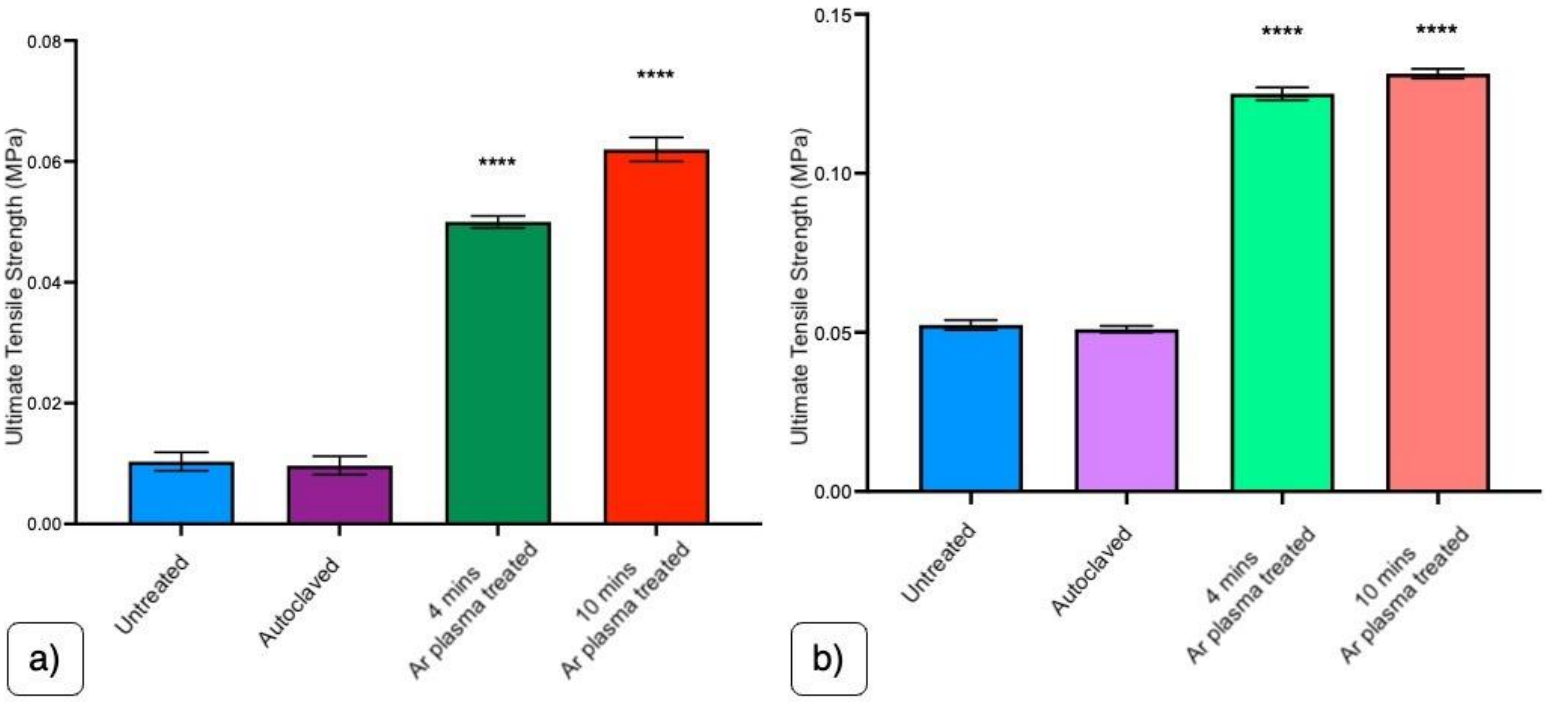

Figure 4.1 – The ultimate tensile strength in MPa resulting from various sterilising procedures for (a) PGSM-50 scaffolds and (b) PGSM-80 scaffolds. The asterisk (*) indicates the significant difference ($P < 0.05$).

According to the data presented in this study, if the maintenance of scaffold ultimate tensile strength (UTS) is a priority, autoclaving emerges as the suitable sterilisation technique. The results indicate no statistically significant difference between untreated and autoclaved PGS-M scaffolds in terms of UTS. Importantly, this observation holds true for both levels of methacrylation that were investigated.

Nevertheless, the treatment of PGS-M scaffolds with Ar plasma, which does not involve heat, exhibited a notable enhancement in mechanical properties. Specifically, Ar plasma treatment appeared to elevate the ultimate tensile strength (UTS) of PGSM-80 in comparison to PGSM-50. This increase in UTS suggests that the scaffolds were better equipped to withstand force during mechanical deformation.

When contrasted with untreated scaffolds, extended exposure to Ar plasma treatment yielded more significant improvements in the mechanical properties of both PGSM-50 and PGSM-80. For PGSM-50, the ultimate tensile strength surged by a factor of 6 with longer exposure, whereas for PGSM-80, this increase was 2.64-fold. The disparity between the untreated scaffold and the scaffold subjected to longer Ar plasma exposure was more substantial than that seen with shorter exposure. Nevertheless, even the shorter exposure duration resulted in a 5-fold increase for PGSM-50 and a 2.5-fold increase for PGSM-80 when compared to untreated scaffolds.

Upon closer examination, the divergence between these two exposure times was more pronounced in the polymer possessing a lower degree of methacrylation. Consequently, it can be inferred that an extended duration of Ar plasma treatment is more effective in enhancing stiffness. Additionally, it's worth noting that the impact of this Ar plasma treatment is more pronounced on PGS-M polymers with a lower degree of methacrylation.

Through the adjustment of curing temperatures, research has revealed the capability to modify the mechanical properties of a PGS polymer scaffold treated with heat. The computation of equilibrium moduli for PGS scaffolds was carried out by Jaafar et al. [104], utilising the correlation between stress (percentage) and strain (MPa). In this pursuit, all scaffolds were cured for 24 hours at temperatures ranging from 120 to 165°C, including increments of 10°C. After the fabrication process, step tensile testing was employed on the PGS scaffolds. The findings indicated that an increase in the curing temperature resulted in heightened elasticity of the PGS scaffold. Significantly, at temperatures of 140 and 150°C, the equilibrium moduli of the scaffolds witnessed a respective increase of 3.6 and 4.7 times, following a mere 10°C increment in curing temperature. This augmentation in mechanical property was notably more substantial than that observed at other curing temperatures, where the increase in elasticity was less than twofold. Despite some variations in data, both studies depicted parallel trends. Chen et al. [103] similarly investigated the mechanical behaviour of PGS sheets across temperatures of 110, 120, and 130°C. In both instances, the researchers found that elevating the curing temperature led to enhancements in the mechanical properties of the PGS sheets. The revelation regarding the influence of temperature on mechanical properties shaped the trajectory of this thesis.

While this thesis predominantly focuses on the PGS-M polymer, it's important to note that the fundamental polymer remains unchanged. To enhance the tensile strength of the scaffolds, an increase in crosslinking density is necessary. In the case of the PGS polymer, the technique hinged on curing temperature adjustments [104, 105], However, for PGS-M, a distinct approach is adopted. The introduction of a methacrylate group in PGS-M

enables UV curing of the scaffolds. This modification renders the material photocurable, eliminating the feasibility of increasing crosslinking density through higher temperatures. Consequently, the utilisation of an autoclave, which employs elevated temperature and pressure for sterilisation, may not impact the crosslinking density of PGS-M scaffolds. This aligns with the findings indicating no statistically significant difference in ultimate tensile strength between untreated and autoclaved PGS-M scaffolds.

Although autoclaving might not induce changes in the mechanical properties of PGS-M scaffolds compared to untreated ones, it might not facilitate cell adhesion and proliferation to the same extent. Previous research conducted demonstrated that human dermal fibroblasts (HDFs) did not effectively proliferate on autoclaved PGSM-50 scaffolds, while showing robust proliferation on tissue culture plastic surfaces [82]. Additionally, the thickness of the scaffold was visibly reduced after autoclaving. The application of high temperature over an extended duration could potentially have a detrimental impact on the PGS-M polymer, leading to a contraction within the scaffold structure. This phenomenon has been observed by other members of the research team using the same polymer (S. Pashneh-Tala, internal communication, May 2019). Unexpected crosslinking of the PGS-M polymer has also been encountered after leaving it at ambient temperature overnight. This occurrence illustrates that the incorporation of the methacrylation group, particularly at higher degrees of methacrylation, amplifies material shrinkage at elevated temperatures. Consequently, the polymer was consistently stored in a freezer until needed for scaffold construction, mitigating the potential for such issues.

Due to the adverse impact of elevated temperature on the polymer, an alternative approach was explored to circumvent the application of heat to the scaffold. Consequently,

an alternative method was sought to avoid heat exposure. This led to the consideration of plasma treatment as a potential solution, which emerged as an interesting option. The interest in this technique was driven not only by its heat-free disinfection process but also by its potential to improve cell attachment.

Beyond its microorganism-destroying capabilities, plasma treatment allows for the adjustment of various features [59, 101]. Despite autoclaving being acknowledged as an effective sterilisation method, it might not always be appropriate [59, 104, 105]. The ability of plasma treatment to ameliorate biomaterial surfaces has garnered mounting attention over time.

Although no published studies currently address the effects of Ar plasma treatment on PGS-M polymers, existing reports delve into the consequences of plasma treatment on other biomaterials. For instance, compared to untreated poly(glycerol sebacate) (PGS)/polycaprolactone (PCL) scaffolds, O_2 plasma treatment has been found to negatively impact tensile strength and Young's modulus in poly(glycerol sebacate) (PGS)/polycaprolactone (PCL) polymers [106]. Yip et al. [62] documented the influence of varying exposure times to Ar plasma on Nylon 6 fabrics. The study followed a protocol involving five distinct exposure durations: 0 (untreated), 5, 10, 20, and 40 minutes. Surprisingly, they found that the plasma exposure time does not linearly correlate with an increase in mechanical characteristics. Specifically, Nylon 6 treated with Ar plasma for 5 minutes displayed lower tensile strength than untreated Nylon, whereas Nylon 6 treated for 10 minutes exhibited higher tensile strength than untreated Nylon 6. This variation in tensile strength mirrors the findings presented in Figure 4.1, where the exposure period didn't enhance the mechanical properties of PGSM-50 scaffolds in the same manner as

it did for PGSM-80 scaffolds. While the impact of Ar plasma treatment on mechanical characteristics of PGSM-80 seems ambiguous, Sarikanat et al. [107] demonstrated that Ar plasma treatment enhances the mechanical properties of flax fibres, aligning with the results presented here. It's plausible that the effects of Ar plasma treatment, including exposure duration, are not uniform across all biomaterials. Instead, they likely depend on the unique characteristics of each biomaterial. Additionally, in cases where a scaffold comprises multiple biomaterials, this could potentially influence both mechanical properties and the outcome of plasma treatment [62, 108].

The water contact angle also attracted attention as it offers insights into the hydrophilicity of a material's surface [58]. Lower contact angle values indicate higher hydrophilicity, where water droplets spread on the surface, while higher contact angle values suggest hydrophobicity, causing water droplets to bead up. By observing the behaviour of water droplets on a surface, images can be captured to determine contact angles. In Figure 4.2(A), water droplets on untreated and autoclaved PGS-M scaffolds exhibited a more spherical shape compared to those on plasma-treated scaffolds. The contact angles derived from these observations indicated that untreated and autoclaved PGS-M scaffolds were more hydrophobic than plasma-treated ones. However, no statistically significant difference emerged among the various exposure times of plasma treatment.

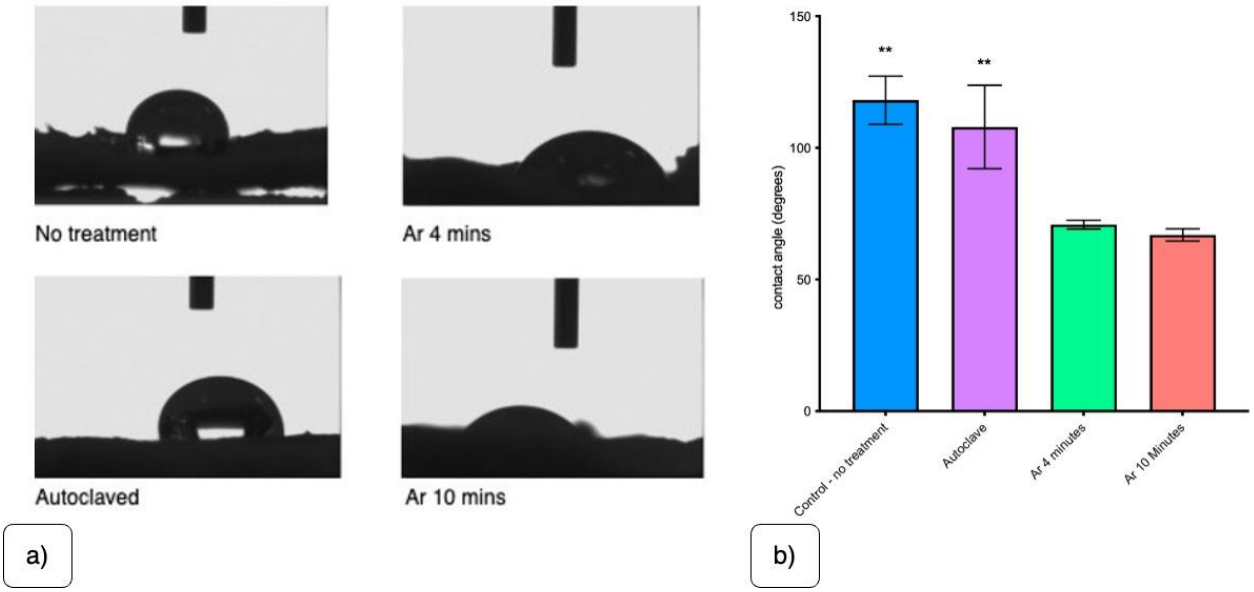

Figure 4.2 – A) Water droplets on different PGS-M surfaces. B) The water contact angle, with asterisks indicate the statistical comparison to the Ar plasma treated PGS-M scaffolds. The asterisk (*) indicates the significant difference in P value < 0.05 (N=1, n=3).

Griffin et al. [109] also reported a comparable discovery. Irrespective of the gases used, plasma treatment enhanced the hydrophilicity of the scaffold surface. The choice of gas during plasma treatment led to diverse alterations in the scaffold surface. Ar plasma treatment, in particular, was found to diminish the presence of carbon on the surface. Instead, it triggered changes in the scaffold surface characteristics, largely due to an augmented oxygen content. This finding aligns well with the observations made by Farr et al. [64]. The use of the secondary electron hyperspectral imaging (SEHI) technique to analyse scaffold surfaces revealed that the detachment of excess methacrylate units from PGS-M enabled the generation of hydroxyl groups, consequently boosting hydrophilicity. Notably, the appearance of OH-bonds on Ar plasma-treated PGS-M scaffolds was linked to an elevation in surface hydrophilicity.

Given that hydrophilicity has been identified as a factor impacting cell attachment, this facet was also subject to investigation. A total of $1x10^5$ HDFs were seeded onto the PGS-

M scaffolds and subsequently cultured for a period of 14 days. To ensure accuracy, the baseline signal originating from cell-free untreated PGS-M scaffolds was subtracted from all obtained results.

When compared to autoclaved PGS-M scaffolds, an elevation in metabolic activity was apparent for Ar plasma-treated scaffolds at both the 7-day and 14-day marks (see Figure 4.3). Notably, no significant difference was noted between various exposure times. The metabolic activity recorded for autoclaved PGS-M scaffolds closely resembled the background value derived from scaffolds lacking cells. This suggests the possibility that cells either did not successfully adhere or, if they did adhere, were unable to endure thereafter.

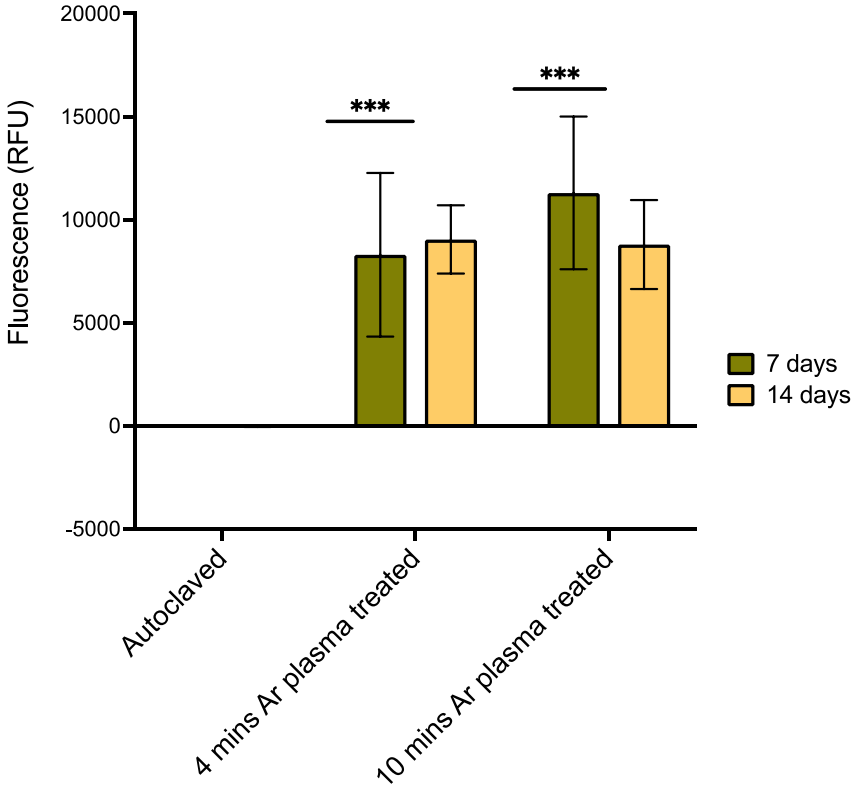

Figure 4.3 –The cell metabolic activity determines from resazurin assay. This data is collected from 7 and 14 days cell culturing on different PGS-M scaffolds. (N=3, n=3). The asterisk (*) indicates the significant difference in P value < 0.001 in comparison with the autoclaved result.

This trend can be ascribed to the hydrophilic characteristic of plasma-treated PGS-M scaffolds. Prior research has substantiated the role of hydrophilicity in facilitating cell attachment [109, 110]. Although a notable variance in cellular metabolic activity was observed among Ar plasma-treated samples, resulting in a substantial standard deviation, it is conjectured that this incongruity stems from divergent plasma conditions prevailing within the plasma chamber across distinct sample positions. This divergence is likely influenced by the positioning of the Ar inlet at the rear of the plasma chamber. The incorporation of more contemporary plasma sources might hold promise in establishing a more uniform plasma environment, thereby mitigating this variability.

The results of these investigations underscored the advantages of Ar plasma treatment compared to autoclaving for scaffold disinfection. Additionally, this approach holds the potential to alter the scaffold surface, augmenting its propensity for cell attachment. While specific tests were not conducted to formally ascertain the sterility of the surface following plasma treatments, observations strongly suggested that Ar plasma treatment adeptly curbed microbial growth on the scaffolds throughout the experimental duration.

4.2 Optimisation of scaffold fabrication techniques

The fabrication of scaffolds using the PGS-M polymer can be achieved through various techniques. This thesis delves into two of these methods: emulsion templating (E) [38] and sugar-leaching (S) [40]. Furthermore, recognizing plasma treatment as the optimal disinfection strategy, supplementary investigations were conducted to explore the effects of different gases employed in the process [109], specifically comparing O_2 with Ar plasma treatment. However, the continuation of emulsion templating for PGSM-50 encountered

challenges that hindered progress in scaffold fabrication. The underlying hypothesis suggested that the lower degree of methacrylation resulted in heightened difficulty in photocuring the scaffold, leading to diminished cross-linking. Importantly, this thesis exclusively explored the lower degree of methacrylation within the context of sugar-leaching, omitting its application in the emulsion technique. This choice was primarily motivated by the substantial variation in the total amount of PGS-M polymer used between the two methods. Consequently, the creation of sugar-leached PGS-M scaffolds proved more feasible and yielded sturdier scaffolds. Despite sporadic instances of successful PGSM-50 scaffold creation using the emulsion technique [39], these scaffolds often displayed fractures and proved unable to withstand the forces exerted during mechanical stimulation.

Additionally, the stability of the emulsion was identified as being susceptible to the presence of residual dichloromethane (DCM) before crosslinking. To rectify this, deliberate measures were taken to eliminate any lingering DCM prior to scaffold fabrication. To achieve this, the PGS-M polymer was subdivided into smaller portions and placed in a vacuum with the container slightly ajar. A metal fragment from the -80°C freezer was employed to uphold low temperatures for the polymer. The weight of the polymer (excluding the container) was then meticulously monitored on an hourly basis until any weight alteration fell below the 1% threshold. This scrupulous protocol ensured that the PGS-M polymer used predominantly consisted of pure polymer.

This procedure underwent refinement through collaboration with colleagues who were concurrently working with this polymer. It was during this collaborative phase that the determination was reached to proceed with the 80% methacrylation degree for the

emulsion technique. This decision was grounded in the fact that its elastic modulus exceeded that of the 50% PGS-M scaffold, providing a robust foundation for subsequent experimentation.

4.2.1 Mechanical testing

When focusing solely on the fabrication methods, the comparison encompassed PGSM-80 emulsion templating (PGSM-80 E), PGSM-50 sugar-leached (PGSM-50 S), and PGSM-80 sugar-leached (PGSM-80 S). Within each category, three scaffolds underwent tensile testing to elucidate the impacts of plasma treatment and construction techniques. As depicted in Figure 4.4, the ultimate tensile strength is governed by both the chosen fabrication methodology and the degree of methacrylation.

From the graph, it is evident that the S technique led to an improvement in the ultimate tensile strength of the PGSM material in contrast to the emulsion technique. This is substantiated by the fact that both PGSM-50 S and PGSM-80 S exhibited significantly higher ultimate tensile strength than PGSM-80 E. Furthermore, the augmentation in methacrylation contributed to the enhancement of ultimate tensile strength in the scaffolds, as evidenced by PGSM-80 S displaying a higher UTS compared to PGSM-50 S.

Notably, across all three categories of PGSM scaffolds, whether argon or oxygen plasma was employed for scaffold sterilisation did not have an impact on the mechanical strength.

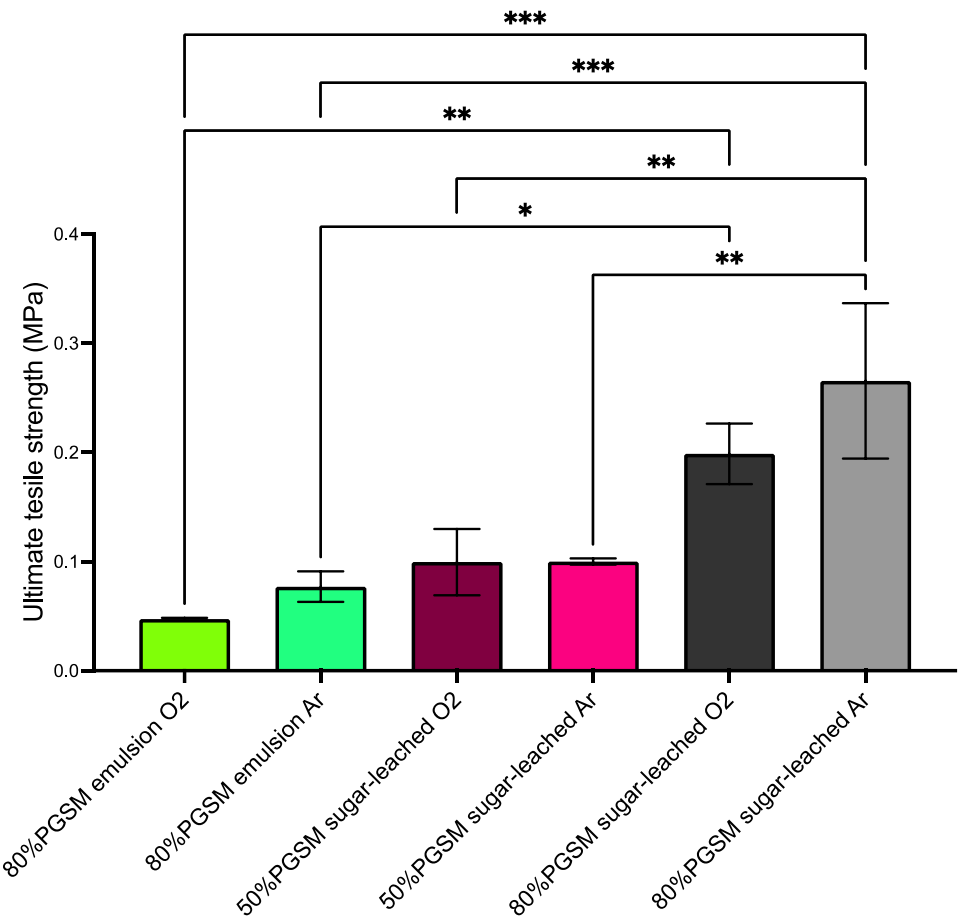

Figure 4.4 – The bar graph demonstrates the ultimate tensile strength of different PGS-M scaffolds (N=3, n=1). The asterisk (*) indicates the significant difference in P value < 0.05.

Pashneh-Tala et al. [38] proposed that crosslink density exerts an influence on mechanical characteristics of PGS-M substance. It indicated that mechanical attributes heightened alongside escalated methacrylation degree. Desirably, this stood true, as scaffolds ought to endure increased force in the presence of heightened methacrylation degree. This clarifies the superior rigidity of PGSM-80 S versus PSGM-50 S scaffolds. An additional supposition arose; sugar-leached scaffolds demanded more force for rupture due to the larger polymer volume necessary with the technique compared to the emulsion approach. This clarifies the outcome wherein PGSM-80 S scaffold surpassed PSGM-50

S. Ifkovits et al.[111] also communicated an elevation in matrix stiffness and tensile strength with ascending methacrylation degree. This pattern is evident in PGS-acrylate and PGS-cinnamate as well [37, 111-113]. Alteration in mechanical robustness might also originate from scaffold porosity. Because emulsion scaffolds possess greater porosity compared to sugar-leached scaffolds, mechanical strength diminishes (F. Claeyssens internal communication, May 2023) [38, 40]. Nonetheless, a comparison between plasma treatment and alternative treatments for PGSM material remains absent. According to this inquiry, sugar-leached scaffolds could potentially endure more force than emulsion templated counterparts. While plasma treatment exerts no impact on tensile strength, it significantly enhances cellular behaviour and rigidity [114].

4.2.2 Hydrophobicity

The subsequent aspect under consideration pertained to wettability. Chapter 4.1 has already demonstrated that plasma treatment enhanced the hydrophilic nature of scaffold surfaces [109], contrasting with autoclave sterilisation. Nonetheless, no studies have addressed the influence of altering plasma gas on PGS-M scaffolds. Consequently, scrutiny of scaffold wettability was undertaken.

Because of COVID-19 restrictions, accessing the goniometer for additional contact angle characterization was unfeasible. Instead, an alternate methodology was adopted, wherein surface hydrophobicity was evaluated through the technique expounded in Chapter 3.1.4.3. The outcomes of this analysis are depicted in Figure 4.5 and Table 4.1. When focusing solely on the sugar-leached PGS-M scaffolds, an observable trend emerges: an increase in methacrylation renders the scaffold more hydrophobic. As the

fabrication of PGSM-50 E was not feasible, it remained impossible to ascertain whether a comparable effect would manifest using the emulsion templating technique. However, in cases where PGSM-80 was employed for scaffold construction, the emulsion templating technique yielded a marked augmentation in surface hydrophilicity compared to the sugar-leached method. Notably, this outcome held true regardless of the plasma gas utilised for surface treatment, highlighting the profound impact of the emulsion approach on hydrophilicity. In terms of the influence of the gas employed in plasma treatment, a significant discrepancy in hydrophobicity was evident in PGSM-80 S scaffolds, with the use of oxygen plasma leading to heightened hydrophilicity. Nonetheless, the disinfection procedures had no discernible effect on PGSM-80 E and PGSM-50 S.

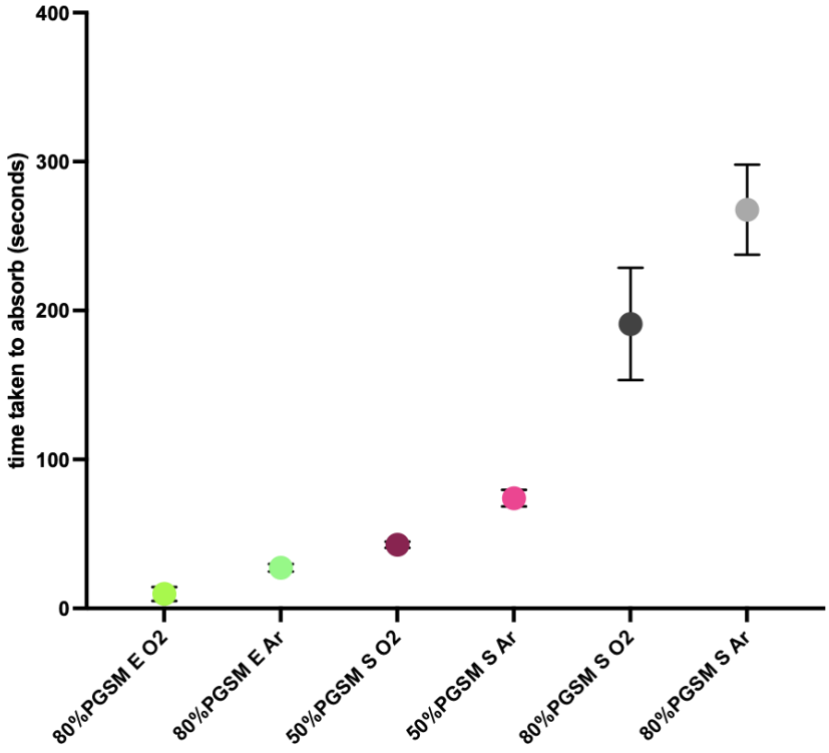

Figure 4.5 – The time requires for each scaffold type to absorb a droplet of water (N=3, n=1).

Tukey's multiple comparisons test	Mean Diff.	Below threshold?	Summary	Adjusted P Value
80%PGSM E O2 vs. 80%PGSM E Ar	-17.67	No	ns	0.8798
80%PGSM E O2 vs. 50%PGSM S O2	-33	No	ns	0.386
80%PGSM E O2 vs. 50%PGSM S Ar	-64.33	Yes	*	0.0189
80%PGSM E O2 vs. 80%PGSM S O2	-181.3	Yes	****	<0.0001
80%PGSM E O2 vs. 80%PGSM S Ar	-258	Yes	****	<0.0001
80%PGSM E Ar vs. 50%PGSM S O2	-15.33	No	ns	0.9286
80%PGSM E Ar vs. 50%PGSM S Ar	-46.67	No	ns	0.1143
80%PGSM E Ar vs. 80%PGSM S O2	-163.7	Yes	****	<0.0001
80%PGSM E Ar vs. 80%PGSM S Ar	-240.3	Yes	****	<0.0001
50%PGSM S O2 vs. 50%PGSM S Ar	-31.33	No	ns	0.4372
50%PGSM S O2 vs. 80%PGSM S O2	-148.3	Yes	****	<0.0001
50%PGSM S O2 vs. 80%PGSM S Ar	-225	Yes	****	<0.0001
50%PGSM S Ar vs. 80%PGSM S O2	-117	Yes	***	0.0001
50%PGSM S Ar vs. 80%PGSM S Ar	-193.7	Yes	****	<0.0001
80%PGSM S O2 vs. 80%PGSM S Ar	-76.67	Yes	**	0.0053

Table 4.1 – The Table demonstrates the statistical comparison between two different scaffolds. This Table related to the bar graph in Figure 4.5.

Within this thesis, two distinct physical properties underwent assessment to determine an ideal scaffold for both cell culture and mechanical stimulation. These properties encompassed the ultimate tensile strength and surface wettability.

Regarding wettability, no publication concerning sugar-leached PGS-M scaffolds has emerged thus far. Nevertheless, Farr et al. [64] have already communicated that plasma treatment augmented the hydrophilicity of emulsion scaffolds. Notably, employing Ar plasma treatment on PGS-M scaffolds rendered them more hydrophilic, yielding a positive influence on cell culture. Griffin et al. [109] also noted an elevation in surface hydrophilicity resulting from plasma treatment. The implementation of oxygen led to modifications in scaffold surface roughness, whereas argon imposed a chemical influence on the scaffold surface's oxygen and carbon composition [64, 109, 115]. These consequences may specifically manifest in sugar-leached PGS-M scaffolds characterized by heightened methacrylation levels. The hypothesis is that the significant degree of methacrylation, in conjunction with the sugar-leaching technique, profoundly impacts water Noteworthy is

the fact that sugar leaching necessitates more polymer for scaffold formation compared to the emulsion technique. Particularly, greater methacrylation degrees could lead to more hydrophobic surfaces. Crucial to underscore is that emulsion templating involves the utilisation of a surfactant to stabilize the water-in-oil emulsion. Given that surfactants are highly surface-active molecules, they predominantly reside at the oil-water interface. Subsequently, these surfactants remain on the polymer surface following curing, potentially enhancing surface hydrophilicity.

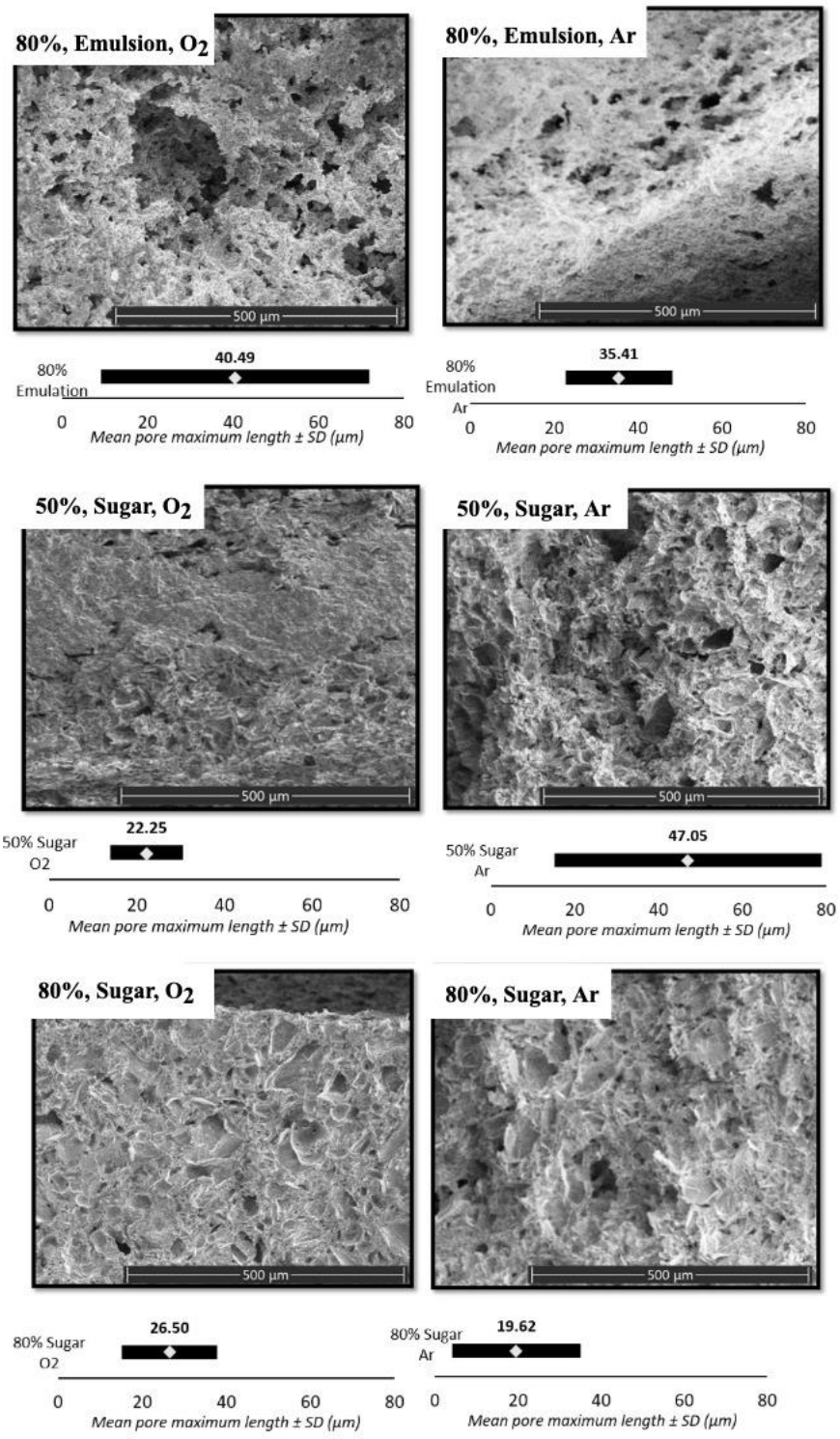

Figure 4.6 – SEM images and pore size analysis of different PGS-M scaffolds. The scale bar is 500 µm.

4.2.3 Pore size and Internal structure

For the imaging of PGS-M scaffolds, the scaffolds were immersed in liquid nitrogen and fractured in half. The images were then captured using SEM. After capturing the images, an analysis of pore size was conducted (as described in Chapter 3). These tasks were performed by Dr. Nicholas Farr during the COVID-19 pandemic.

As illustrated in Figure 4.6, the pore size ranges of PGSM-80 S were notably smaller than those of PGSM-80 E. The choice of gas for the surface plasma treatment did not influence this outcome. In the case of PGSM-50 S scaffolds subjected to O_2 plasma treatment, both a broader pore range and larger average pore size were observed compared to the Ar plasma treated PGSM-50 S scaffolds. Furthermore, a similar pattern to that observed with PGSM-80 E scaffolds emerged, where O_2 plasma treated PGSM-80 E exhibited a wider pore range and greater pore size compared to Ar plasma treated PGSM-80 E scaffolds. This trend is once again depicted in Figure 4.6.

When evaluating the construction methodologies and degrees of methacrylation inherent in the PGS-M scaffolds, the emulsion scaffolds displayed a promising tendency towards greater average pore size and a wider range of pore sizes. This observation suggests that emulsion technology holds potential as a suitable option within the scope of this thesis. Nevertheless, an observation emerges that the pore ranges obtained from diverse settings of PGS-M scaffolds were limited in size and potentially insufficient to facilitate cell ingrowth. The optimal pore sizes for fibroblast culture typically fall within the range of 38-150 μm. This circumstance could potentially be attributed to the freeze-drying process employed prior to immersing the scaffolds in liquid nitrogen. This sequence of actions might result in the internal structures of the scaffolds collapsing. Additionally, due to the

constraints imposed by the COVID-19 outbreak, the samples were prepared days before SEM imaging. This temporal gap might conceivably contribute to the collapse of the interior scaffold structures.

4.2.4 Cell metabolic activity

Given that the primary objective of this thesis is to refine the fabrication process of biohybrid scaffolds by enhancing collagen production from human dermal fibroblasts (HDFs), the aspect of cell culture assumes paramount importance. For this purpose, cells were seeded onto tissue culture plastic (TCP) as well as PGS-M scaffolds, specifically 1x105 HDFs. It's important to note that HDFs seeded on TCP were treated as a baseline control for the experiment. Subsequently, both the cells adhered to TCP and those on scaffolds were afforded a day for initial adherence before quantifying cell attachment. Following this, the cells were cultured in Complete DMEM for a total duration of 3 weeks, with resazurin testing conducted at intervals of 1 week, 2 weeks, and 3 weeks, successively.

By cultivating cells within 3D models, the expectation is that cells will not only establish themselves on the surface but also permeate the scaffold structure. As a result, the metabolic activity of cells over a span of two weeks was also assessed. In this scenario, resazurin remained a viable option since it facilitated the continuation of the experiment post quantification. The benefit of using this assay lies in its non-toxic nature, which allows the experiment to proceed without requiring termination after quantification [116]. While this test does not directly pertain to cell count or proliferation, it can serve as supplementary data once the actual cell count is determined [117].

Figure 4.7 illustrates the metabolic activity following a three-week period of cell culture. The bar graph conveys that there existed no noteworthy distinction between the 2D control and the PGS-M scaffolds. Moreover, there were no statistically significant differences across the various scaffolding conditions. This observation underscores the ability of cells to adhere to the PGS-M scaffolds, a trait mirrored in the performance of the 2D control template.

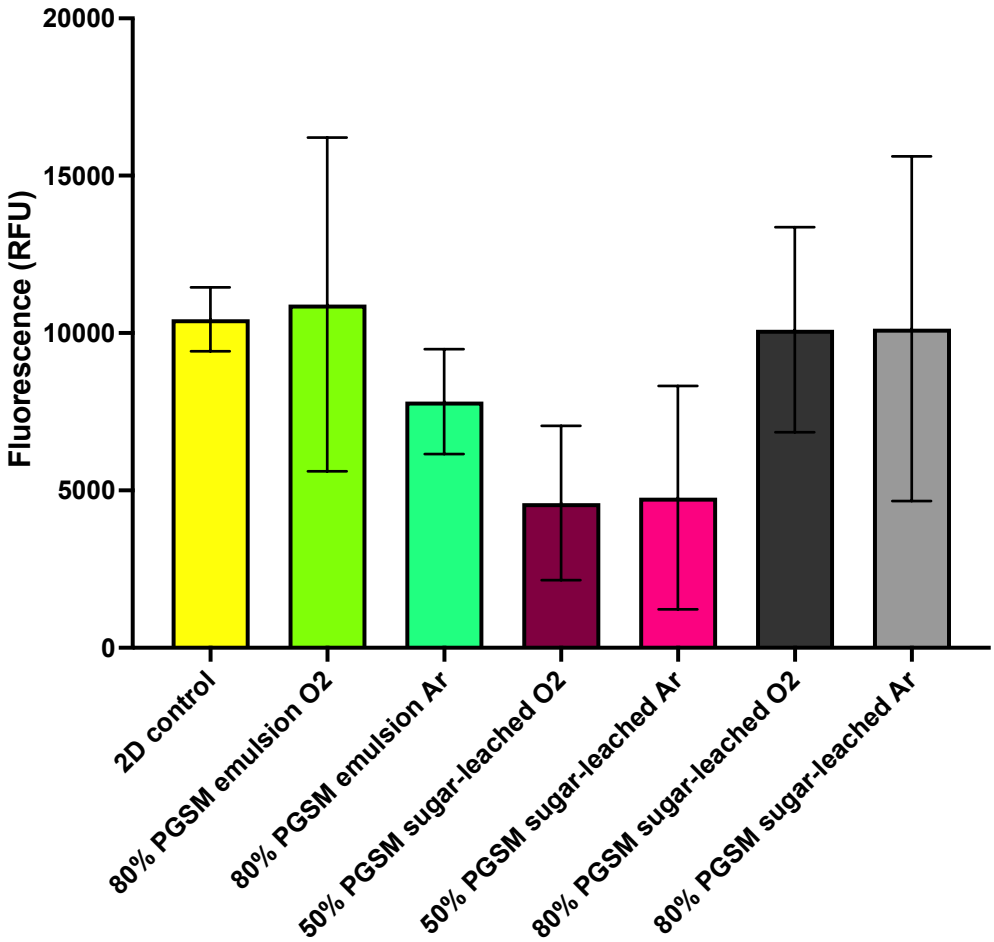

Figure 4.7 – A bar graph demonstrates the metabolic activity of HDFs seeded on different condition of PGS-M scaffolds after one day of cell culture. The outcomes are evaluated using one-way ANOVA (N=2, n=3).

After one week of cell culture, HDFs displayed varying responses dependent on the specific scaffold conditions. As a result, the results were categorized and grouped according to the employed fabrication technique, the gas type employed for plasma treatment, and the percentage of PGS-M polymers incorporated.

To acquire a more comprehensive understanding of the sugar leaching process, an examination was carried out on PGSM-50 S and PGSM-80 S scaffolds treated with both Ar and O_2 (depicted in Figure 4.8 a)). Remarkably, only the cell metabolic activity obtained from PGSM-80 S scaffolds treated with O_2 plasma exceeded the results of PGSM-50 S scaffolds treated with Ar plasma. No statistically significant differences were evident among the remaining conditions. It is noteworthy that the outcomes obtained from the scaffolds were generally lower compared to the TCP control, except for PGSM-80 S treated with oxygen.

The subsequent variable under investigation was the Ar plasma treatment. Considering its previous application for comparison with autoclaving, a practice that yielded significant improvements in PGS-M scaffolds, this treatment was also subject to examination in this test to facilitate a deeper comprehension.

As depicted in Figure 4.8 b), it became apparent that the metabolic activity of cells seeded on both PGSM-50 S and PGSM-80 S scaffolds was comparatively lower than that of cells on PGSM-80 E scaffolds. The metabolic activity of HDFs seeded on PGSM-80 E scaffolds was approximately four times higher than that observed on PGSM-50 S scaffolds. Similarly, the results derived from PGSM-80 E were twice as substantial as those from PGSM-80 S. However, no statistically significant distinction existed between the 2D TCP

control and emulsion scaffolds. This observation underscores that, akin to tissue culture plastic, emulsion scaffolds effectively maintained cell viability.

Figure 4.8 c) presents the data on cell metabolic rates collected from the 2D control and various manufacturing approaches of PGS-M scaffolds treated with O_2 plasma. As depicted in the graph, after one week of cell culture, PGSM-80 E scaffolds displayed the capability to support cell adhesion and proliferation. The measured metabolic activity on PGSM-80 E scaffolds was approximately 2.5 times higher than that observed for PGSM-50 S. In contrast, under O_2 plasma treatment, no significant differentiation was evident among PGSM-80 E, PGSM-80 S, and the 2D TCP control.

The subsequent aspect under investigation for a one-week cell culture pertains to the fabrication procedures for PGSM-80 scaffolds. As portrayed in Figure 4.8 d), the PGSM-80 S scaffolds treated with Ar plasma produced less favourable outcomes when contrasted with the other scaffolds, including the 2D control. This observation highlighted that Ar plasma-treated PGSM-80 S scaffolds did not sustain cell viability. However, the rest of the PGSM-80 scaffolds, regardless of plasma treatment and fabrication methods, maintained cell viability as anticipated in tissue culture plastic.

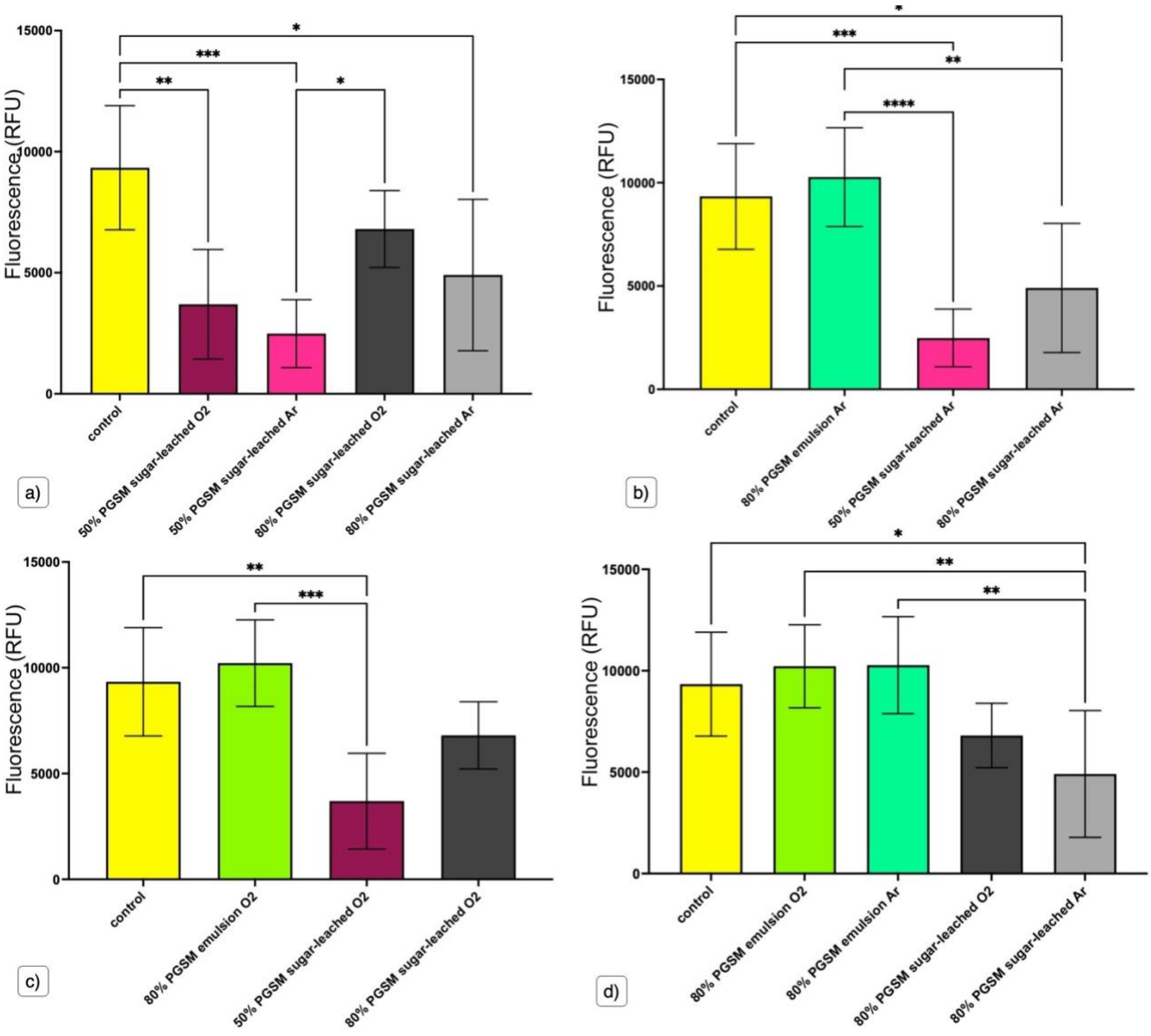

Figure 4.8 –The metabolic activity of cells after one week of cell culture on the (a) sugar-leached, (b) Ar plasma treated, (c) O_2 plasma treated, and (d) higher methacrylation degree of PGS-M scaffolds. The outcomes are evaluated using one-way ANOVA (N=2, n=3). According to the line, the asterisk indicated the statistical difference between two conditions ($P < 0.05$).

Upon meticulous examination of all the data gathered over a one-week duration, it becomes apparent that the type of gas employed in plasma treatment exerted minimal influence on cell culture. This deduction is drawn from the comparable metabolic activity observed in cells cultured on TCP. However, noteworthy is the substantial discrepancy in

metabolic activity exhibited by cells cultured in sugar-leached PGS-M scaffolds with a lower degree of methacrylation, in contrast to other scaffold types. This stark difference implies that this particular subset of scaffolds did not sustain cell viability as originally anticipated. This circumstance could potentially emanate from the pore size and interconnectivity within the scaffolds. As previously posited, the fabrication technique's impact on pore size is plausible. Nonetheless, drawing any decisive inferences necessitates an extended cultivation period to adequately gauge potential effects.

Following two weeks of cell culture, all outcomes were categorized in a manner consistent with the reporting after the first week. Figure 4.9 a) illustrates a comparison between the PGSM-50 and PGSM-80 scaffolds. As depicted in the graph, the pattern remained consistent with the one-week results, wherein the metabolic activity observed on Ar plasma-treated PGSM-50 scaffolds was markedly lower than that of PGSM-80 scaffolds. Furthermore, the metabolic activity exhibited by PGSM-80 scaffolds was substantially higher than that of PGSM-50 scaffolds when the same gas was employed for plasma treatment.

Notably, after 2 weeks in culture, the sole scaffold that continued to exhibit significantly lower metabolic activity than the 2D control was the PGSM-50 S scaffold treated with Ar plasma. While the average metabolic activity observed for cells on O_2 plasma-treated PGSM-50 S scaffolds remained lower than the 2D control in the second week, the substantial variability in responses among samples rendered this difference no longer statistically significant. Meanwhile, for O_2 and Ar-treated PGSM-80 S scaffolds, although they displayed lower metabolic activity than the 2D control in the first week, cell proliferation increased over the second week, bringing the results more in line with the

2D control. This suggests that low cell attachment on PGSM-80 S was potentially attributed to its hydrophobic nature. However, once cells established attachment, they could proliferate freely within this scaffold.

Figure 4.9 b) illustrates a comparison among different scaffolds treated with Ar plasma. The findings sustained the same trend as the one-week results, wherein the metabolic activity registered from PGSM-50 S scaffolds treated with Ar plasma remained significantly lower than that observed in other situations. However, the data extracted from Ar plasma-treated PGSM-80 S scaffolds exhibited a noticeable increase and were no longer statistically distinguishable from 2D control scaffolds or PGSM-80 E scaffolds.

Figure 4.9 c) provides a comparison of two-week cell culture outcomes across varying degrees of methacrylation and manufacturing processes of O_2 plasma-treated PGS-M scaffolds. As depicted in the graph, the metabolic activity on PGSM-50 S scaffolds was significantly lower than that on either PGSM-80 S or PGSM-80 E scaffolds. Importantly, by the second week, the results obtained from PGSM-80 E scaffolds treated with O_2 plasma had become statistically higher than the 2D control. Nonetheless, there was no significant difference in metabolic activity between PGSM-80 E and PGSM-80 S scaffolds. When compared to the one-week results, this graph substantiates that emulsion scaffolds upheld cell viability and harboured the potential to facilitate cell growth within the scaffolds. This is underscored by the marked increase in metabolic activity measured within this type of scaffold, surpassing levels observed in the 2D control. This finding suggests that PGSM-80 E scaffolds treated with Ar plasma supported cell metabolism upon cell attachment and might also facilitate cell ingrowth.

Figure 4.9 d) presents a comparison of the PGSM-80 scaffolds under different conditions. As indicated by the graph, most scaffolds did not exhibit significant differences from one another in terms of metabolic activity. Only the results from the oxygen plasma-treated PGSM-80 E scaffold showed a significantly higher metabolic activity than the 2D control. Furthermore, it was notably higher than that observed in the Ar plasma-treated PGMS-80 S scaffold. This contrast, particularly in relation to the one-week results where data from emulsion scaffolds did not differ statistically from the 2D control, highlights the evolving impact of cell culture duration on scaffold performance.

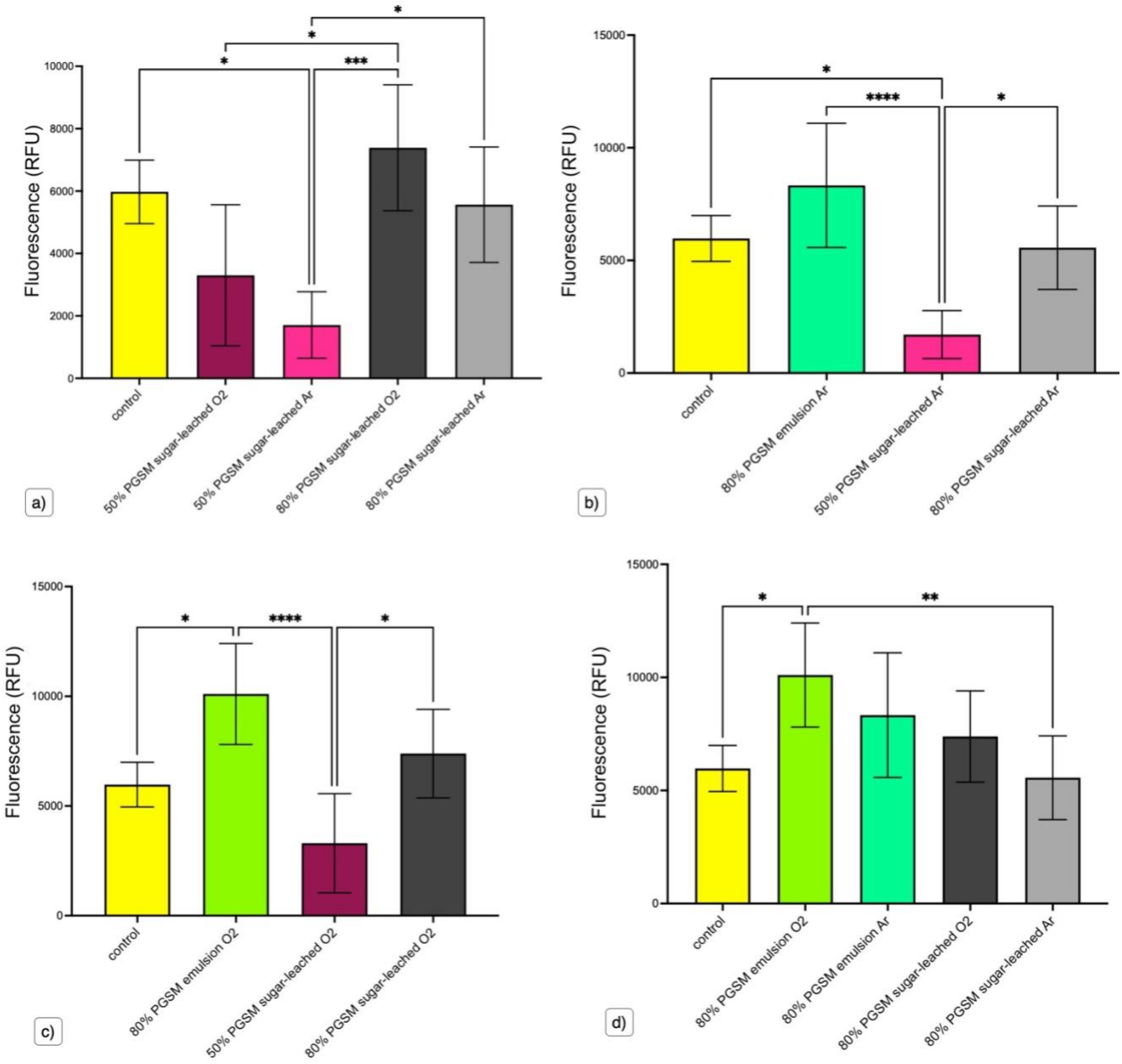

Figure 4.9 – The metabolic activity of cells after two-weeks of cell on the (a) sugar-leached, (b) Ar plasma treated, (c) O_2 plasma treated, and (d) higher methacrylation degree of PGS-M scaffolds. The outcomes are evaluated using one-way ANOVA (N=2, n=3). According to the line, the asterisk indicated the statistical difference between two conditions ($P < 0.05$).

Following the measurement of metabolic activity in HDFs cultivated under various conditions of PGS-M scaffolds, cell culture was extended for an additional week to analyse the metabolic trend. Figure 4.10 a) presents the results obtained from both

PGSM-50 S and PGSM-80 S scaffolds. As depicted in the graph, the metabolic rate of the 2D control was significantly higher than that of most sugar-leached PGS-M scaffolds. Only the PGSM-80 S O_2 plasma-treated scaffolds supported a metabolic activity similar to the 2D control. This observation suggests that sugar-leaching may not be an ideal scaffold for sustained cell growth, as the metabolic activity recorded from the scaffolds, regardless of the gas employed in plasma treatment, remained lower than that of the 2D control. This also indicates that the cells might become less metabolically active after extended cell culture. With the exception of O_2 plasma-treated PGSM-80 S scaffolds, where there was no significant difference, the scaffolds may not provide the level of support initially anticipated. This discrepancy could be attributed to the scaffold's properties or the experimental conditions, particularly the repeated use of a high concentration of resazurin, which is generally considered non-toxic to cells but was frequently applied throughout the experiment.

Figure 4.10 b) illustrates the metabolic activity data obtained from Ar plasma-treated PGS-M scaffolds. The graph indicates that only the metabolic activity observed on Ar plasma-treated PGSM-80 E scaffolds was on par with that of the 2D control. In contrast, the outcomes from both sugar-leached scaffolds were significantly lower than those of the 2D control. This suggests that among all the PGS-M scaffolds treated with Ar plasma, the emulsion approach exhibited the greatest capacity to support cell culture over an extended period. This enhanced performance could be attributed to the emulsion scaffolds' hydrophilicity and pore size.

Figure 4.10 c) presents a comparison of the metabolic activity obtained from various PGS-M scaffold types in response to O_2 plasma treatment. Similar to the week 2 results, the

mean metabolic activity for PGSM-80 E is higher than that of the 2D control. However, the substantial variation in activity observed for the control has led to this difference no longer being statistically significant. While most conditions did not exhibit significant differences from one another, the metabolic activity of the PGSM-50 S scaffolds was lower than that of both the 2D control and the PGSM-80 E scaffolds. These findings reinforce the notion that the lower methacrylation degree of sugar-leached scaffolds may not be conducive to cell growth.

Figure 4.10 d) portrays the metabolic activity on PGSM-80 scaffolds depending on the fabrication process and plasma treatment. According to the graph, the results obtained from Ar plasma-treated 80% PGS-M scaffolds were significantly lower than those obtained from 2D control scaffolds and emulsion scaffolds treated with O_2 plasma. Conversely, the remaining scaffolds exhibited a significant variation between one another. Although no significant difference was observed between Ar and O_2 plasma treatment when comparing PGSM-80 E and S, this could be attributed to the high error bars in the results. This substantial variation might arise from differences in conditions between the two repetitions of the experiment. Furthermore, as primary cells were employed in the experiments, there might be inherent variability associated with their use. Consequently, this observation might suggest that Ar plasma treatment enhanced the cell metabolic rate after three weeks of cell culture.

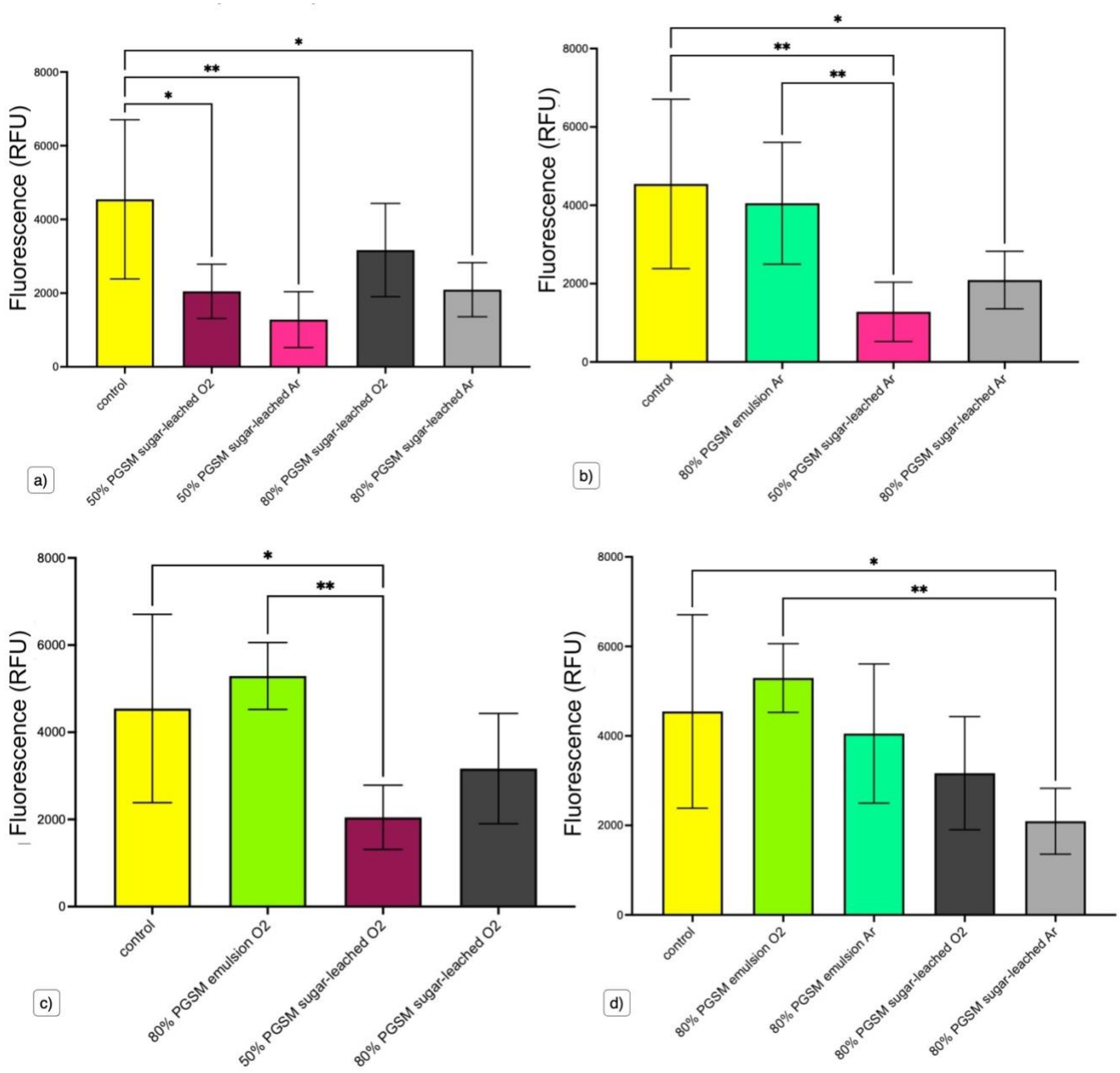

Figure 4.10 –The metabolic activity of cells after three-weeks of cell culture the (a) sugar-leached, (b) Ar plasma treated, (c) O_2 plasma treated, and (d) higher methacrylation degree of PGS-M scaffolds. The outcomes are evaluated using one-way ANOVA (N=2, n=3). According to the line, the asterisk indicated the statistical difference between two conditions ($P < 0.05$).

When comparing metabolic activity results over time, it becomes evident that PGSM S scaffolds, irrespective of the gas employed in plasma treatment, did not prove suitable for in vitro cell culture. The emulsion templating technique emerged as the preferred method

for scaffold manufacturing, as the cell metabolic activity data obtained from these scaffolds demonstrated an encouragingly high level. Concerning plasma surface treatment, earlier findings (as detailed in Chapter 4.2.2) have underscored the necessity of surface treatment for successful cell adhesion. The prevailing trend suggested that O_2 plasma sterilisation tended to elicit greater cell activity compared to the Ar plasma method for equivalent scaffolds. However, it's important to note that in each case, these differences failed to reach statistical significance.

Additionally, it is worth noting that the fluorescence measurements obtained for all conditions after three weeks of cell culture were lower than those obtained after two weeks of cell culture. This observation extended to the metabolic activity recorded for the 2D control as well. One possible explanation for this could be the variations in the concentrations of resazurin used in each measurement. It's important to acknowledge that while this methodology was employed to accurately assess the metabolism of HDFs in a 3D environment, it may not be ideally suited for use over an extended period. This declining trend over the course of the cell culture duration was consistent across both repeated experiments.

An additional hypothesis concerns scaffold degradation potentially impacting cell proliferation. However, this scenario appears unlikely, as data obtained from the 2D control also displayed a decrease following a similar pattern as observed in 3D cell culture. Furthermore, the age of primary cells can also influence the capacity for proliferation. Primary cells were chosen for this thesis due to their ability to generate extracellular matrix (ECM). It's important to note that these primary cells, while valuable, are not immortal and eventually reach their proliferation limit. Given the prolonged duration of the experiment

and the utilisation of cells with a high passage number, it's plausible that the rate of cell proliferation decreased due to their age [120, 121]. In light of these considerations, it might be more suitable to employ the optimised resazurin concentration as the endpoint assay and work with cells at an earlier passage number in future experiments.

4.2.5 DNA quantification

The Picogreen test assessed the DNA content of cells cultured on all scaffold types. Figure 4.11 presents the results of two repeated trials, with two samples in each experiment (N=2, n=1). Simultaneously, Table 4.2 illustrates the statistical comparison between two distinct scaffolds from Figure 4.20.

Only the outcome from Ar-treated PGSM-50 S scaffolds was considerably lower than the control after three weeks of cell culture. The others did not differ significantly. In terms of fabrication methods, emulsion scaffolds produced the best results, followed by PGSM-80 S and PGSM-50 S scaffolds. Regarding plasma treatment, there was no statistical difference among the scaffolds of the same kind. According to the graph, PGSM-80 scaffolds appeared to be the best platform for the proliferation of HDFs, regardless of the manufacturing and sterilising technique. In contrast, the DNA levels from PGSM-50 S scaffolds were considerably lower than that of PGSM-80 E scaffolds. This finding agreed with the resazurin result. Hence, the hypotheses were that the gas used in plasma treatment is insignificant when considering cell proliferation. However, the technique used in fabrication and the degree of methacrylation of PGS-M played such an important role for cell proliferation.

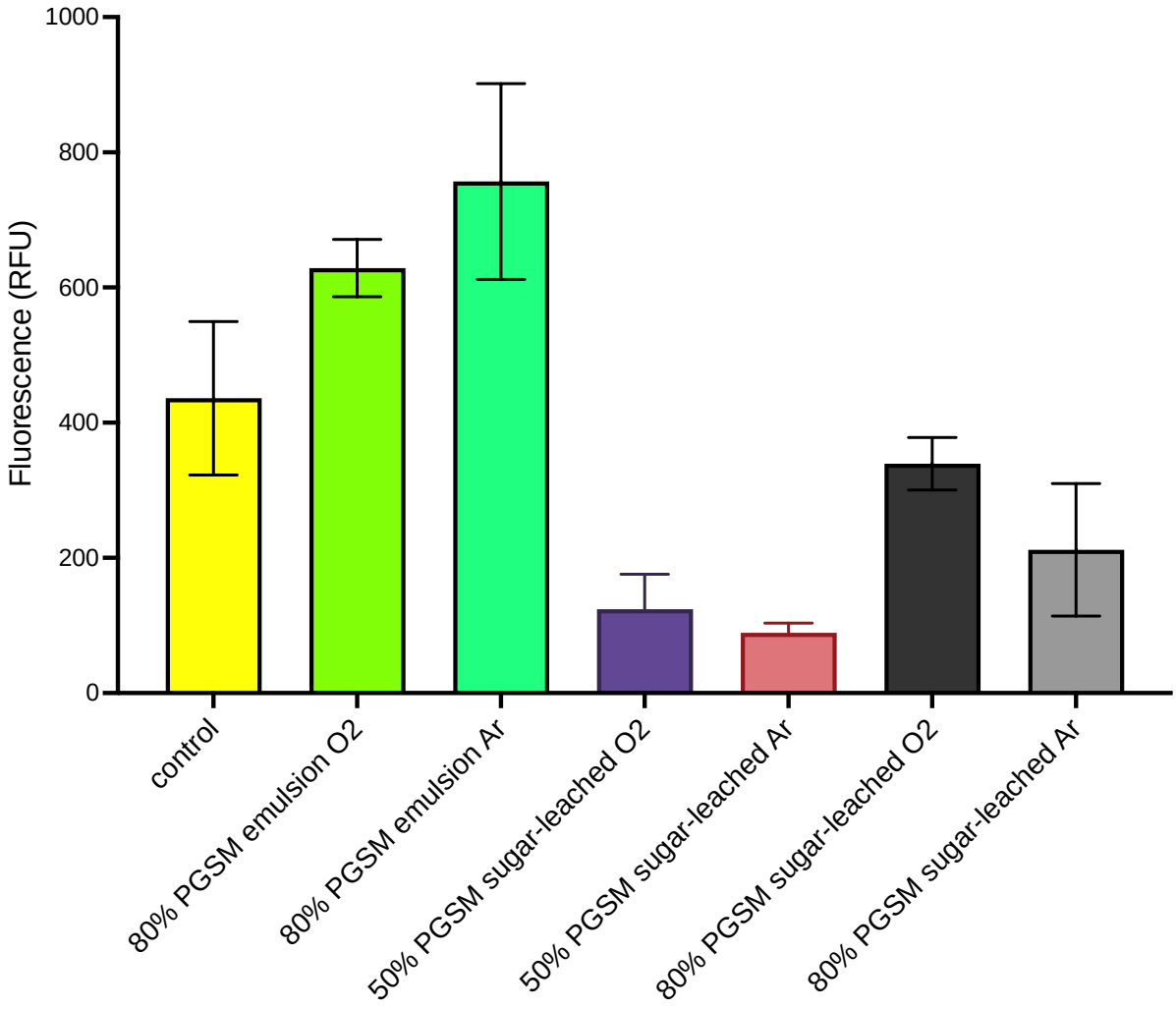

Figure 4.11 –The DNA concentration after three-weeks of cell culture on different conditions of PGS-M scaffolds. The outcomes are evaluated using one-way ANOVA (N=2, n=3).

Tukey's multiple comparisons test	Mean Diff.	Below threshold?	Summary	Adjusted P Value
80% PGSM emulsion O2 vs. 80% PGSM emulsion Ar	-128.3	No	ns	0.7272
80% PGSM emulsion O2 vs. 50% PGSM sugar-leached O2	504.7	Yes	**	0.0057
80% PGSM emulsion O2 vs. 50% PGSM sugar-leached Ar	539.3	Yes	**	0.0039
80% PGSM emulsion O2 vs. 80% PGSM sugar-leached O2	289.3	No	ns	0.0936
80% PGSM emulsion O2 vs. 80% PGSM sugar-leached Ar	416.7	Yes	*	0.0166
80% PGSM emulsion O2 vs. control	192.3	No	ns	0.3614
80% PGSM emulsion Ar vs. 50% PGSM sugar-leached O2	633	Yes	**	0.0015
80% PGSM emulsion Ar vs. 50% PGSM sugar-leached Ar	667.7	Yes	**	0.0011
80% PGSM emulsion Ar vs. 80% PGSM sugar-leached O2	417.7	Yes	*	0.0164
80% PGSM emulsion Ar vs. 80% PGSM sugar-leached Ar	545	Yes	**	0.0037
80% PGSM emulsion Ar vs. control	320.7	No	ns	0.0601
50% PGSM sugar-leached O2 vs. 50% PGSM sugar-leached Ar	34.67	No	ns	0.9993
50% PGSM sugar-leached O2 vs. 80% PGSM sugar-leached O2	-215.3	No	ns	0.2662
50% PGSM sugar-leached O2 vs. 80% PGSM sugar-leached Ar	-88	No	ns	0.9265
50% PGSM sugar-leached O2 vs. control	-312.3	No	ns	0.0675
50% PGSM sugar-leached Ar vs. 80% PGSM sugar-leached O2	-250	No	ns	0.1639
50% PGSM sugar-leached Ar vs. 80% PGSM sugar-leached Ar	-122.7	No	ns	0.7608
50% PGSM sugar-leached Ar vs. control	-347	Yes	*	0.0417
80% PGSM sugar-leached O2 vs. 80% PGSM sugar-leached Ar	127.3	No	ns	0.7332
80% PGSM sugar-leached O2 vs. control	-97	No	ns	0.8922
80% PGSM sugar-leached Ar vs. control	-224.3	No	ns	0.2352

Table 4.2 – The table demonstrates the statistical comparison between two different scaffolds. This table relates to the bar graph shown in Figure 4.20

4.2.6 Collagen production

After three weeks of cell culture, collagen formation data were analysed using the picrosirius red test in two repeated trials (N=2, n=2). Figure 4.12 presents a bar graph of collagen production obtained from various conditions of PGS-M scaffolds, while Table 4.3 provides a statistical comparison of collagen production. According to the graph, the outcomes were categorized into two sterilisation techniques: O_2 and Ar plasma treatment. Among the scaffolds treated with O_2 plasma, the PGSM-50 S scaffolds produced the least collagen, while there was no significant difference between the PGSM-80 E and PGSM-80 S scaffolds. However, for Ar plasma sterilisation, there was no substantial difference between the three types of PGSM scaffolds. Only O_2-treated PGSM-80 E and O_2-treated PGSM-80 S scaffolds demonstrated a greater collagen content than the 2D control.

However, there was no significant difference among scaffolds of the same kind that utilised varying gases in plasma treatment.

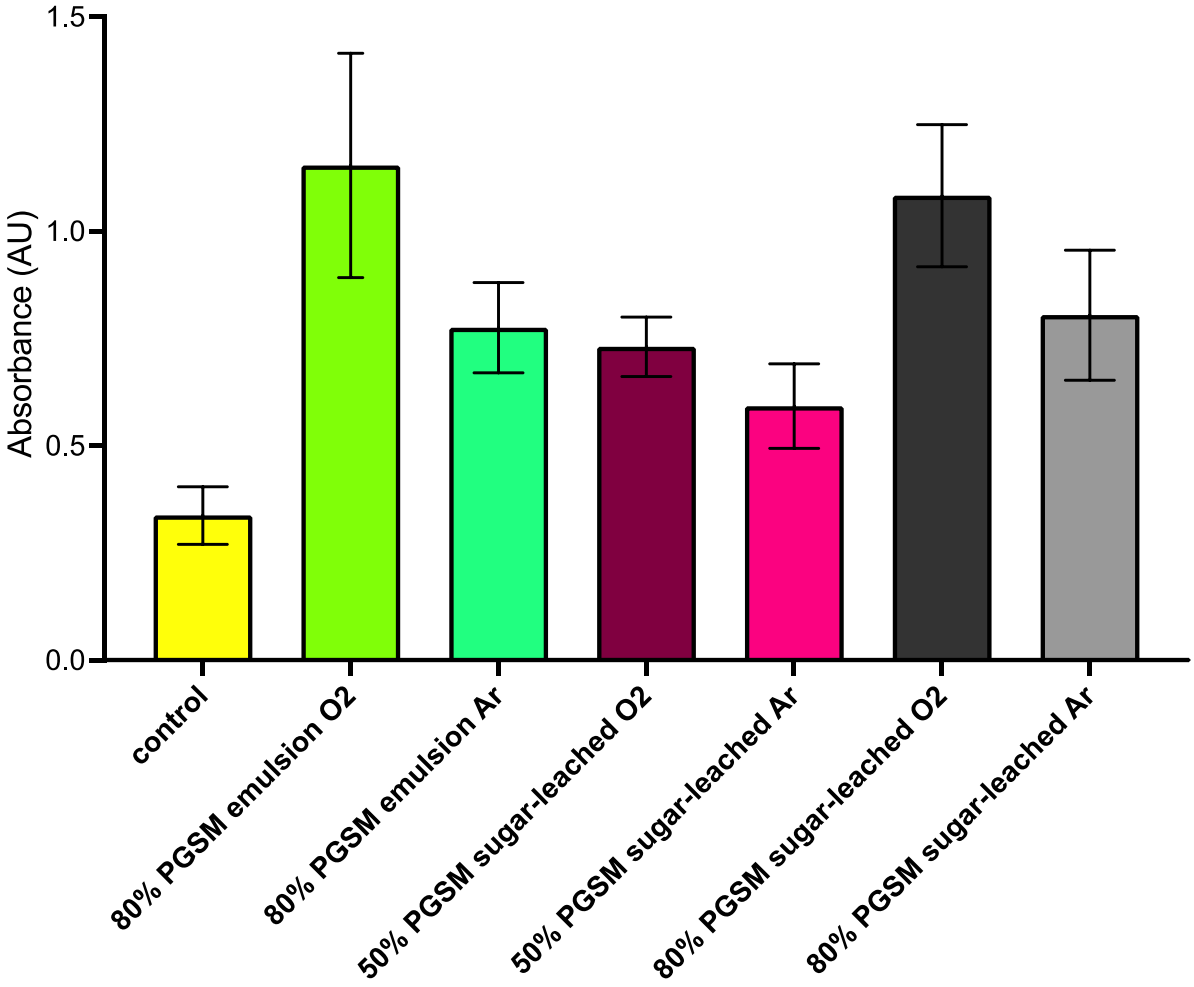

Figure 4.12 – A bar graph depicts the collagen production after three-weeks of cell culture on different conditions of PGS-M scaffolds. The outcomes are evaluated using one-way ANOVA (N=2, n=3).

Tukey's multiple comparisons test	Mean Diff.	Below threshold?	Summary	Adjusted P Value
80% PGSM emulsion O2 vs. 80% PGSM emulsion Ar	0.3782	Yes	*	0.025
80% PGSM emulsion O2 vs. 50% PGSM sugar-leached O2	0.4225	Yes	*	0.01
80% PGSM emulsion O2 vs. 50% PGSM sugar-leached Ar	0.561	Yes	***	0.0005
80% PGSM emulsion O2 vs. 80% PGSM sugar-leached O2	0.07067	No	ns	0.9928
80% PGSM emulsion O2 vs. 80% PGSM sugar-leached Ar	0.349	Yes	*	0.0448
80% PGSM emulsion O2 vs. control	0.816	Yes	****	<0.0001
80% PGSM emulsion Ar vs. 50% PGSM sugar-leached O2	0.04433	No	ns	0.9995
80% PGSM emulsion Ar vs. 50% PGSM sugar-leached Ar	0.1828	No	ns	0.5996
80% PGSM emulsion Ar vs. 80% PGSM sugar-leached O2	-0.3075	No	ns	0.0982
80% PGSM emulsion Ar vs. 80% PGSM sugar-leached Ar	-0.02917	No	ns	>0.9999
80% PGSM emulsion Ar vs. control	0.4378	Yes	*	0.0143
50% PGSM sugar-leached O2 vs. 50% PGSM sugar-leached Ar	0.1385	No	ns	0.8359
50% PGSM sugar-leached O2 vs. 80% PGSM sugar-leached O2	-0.3518	Yes	*	0.0424
50% PGSM sugar-leached O2 vs. 80% PGSM sugar-leached Ar	-0.0735	No	ns	0.9911
50% PGSM sugar-leached O2 vs. control	0.3935	Yes	*	0.0331
50% PGSM sugar-leached Ar vs. 80% PGSM sugar-leached O2	-0.4903	Yes	**	0.0024
50% PGSM sugar-leached Ar vs. 80% PGSM sugar-leached Ar	-0.212	No	ns	0.4349
50% PGSM sugar-leached Ar vs. control	0.255	No	ns	0.316
80% PGSM sugar-leached O2 vs. 80% PGSM sugar-leached Ar	0.2783	No	ns	0.1637
80% PGSM sugar-leached O2 vs. control	0.7453	Yes	****	<0.0001
80% PGSM sugar-leached Ar vs. control	0.467	Yes	**	0.0082

Table 4.3 – The table demonstrates the statistical comparison of collagen production between two different scaffolds. This table relates to the bar graph shown in Figure 4.21.

4.2.7 Cell Ingrowth

Light sheet imaging was employed to observe cell ingrowth behaviour after three weeks of cell culture. This technique enables the observation of a sample's 3D structure in 360 degrees without the need for manual rotation. Additionally, it allows for working with the sample without generating heat, which is beneficial for PGS-M scaffolds, known for their sensitivity to high temperatures [118]. With the assistance of a Light Sheet fluorescent microscope, the pattern of cell proliferation within 80% PGSM scaffolds seeded using the emulsion approach was examined. Figure 4.13 displays light sheet microscopy images of cell proliferation and penetration on the surface and within samples. In Figure 4.13 a) and b), it is evident that cell ingrowth was promoted inside emulsion scaffolds. Moreover, HDFs successfully attached to the surface of the PGS-M scaffolds, as shown in Figure

4.13 c) and d). This indicates that, regardless of plasma treatment, 80% PGS-M scaffolds fabricated using the emulsion technique supported cell ingrowth.

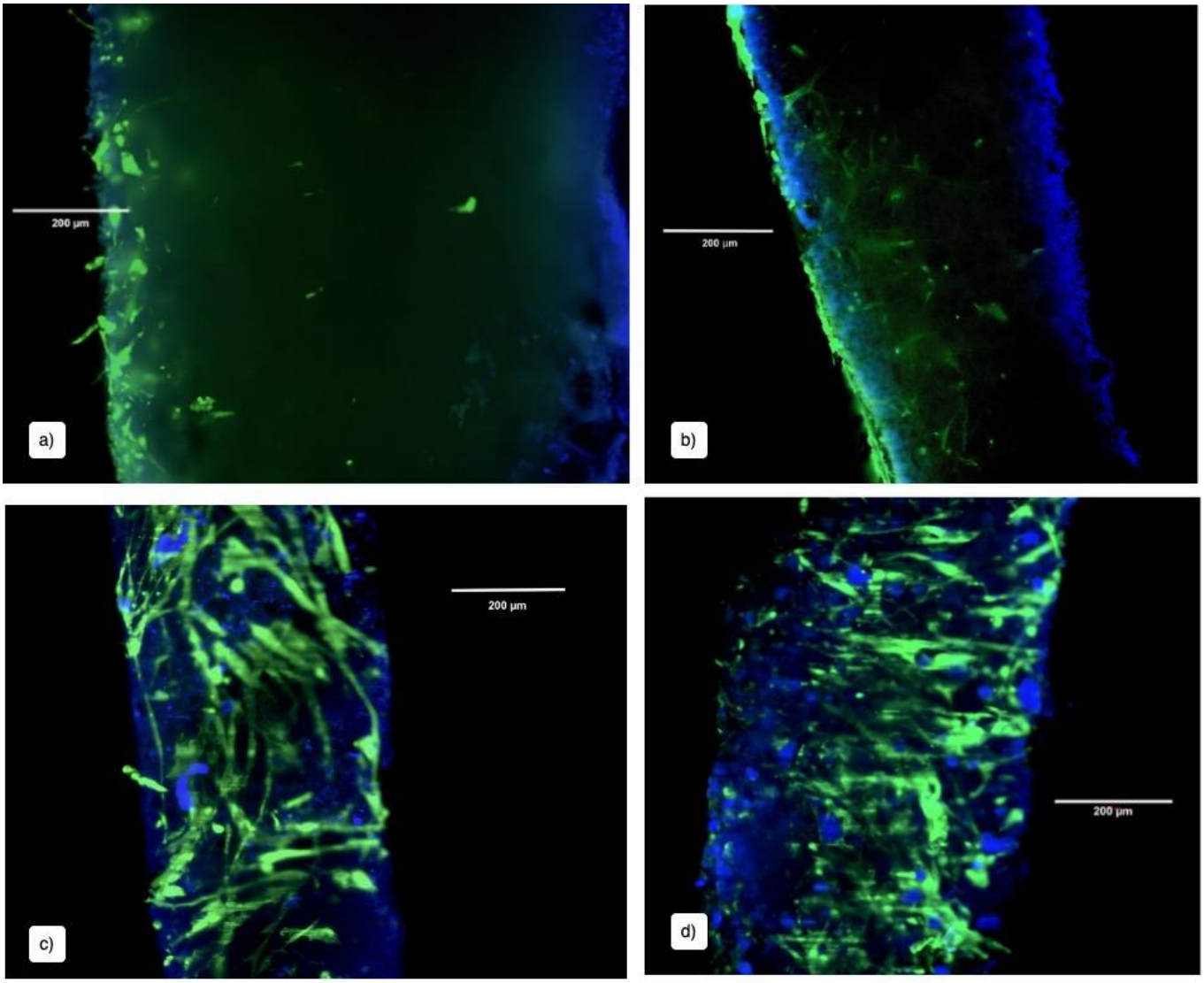

Figure 4.13 – Lighsheets images depicts the surface and side views of DAPI- and Phalloidin-stained emulsion PGSM scaffolds. The scale bar in every image is 200 µm.. The lightsheet photos of the side view of (a) O_2 plasma treated 80% PGS-M scaffolds and (b) Ar plasma treated 80% PGS-M scaffolds manufactured using the emulsion process. The bottom row displayed the top view of emulsion 80% PGS-M scaffolds treated with (c) O_2 and (d) Ar plasma treatment (N=2, n=3).

The emulsion templating approach emerged as the most favourable technique for in vitro cell culture, yielding the highest cell metabolic activity, DNA concentration, and collagen production.

PGSM scaffolds have been shown to support cell growth [39]. Different fabrication techniques, including sugar-leaching [40] and emulsion templating , have been employed to create materials with specific properties for various applications. Surprisingly, there is no published comparison between these two approaches concerning cell behaviours and mechanical properties. Furthermore, although plasma treatment has been previously acknowledged as a superior sterilisation method for PGSM scaffolds compared to autoclaving [64], no research has compared different plasma treatments. Consequently, this study elucidates the effects of various construction and sterilisation processes of PGSM scaffolds for in vitro cell culture.

Pashneh-Tala et al. reported the results of seeding fibroblasts on porous PGSM scaffolds, employing both emulsion and sugar-leaching techniques to assess material biocompatibility. It was demonstrated that PGSM scaffolds constructed using the emulsion method supported better cell growth compared to those fabricated through sugar leaching [38]. The study utilised smooth muscle cells (SMCs), human adipose-derived stem cells, and HDFs.

Picogreen was employed in the study by Pashneh-Tala [38] on the emulsion technique of porous PGSM scaffolds to quantify the DNA content of three cell types, as previously disclosed. Both SMCs and HDF cells were confirmed to be viable on PGSM after seven days of culture [29, 111, 112, 119]. In the case of the sugar-leaching approach, Pashneh-Tala et al. [40] demonstrated that sugar-leaching PGSM can enhance cell proliferation by

comparing day 1 and day 7 results, although no comparison was made with a 2D environment. Our study evaluated the outcomes between 2D and 3D environments, revealing that both approaches of 80% PGSM not only supported cell viability but also promoted cell proliferation and growth. The images obtained from the light sheet microscope supported these results, depicting HDFs adhering, proliferating, and migrating within emulsion scaffolds [38, 120-122].

Surface modification techniques, such as plasma treatment and growth factor coating, have been proposed to enhance cell activity Farr et al. [64], applied this enhancement but only for scaffolds manufactured using the emulsion approach. They improved scaffold surface chemistry by sterilising them with Ar plasma treatment and compared the outcomes to autoclaved scaffolds, the conventional sterilisation method. According to Farr et al., altering surface chemistry influenced cell proliferation by promoting cell adhesion. However, no report has compared the two procedures when implementing the same sterilisation method. Plasma treatment was chosen for this study because it is a well-established sterilisation method [101] that has also been shown to enhance cell growth, adhesion, and metabolism [60, 123, 124]. Both Ar and O_2 plasma treatments were applied to assess their effects. While the fabrication method had no impact on cell attachment, the results indicated that PGS-M scaffolds manufactured using the emulsion method promoted cell growth over time. During three weeks of cell culture, various plasma treatments had no discernible effect on cell attachment or metabolic activity. The choice of O_2 plasma treatment was based on its ease of application and cost-effectiveness compared to Argon, as the gases used in plasma treatment did not significantly differ in terms of cell activities, wettability, and ultimate tensile strength.

4.3 Assay optimisation

4.3.1 Resazurin assay optimisation

Each parameter requires different assays to observe cell activity and collagen formation. Typically, the MTT assay is used to detect cell metabolic rate, cytotoxicity, and cell proliferation, all of which were intended to be measured in this experiment. However, the MTT assay poses challenges when eluting the color from a 3D scaffold compared to a 2D surface due to the formation of formazan crystals by the cells during staining [125]. Previous attempts to measure cell metabolic rate using the MTT assay resulted in inaccurate results [82]. Therefore, the resazurin test was chosen to measure metabolic rate in this study. The resazurin test, also known as alamar blue, is an assay that measures the metabolic rate of active cells in a specific environment. This assay relies on the enzymatic reduction of a substrate to produce a fluorescent product. It is commonly used in scientific research to determine cell proliferation and viability because it is easy to conduct and observe using a conventional or fluorescence plate reader. Additionally, this method is cost-effective and non-toxic to cells, allowing the experiment to continue after the assay has been performed [117].

To optimise the appropriate concentration and incubation periods of resazurin for cultured HDFs on PGS-M scaffolds, the number of cells after approximately 18 hours of cell culture was examined. The aim was to ensure that the number of cells before and after quantification was as close as possible since the cells were allowed to attach to the surface but not proliferate during this period. To achieve this, a range of cell quantities was seeded on both 2D and 3D surfaces. First, a standard 2D calibration curve was generated. This graph plotted fluorescence (from the 2D surface) against the seeded

number of cells. This 2D calibration curve for each resazurin regimen provided the R^2 value and formula, which would subsequently be used to calculate seeded cells on 3D scaffolds. Similarly, a 3D calibration curve was then created, correlating the calculated number of attached cells (from 3D scaffolds) with the seeded cells. These same steps were applied for optimising the picogreen assay, with the addition of a DNA concentration standard curve from commercialized DNA concentration. To generate the 2D calibration curve for cell metabolic rate and the 3D standard curve for cell number using different concentrations of resazurin, it was crucial to maintain the same number of cells as when they were initially seeded. However, the cells still needed to properly attach to the surfaces. Therefore, the incubation time needed to be long enough for HDFs to attach but not too long to allow them to start proliferating. HDFs typically take approximately 24 hours to proliferate [72]. To prevent cell proliferation, cells from the same passage number of human dermal fibroblasts, obtained from the same donor, were cultured for 18 hours before conducting the experiment. For the 2D and 3D calibration curves, HDFs were seeded at quantities of $6.25x10^4$, $1.25x10^5$, $2.5x10^5$, $5x10^5$, and $1x10^6$ cells to evaluate the performance of resazurin at various incubation times. In 2D experiments, the control consisted of an empty well plate, and in 3D experiments, the scaffold was not seeded. After one night of cultivation, the cells were incubated for 2, 4, and 6 hours, respectively, in resazurin with fresh medium.

To determine the optimal resazurin assay treatment for use with PGS-M scaffolds, two different concentrations of resazurin in fresh medium were tested: 1 in 50 (v/v) (higher concentration) and 1 in 100 (v/v) (lower concentration). The results of multiple resazurin concentration assays at various time points in a 3D setting are depicted in Figure 4.14.

As illustrated in Figure 4.14 a), the standard curve for the higher concentration was established using the fluorescence values obtained from 2D cell culture and the known number of seeded cells. Once the standard equation was determined, Figure 4.14 b) presents the number of attached cells calculated from the standard equation for each time period, plotted against the number of initially seeded cells. In Figure 4.14 c), the standard curve for the lower concentration is displayed, while Figure 4.14 d) shows a bar graph comparing the number of attached cells to the number of seeded cells obtained from the lower concentration of resazurin.

The number of attached cells was found to be closer to the number of seeded cells in medium containing a higher concentration of resazurin stain compared to medium with a lower concentration. Therefore, it was determined that the assay using the higher concentration of resazurin was optimal for assessing the metabolic activity of cells in PGS-M scaffolds. Furthermore, the optimal incubation period for the resazurin assay was determined by seeding cells overnight and incubating them in resazurin stain in medium for different durations, specifically 2, 4, and 6 hours in an incubator. Figure 4.14 d), which considers both concentrations, indicates that incubating cell-seeded scaffolds in resazurin-containing medium for 2 hours was insufficient. This was evident as the initial results for the number of attached cells were negative, despite seeding $2.5x10^5$ cells. At 4 hours of incubation, the dye appeared to be more effective, as the number of attached cells aligned with the number of seeded cells. However, when using a seeding concentration of $2.5x10^5$ cells, the number of attached cells after 6 hours of incubation was approximately $4x10^5$, exceeding the number of initially seeded cells. This information

suggests that a 4-hour incubation period with the higher concentration of resazurin stain is the optimal condition for assessing the metabolic activity of cells in PGS-M scaffolds.

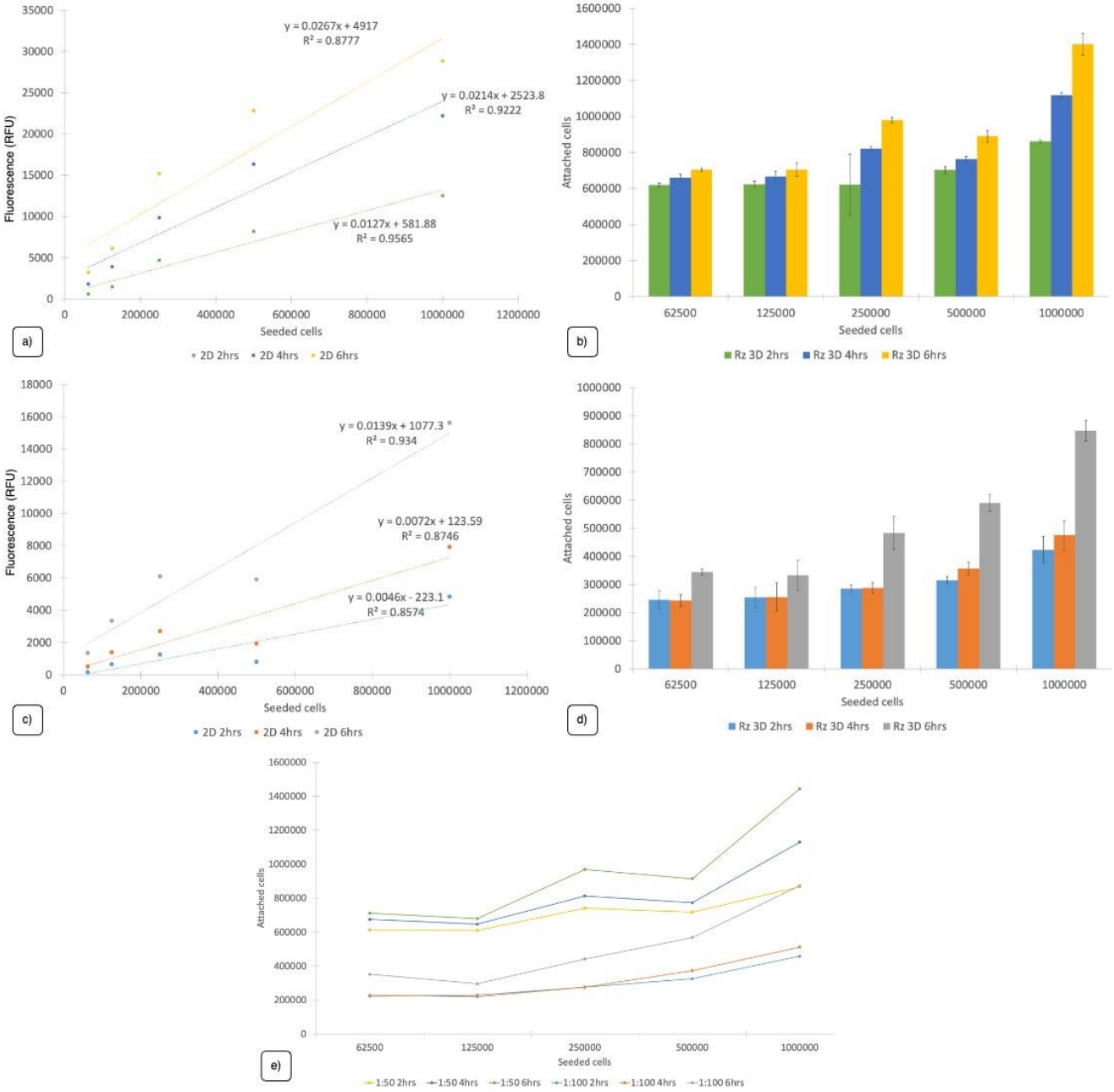

Figure 4.14 - The comparison of resazurin stain in 1:50 ratio (v/v) and 1:100 (v/v) in DMEM where (a) and (c) showed the 2D calibration curve of fluorecence of the metabolic activity retrieved from HDFs cultured on TCP, and the number of seeded cells and (b) and (d) demonstrated the comparison between the number of attached cells on 3D scaffolds and the number of seeded cells after 18 hours in culture.

There were concerns regarding the impact on cell survival, the reversibility of growth inhibition, and the decline in resazurin concentration during incubation with the resazurin test, as highlighted by Xiao et al. [126] in their study using CHO cells. To assess cell viability, they increased the resazurin concentration and found that 100 µM of resazurin inhibited CHO cell vitality. Regarding the reversibility of growth inhibition and the incubation period, they observed that four hours of incubation in resazurin resulted in little to no growth inhibition. Additionally, the proportion of resazurin concentration decreased when the number of cells and incubation period exceeded 5 x 10^5 microencapsulated CHO cells and 5 hours, respectively [126]. Similarly, Magnani and Bettini [127] explored the effects of varying resazurin concentration and incubation period in their research with PC12 cells to monitor the decrease in resazurin fluorescence. In contrast to Xiao et al., Magnani et al. tested the effects with a higher concentration of resazurin, ranging from 497.671 to 3981 µM. They observed that at a concentration of 3981 µM of resazurin in the medium, the fluorescence increased linearly with the number of cells until reaching approximately 1x10^5 cells, at which point the signal began to diminish. This finding was consistent with Xiao et al.'s report that 100 µM of resazurin inhibited growth in medium. Additionally, Magnani et al. [127] demonstrated that as the incubation duration increased, the resazurin fluorescence signal decreased after a certain point, similar to the findings of Xiao et al. Considering these findings, experiments were designed to investigate the limitations of human dermal fibroblasts and PGS-M scaffolds. Since primary cells within the polyHIPE scaffolds may have different dye concentration requirements, the standard technique in the lab involved using a concentration of 1:100 (v/v) resazurin (400 µM) in fresh medium with one hour of incubation. Consequently, experiments were conducted

with resazurin concentrations of 1:100 (v/v) (398.137 µM) and 1:50 (v/v) (796.27 µM) in medium, with incubation times of 2, 4, and 6 hours.

As shown in Figure 4.14 d), the approximate number of attached cells detected after 2 hours of incubation was lower than that at 4 and 6 hours of incubation for both concentrations. This was despite using the same incubation time to determine the cell number via a standard curve. However, at 6 hours of incubation, the signal from 796.273 µM resazurin became excessively strong, as the number of attached cells determined by the assay ($4x10^5$ cells) exceeded the number of initially seeded cells ($2.5x10^5$ cells). This contradicted both publications and indicated that the concentration that may inhibit cell growth was not reached. Therefore, the appropriate protocol for evaluating human dermal fibroblasts in PGS-M scaffolds involved a 4-hour incubation with 796.273 µM resazurin, and this protocol was used for all subsequent experiments.

4.3.2 Picogreen DNA assay optimisation

The Picogreen assay is a technique that directly stains DNA, providing a more precise cell count compared to resazurin and MTT assays. In a 3D environment, it can be challenging to ensure complete cell lysis for accurate counting [127-130]. This thesis explores the effectiveness of using both the resazurin and Picogreen assays to determine the cell proliferation rate in PGS-M material. Picogreen assay, which quantifies DNA content, was employed to obtain cell number information. To prevent cell proliferation, human dermal fibroblasts from the same donor and at the same passage number were cultured on the scaffolds for one night. Three cell lysis protocols were evaluated: one using 1% TE buffer with Triton-X solution for two hours, a second using 1% TE buffer with

Triton-X solution for three hours, and a third using six cycles of freeze and thaw with deionized water (30 minutes in the freezer for each cycle). Figure 4.15 a) and b) served as standard curves for calculating DNA content and the number of attached cells after one week of cell culture. As shown in Figure 4.15, the outcomes of two and three hours of incubation in TE buffer solution were comparable (Figure 4.15 c) and 4.15 e), but the outcomes of freezing and thawing were different (Figure 4.15 d) and 4.15 f)). At a low number of seeded cells, there was no significant difference in DNA content and the number of attached cells between the two methods. However, as the number of seeded cells increased, the disparity between the two methods became significant. Two and three hours of incubation in TE buffer solution resulted in DNA concentrations of 0.180 and 0.179 (approximately $1.55x10^5$ and $1.74x10^5$ cells) at $1x10^6$ seeded cells, while six cycles of freeze and thaw in dH_2O resulted in a DNA concentration of 0.325 (approximately $3.42x10^5$) at $1.25x10^6$ seeded cells. Despite a 25% increase in the number of seeded cells, the DNA yield from the freeze-thaw technique exceeded that of the Triton-X solution by more than 100%. However, even with the higher DNA yield from freeze and thaw, the number of attached cells was approximately half of the number of seeded cells ($1.25x10^6$ cells).

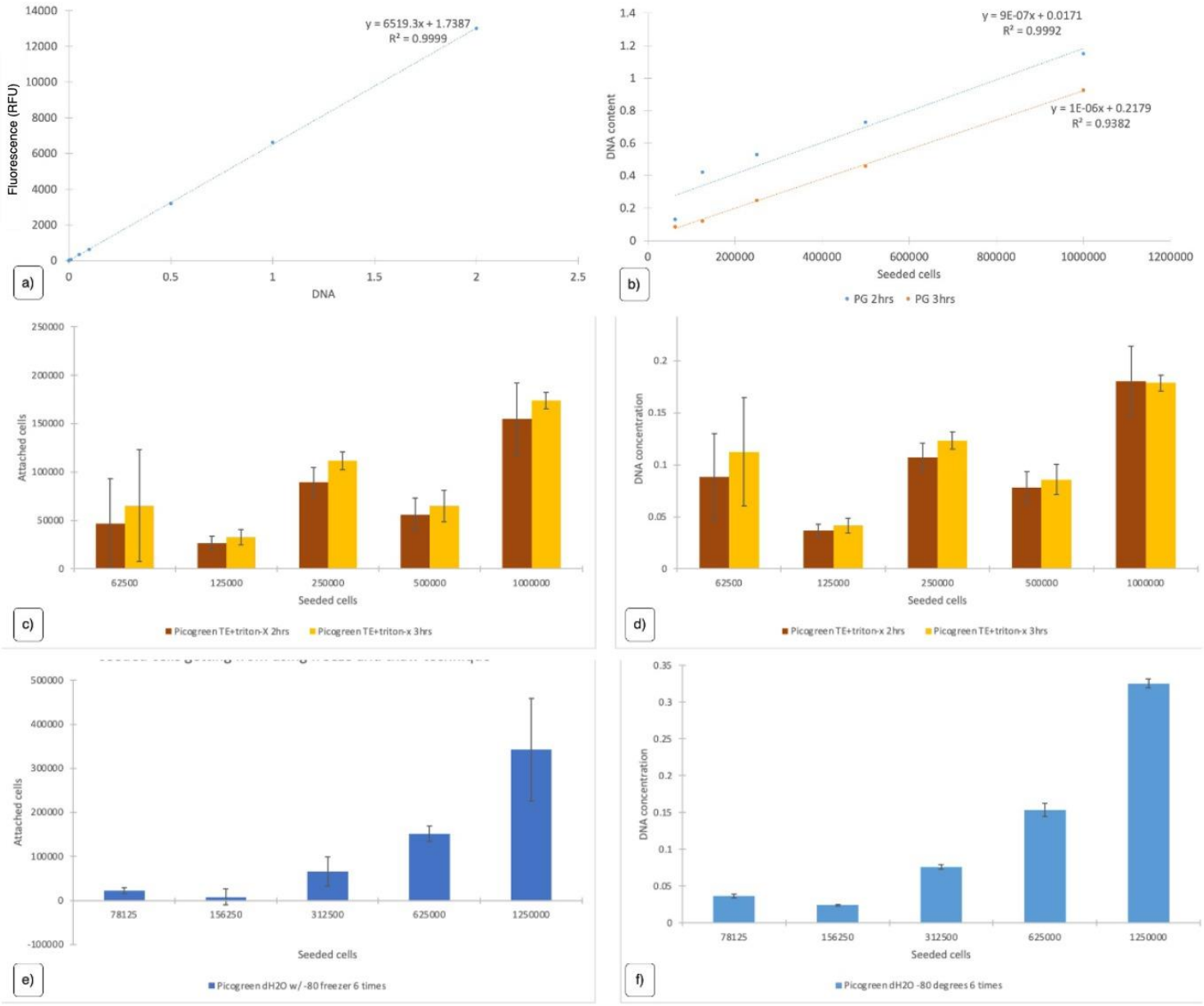

Figure 4.15 - the graphs showed the comparison of DNA concentration retrieved from different washing reagents and cell liaising techniques (N=1, n=3). (a) showed the DNA concentration obtained from the concentration of λDNA standard provided as the reference and its fluorescence. (b) showed the standard curve of the DNA concentration calculated from the λDNA standard curve and the number of seeded cells. The graphs demonstrated the impact of different duration of using Triton-x as the liaising technique where (c) showed the relationship between the attached cells calculated from standard curve and the number of seeded cells, and (d) the relationship between the DNA concentration and the number of seeded cells. The bottom row showed the effects of the freeze and thaw technique where (e) showed the relationship between the number of attached cells and the number of seeded cells and (f) showed the relationship between the DNA concentration and the number of seeded cells.

Complete cell membrane lysis is crucial for accurate Picogreen staining of DNA [130]. The use of Picogreen to measure DNA content on various scaffolds was investigated by Forsey et al. [128]. In contrast to cells cultured on tissue culture plastic, which increased 2-fold after 7 days of culturing, their investigation found that cell concentrations from hydrogel, collagen gel, and PGA fleece were only slightly higher than the seeding density. This finding contradicts the notion that cellular growth rates in 3D structures should be higher than those on 2D surfaces but may have been due to the inability to extract 100% of the DNA from the scaffolds, rather than a reduction in cell proliferation. It was necessary to use the appropriate lysis buffer or procedure to increase the likelihood of extracting more DNA from the cells housed within the scaffolds. Different lysis buffers were evaluated at various concentrations by Chen et al. [129]. The only buffer that worked well with every dilution was Triton-X. The cells were observed after various incubation times with Triton-X. However, fewer attached cells were detected than predicted. Then the freeze and thaw procedure was employed, which produced superior results by bringing the number of attached cells closer to the number of seeded cells. This indicated that, in contrast to the Triton-X approach, more cells were lysed. This approach was then used as the protocol for the rest of this thesis.

4.3.3 Picrosirius red optimisation

The picrosirius red assay is one of the most effective methods for measuring collagen formation in vitro because it is relatively simple to perform and allows researchers to both quantify and characterize the total collagen network [130]. However, to obtain accurate data from each experiment, the assays used to detect specific parameters must be

adapted to the particular cell and material being studied. In the case of the picrosirius red assay, it worked effectively with collagen production derived from tissue culture plastic. However, there was a previous challenge where unbound stain remained within the scaffolds and could not be adequately rinsed during the washing stage. In the past, the use of deionized water (dH_2O) was ineffective at removing unbound stains from the samples. To accurately assess the total collagen content produced by human dermal fibroblasts seeded on a PGS-M scaffold, adjustments were needed to adapt the picrosirius red assay to match the scaffold's unique architecture.

This study compared dH_2O, 0.01M HCl, and 0.5M acetic acid to determine the optimal washing solution for the picrosirius red assay. Initially, PBS was included in the original proposal for establishing a picrosirius red test to detect total collagen production. However, it was found that PBS eliminated both the surplus stain and the stain associated with a particular type of collagen. Consequently, PBS could not be used as a washing agent in the picrosirius red test. For this experiment, the same number of passages of human dermal fibroblasts (HDFs) obtained from the same donor were cultured for two weeks before completing the assay. The scaffolds were rinsed with three different washing solutions until there was no trace of unbound picrosirius red in the liquid taken from the well. As depicted in Figure 4.16, the use of deionized water as a washing solution failed to remove excess picrosirius red staining, as the absorbance of total collagen production was significantly lower compared to the absorbance obtained when using 0.01M HCl and 0.5M acetic acid as washing solutions. In the washing step of the picrosirius experiment, there was no statistically significant difference between the use of 0.01 M HCl and 0.5M acetic acid. The efficacy of the different reagents can also be visually observed by the

amount of the remaining stain on the scaffolds. As shown in Figure 4.17 the remaining picrosirius red stain on the HCl and acetic acid washed background (BG) was less than the dH_2O sample. In the Figure, PBS was also tested and being excluded from the analysis since PBS seemed to wash both bound and unbound stain from the scaffold.

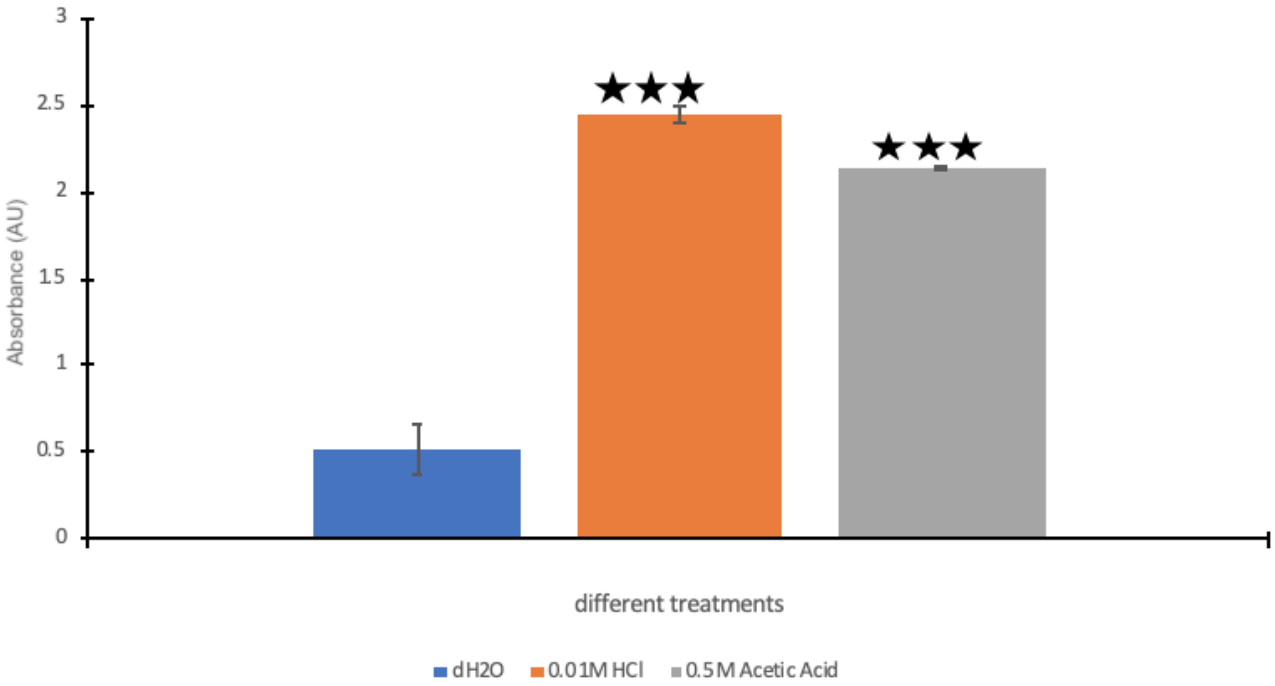

Figure 4.16 - the graphs showed the comparison of picrosirius red retrieved from different washing reagents (N=1, n=3). The asterisk (*) indicates the significant difference in P value < 0.05 compared to the method that use dH_2O as a reagent.

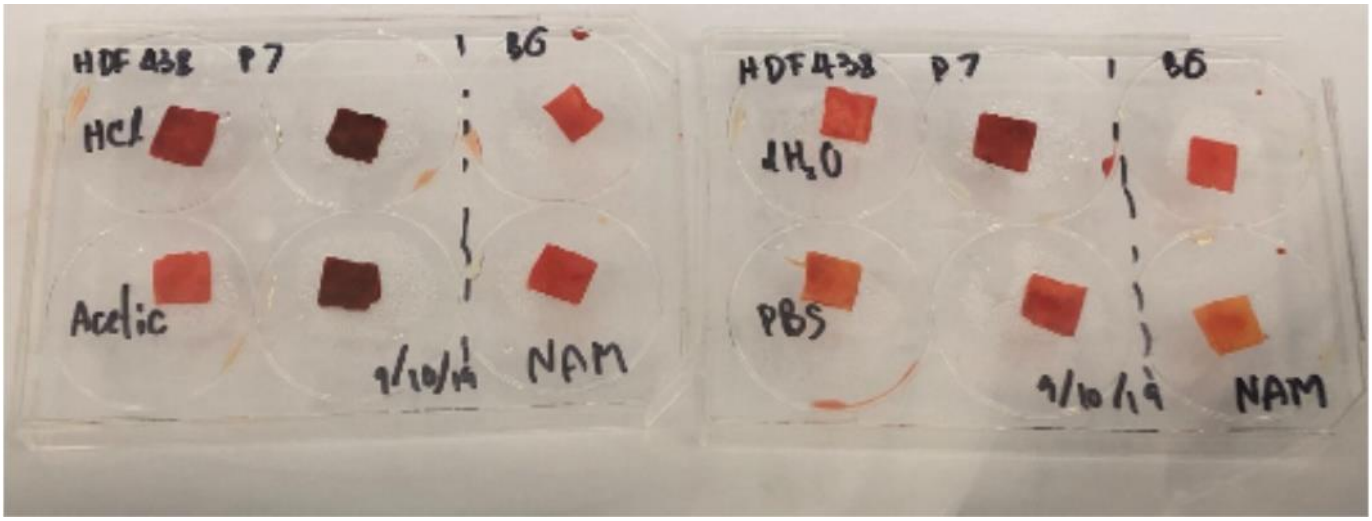

Figure 4.17 – The representative sample of the background (unseeded and untreated) and the cultured PGS-M scaffolds after being washed by different washing reagents.

Typically, deionized water was used to determine the total amount of collagen produced during an experiment. However, as previously stated, the assessment of a washing reagent was required to remove unbound colour from PGS-M scaffold. Taskiran et al. [131] identified the procedures for measuring the total collagen in rabbit tendon; one of the ways employed was Sirius red, and the samples were washed three times with 0.5 M acetic acid. The overall collagen content of Sirius red was considered suitable for clinical and research applications. Caputo et al. [132] evaluated the collagen extraction methods of the Sirius red assay based on acetic acid (CH_3COOH) and hydrochloric acid (HCl) to determine the amount of collagen in bone. In contrast, the data derived from the acetic acid-based Sirius red assay contained a greater proportion of total collagen formation than the data derived from the HCl-based Sirius red assay. Based on these findings, adjustments were made only to the washing phase of the picrosirius red assay, and the samples were rinsed until there was no trace of extra stain in the liquid resulting from

washing. It was discovered that using an acidified solution (both acetic acid and HCl) in the washing step yielded superior results versus using deionized water. There was no statistically significant difference between 0.5M HCl and 0.2M acetic acid, so 0.2M NaOH was used in the remainder of the experiments for ease of preparation.

The optimisation of both the scaffolds and assays plays a crucial role in this research. The term "scaffold" refers to the 3D cell culturing environment, and the accuracy of the results is significantly influenced by the chosen assays.

Regarding the optimisation of the PGS-M scaffold, two distinct fabrication techniques and three disinfection methods were explored. Ultimately, the PGS-M scaffolds created using the emulsion technique and disinfected with O_2 plasma treatment were selected due to their cell-friendly properties and favourable mechanical characteristics.

In terms of assay optimisation, this thesis focuses on three different assays: resazurin, picogreen, and picrosirius red. For the resazurin assay in 3D cell culture, the optimal conditions involve a 4-hour incubation on a rocker in an incubator using a resazurin concentration of 1:50 (v/v) resazurin stock in fresh DMEM.

The cell lysis technique for the picogreen assay was also fine-tuned, with the freeze and thaw method involving 5 cycles with dH_2O proving to be effective and suitable for this thesis.

Lastly, during the picrosirius red staining process, 0.2M NaOH is employed as the solvent to wash away any excess stain from the scaffold.

Chapter 5 – Decellularisation of Tissue engineered PGS-M scaffolds

In tissue engineering, the choice of material is of utmost importance. While native tissues like autografts and allografts are the preferred scaffolds for clinical applications, they come with limitations such as the risk of disease transmission, the challenge of sourcing sufficient donor tissue for allografts, and the necessity of additional surgery for autografts. Availability is a significant constraint when using these types of scaffolds. Consequently, synthetic biomaterials have been introduced into the field because they can be readily manufactured and customized to suit specific applications. However, synthetic materials cannot replicate the intricate structure of the target organ, may trigger an inflammatory response, and might impact the effectiveness of the implant [1-3]. Hybrid scaffolds, which combine synthetic and natural materials, have shown promise as they incorporate elements of the extracellular matrix (ECM) structure [4-6]. The selection of the polymer is crucial and hinges on the mechanical properties of the material.

Decellularisation is a crucial process involving the removal of cells and their components, particularly DNA and RNA, from biomaterials. This is done to minimize the risk of rejection by the host. Decellularisation can be applied to both biological tissues [133, 134] and synthetic scaffolds [95, 135, 136]. In the context of soft-tissue applications, there's a growing interest in utilising cell-derived extracellular matrices because they provide a naturally occurring, intricate array of physiologically functional cues for cell growth. These matrices are rich in collagen, elastin, and glycosaminoglycans (GAGs). They serve as attachment sites for cells and provide robust mechanical support for tissue engineering

endeavours. Therefore, the decellularisation process is pivotal, as it impacts the ability to effectively eliminate the majority of cellular components while minimally disturbing the ultrastructure and composition of the extracellular matrix [133]. In the context of soft-tissue applications, there's a growing interest in utilising cell-derived extracellular matrices because they provide a naturally occurring, intricate array of physiologically functional cues for cell growth. These matrices are rich in collagen, elastin, and glycosaminoglycans (GAGs). They serve as attachment sites for cells and provide robust mechanical support for tissue engineering endeavours. Therefore, the decellularisation process is pivotal, as it impacts the ability to effectively eliminate the majority of cellular components while minimally disturbing the ultrastructure and composition of the extracellular matrix [137, 138]. Preserving the native structure of the ECM is critical because it plays a significant role in proper cell functioning. Furthermore, the ECM's structure is highly organ-specific, as its components induce cell specialization and tissue remodelling for organ function. The ultimate goal of decellularisation is to produce either a complete organ scaffold or unstructured decellularised ECM tissue. In the case of decellularised whole organs, the structure is preserved to maintain the vascular network's integrity. The loose decellularised ECM tissue is a section cut from the organ, possessing the same structure as the native organ but not forming the entire organ [139].

Concerning biocompatible synthetic materials, decellularisation is employed in the fabrication of ECM-based hybrid scaffolds. 3D scaffolds play a pivotal role in in vitro cell culture as they provide a platform and physical guidance for the development of new tissues or organs. To mitigate the impact of the decellularisation method on the ECM structure, various approaches have been explored in several studies [95, 135, 136, 140].

Common techniques utilised with 3D hybrid scaffolds include multiple freeze-thaw cycles, osmotic shock, exposure to acidic or alkaline conditions, and the use of detergents such as Triton-X, as well as combinations of these techniques. However, the effectiveness of a particular decellularisation approach is highly dependent on the base polymer, and results may not always be consistent. Recommended methods for decellularisation vary depending on the cell types and scaffolds being used. Therefore, it is essential to tailor the decellularisation approach to each specific application and cell type [95].

It has been noted that the use of a detergent can lead to more efficient removal of cells. Furthermore, combining physical techniques such as freeze and thaw cycling and osmotic shock with a detergent may enhance the decellularisation process even further. Lu et al. [95] conducted a comparative study of seven decellularisation methods, including combinations of these methods. Their findings indicate that the combination of the freeze and thaw technique with NH_4OH detergent effectively removes the majority of cells from the scaffolds. Similarly, the use of an alkaline buffer with Triton-X detergent yielded comparable results, while other methods demonstrated moderate effectiveness.

To create the hybrid scaffold using the PGS-M scaffold as a template, it's essential for cells to first adhere and proliferate within the scaffold. After optimising this process, which has been detailed in Chapter 4.2, O_2 plasma-treated PGSM-80 E scaffolds were employed in the experiments. These are simply referred to as PGS-M in this chapter. During the cell culture, fibroblasts generate the extracellular matrix, which will enable the formation of the hybrid scaffold. Additionally, the polymer scaffold should be biodegradable to allow the biological material to eventually replace the synthetic scaffold after implantation. Since PGS-M scaffolds are biodegradable, they are chosen as the

base scaffold for in vitro cell culture. However, there is still no report on the appropriate protocol to effectively decellularise cultured PGS-M scaffolds. In this thesis, two different approaches were tested: using dH_2O at 37°C and the freeze and thaw technique.

To optimise the decellularisation protocol, the experiments involved controlling the use of cell-seeded PGSM-80 E scaffolds with O_2 plasma treatment, later referred to as PGS-M scaffolds. Chapter 4 provides explanations regarding the impact of this specific treatment and the fabrication technique on the scaffolds, in which cell activities and mechanical properties were related. For these experiments, $1x10^4$ HDFs were cultured on the PGS-M scaffolds. The control group comprised scaffolds in which cells were not subjected to decellularisation before data collection, serving as evidence of cell viability within the scaffolds.

5.1 Decellularisation

Multiple tests were conducted to assess the effectiveness of various decellularisation techniques on PGS-M scaffolds. PGSM-80 E was chosen as the primary scaffold for this thesis based on the optimisation described in Chapter 4.2 and will be referred to as PGS-M scaffolds. While both gases used in plasma treatment had beneficial effects on changes in cell activity, O_2 plasma treatment was chosen as the primary disinfection method because it provided a wider range of pores.

Using a resazurin assay, the metabolic rate of decellularised scaffolds was compared to that of 3D control scaffolds on which cells were cultured for the same period of time. Additionally, the fluorescence measured from an unsown 80% PGS-M emulsion scaffold was considered background and was subtracted from each data set. Four different conditions were tested in this chapter:

1. 80% PGS-M scaffold with no cells (background).
2. PGS-M scaffold with two weeks of cell culturing (control).
3. Decellularised PGS-M scaffold using Protocol 1.

   Cell-seeded PGS-M scaffolds were immersed in dH_2O at 37°C for 30 minutes on a rocker, and then the water was removed. This step was repeated for three cycles.
4. Decellularised PGS-M scaffold using Protocol 2.

   the cultured PGS-M scaffolds were submerged in dH_2O at -80°C for 30 minutes, then allowed to thaw at room temperature, and the water was removed. This was also repeated for three cycles.

5.1.1 Colourimetric assays

To collect information from two decellularised scaffolds, a range of colourimetric assays were conducted. The protocols for these assays were the optimised protocols as presented in Chapter 4.

Figure 5.1 shows the comparison of PGS-M scaffolds after one of these decellularisation protocols. In comparison with the positive cell-seeded 3D control, both decellularised techniques significantly decreased the metabolic rate of HDFs, which could refer to cell inactivity after the decellularised protocol. However, there was no significant difference between the two decellularised protocols. It indicated that both decellularised methods successfully removed HDFs from the PGS-M scaffolds and either could be used as the decellularised process by considering the metabolic rate of cells.

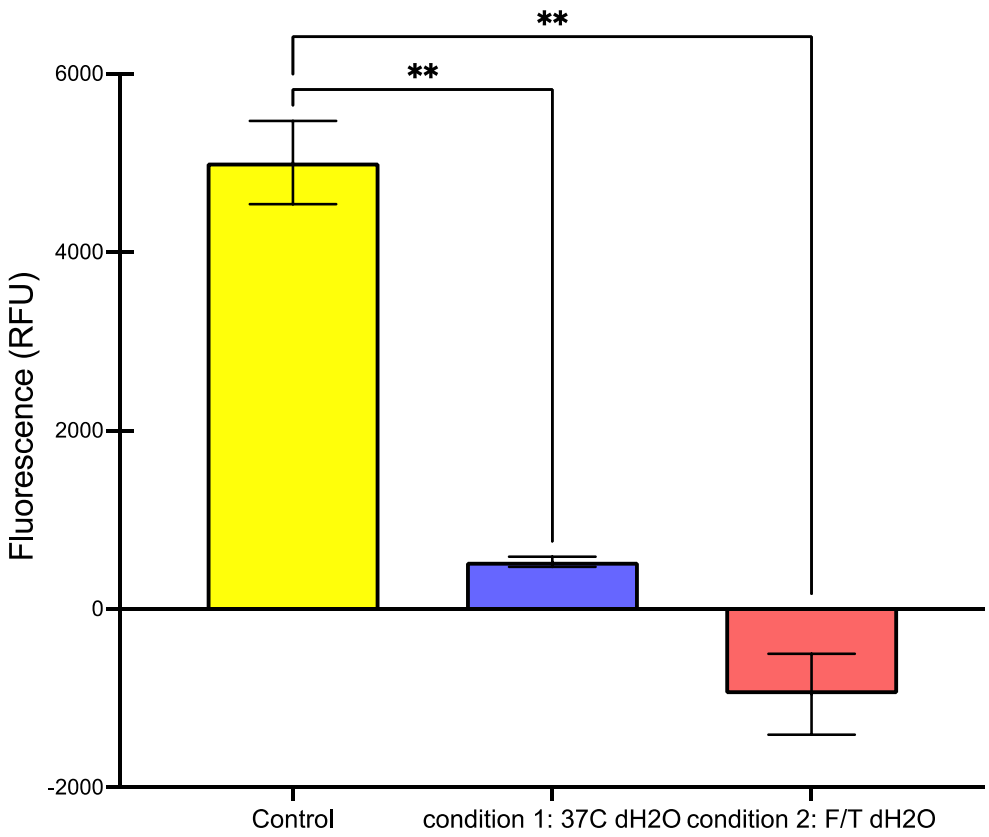

Figure 5.1 - The bar graph depicts the metabolic activity extracted from 80% emulsion PGS-M scaffolds using both decellularisation methods. The examination was conducted using a resazurin assay. One-way ANOVA was used to analyse the data (N=1, n=3). The asterisk (*) indicates the significant difference in P value < 0.05.

The next aspect to determine was the cell number. The Picogreen assay was utilised to calculate the number of cells by measuring the DNA concentration. Figure 5.2 illustrates the comparison of the cell number between the 3D control and the decellularised scaffolds. According to the graph, the number of cells extracted from both treatments was significantly lower than that of the control. However, there was no significant difference between the two techniques. This result suggests that both techniques can be used for decellularising the PGS-M scaffolds when considering only DNA quantification perspective.

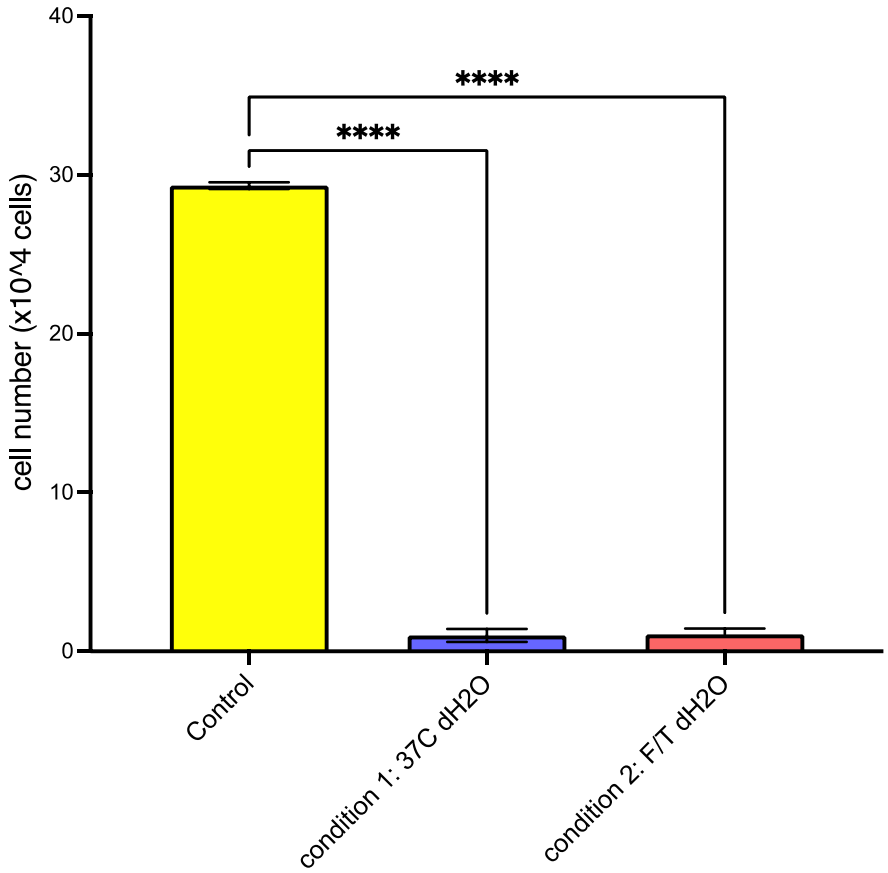

Figure 5.2 - The bar graph shows the cell number (x10^4) extracted from 80% emulsion PGS-M scaffolds using both decellularisation methods. The examination was conducted using a picogreen assay. One-way ANOVA was used to analyse the data (N=1, n=3). The asterisk (*) indicates the significant difference in P value < 0.05.

Figure 5.3 illustrates the amount of collagen produced by HDFs present on the scaffold after two weeks of cell culture, both before (control) and after decellularisation. According to the graph, there was no statistically significant difference in the amount of collagen on scaffolds between the control and both decellularised scaffolds. This result suggests that both techniques preserved the collagen produced by the fibroblasts during culture.

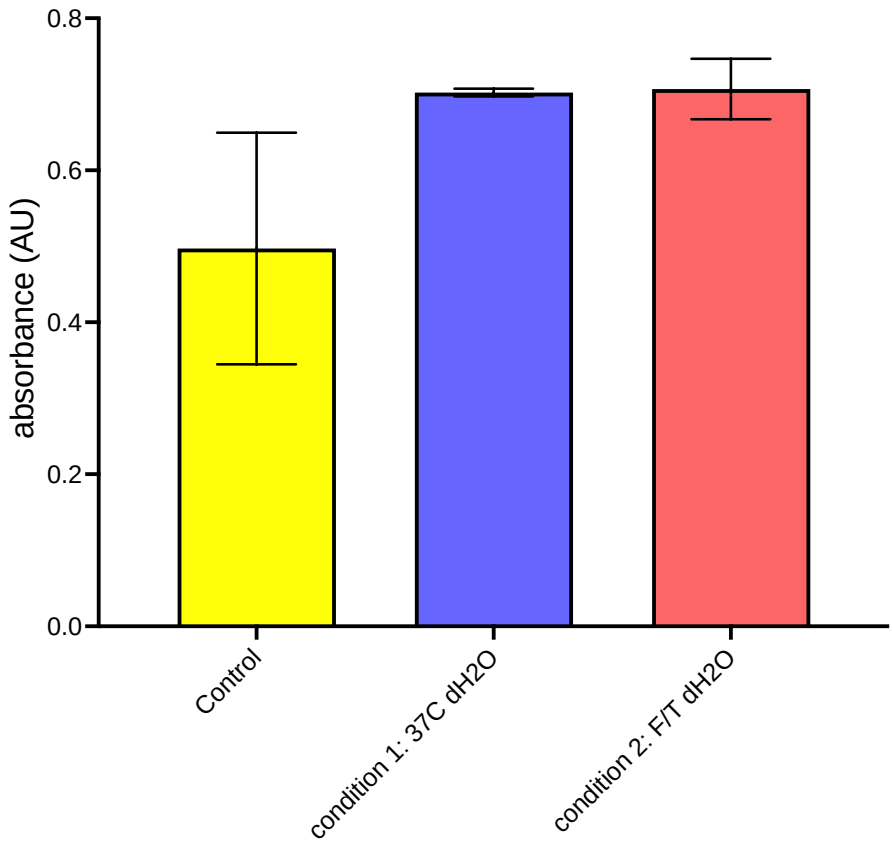

Figure 5.3 - The bar graph shows the absorbance of picrosirius red which indicated the collagen production extracted from 80% emulsion PGS-M scaffolds using both decellularisation methods. The examination was conducted using a picrosirius red assay. One-way ANOVA was used to analyse the data (N=1, n=3).

Resazurin, picogreen, and picrosirius red assays were utilised to quantify the effectiveness of the decellularisation techniques. The goal was to assess the impact of both decellularisation methods and identify a suitable approach for PGS-M scaffolds. Based on the presented graphs, both techniques yielded promising results and could be potential methods for this polymer.

5.1.2 Histological staining

Haematoxylin and eosin (H&E) staining has been a staple in the field for many years. This staining method is employed to colour the cell nuclei (haematoxylin), cytoplasm, and extracellular matrix (ECM) structure (eosin). Haematoxylin stains the nuclei dark purple or blue, while eosin stains the ECM structure and cytoplasm pink [141]. The H&E staining process typically involves tissue or sample fixation, dehydration, and paraffin embedding when using the wax-embedding approach [142]. Researchers, such as Pashneh-Tala et al. [38, 40], have successfully applied this technique to PGS-M scaffolds, confirming its suitability for these scaffolds without the risk of self-staining. H&E staining is effective for porous scaffolds, allowing for clear visualization of nuclei, the ECM network, and cytoplasmic components [143].

Elastin Verhoeff-Van Gieson (EVG) staining is a specific stain used for visualizing elastin fibres in tissues. It is primarily employed to examine abnormalities in elastin fibres within tissue samples. In EVG staining, elastic fibres appear black, collagen fibres are stained red, and cells are typically stained brown or yellow [144]. Kazlouskaya et al. [145] provided a comparison of various elastin stains, including EVG, gomori, Miller's elastic stain, humberstone, and orcein. Among these stains, EVG is favoured because it does not require paraformaldehyde for fixation, is relatively easy to perform, and can effectively stain the entire elastic network. Therefore, EVG staining is particularly useful for observing elastin fibres [146].

Immunohistochemistry (IHC) is a valuable technique that enables researchers to visualize various markers by using specific antibodies. In the context of this thesis, which focuses on cell proliferation, two stains of particular interest are Ki-67 and DAPI. Ki-67 staining is

utilised to observe cells that are actively undergoing mitosis, indicating proliferating cells. Ki-67 is a marker that becomes visible during the proliferation process[88, 147, 148]. To stain this marker, an anti-Ki-67 antibody is used as the primary antibody. This primary antibody binds to the Ki-67 marker. Subsequently, a secondary antibody, derived from the host species used in the primary antibody, is employed to produce a fluorescent signal [149]. Ki-67 staining helps identify and quantify actively proliferating cells within the sample. DAPI staining, on the other hand, is a common technique in tissue engineering. DAPI stains the DNA within cells, typically producing a bright blue fluorescent signal when viewed under a microscope. The staining procedure is straightforward, involving incubating the sample with the stain for a specified duration before mounting for observation [150]. DAPI staining can complement Ki-67 staining by providing insight into the overall cell proliferation profile within the scaffolds.

To qualitatively observe 3D samples, various techniques are employed, depending on the specific objectives of the observation. In the field of tissue engineering and biomaterials research, two common techniques for obtaining images are histological imaging and immunohistochemistry (IHC) imaging [151]. Histological imaging involves the use of a microscope to examine stained sections. This technique is commonly used in autopsies, medical diagnoses, educational settings, and histological research. It plays a crucial role in the study of diseased tissues to aid in diagnosis and treatment. The histological staining process typically consists of five essential steps: fixation, tissue processing to dehydrate the samples, embedding, sectioning, and staining. Advances in histological staining methods, which combine chemical, molecular biology, and immunological techniques, have greatly improved the study of organs and tissues. One of the variations in this

method is the choice of stain used during the staining phase. Different stains can be employed to colour different cellular or tissue components of interest [152, 153]. This technique is particularly useful for imaging cells and their constituents, as well as for staining multiple variables simultaneously within the same tissue section.

Although histological imaging is a valuable technique in tissue engineering because it allows researchers to investigate various parameters by using different stains, it does have its limitations. One major drawback is that it is a destructive method and can sometimes yield inaccurate results [151]. Scanning Electron Microscopy (SEM), on the other hand, offers researchers the ability to capture detailed information about the surface, chemical composition, electrical properties, and crystalline structures of biomaterials. SEM provides the advantage of examining a larger area compared to a conventional optical microscope and allows for high-magnification observations. It operates by using an electron beam to generate images based on the reflection of electrons, and in many cases, it doesn't require staining, although coating may be necessary for improved resolution [154, 155]. SEM is particularly well-suited for observing the pore size and interconnectivity of scaffolds due to its high-resolution surface imaging capabilities. However, it may not be the best choice for studying cell activities, as the sample needs to be dried before examination, which can lead to structural changes and the loss of information during the process.

Histological and immunohistochemistry (IHC) approaches were selected to examine the structure of extracellular matrix (ECM) production and how cells re-proliferate within the scaffold. Several staining techniques were employed:

1. Haematoxylin and eosin (H&E): H&E staining provided an overview of the protein structure and nuclei within the scaffolds. It allowed researchers to observe the overall tissue structure.
2. Elastic Van Gieson (EVG): EVG staining was specifically chosen to visualize elastin structures that might be produced by human dermal fibroblasts (HDFs). This stain is particularly effective for highlighting elastin fibres.
3. DAPI: DAPI staining was used in immunohistochemistry to label the cell nuclei within the samples. DAPI stains the nuclei with a bright blue fluorescence, aiding in the visualization of cell distribution.
4. Ki-67: Ki-67 staining was utilised to identify actively proliferating cells within the scaffold. Ki-67 is a marker that becomes visible during cell proliferation, making it a valuable tool for assessing cell growth.

These histological staining techniques were applied to gain a better understanding of how the scaffolds responded, simulating potential in vivo clinical implantation scenarios. Human dermis served as the positive control for all staining procedures, while undecorated PGS-M scaffolds were used as the negative control for comparison.

Figure 5.4 demonstrates the H&E-stained sections of skin (D477) and blank scaffold. The images were taken using two different objective lenses: (a and c) 4x and (b and d) 10x by using a light microscope. Cell nuclei are stained dark purple, while intra- and extracellular proteins, including collagen, are stained pink. As shown in Figure 5.4, the PGS-M scaffold was not stained by H&E.

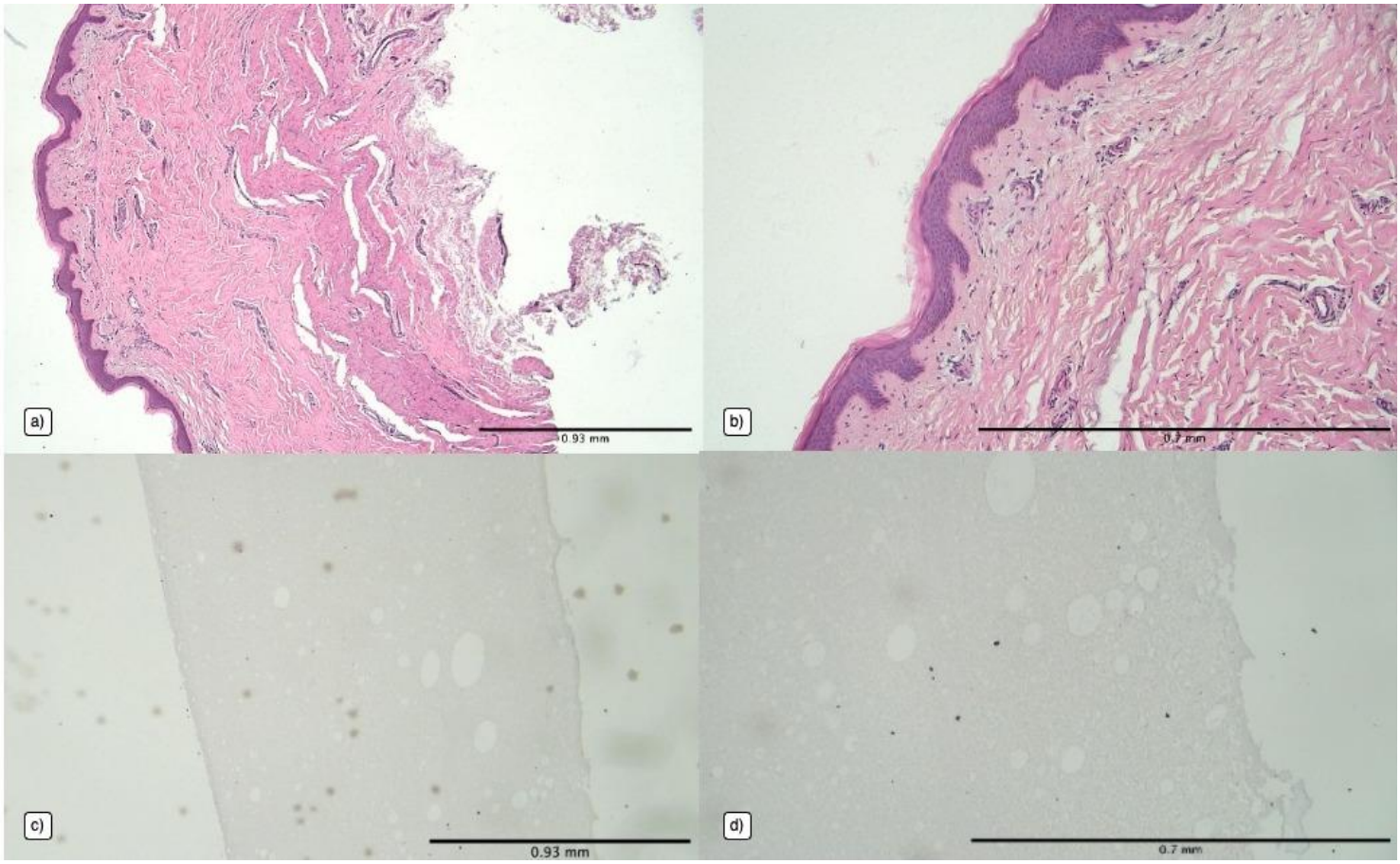

Figure 5.4 – The H&E-stained images of donor's skin with (a) 4x and (b) 10x objective lens where dark purple refers to cell nuclei and pink refers to the ECM structure, and the blank, unseeded PGS-M scaffolds with (c) 4x and (d) 10x objective lens (N=1, n=2).

Figure 5.5 displays the decellularised scaffolds after treatment using (a and b) condition 1 and (c and d) condition 2 protocols. The images were captured using (left) a 4x and (right) a 10x objective lens. When compared to the background scaffold (Figure 5.4, c and d), the pink colouration of the decellularised scaffolds from both conditions appeared darker. Since this colour corresponds to the protein content, it may indicate the presence of soluble proteins produced by HDFs within the scaffolds. Additionally, there was no noticeable dark purple colour on the scaffold, suggesting that HDFs were successfully

lysed, and their DNA was removed by both techniques. This outcome aligns with the metabolic rate data (Figure 5.1) and the cell count data (Figure 5.2).

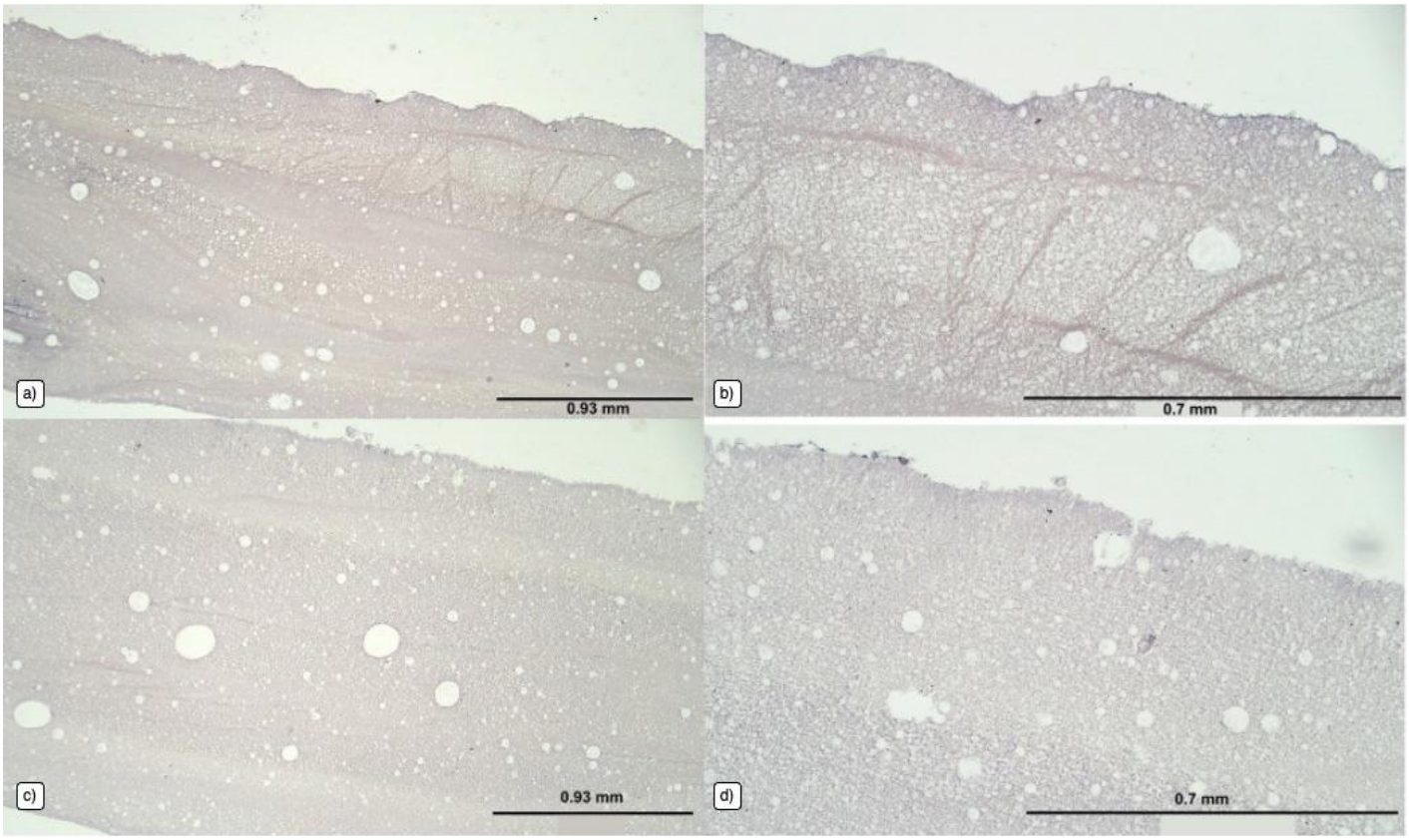

Figure 5.5 – The H&E-stained images of decellularise condition 1 with (a) 4x and (b) 10x objective, and the images of condition 2 scaffolds with (c) 4x and 10x (d) objective lens (N=1, n=2).

Elastin Verhoeff-Van Gieson (EVG) staining was employed to confirm the presence of elastin in this hybrid scaffold. Sections of skin (D477) and the background of PGS-M scaffolds were stained to verify the technique. As shown in Figure 5.6, the positive control exhibited appropriate EVG staining, with black representing cell nuclei, red indicating collagen content, and yellow/brown indicating muscle and other components. However, when the stain was applied to the negative control, it was evident that the entire PGS-M scaffold stained black (Figure 5.6). This suggested that EVG staining might not be suitable for use with PGS-M scaffolds. Consequently, the test was not continued, as

Figure 5.6 (right) indicates that PGSM appears to retain a large number of stains non-specifically.

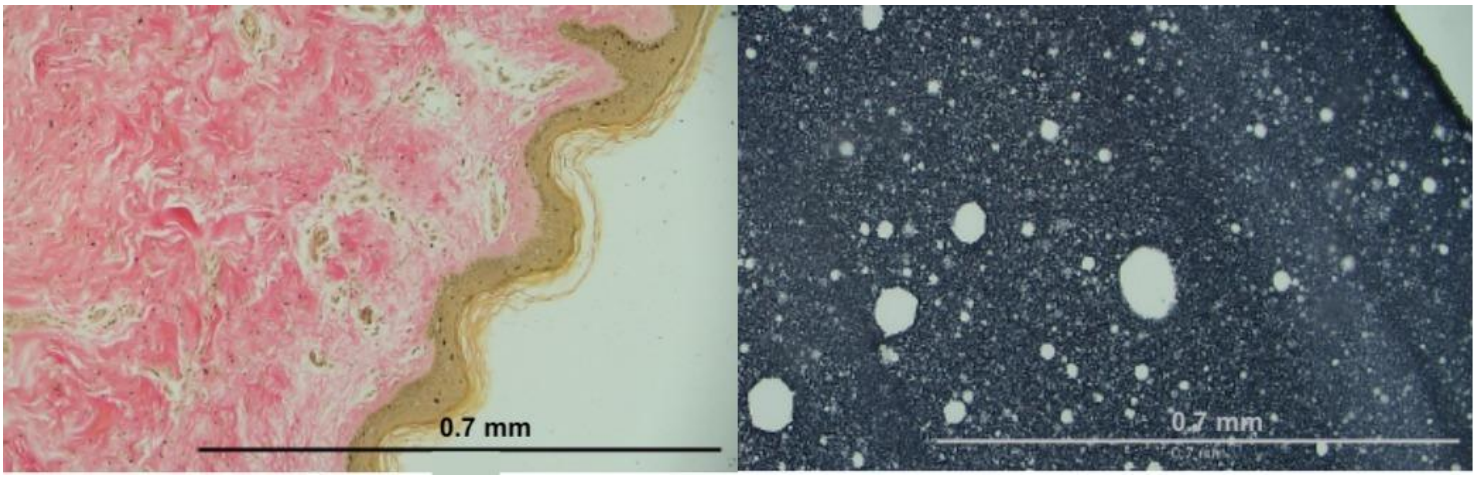

Figure 5.6 – The EVG stained images of (left) stained sections of skin (D477) where black refers to cell nuclei, red refers to collagen content and yellow/ brown for muscle and other, and (right) the blank, unseeded PGS-M scaffolds (N=1, n=2).

5.1.3 Immunohistochemistry staining

The IHC (Immunohistochemistry) technique was also used to confirm the performance of the two decellularisation methods. Two stains, DAPI and Ki-67, were employed in this process. DAPI is a stain that binds to and stains nucleic acids, and it was used to indicate the presence of residual DNA after decellularisation. Ki-67, on the other hand, is a nuclear protein that plays a crucial role during mitosis and is a recognized marker of actively proliferating cells. These stains were chosen to assess the presence of DNA and the level of cell proliferation within the decellularised scaffolds.

Figure 5.7 (a) illustrates that the unseeded PGS-M scaffold exhibited slight autofluorescence, or it might have been stained by Ki-67. However, this noise was deemed acceptable and was corrected by adjusting the offset. This same setting was applied to all images taken of the PGS-M scaffold. Figure 5.7 (bottom) shows the IHC

images of the decellularised scaffolds. Figure 5.7 (b) representing condition 1 and (c) representing condition 2. These images were captured using a 10x objective lens. As seen in Figure 5.7 (b), when the PGS-M scaffolds were incubated in an incubator (condition 1), the cells were entirely removed from the hybrid scaffold, as there was no positive DNA stain (blue colure) in the image. However, when the freeze-thaw technique (Figure 5.7 (c) was used for decellularisation (condition 2), a layer of cells could still be observed attached to the surface of the scaffold. This can be inferred from the thin blue line at the edge of the scaffold. Based on this result, it appears that the freeze-thaw method might not completely lyse the cells from the scaffold.

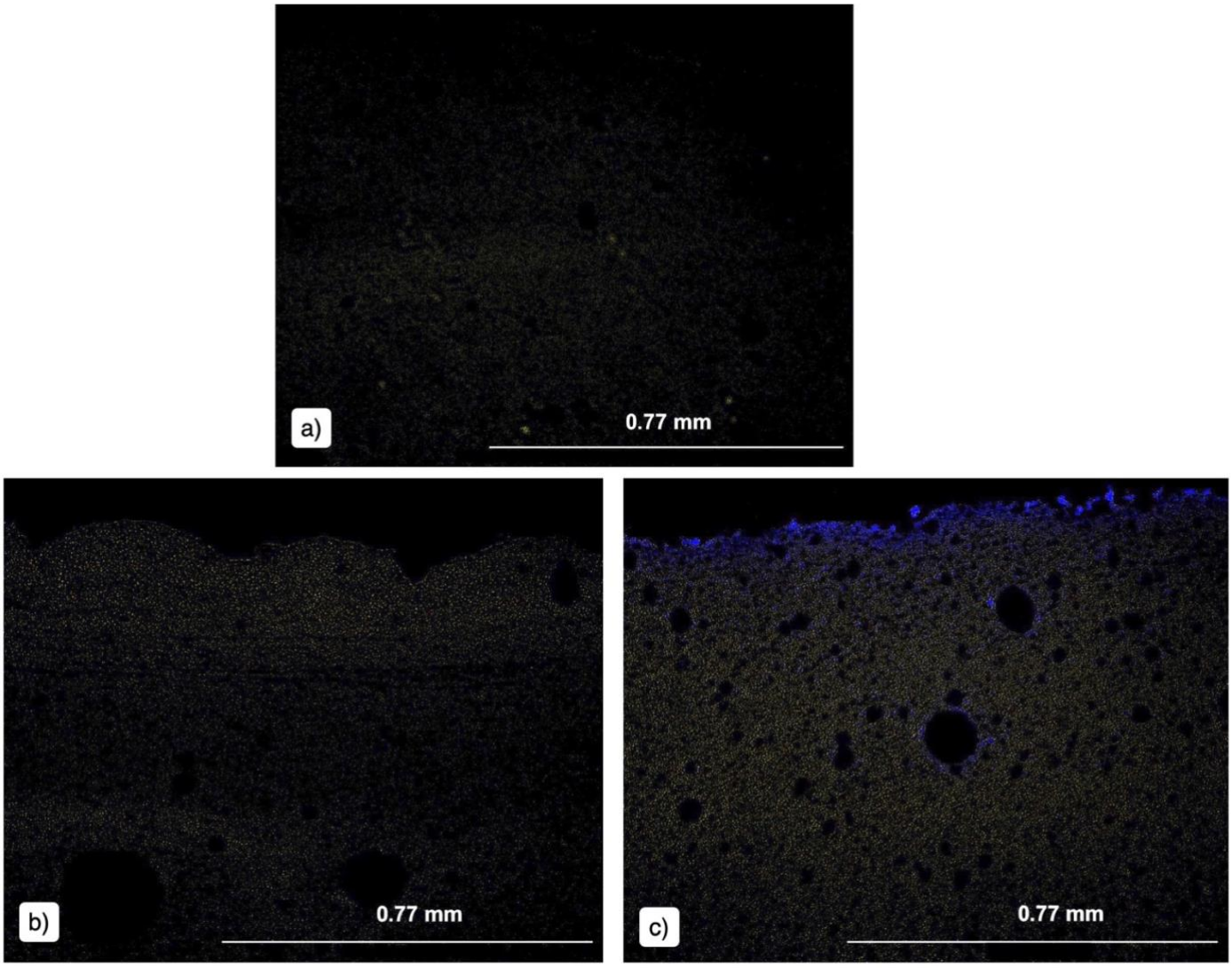

Figure 5.7 – The IHC-stained images of (a) unseeded PGS-M scaffold, decellularised (b) condition 1 and (c) condition 2 PGS-M scaffold.

Concerning the proliferating marker stained by Ki-67, the signal appeared stronger in the condition 2 decellularised scaffolds, with the yellow marker being noticeably more pronounced compared to condition 1. This difference could be attributed to the success of the condition 1 protocol in removing most of the cells, along with their DNA, from the scaffold. In contrast, the condition 2 protocol, where the signal remained strong and a line of cells was visible, might have had a milder effect on the cells and their DNA.

Nonetheless, both scaffolds still exhibited the yellow highlight, indicating the presence of Ki-67 markers and suggesting the existence of actively proliferating cells. It is important to mention that PGS-M itself also displayed autofluorescence in this channel (as observed in the visible yellow marker in Figure 5.7(a)), which is deemed acceptable for the decellularisation protocols [95, 156].

5.1.4 Mechanical properties

In terms of mechanical properties, this thesis examined the ultimate tensile strength and hydrophilicity of the scaffolds. Figure 5.8 presents the ultimate tensile strength data obtained from background scaffolds, 3D controls, and seeded scaffolds after decellularisation. The graph indicates that, when comparing the two different decellularisation techniques, the ultimate tensile strength of condition 1 was statistically lower. However, condition 2 showed no significant difference compared to the 3D control and background scaffolds. This suggests that condition 1 decreased the ultimate tensile strength of the seeded scaffolds, while condition 2 appears to be a promising technique and can be used as a decellularisation method for PGS-M polymer.

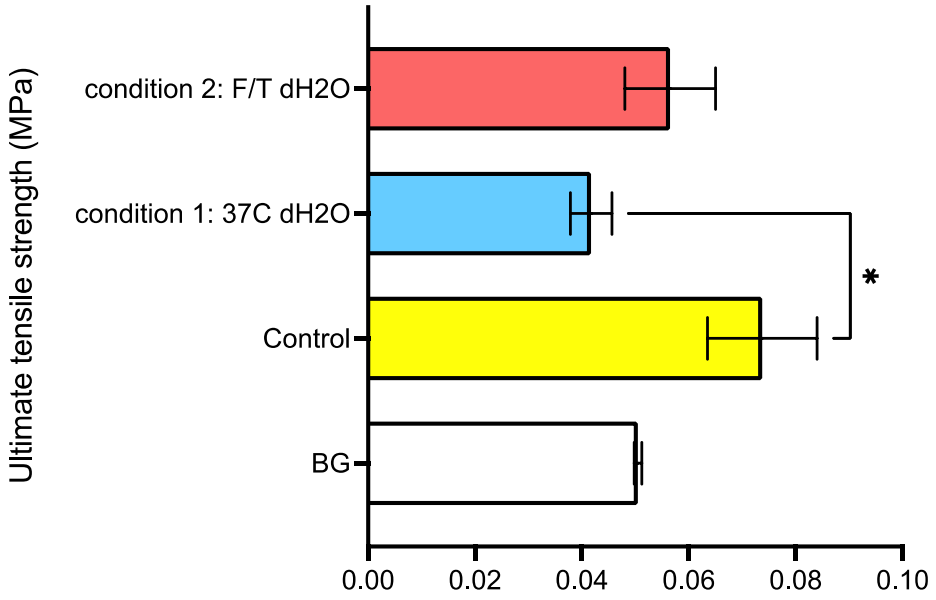

Figure 5.8 - The bar graph demonstrates the ultimate tensile strength collected from 80% emulsion PGS-M scaffolds after decellularisation. BG stands for untreated, unseeded background scaffold. One-way ANOVA was used to analyse the data (N=1, n=3). The asterisk (*) indicates the significant difference in P value < 0.05.

Wettability was assessed to determine the hydrophilicity of the scaffold surfaces. Due to the unavailability of the wettability measurement machine during the COVID-19 pandemic, an alternative method was employed. This alternative method involved using only 5 µL of dyed water and visually recording the absorption over time. Two samples were quantified for each type of scaffold (N=1, n=2).

Figure 5.9 illustrates that the unseeded PGS-M scaffold exhibits higher hydrophilicity compared to the seeded scaffolds. This difference could be attributed to the exposure of ECM components on the surface after decellularisation. This change is advantageous as it can improve cell attachment during subsequent recellularisation. However, there was no statistically significant difference between both conditions and the 3D control (seeded scaffolds that have already been fixed). The results suggest that hydrophilicity decreased after seeding the cells onto the scaffolds. Additionally, these results indicate that the two

decellularisation processes used in this study did not have a significant impact on the hydrophilicity of the surface when compared to the control.

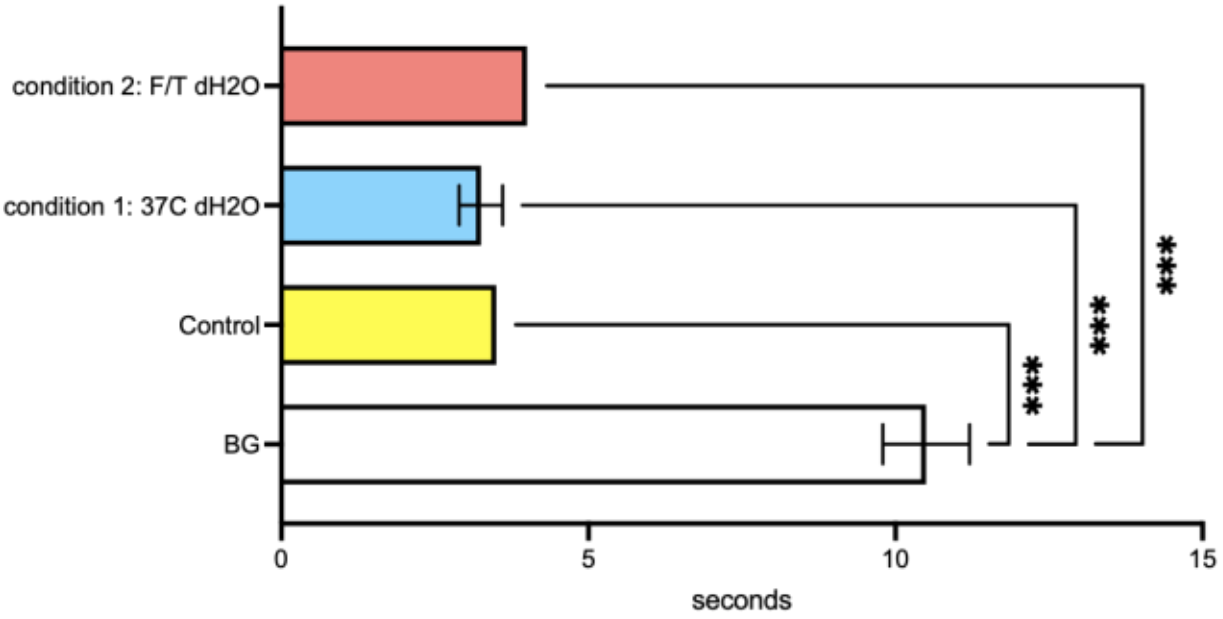

Figure 5.9 - The bar graph demonstrated the period (in seconds) the scaffold used to absorb 5µL of red-dyed dH_2O collected from the PGS-M scaffolds after decellularisation. One-way ANOVA was used to analyse the data (N=1, n=2). The asterisk (*) indicates the significant difference in P value < 0.05.

The effectiveness of a specific decellularisation method depends significantly on the specific target tissue. For instance, in cardiovascular applications, the emphasis is on preserving vascularization after decellularisation, optimising the chemical composition, and maintaining the mechanical properties and 3D structure [157].

To decellularise cells from a 3D template, multiple methods and various reagents can be employed to achieve the goal of removing the cells and their immunogenic components [156]. However, considering that this is the first attempt at performing decellularisation on PGS-M scaffolds, it is advisable to use physical approaches, such as osmotic shock and freeze-thaw techniques with deionized water (dH_2O). This minimizes the risk of damaging

the matrix with detergents. Wang et al. [140] reported a trend where using detergents was more efficient. However, the freeze-thaw technique, while slightly less efficient in terms of cell removal compared to the physical approach, preserves the matrix with minimal destructive effects. Xing et al. [133] also employed the freeze-thaw technique in their research. They used ECM scaffolds produced from decellularised fibroblast cell sheets as the main scaffold. Their results indicated that, compared to using sodium dodecyl sulphate (SDS) at two different concentrations, the freeze-thaw technique showed promising results in removing viable cells from the scaffolds while preserving ECM production, cellular components, and the scaffold's strength. In contrast, the SDS used in the decellularisation protocol had a negative effect on ECM content and mechanical properties. Lu et al. [95] also reported using the freeze-thaw technique in comparison with various reagents such as 25 mM NH4OH and 0.1% Triton™ X-100. They used Poly (lactic-co-glycolic acid) (PLGA) mesh as the template. Their findings indicated that the freeze-thaw technique enhanced the performance of NH4OH during the decellularisation process. Additionally, this method, when combined with 0.1% Triton™ X-100, resulted in mild host responses in in vivo experiments. The freeze-thaw technique has also been reported to successfully decellularise natural tissue, reduce immune responses, and preserve necessary cellular components. The results collected in this thesis, particularly in terms of cell metabolic rate (Figure 5.1) and cell number (Figure 5.2), align with the trends found in other studies. The freeze-thaw technique proved to be an efficient method for decellularising HDFs cultured in PGS-M scaffolds while preserving mechanical properties like ultimate tensile strength and hydrophilicity. [134, 136, 140].

5.1.5 FTIR analysis

FTIR (Fourier-transform infrared) spectroscopy was employed to verify the presence of collagen and the intact extracellular matrix (ECM) structure within the PGS-M scaffold following the decellularisation process. This analytical technique enabled the examination of the scaffold's surface and its uppermost layer to assess the composition of various components. The FTIR spectra were acquired within the range of 1000 to 4000 cm^{-1} from four distinct samples. The fingerprint region of interest spanned from 1000 to 1800 cm^{-1} and contained critical information about the scaffold's composition. To ascertain the presence of the PGS-M prepolymer, the FTIR spectrum at 1724 cm^{-1} was examined. This spectral region corresponds to the C=O stretching vibrations of the aldehyde group. Additionally, the peak observed at 1169 cm^{-1} was indicative of the C-O stretching bond associated with the ester group.

The FTIR analysis provided insights into the composition and structural changes in the PGS-M scaffolds after decellularisation. Specifically, it allowed for the identification of key functional groups and their relative abundance within the scaffolds. One notable observation was the presence of the aldehyde group in the FTIR spectra. The aldehyde group was most prominent in the background scaffold, followed by the control scaffold, with conditions 1 and 2 having similar, lower levels. This aldehyde group is associated with the PGS-M prepolymer, indicating the presence of PGS-M polymer in the scaffolds. This suggests that the percentages of PGS-M prepolymer were relatively high in the control and condition 2 scaffolds, while condition 1 had the lowest levels.

The analysis also considered the peak associated with the ester group, which is related to glycerol used in the production of PGS-M polymer. In the background scaffold (no cells),

the ester group peak was the highest, followed by the control scaffold, with conditions 1 and 2 showing similar, lower peak heights. This suggests that in the background scaffold, the PGS-M polymer remained relatively preserved. In contrast, in the control and condition 1 scaffolds, where cells were present and had proliferated, the polymer appeared to have started degrading, or perhaps the ECM components were exposed on the surface of the PGS-M scaffold. Condition 2 showed the lowest percentage of polymers compared to the other conditions.

Overall, the FTIR results indicate differences in the preservation of PGS-M polymer and suggest changes in scaffold composition due to the presence of cells and the decellularisation process.

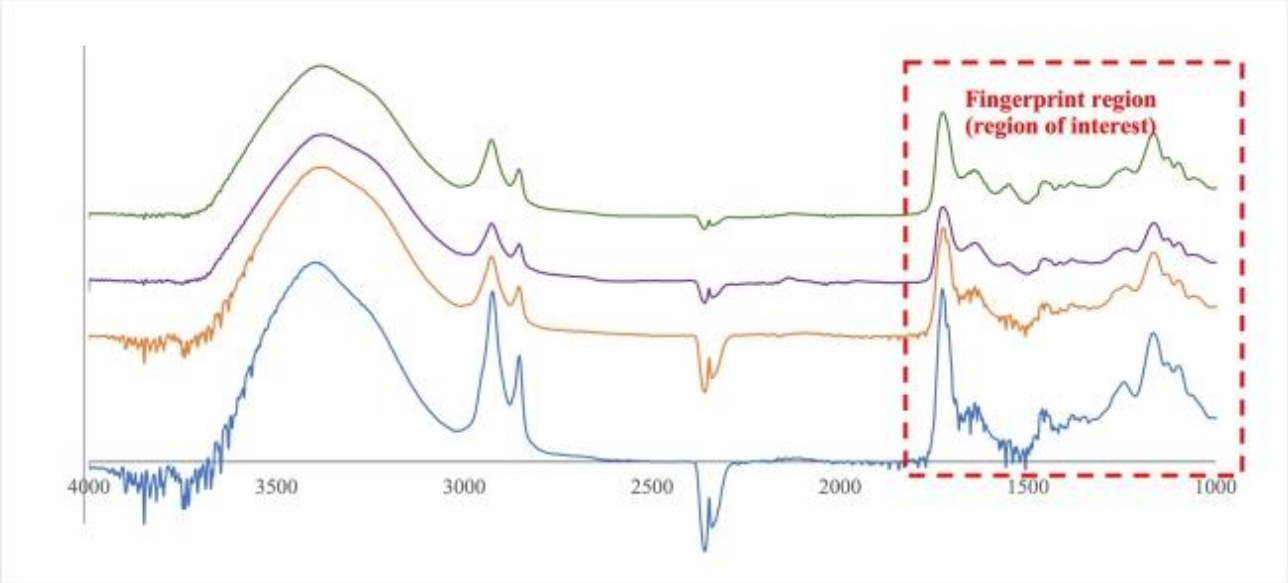

Figure 5.10 - FTIR spectra of different treated PGS-M scaffolds normalised at the amide I peak (1645 cm^{-1}). The main peaks and regions of interest are indicated.

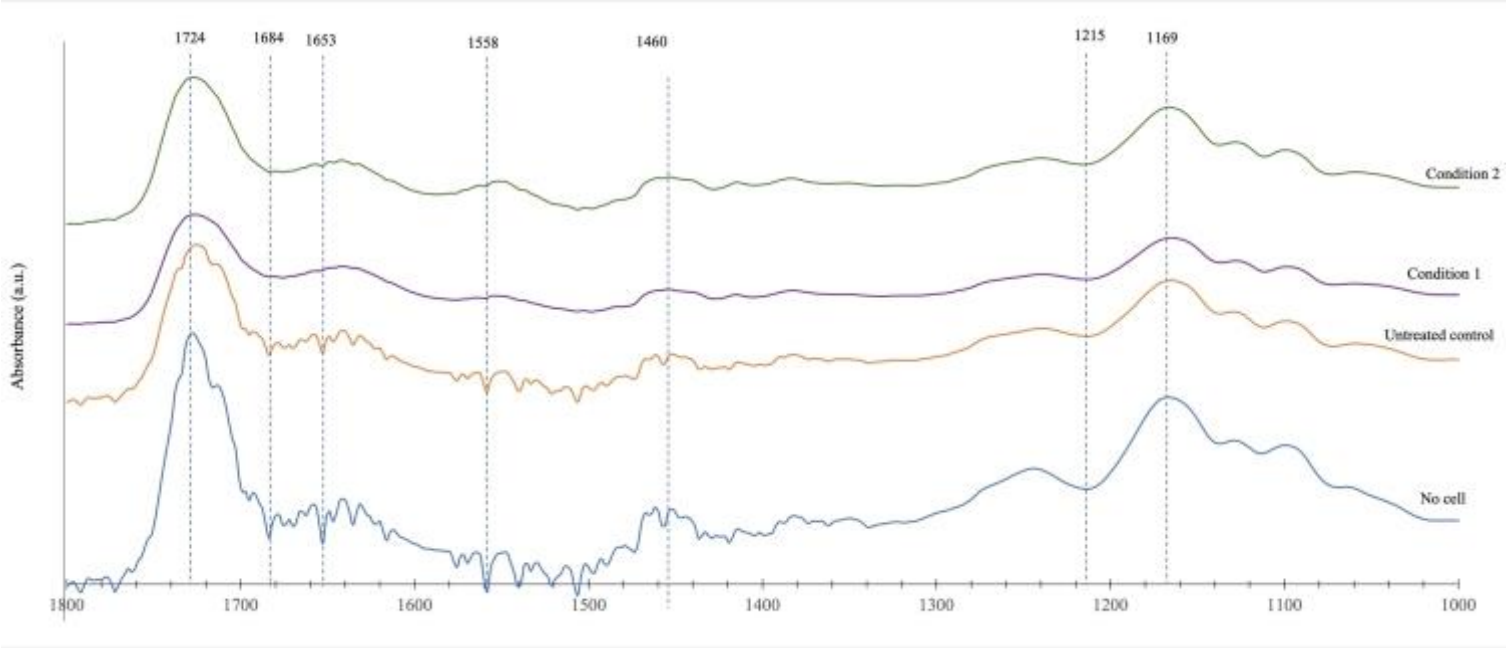

Figure 5.11 – FTIR spectra at fingerprint region (1000-1800 cm^{-1}) of blank PGS-M scaffold, untreated PGS-M with cells, and 2 different decellularised conditions of PGS-M scaffold; 3 cycles of dH_2O at 37 degrees and 3 cycles of freeze and thaw dH_2O.

Figure 5.10 exhibits the spectra collected by using FTIR technique. Since FTIR analysis also able to examine the presence of the amine group, which is associated with collagen I, Figure 5.11 represents the focused spectra where the amine group's wavelength is included. Interestingly, the amine group peak was more pronounced in condition 1 and condition 2 scaffolds, while it dropped in both the control and background scaffolds. This suggests that the amine group, and by extension, collagen I, may be more preserved in condition 1 and condition 2 scaffolds compared to the control and background scaffolds. Furthermore, the analysis indicated that the percentage of collagen I was higher in condition 1 and condition 2 scaffolds compared to the control and background scaffolds. This observation aligns with the trend observed in the amine group peak, further suggesting that collagen I content was relatively well-preserved in condition 1 and

condition 2 scaffolds. These findings provide valuable insights into the retention of collagen I, an essential extracellular matrix component, in the PGS-M scaffolds following the decellularisation process.

This thesis introduced two methods aimed at minimizing negative effects on the extracellular matrix (ECM) structure. Both techniques appeared to successfully lyse the cells inside the PGS-M scaffolds and maintain the hydrophilicity of the scaffold compared to the control. However, the freeze and thaw technique seemed to offer an advantage in terms of ultimate tensile strength, as it showed no significant difference compared to the control and background scaffold. In contrast, incubating the scaffold in dH_2O inside an incubator decreased the ultimate tensile strength. One hypothesis is that the scaffold started to degrade more rapidly at higher temperatures, and the physical approach using the rapid change of temperature in the freeze and thaw technique may be a promising method compared to the osmotic shock approach alone. These findings highlight the potential of the freeze and thaw technique for effective decellularisation of PGS-M scaffolds while preserving their mechanical properties, making it a promising method for various tissue engineering applications.

5.2 Recellularisation

5.2.1 DNA quantification of recellularised scaffolds

To confirm that the hybrid PGS-M scaffolds can support HDF re-culture, a recellularisation experiment was conducted. The objective was to validate the hypothesis that the decellularised PGS-M scaffold is capable of facilitating cell adhesion and can serve as a suitable scaffold for cell culture when compared to blank PGS-M scaffolds. Given that this

test focuses on assessing cell activities, no collagen-related assay or test was performed. Instead, the resazurin and picogreen assays were utilised to assess the cells and ensure their successful reattachment to the scaffold surface.

Figure 5.12 presents the cell metabolism data of HDFs on decellularised scaffolds. HDFs were also seeded onto freshly prepared PGS-M scaffolds, which served as the 3D control for this experiment. After one week of cell culture, the cell metabolism was quantified. As depicted in Figure 5.12, there was no significant difference observed among the three different sets of scaffolds. This suggests that after one week of cell culturing on decellularised scaffolds, the cells are capable of attaching and growing within the scaffolds, comparable to the 3D control.

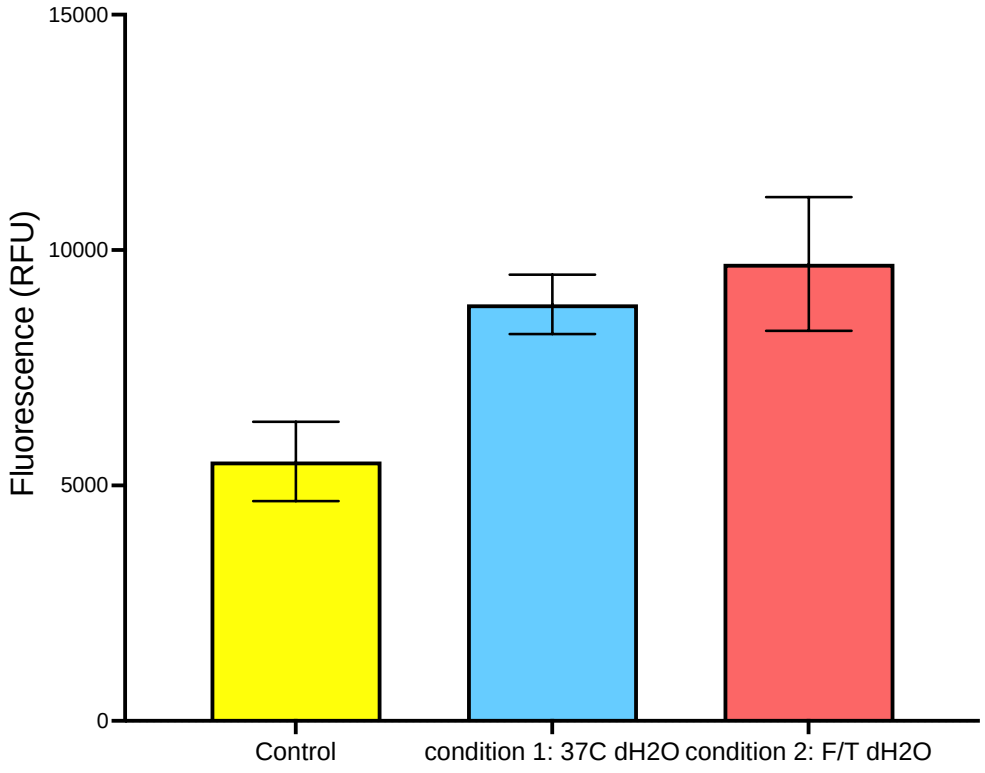

Figure 5.12 – The bar graph depicts the metabolic activity extracted from 80% emulsion PGS-M scaffolds after recellularisation. The examination was conducted using a resazurin assay. One-way ANOVA was used to analyse the data (N=1, n=3).

Picogreen was used to quantify the number of cells, serving as a quantifying assay. In terms of cell number, condition 1 yielded results similar to what was expected from the PGS-M scaffold, as represented by the control. However, in contrast, the number of HDFs cultured from condition 2 significantly increased and surpassed both the control and condition 1. The results from the decellularisation step had already confirmed the successful removal of cells by both techniques. Therefore, Figure 5.13 indicates that condition 2 was the superior choice for decellularising the scaffold and supporting cell regrowth.

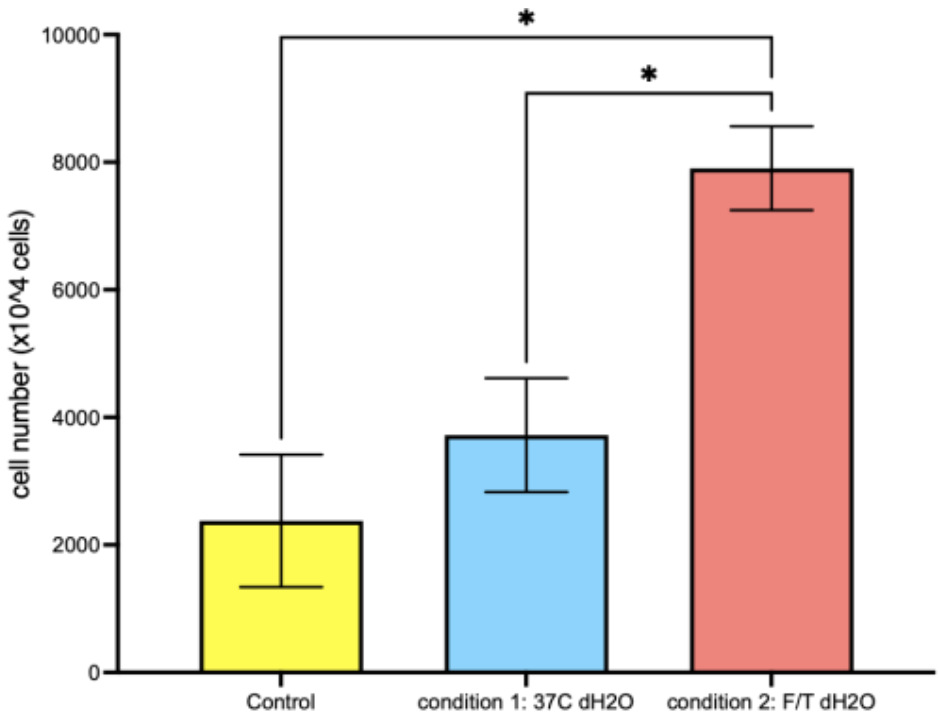

Figure 5.13 – The cell number extracted from 80% emulsion PGS-M scaffolds after recellularisation. The examination was conducted using a picogreen assay. One-way ANOVA was used to analyse the data (N=1, n=3). The asterisk (*) indicates the significant difference in P value < 0.05.

This thesis employed two techniques to establish a guideline for further research. While Figure 5.12 showed no difference between the decellularised conditions, Figure 5.13,

which evaluated the number of cells, suggested that the ECM on the hybrid scaffold could influence cell adhesion initially, potentially increasing the rate of cell proliferation in condition 2. This phenomenon may be attributed to the effect of the decellularisation technique on the PGS-M polymer. The freeze and thaw technique has been applied in the decellularisation of various tissue-engineered organs, such as the lungs [134], meniscus [158], and tendon [159]. Reports indicate that when the freeze and thaw technique is used for cell lysis, it preserves most of the mechanical properties [95, 134, 158]. According to Ding et al. [158], this technique is more suitable for less dense tissues, which aligns with the PGS-M hybrid scaffold's intended use in soft tissue engineering. Considering that the PGS-M polymer is sensitive to higher temperatures and that exposure to temperatures below 0°C does not negatively affect the scaffold, the freeze and thaw technique (condition 2) appears to be a superior approach compared to incubation at 37°C (condition 1). When combining the data from decellularisation and recellularisation, it becomes evident that the freeze and thaw technique is an appropriate approach for cell lysis, DNA removal, and recellularisation of the biohybrid scaffold. This technique effectively lyses cells while preserving the scaffold's mechanical properties.

5.2.2 Histological staining

After one week of cell culture on the decellularised PGS-M scaffolds, the scaffolds were fixed and then underwent recellularisation. Figure 5.14 displays the H&E-stained sections of (a and b) recellularised condition 1 and (c and d) condition 2 scaffolds. The images were captured using (a and c) a 4x and (b and d) a 10x objective lens. Based on Figure 5.14, the cells were able to grow inside the scaffold and on the surface. When comparing the pink colouration between the two techniques, condition 2 appeared to be darker, which might indicate a higher amount of soluble protein produced by HDFs. In terms of the cell number indicated by dark purple staining, the number observed in condition 2 was higher than in condition 1. This result is consistent with the cell count data collected from the picogreen assay (Figure 5.13). Considering the cell distribution, most of the cells were located at the top part of the scaffold near the surface in both conditions. However, as some of them had already proliferated inside the PGS-M scaffolds, both techniques still served as a 3D template and supported cell proliferation.

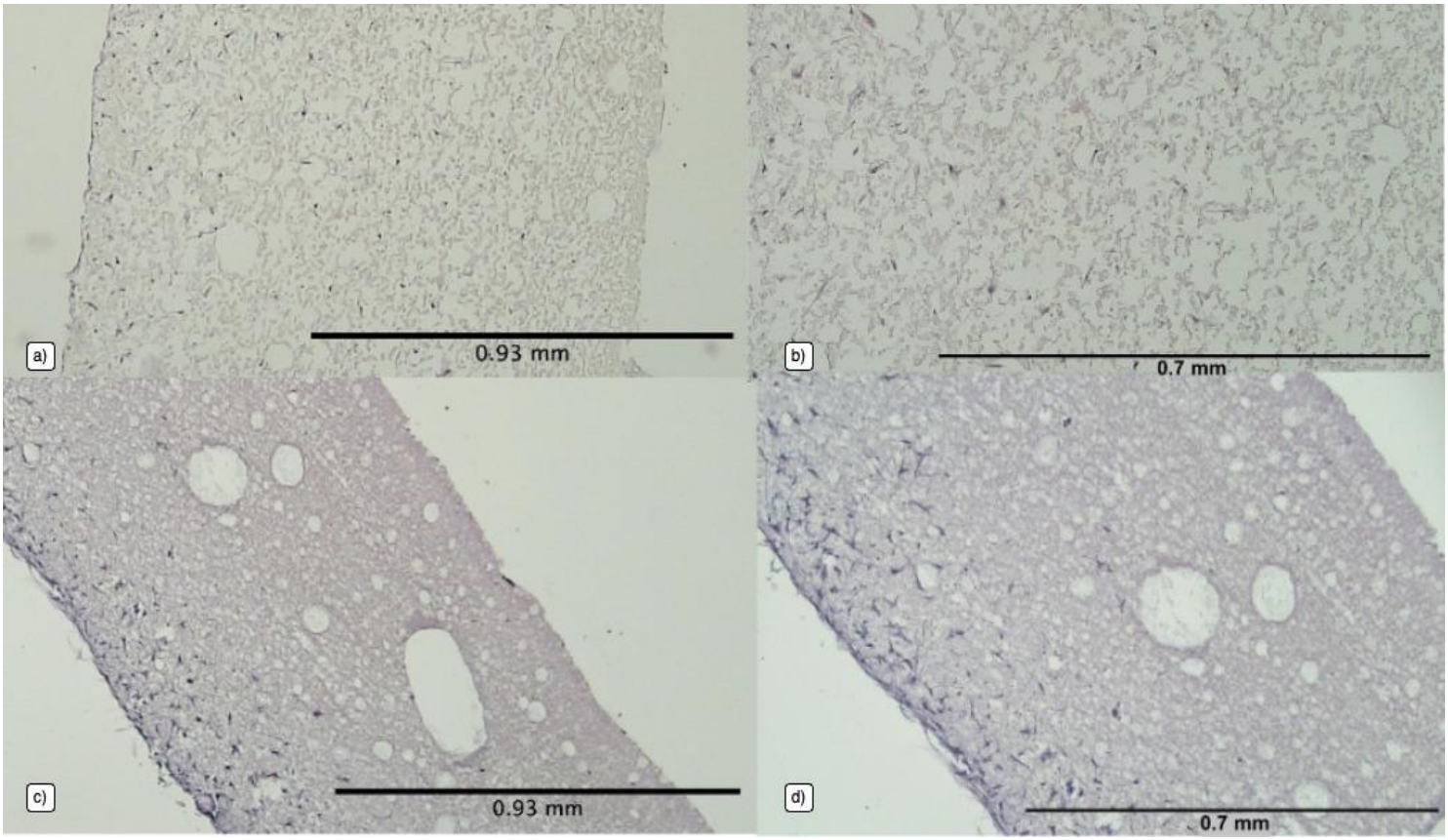

Figure 5.14 – The H&E -stained images after one week cell culture of the (a and b) condition 1 and (c and d) condition 2 decellularised scaffolds (N=1, n=2).

The results of the H&E staining already indicated that after 3 weeks of cell culture (2 weeks before decellularisation and 1 week after recellularisation), the cells still could not produce a proper ECM structure and needed more time to proliferate and fill the scaffold.

The IHC technique was also employed to assess the cell response after decellularisation. The recellularisation step aimed to observe the potential of the hybrid scaffold after being decellularised. Figure 5.15 displays the recellularised (left) condition 1 and (right) condition 2 PGS-M scaffolds. From the images, it appears that both techniques supported recellularisation. Blue and yellow markers were visible in both samples, indicating that the cells were able to proliferate inside the scaffolds and were in a state of readiness for further proliferation.

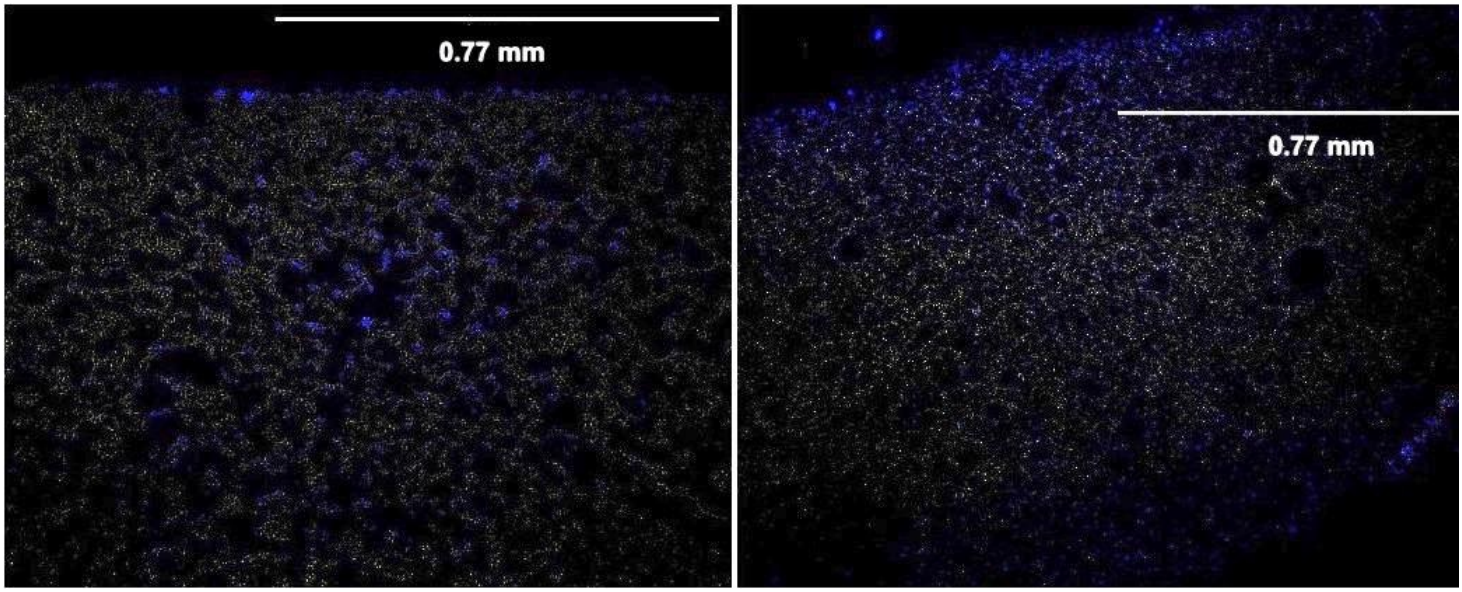

Figure 5.15 – The IHC-stained images of recellularised (left) condition 1 and (right) condition 2 scaffolds, where blue refers to cell nuclei (DAPI) and yellow refers to actively proliferating cells (Ki-67) (N=1, n=2)

Based on the recellularisation results, where other outcomes showed no significant difference, the cell number extracted from condition 2 exceeded the cell number extracted from condition 1. Notably, collagen is typically insoluble in water, but it can become soluble with changes in pH. The collagen's form significantly impacts its mechanical properties [160]. H&E staining (Figure 5.11) indicated that collagen had merged with the

scaffold. This suggests that after two weeks of cell culture, HDFs may primarily produce soluble collagen. Collagen VI, found in many connective tissues including skin, can be produced in a water-soluble form [161, 162]. Hatamochi et al. [163] have demonstrated that collagen VI levels increase with higher cell density. This corresponds with the cell number results, particularly near the surface where cell numbers were higher. Nevertheless, additional research is required to optimise the appropriate duration for culturing HDFs to achieve the desired ECM structure.

Regarding Ki-67 staining, condition 2 demonstrated the inability to eliminate HDFs while preserving the proliferating marker within the scaffolds. Conversely, condition 1 treatment resulted in the removal of all cells and most proliferating markers. A similar trend was observed by Ning et al. [159], who found that repeated freeze and thaw cycles were ineffective in removing cells and nuclear debris. To enhance the lysing capability, Lu et al. [95] successfully optimised the freeze and thaw technique by incorporating NH4OH or ammonia as a detergent. Their study reported that the use of ammonia in conjunction with the freeze and thaw technique effectively removed all cells and induced a mild host response, which was deemed acceptable. Therefore, the use of nucleus treatment or detergent in combination with the freeze and thaw technique was recommended. Interestingly, not only detergents but also a physical approach has been employed to optimise decellularisation using the freeze and thaw technique. Ding et al. [158] combined these two approaches by incorporating DNase while grinding the meniscus. By mincing and grinding the bovine meniscus before decellularisation, the surface area in contact with the solution was increased, enhancing the chances of effectively eliminating cells.

As no reports exist on the appropriate decellularisation technique for the PGS-M scaffold, this thesis preliminarily focused on two physical approaches, excluding the use of detergent. This choice was made due to the unknown effects of different detergents on this polymer. Utilising only physical approaches does not aggressively impact the scaffold and lays the groundwork for further research involving various reagents and the combination of multiple techniques.

The suitability of PGS-M scaffolds as a platform for cell cultivation has been demonstrated. However, recellularisation remains essential, particularly considering the intended use of the scaffold within the human body. Given the sensitivity of the PGS-M polymer to heat, the freeze and thaw technique (condition 2) may serve as a suitable method for lysing cells when compared to the use of heat (condition 1). Freeze and thaw also support recellularisation. Therefore, the preferred decellularisation technique for PGS-M scaffolds is the freeze and thaw method.

Chapter 6 – Mechanical Stimulation

To produce the hybrid scaffold, cells and ECM production play a crucial role [22]. Therefore, mechanical stimuli are employed to enhance cell proliferation and ECM production [39, 82]. Detailed discussions on this topic can be found in Chapter 2. Numerous adjustments and refinements were made to achieve optimal settings for fabricating the hybrid PGS-M scaffold. The optimisation of the manufacturing, sterilisation, quantification, and decellularisation processes has been previously addressed in earlier chapters of this thesis. It has been previously observed that mechanical stimulation increases collagen synthesis in HDFs cultivated on a PGS-M scaffold in vitro [82]. This section will delve into various mechanical stimulation regimes. These routines were developed when it was discovered that some of the stimulating effects had already been mentioned in the literature and my master's thesis.

6.1 pH control using HEPES buffer

The Ebers incubator serves as the main incubator for studies requiring mechanical stimulation. All components of this bioreactor collaborate to create a self-contained unit; the Ebers chambers can be loaded quickly and easily, allowing experiments to resume without disruption. Typically, this bioreactor operates within a customized incubator, which maintains a pH and temperature-controlled environment for the cells. Within these incubators, pH stability is ensured at a physiological level through a combination of a 5% CO_2 atmosphere and a bicarbonate buffer in the culture medium. Unfortunately, during the course of this project, an issue arose when both the gas inlet and temperature controls

failed simultaneously. The temperature exceeded 37°C, and the CO_2 level fell well below the minimum required of 5%. The colour of the cell culture medium also changed from pink to yellow, indicating an acidic pH condition. Consequently, the experiment had to be prematurely halted.

The two issues became the focus of numerous attempts at resolution. Although the temperature control problem was readily resolved with the installation of a new temperature probe, replacing the gas inlet valve controller proved impossible, and pH levels in the culture medium remained uncontrolled, rendering it unsuitable for cell growth. Consequently, attempts were made to address this problem by incorporating a HEPES buffer into the culture medium. In the absence of CO_2, HEPES buffer is capable of adjusting the pH of the medium to a level similar to that found in the human body (approximately pH 7) [164, 165].

The effects of varying HEPES buffer concentrations in a Complete DMEM medium on pH are depicted in Figure 6.1, while a statistical comparison of the results is presented in Table 6.1. A significant difference in pH was observed in the culture medium when using a 5% CO_2 environment compared to a low CO_2 environment. However, no difference in pH was observed with the increase in HEPES concentration in either case. Despite the incorporation of several HEPES buffer concentrations, no discernible change was evident. The data obtained from the Ebers incubator indicated no significant pH change between the two concentrations. When measuring the pH of the medium after incubation in both the standard and the Ebers incubators, it was found that the standard incubator had a pH value approximately 2 levels lower.

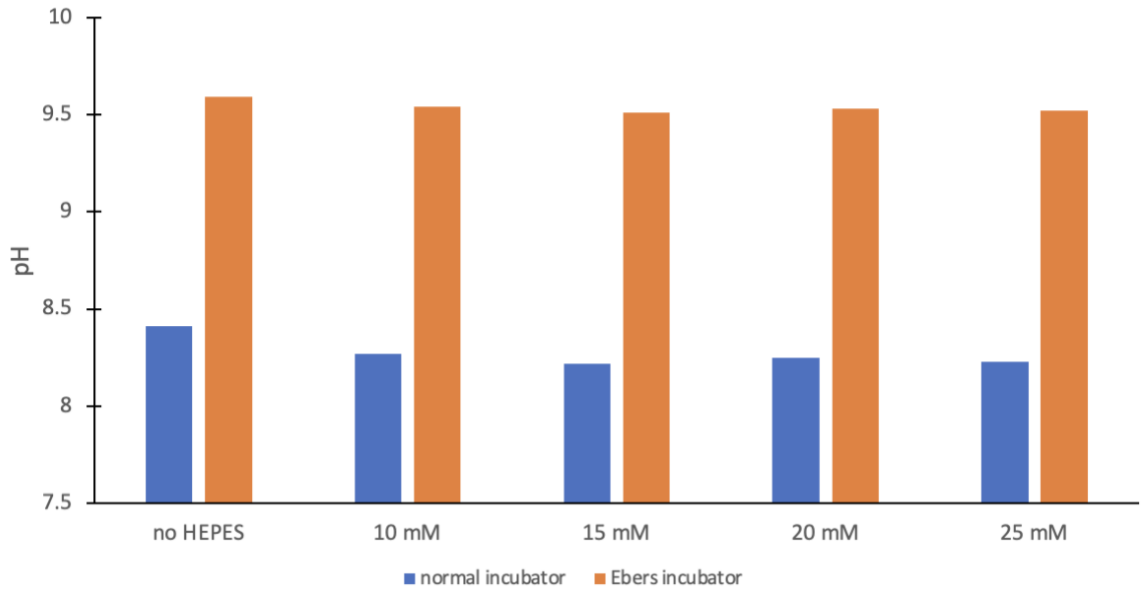

Figure 6.1 – the bar graph demonstrates the pH of the medium when different concentration of HEPES buffer is added to complete DMEM medium after 7 days. Blue represents the pH obtained in a 5% CO_2 environment, while orange shows the pH in the Ebers incubator, without a controlled CO_2 environment (N=1, n=3)

	normal no HEPES	10 mM	15 mM	20 mM	25 mM	Ebers no HEPES	10 mM	15 mM	20 mM	25 mM
no HEPES		*	*	*	*	****	****	****	****	****
10 mM			x	x	x	****	****	****	****	****
15 mM				x	x	****	****	****	****	****
20 mM					x	****	****	****	****	****
25 mM						****	****	****	****	****
no HEPES							x	x	x	x
10 mM								x	x	x
15 mM									x	x
20 mM										x
25 mM										

Table 6.1 – the table depicts the statistical comparison between the complete DMEM medium incubated in the normal 5% CO_2 environment and the low CO_2 environment of the Ebers incubator.

The pH of the human body is buffered and naturally maintained in a healthy state without reliance on external buffers. However, when conducting an in vitro experiment, this natural regulation becomes irrelevant. To counteract the acidic conditions inherent in in vitro experiments, HEPES buffer, a naturally occurring chemical, is employed. It is used

to simulate the internal human environment in cases where the pH is suboptimal for cell culture [165].

Since the CO_2 level in the Ebers incubator was unstable and uncontrollable due to the gas valve failure, a new plan had to be devised before resuming the experiment. To address this issue, measures were taken to chemically buffer the pH. HEPES buffer was chosen, as it maintains a healthy pH of 7.4 [166, 167].

It has been reported that HEPES buffer can be utilised to maintain pH stability, although the results of experiments in this thesis with varying doses of HEPES appeared to contradict those studies. Inside the Ebers incubator, CO_2 levels were maintained at a minimum unless the lid was opened. Since it was necessary to retain both heat and moisture, the lid could not remain open. Consequently, CO_2 concentration had not reached the target level and was unable to self-regulate. The primary differentiating factor between the findings and the actual scenario was the levels of CO_2. The experiments were reported to have a sufficient concentration of carbon dioxide for the HEPES buffer to maintain an appropriate pH level. Itagaki et al. [168] reported that even in an open flask where gases can freely interchange, a sufficient CO_2 level was necessary for cells to function normally. As CO_2 is still required, using HEPES buffer is not usually conducive to this type of experiment. In cases where the experiment is conducted in a stoppered flask, cells benefit from this buffer. Prior to conducting the test, the pH of the HEPES buffer solution was adjusted to pH 7 using NaOH. The final solution was then sterilised and filtered with a 0.22 µm filter. This was done to ensure that the buffer was at the required pH before being added to the experiment. Since all experiments in this thesis

used open flasks, this explains why the HEPES buffer did not modulate the pH in the well plate, as observed in Figure 6.1.

After the inability to control pH using HEPES buffer, another suitable incubator was acquired, possessing the capability to regulate both CO_2 and temperature at the desired levels. This incubator was utilised for all subsequent experiments.

6.2 Mechanical stimulation

Although established that mechanical stimulation can enhance both cell proliferation and collagen formation, as extensively discussed in Chapter 2, there is scarce published research detailing the optimal regimes for augmenting collagen production. To attain the desired outcomes, various potential parameters can be modified. These include travel distance, frequency, amplitude, resting and stimulating periods, and the incremental adjustment of a parameter during an experiment.

In preliminary work conducted during my MSc, mechanical regimes were initially assessed using PGSM-50 E scaffolds (50% methacrylate, fabricated through the emulsion templating process) [82]. This investigation revealed that one week of continuous incremental stimulation yielded the highest collagen production per cell, while increasing the stimulation amplitude resulted in an overall increase in total collagen production.

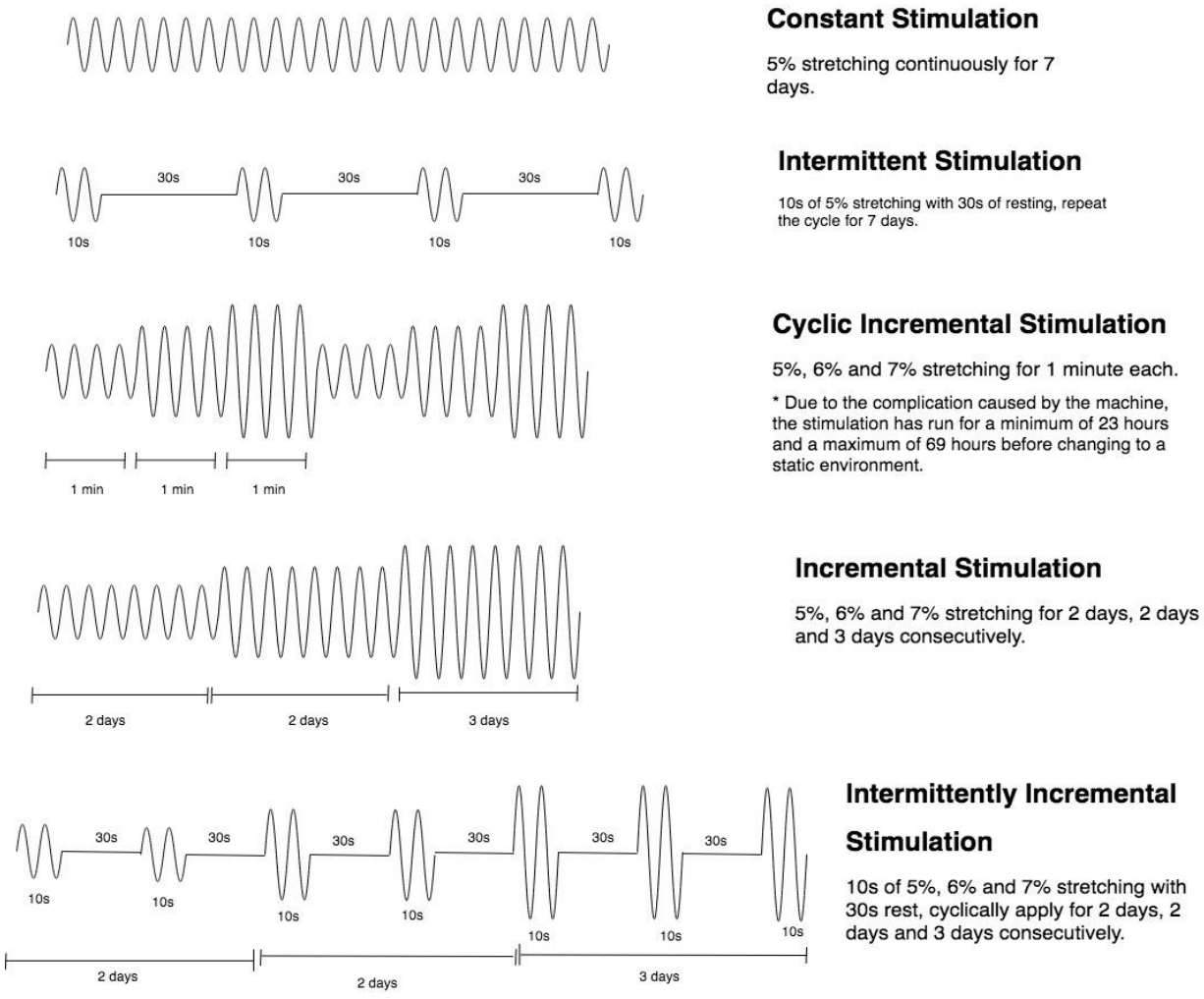

Figure 6.2 – The mechanical regimes used in the preliminary study [82]. The experiments were set to run for one week before quantifying cell proliferation and collagen production. The amplitude indicates the level of strain applied at a given time.

A preliminary set of mechanical regimes was designed, drawing upon the initial study (Figure 6.2). In all instances, a strain was applied at a frequency of 1 Hz throughout the experiment. It has previously been established that both cell proliferation and collagen formation benefit from the inclusion of a resting interval within each stimulation cycle [82]. The work presented in this thesis builds upon the preliminary data, with regimes applied over a 2-week culture period to further enhance collagen production (Figure 6.3). Similar regimes were employed, with the exception of varying the stimulation amplitude between

five and ten percent of the scaffold's length. Additionally, the same ratio of stimulation, with an extended resting period, is evaluated in this thesis, with two amplitudes. This is in accordance with Schmidt et al.'s [83] suggestion of the benefits of increasing the resting period to 6 hours. The ratio of the length of the stimulating interval to the resting interval was set at 1:3. The thesis concludes with a discussion of the four regimes used throughout: 5% elongation with 10 seconds active and 30 seconds rest (stimulation 1); 10% elongation with 10 seconds active and 30 seconds rest (stimulation 2); 5% elongation with 2 hours active and 6 hours rest (stimulation 3); and 10% elongation with 2 hours active and 6 hours rest (stimulation 4).

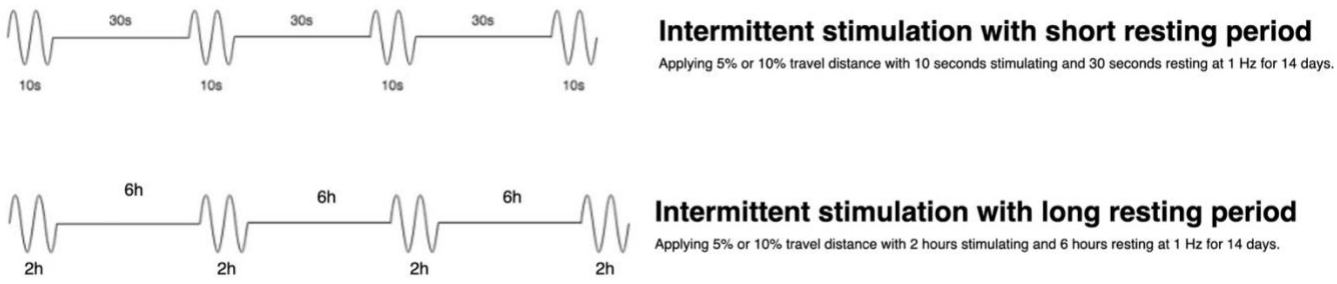

Figure 6.3 – The mechanical regimes used in this thesis. The stimulations were continued for 14 days before examining.

The PGSM-50 E scaffold, sterilised using autoclave, served as the template for cell culture in my MSc report [82]. However, given the optimisation of both the PGS-M scaffold and the sterilisation technique in this thesis (as detailed in Chapter 4), a change was made. For these experiments, the utilised scaffolds were PGSM-80 E, which had undergone O_2 plasma treatment and will be referred to as the PGS-M scaffold. To minimize the potential impact of differing passage numbers of the HDFs on the obtained results, all outcomes were normalized against their respective 3D static control.

The comparison of the metabolic rate of the cells under each stimulation condition is shown in Table 6.2. The Table shows that HDFs had a higher metabolic rate after being exposed to stimulation 1 in comparison to other regimes. However, there was no significantly discernible difference between the control and other stimulation regimes.

Welch's T Test	Below Threshold?	Summary	P Value
No stimulation vs. Int 5% elongation with 10s resting	Yes	*	0.0458
No stimulation vs. Int 10% elongation with 10s resting	No	ns	0.1951
No stimulation vs. Int 5% elongation with 2h resting	No	ns	0.1771
No stimulation vs. Int 10% elongation with 2h resting	Yes	*	0.0225
Int 5% elongation with 10s resting vs. Int 10% elongation with 10s resting	Yes	**	0.0064
Int 5% elongation with 10s resting vs. Int 5% elongation with 2h resting	Yes	*	0.0155
Int 5% elongation with 10s resting vs. Int 10% elongation with 2h resting	Yes	*	0.0318
Int 10% elongation with 10s resting vs. Int 5% elongation with 2h resting	No	ns	0.4911
Int 10% elongation with 10s resting vs. Int 10% elongation with 2h resting	No	ns	0.2945
Int 5% elongation with 2h resting vs. Int 10% elongation with 2h resting	No	ns	0.1021

Table 6.2 – The comparison of Cell metabolic activity under different mechanical regimes after two weeks of stimulation. All the experiments were normalised with its 3D control. The results were statistically analysed with T- Test (N=1, n=2). The asterisk (*) indicates the significant difference in P value < 0.05.

The Picogreen assay was utilised to quantify DNA levels and ascertain whether changes in metabolic activity correlated with alterations in cell number. Table 6.3 presents a comparison of cell numbers under different stimulation regimens, with each result normalized against its corresponding 3D static control. Although HDFs subjected to stimulation 1 displayed a threefold higher cell metabolism compared to those subjected to other regimens, no significant difference was detected between the various stimulation protocols and the control group. This observation could be attributed to the inconsistency

of the technique and might also have been influenced by the presence of a relatively large error bar.

Welch's T Test	Below Threshold?	Summary	P Value
No stimulation vs. Int 5% elongation with 10s resting	No	ns	0.1308
No stimulation vs. Int 10% elongation with 10s resting	No	ns	0.9413
No stimulation vs. Int 5% elongation with 2h resting	No	ns	0.8542
No stimulation vs. Int 10% elongation with 2h resting	No	ns	0.7833
Int 5% elongation with 10s resting vs. Int 10% elongation with 10s resting	No	ns	0.1618
Int 5% elongation with 10s resting vs. Int 5% elongation with 2h resting	No	ns	0.0664
Int 5% elongation with 10s resting vs. Int 10% elongation with 2h resting	No	ns	0.0645
Int 10% elongation with 10s resting vs. Int 5% elongation with 2h resting	No	ns	0.9984
Int 10% elongation with 10s resting vs. Int 10% elongation with 2h resting	No	ns	0.9676
Int 5% elongation with 2h resting vs. Int 10% elongation with 2h resting	No	ns	0.9392

Table 6.3 –The comparison of the number of cells from different mechanical regimes after two weeks of stimulation. All the experiments were normalised against the equivalent 3D control. The results were statistically analysed with T-Test (N=1, n=2).

Considering that the primary objective of this thesis is to develop a hybrid, ECM-based scaffold from a synthetic PGS-M scaffold, the total collagen content is regarded as one of the most crucial factors. To quantify the collagen content following stimulation, the optimised picrosirius red methodology, as described in Chapter 4, was employed. Table 6.4 presents a comparison of the total collagen measured after each stimulus. As shown in the table, only stimulation 4 exhibits a significant increase compared to both the 3D control and the other regimens. In stimulation 4, characterized by a longer stimulation duration and greater amplitude, approximately five times more collagen is generated than in the static 3D control. These results suggest that exposing HDFs to an extended resting period in conjunction with a higher strain leads to increased collagen production, a vital component of the ECM matrix.

Welch's T Test	Below Threshold?	Summary	P Value
No stimulation vs. Int 5% elongation with 10s resting	No	ns	0.3752
No stimulation vs. Int 10% elongation with 10s resting	Yes	*	0.0275
No stimulation vs. Int 5% elongation with 2h resting	No	ns	0.1656
No stimulation vs. Int 10% elongation with 2h resting	Yes	*	0.0335
Int 5% elongation with 10s resting vs. Int 10% elongation with 10s resting	No	ns	0.1427
Int 5% elongation with 10s resting vs. Int 5% elongation with 2h resting	No	ns	0.3384
Int 5% elongation with 10s resting vs. Int 10% elongation with 2h resting	Yes	**	0.0092
Int 10% elongation with 10s resting vs. Int 5% elongation with 2h resting	No	ns	0.0842
Int 10% elongation with 10s resting vs. Int 10% elongation with 2h resting	Yes	*	0.0256
Int 5% elongation with 2h resting vs. Int 10% elongation with 2h resting	Yes	**	0.0086

Table 6.4 – The comparison of collagen production collected from different mechanical regimes after two weeks of stimulation. Results are shown as a % of the static 3D control. All the experiments were normalised with its 3D control. The results were statistically analysed with T-Test (N=1, n=2). The asterisk (*) indicates the significant difference in P value < 0.05.

Since this finding suggests that an increase in cellular metabolism is relevant to cell growth, the experiments investigated the effects of varying the resting period and the amplitude size on cell proliferation and collagen production. Stimulation 1, characterized by smaller displacement and a shorter resting period, is reported to stimulate cell proliferation. Ugolini et al. [88] reported a similar effect through the reduction of strain. In their study, they employed 2% and 8% cyclic strains to stimulate cardiac fibroblasts. The 2% cyclic strain induced a higher rate of cell proliferation in cardiac fibroblasts compared to the 8% strain. Park et al. [147] also examined the impact of uniaxial strain on cutaneous fibroblasts cultured on a chitosan scaffold. Their research investigated the effects of cyclic mechanical strain. According to their findings, mechanical stimulation not only increased the quantity of cells but also stimulated the secretion of growth agents such as IL-6 and VEGF. Although their study used a single amplitude, the increase in growth factor

secretion resulting from stimulation suggests that with the use of an appropriate amplitude, cells will secrete more growth factors, thus promoting cell proliferation and metabolism.

Joshi et al [169] revealed that fibroblasts have the capacity to respond to various stimuli. In their experiments, they assessed multiple parameters, including force amplitude (2.5-10%), frequency (0.1-1 Hz), and the number of daily cycles. They found that the elastic modulus was enhanced by low amplitude (2.5% strain) at a lower frequency (0.1-0.5 Hz). Unfortunately, due to the limitation of only being able to set three scaffolds per chamber, I couldn't explore this property in this thesis. At the time of the experiments, there were only two usable chambers, and all six scaffolds were meticulously allocated to different tests.

However, as reported by Joshi et al.[169], the increase in elastic modulus is linked to ECM production by cells. It's possible that the signaling pathways necessary for increased ECM synthesis and subsequent mechanical strength are not activated under regimes characterized by low total cycle numbers or low frequency combined with limited duration. This could explain the result of enhanced collagen production observed with larger amplitude and longer exposure time. Since they also reported that fibroblasts can sense multiple stimuli simultaneously, this observation that cells can detect various stimuli explains the interaction plots, where cells respond differently to each combination of amplitude and resting time.

The effect of uniaxial stretching on cell proliferation was described by Yang et al. [170]. Human patellar tendon fibroblasts were subjected to intermittent mechanical stretching at 4% and 8% displacement (0.5 Hz for 4 hours of stimulation and 20 hours of resting). Activating the cells by subjecting them to a greater degree of elongation was found to

boost the rate of cell proliferation. However, there was no significant difference between the stimulated and unstimulated models for the smaller strain amplitude.

Schmidt et al. [83] 83] previously published a comparison of constant, intermittent, and gradual stimulation on cutaneous fibroblasts. This study reported that resting time increases the levels of extracellular signal-regulated kinase 1/2 (ERK1/2), which are proteins involved in the cell mitotic process. The article also indicated that ERK1 and ERK2 were fully reactivated after a 6-hour rest period for the cells. However, when the rest period was shorter, the level of ERK1/2 was lower than the initial stage. Since ERK1/2 signaling pathways are essential for collagen transcription, the reactivation of both ERK1 and 2 resulted in higher collagen production.

In the context of collagen formation, several studies have highlighted the routines that can promote collagen production. Multiple articles [87, 89, 92] have confirmed that uniaxial mechanical stretching enhances collagen content. Yang et al. [170] revealed that intermittent uniaxial stretching stimulates not only cell proliferation but also collagen synthesis. Similarly, Manuyakorn et al. [89] reported that cyclic mechanical stimulation increased collagen production by bronchial fibroblasts, specifying the elevated collagen types as types I and II. To provide more specificity, Lohberger et al. [93] subjected degenerative rotator cuff fibroblasts to intermittent stimulation for 7 and 14 days. Their findings showed a substantial increase in overall collagen content after intermittent stimulation.

Remarkably, Coeyman et al. [171] depicted the effect of mechanical stimulation in such a way that tissue stiffness improved after three days of stimulation. This suggests that

mechanical stimulation, particularly intermittent stimulation, can enhance collagen formation and improve tissue stiffness [169].

According to research articles provided by scientists, even though mechanical stimulation enhances cell growth and collagen content, the best procedure remains dependent on various factors and can assume multiple forms. This variability may arise from differences in cell type, scaffold material, and stimulation conditions. As there is a lack of a direct comparison of the effects of different resting intervals and amplitudes on HDFs cultured on PGS-M scaffolds, it is conceivable that the recommendations found in these publications may not be directly applicable to the primary fibroblasts used in this research. Further research is still necessary to determine the optimal regimen suitable for this specific application.

To evaluate the effects of mechanical stimulation, histological techniques were employed alongside colourimetric assays. In order to gain insights into the potential elastin structure produced by HDFs, the EVG assay was also conducted. However, the PGS-M scaffold, as demonstrated in the previous chapter, absorbed the stain, rendering it unobservable. In this case, the cells and ECM synthesis were examined using the H&E assay. Immunohistochemistry (IHC) was conducted to analyse the behaviour of HDFs post-stimulation, utilising DAPI and Ki-67 staining.

Figure 6.3 presents typical examples of H&E stained sections from various categories. Figures 6.3 a), c), and e) were acquired using a 10x objective lens, while 6.3 b), d), and f) were captured using a 20x objective lens. The same staining procedure was employed for all sections. Figures 6.3 a) and b) serve as positive controls for the staining process, depicting the human epidermis. In order to evaluate the staining procedure on the PGS-

M scaffold, the background scaffold was stained, as illustrated in Figure 6.3 b) and d). In Figures 6.3 e) and f), which depict scaffolds that did not undergo mechanical stimulation, the weak staining of the background scaffold with H&E indicated that the PGS-M scaffold itself was not stained by H&E. Without mechanical stimulation, these images demonstrate that HDFs were primarily observed on the scaffold's surface, although some cells were also observed within the scaffold after two weeks of stimulation.

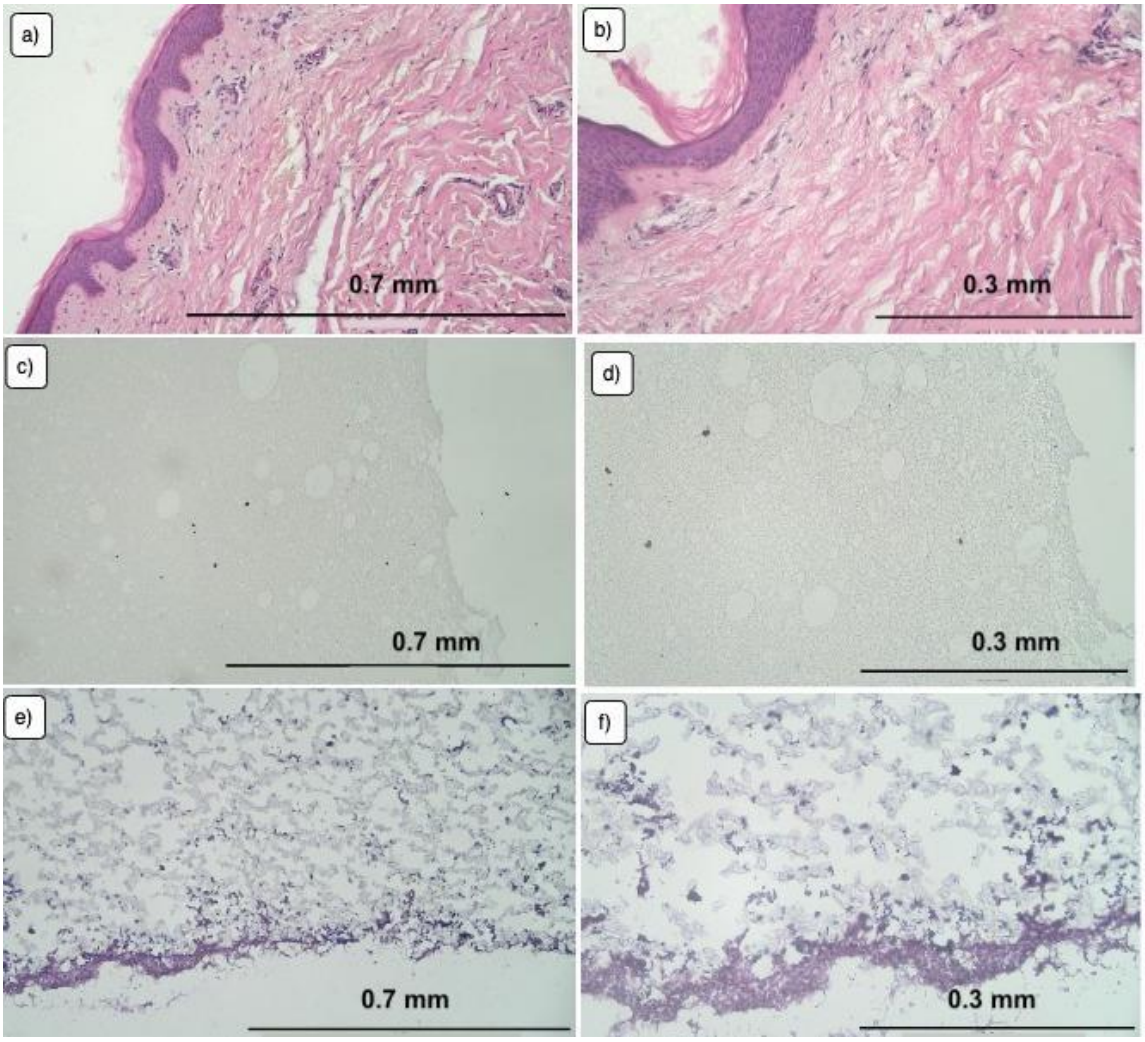

Figure 6.3 – the H&E images of (a and b) from human epidermis, (c and d) the unseeded PGS-M scaffold or 'background' and (e and f) the static, cultured PGS-M scaffolds or '3D control'. Both images from each category were representative images from different magnification in which the scale bar is attached. Purple colour represents the cells and pink demonstrates the ECM structure.

Figure 6.4 displays H&E-stained sections using four distinct regimes as examples. The photographs on the left were taken with a 10x objective lens, while the images on the right were captured with a 20x objective lens. Metabolic activity and collagen quantification assays have indicated that stimulation 1 promoted the highest level of cell growth, while stimulation 4 resulted in maximum collagen production. Unfortunately, Figure 6.4 reveals partially deteriorated scaffolds that are challenging to analyse. This could be attributed to the scaffolds being stimulated for two weeks before fixation and storage in PBS for several months, as they could not be processed and stained immediately due to Covid-19 limitations. Nonetheless, it is still evident that all stimulations led to cell infiltration into the scaffolds.

It is worth noting that there appears to be an increase in cells within the scaffold with stimulation 1 (Figure 6.4 a and b). Additionally, stimulation regime 4 seems to have produced a more pronounced layer of cells on the surface, displaying some pink staining indicative of ECM generation.

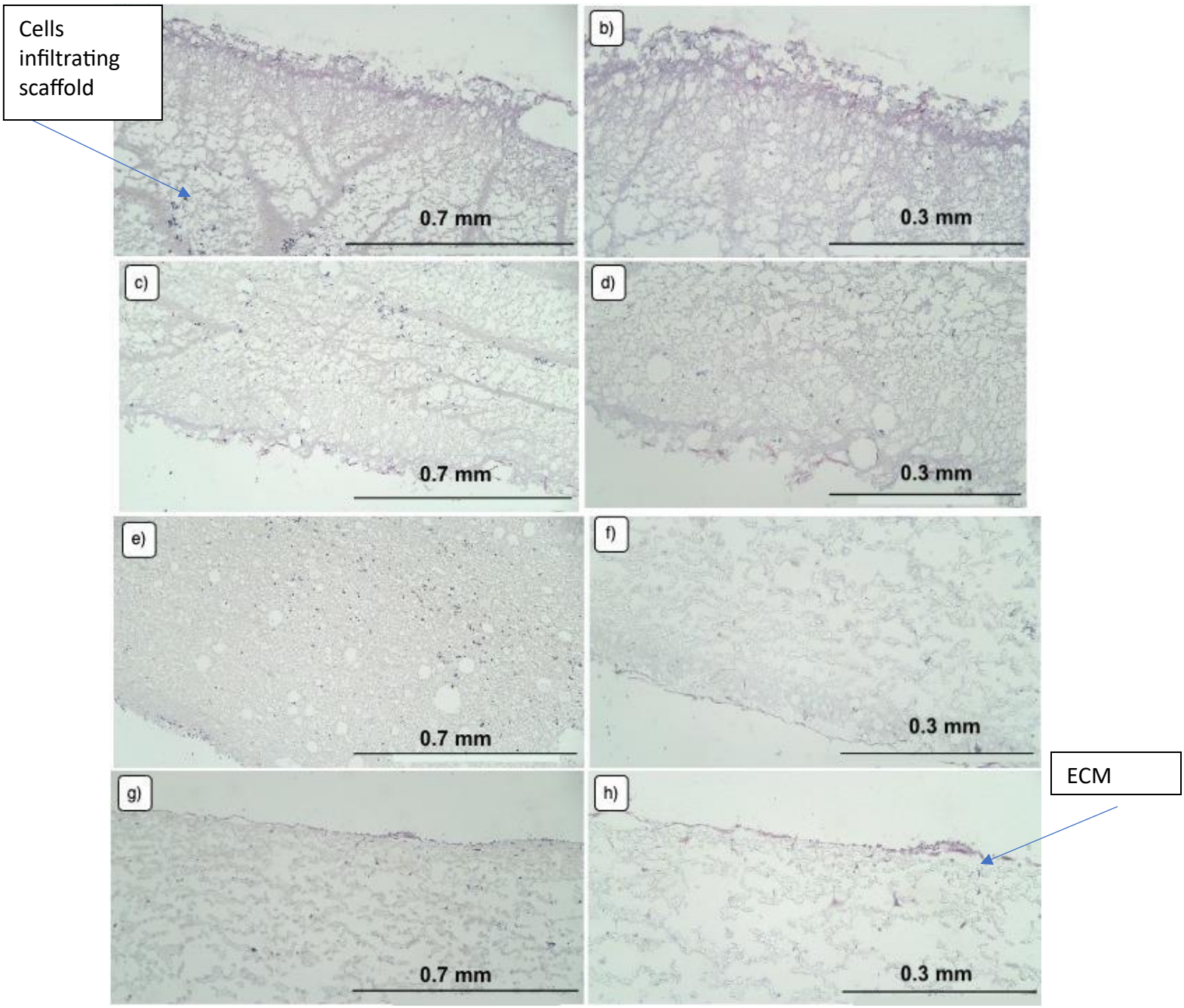

Figure 6.4 – the H&E images of the cultured PGS-M scaffolds after being stimulated by (a and b) stimulation 1, (c and d) stimulation 2, (e and f) stimulation 3 and (g and h) stimulation 4. Both images from each category were representative images from different magnification in which the scale bar is attached. Purple colour represents the cells and pink demonstrates the ECM structure. The arrows indicate the cell infiltration into the scaffold and the ECM production.

DAPI and Ki-67 were employed to investigate cell nuclei and cells undergoing mitosis, providing a closer examination of cell behaviour. Figure 6.9 presents images obtained using the IHC approach, depicting the human epidermis, an unseeded background scaffold, and a static, cultured 3D control scaffold. All photos were captured with a 10x objective lens and a scale bar of 0.77 mm.

The representative image of human skin after protocol optimisation (Figure 6.5 a)) clearly shows cobblestone-shaped nuclei (blue) and the Ki-67 marker (yellow). Each IHC image underwent the same optimisation process. An image of the background PGS-M scaffold was also obtained, revealing that the scaffold exhibits autofluorescence or non-specific staining (Figure 6.5 b). The 3D control image (Figure 6.5 c) displays the cell clusters that adhered to and proliferated on the PGS-M scaffold.

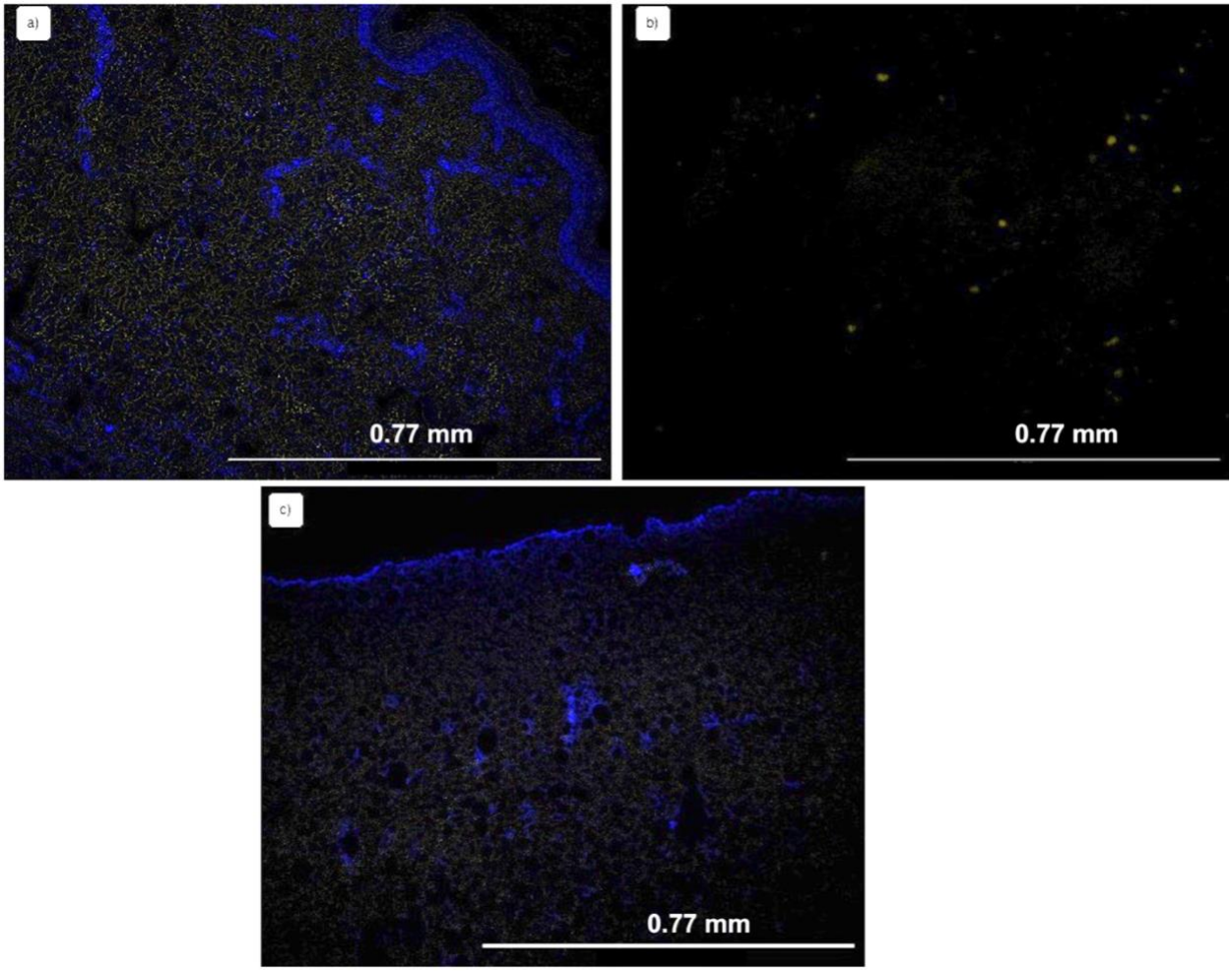

Figure 6.5 – the IHC images of (a) the donor's epidermis, (b) the unseeded PGS-M scaffold or 'background' and (c) the static, cultured PGS-M scaffolds or '3D control'. Both images from each category were representative images from different magnification in which the scale bar is attached. Blue colour (from DAPI) represents the nuclei and yellow (from Ki-67) demonstrates the cells that were duplicating at the time of fixing.

Each stimulus was applied to the cultured PGS-M scaffolds for a two-week period before fixation with 3.7% formaldehyde. Subsequently, the scaffolds were stored in PBS at 4 °C until staining. Figure 6.6 presents fluorescent images of the stimulated PGS-M scaffolds. Consistent with the H&E staining, staining of the cell nuclei (blue) reveals that the majority of cells were situated on the surface of the PGS-M scaffold, although some cells can still be observed within the scaffold. Notably, in the case of the DAPI signal in Figure 6.6 d),

derived from stimulation 1 and 4, the cells appeared to fill the scaffold more extensively compared to other regimes.

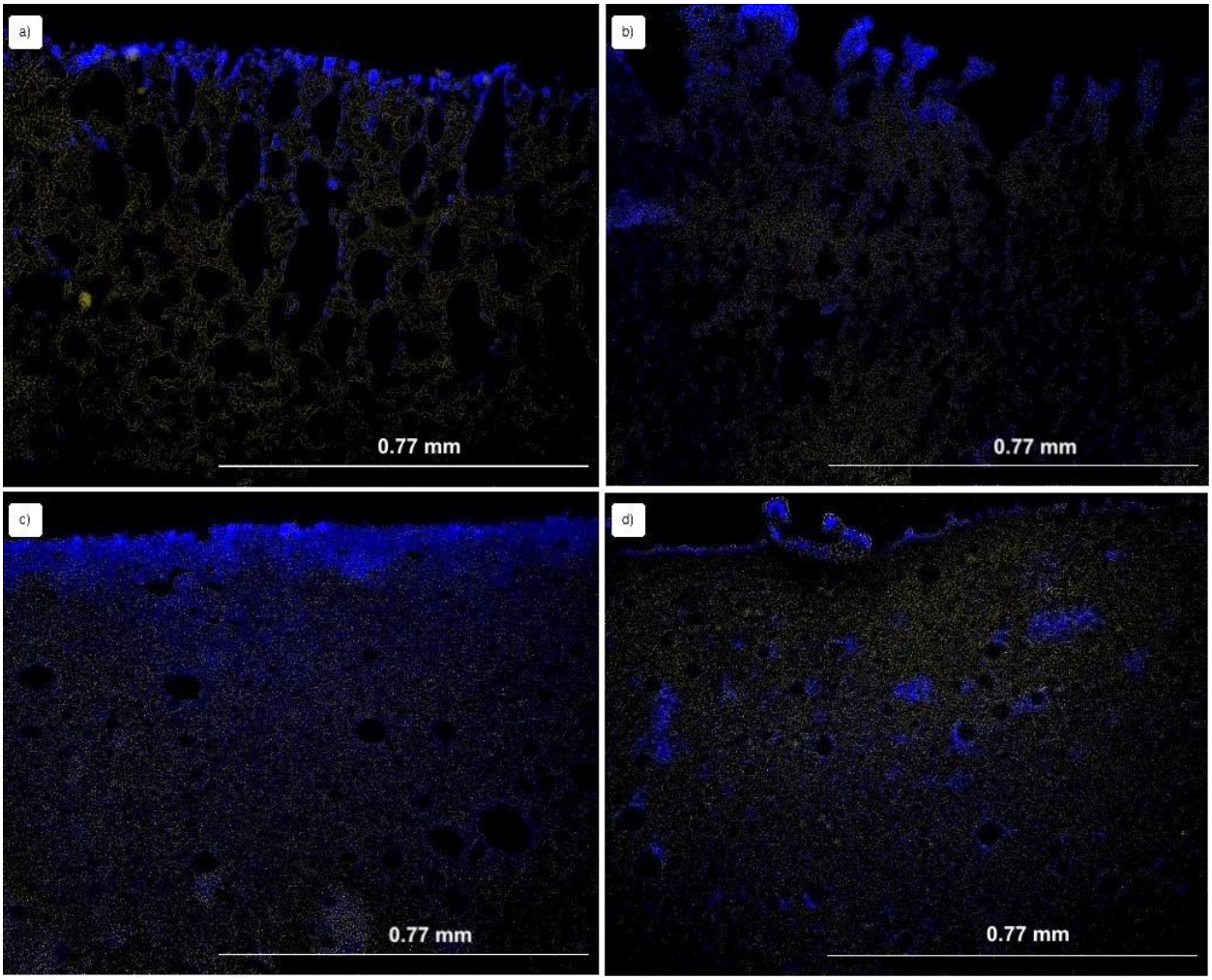

Figure 6.6 – the IHC images of the cultured PGS-M scaffolds after being stimulated by (a) stimulation 1, (b) stimulation 2, (c) stimulation 3 and (d) stimulation 4. Both images from each category were representative images from different magnification in which the scale bar is attached. Blue colour (from DAPI) represents the nuclei and yellow (from Ki-67) demonstrates the cells that were duplicating at the time of fixing.

The scaffolds might have initiated degradation, and some information could have been lost due to their storage in the fridge for several months. Previous quantitative analysis indicated that stimulation 1 (depicted in Figure 6.6 a) induced the highest rate of cell proliferation. DAPI staining confirmed the infiltration of cells into the scaffolds subjected

to this stimulation, although it remains unclear from this data whether this occurred at a higher level than with other stimulation regimes.

Minitab software was employed to examine the impact of displacement and resting time on cell metabolic rate, cell number, and total collagen content. This software enables the understanding of the relationship between two factors and the estimation of possible regimes for future research [172]. Figure 6.7 illustrates the interaction plot of (a) cell metabolic rate, (b) cell number, and (c) collagen production based on the data presented in Tables 6.2 – 6.4. The interaction plots of cell metabolism and cell number (Figure 6.7 a and b) reveal a similar trend, suggesting that stimulation 1, characterized by a lower percentage of elongation and a shorter resting time, appears to be highly beneficial for cell proliferation. These two graphs also indicate that a greater amplitude, regardless of the resting time, has an adverse effect on cell metabolism and proliferation.

In contrast, the regimen that resulted in the most collagen formation was the combination of greater amplitude and a longer resting period. Additionally, Figure 6.7 c) shows that the rate of collagen formation remains consistent irrespective of the duration of the resting time for the smaller displacement. This suggests that cells are more sensitive to variations in the smaller amplitude than to the duration of the resting period.

Considering all three interaction graphs, these results indicate that the modification of these parameters has distinct effects on cell proliferation and collagen synthesis. Furthermore, the plots presented in Figure 6.7 support and confirm the findings reported above and in the literature.

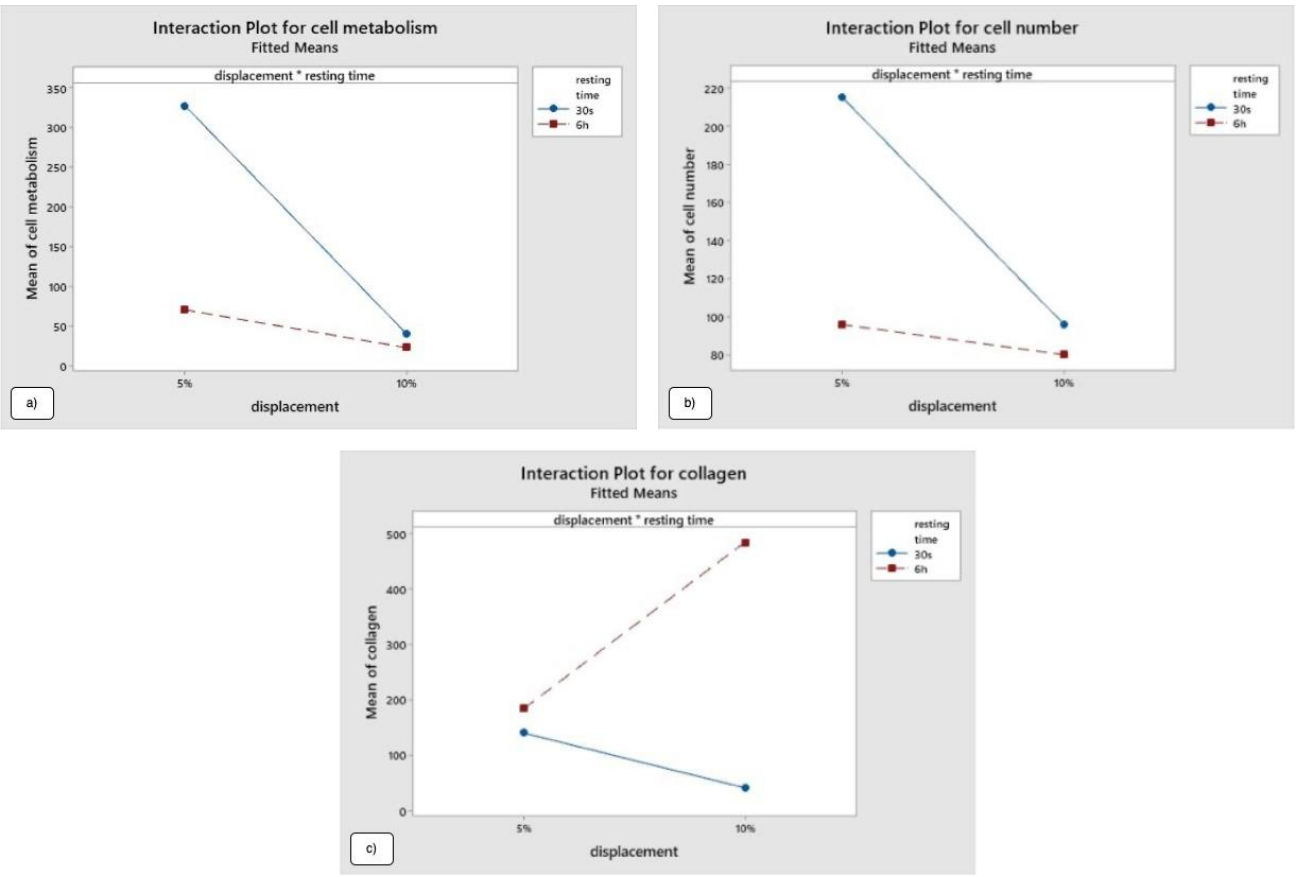

Figure 6.7 – the interaction plots demonstrate the effect of displacement and resting time on a) cell metabolism, b) cell number and c) the collagen content. The plots are generated by using Minitab software.

Minitab software played a crucial role in this thesis due to its data analysis capabilities and its capacity to provide recommendations for further experimentation [172], as mentioned earlier [173]. The process involves gathering and inputting all the data into the program to create interaction graphs. Predictive analysis is then performed to identify potential areas for future research. The modified parameters include displacement, which the program suggests adjusting by 2.5% in both directions, and resting time, which can be adjusted based on the specified ratio.

Furthermore, the interaction plots have provided insights into effective regimes for improving various elements. Combining two such effective regimes might yield even more

promising results, where one regime enhances cell proliferation while the other promotes collagen production. However, this idea could not be explored in this thesis due to time constraints.

In terms of future research using Minitab to predict potential approaches, this software is gaining recognition in the engineering field as a valuable tool for deepening knowledge and understanding through its analysis [173]. Its algorithms enable researchers to input recent results and predict new approaches that may be beneficial [172, 174]. In the context of this thesis, with the results already obtained, future research can be designed in a rational and systematic manner for each parameter.

Chapter 7 – Inhouse Robotic Bioreactor

Bioreactor is a crucial piece of equipment in tissue engineering, as it enables scientists to manage the proper environment for cell culture. Also, it permits an experiment to replicate in a specific environment. A bioreactor can be used for a variety of objectives, including promoting cell proliferation, creating 3D-structured tissue in vitro, delivering shear stress to an organism, and providing tissue support. There are various types of bioreactors that serve different purposes, such as stirred tank bioreactors (air is circulated in a large vortex), airlift bioreactors (pressurised air is circulated; used in tissue engineering), and immobilised systems (air circulates over a microorganism membrane) [175-177].

There are numerous commercially available bioreactors that can be used to stimulate the sample. I compared and evaluated numerous commercial bioreactors (Table 7.1). According to the chamber size and configuration protocol, Biotense [178] is difficult to work given the space and the setting up procedure. Cartigen [179] and LigaGen [180] are acceptable for use in orthopaedics. Several scaffolds cannot be stimulated simultaneously by BioDynamic [181]. As it can stimulate many samples simultaneously, Ebers TC-3 is often a good choice for use in research. The programme is simple to install and makes it easier for researchers to work. In addition, the lid is transparent, allowing users to examine the condition within the chamber without removing the top. This will assist in decreasing the likelihood of contamination.

Devices	PRO	CON
Biotense[178]	- Support extended investigation - Real time strain and temperature - Capable of observing cells with a high magnification microscope without relocating the chamber - Height-adjusTablechamber to ensure cells are below the medium level	- need the whole box in order to control environment.; too large and complicate to set up - limited number of scaffolds - no force sensor - hard to use - small chamber (30 mm diameter with 5 mm thickness)
CartiGen[179]	- multi samples (12 scaffolds with 10mm diameter) - window on the bottom with confocal - able to measure compressive stress - able to investigate cell functions and replication	- too big/ hard to set up - need to be circle scaffolds
LigaGen[180]	- chamber: 30 mm in length - can be single/ multi chambers - scaffolds can be up to 4mm width	- work with scaffolds 3mm thickness in maximum - narrowed chamber
BioDynamics 5200[181]	- can be multi-chamber - able to stimulate in different type of stress and strain - easy to maintain - force sensor availability	- one scaffold per chamber
Ebers TC-3[182]	- easy to use - user interface is easy to use - can be multiple scaffolds in one chamber - various types of clamps - transparent lid; easy to observe	- no force sensor - using glass as a window; easy to crack

Table 7.1 – Table represents brief reviews of commercial bioreactors.

The Ebers TC-3 bioreactor consists of three chambers that allow researchers to stimulate numerous scaffolds at the same time, sensors that regulate CO_2 and O_2 levels, and a tension and compression control box that regulates all chamber movements. Some materials are stimulated along uniaxial axis by Ebers TC-3 bioreactor. The glass at the bottom of the chamber is meant to allow microscopic inspection of the ongoing experiment. The cover was designed to be clearly visible so that users could approximate the colour of the medium [182].

In accordance with the user interface and stimulation programming (Figure 7.1), users can control the frequency of the stimulation, the elongation or travel distance, the pausing

or resting period (if applicable), the acceleration of the movement, and the different pattern of regimes if they wish to apply varying stimulation throughout the experiment. Since a single actuator is attached to the control box, all three chambers are stimulated with the same pattern. Depending on the selected mode, the graph of the journey distance or stimulation frequency is displayed on the display. The duration of an experiment is displayed in 24 hours and is reset every 24 hours; the experiment is terminated if the actuator exceeds the zero-setting point, which must be set prior to beginning a particular experiment.

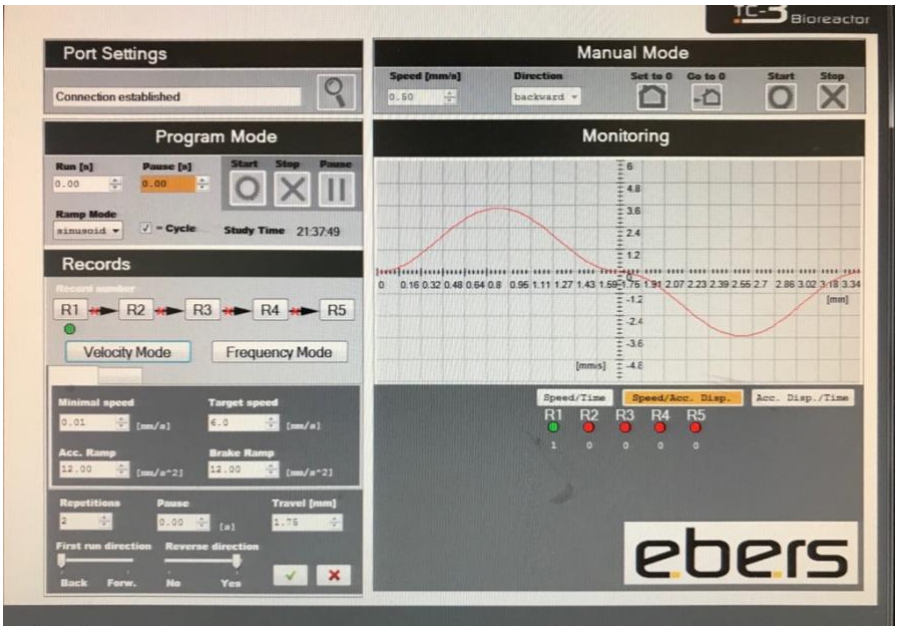

Figure 7.1 – The image of Graphic User Interface (GUI) captured from Ebers TC-3 programme.

7.1 The first design of robotic bioreactor

The general definition of a bioreactor is a device that allows biological and biochemical reactions to occur under strictly controlled, closely watched environmental conditions, such as pH, temperature, pressure, nutrition, and liquid exchanging system. Bioreactors have been essential for the transfer of unique experimental bioprocesses to large-scale

applications because of the great degree of reproducibility, control, and automation they have provided.

Despite the advantages and disadvantages of commercial bioreactors being examined, there is still no bioreactor that can sense and auto-adjust the displacement and force put on the scaffold during an experiment. This adjustable displacement and force during the experiment minimises the risk of scaffold damage and the need to immediately stop the experiment. My master's thesis served as the foundation for this thesis; hence, the issues were predetermined. One of the main issues was that the trials required immediate stop since the scaffolds shattered during the tests. After that, it would be necessary to prepare the extra sets of HDFs and PGS-M scaffolds. This occurred as a result of a force that exceeded what the scaffolds could sustain when it was applied to them. The fact that the mechanical characteristics of the scaffolds could not be measured after stimulation was another issue. The first robotic bioreactor was designed with these issues in mind.

The prerequisites outlined in the introduction served as the foundation for the specifications for this bioreactor. In addition to providing mechanical stimulation to the cells, the robotic reactor was designed to keep track of how the scaffold's mechanical properties changed while the cells were being cultivated, and the ultimate aim was to generate a bioreactor which could then respond to these changes and modify the force applied during the culture period. This would allow the robotic bioreactor to react to factors like ECM production and scaffold degradation as well as prevent the scaffold from being damaged by the application of excessive force. The Ebers TC-3, the Bose BioDynamic 5200[181], and a bioreactor constructed by former bioengineering undergraduate students [183] served as the basis for the prototype's design in Solid works. The design

of this robotic bioreactor was then implemented by Theo Le Signor, Hiba Khalidi and me. The system of the robotic bioreactor was first written in Python language by Theo Le Signor. The works were then carried on by Abigail Smith where some parts were re-designed. The system including the graphic user interface (GUI) was rewritten in MATLAB. Raspberry Pi was used as a portable CPU for this robotic bioreactor.

7.1.1 Designs of the robotic bioreactor

A square chamber was built to stimulate the various scaffolds uniaxially and simultaneously. In order to preserve the viability of cells in bioreactors, it is crucial to take into account oxygen tension, pH, chamber temperature, and aseptic atmosphere. Moreover, because a bioreactor is employed to manage the environment, an automatic control system is required to maintain the statistical reliability and reproducibility of an experiment and the routine fabrication for clinical application [184]. Moreover, physical stimulation is also another requirement for a bioreactor requirement[177]. Despite the widespread use of bioreactors in tissue engineering, there are still certain drawbacks. Mass transferring (e.g., oxygen transmission, nutrition supplying, and toxin removal), the size of a chamber (relatively tiny, the sample cannot integrate blood supply because it typically receives nutrition via diffusion), and oxygen supplying are the essential issues. According to the research [176, 177, 184, 185] and the key elements found during setting up the experiments in the dissertation [82], Table 7.2 represents the summary of the fundamental requirements for designing a bioreactor. The information in this table is from reviewing what is available commercially, and the important factors for setting up the experiment.

Requirements	Explanation
No toxicity/ biocompatibility	When creating this prototype, priority is given to biocompatibility. Emphasis is placed on ensuring that cells can grow healthily within the robotic bioreactor. The selection of biocompatible materials is based on their non-toxicity to cells and resistance to dissolution in the medium, thus preventing chamber and component corrosion and decomposition.
Prevent contamination from air and liquid	Contamination is the most detrimental feature of an experiment. To continue the experiment and decrease the chance of air contamination, the air must be filtered before entering the chamber. In addition, the medium within the chamber must be separated from the unsterile vapour and liquid outside the chamber to prevent liquid contamination.
Heat resistant capability	As the robotic bioreactor must be reusable, all components in contact with medium and scaffolds must be sterilised prior to reuse to prevent contamination. Autoclaving became the preferred method for sterilising tools since it was a simple and quick process. Moreover, the autoclave is a frequent machine in the S20 laboratory. All of the bioreactor's components, with the exception of the electronic components, must be able to sustain temperatures above 100 degrees Celsius without corroding or breaking.
Easily and visually check the scaffolds and medium	During the experiment, it is crucial that scaffolds and medium may be examined without reopening the container's cover, as doing so raises the risk of contamination. The transparent cover satisfies this criterion because the user can observe the chamber's inside while the experiment is in progress.
Ease of handling	Before transferring to a specific incubator, the experiment must be set up beneath a safety cabinet, and the chamber and components must be simple to manipulate to prevent complications.
The ability to simultaneously stimulate multiple scaffolds	To assure the validity of the results, the quantity of models or scaffolds is critical. The grips and chamber must be large enough to accommodate scaffolds wider than 10 mm.
Reusable	According to the repeatability and cost-effectiveness of the trials, the robotic bioreactor should be able to be reused multiple times.
Simple to operate and conduct experiments	Keeping the lid open and introducing sterile instruments into the chamber for experiment setup carries the risk of bacterial contamination from the air or the instruments. Therefore, the ease and speed of setting up the experiment are crucial factors to consider. The robotic bioreactor should have a straightforward setup process to minimize the time needed to start the operation. Additionally, a bioreactor with an uncomplicated setup procedure reduces the risk of having to reopen the lid for adjustments after the initial setup is completed.

Table 7.2 - the requirements for building a bioreactor.

To more easily meet the needs, an effort was made to design a few bioreactor components in a different way. The final layout of the first robotic bioreactor prototype is

depicted in Figure 7.2. As mentioned earlier, this final design is based on the design from the bioengineering undergraduate students [183] and the table 7.2. This work was from the collaboration between myself, Theo Le Signor and Hiba Khalidi. The change in chamber's material, transferring the system from python to MATLAB and Raspberry Pi and the fine adjustment for the screw and membrane was done by Abigial Smith.

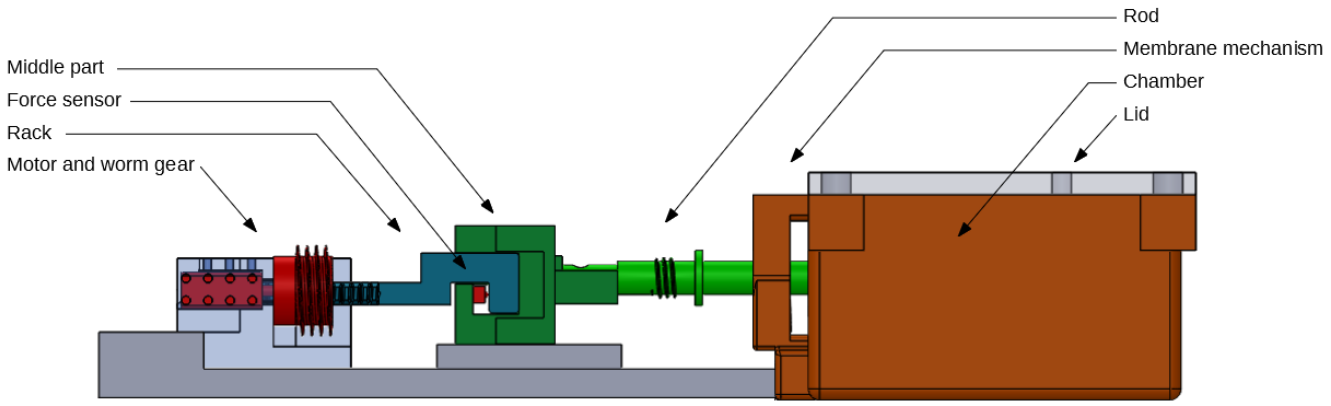

Figure 7.2 –The robotic bioreactor components.

7.1.1.1 Bioreactor chamber

A square chamber was constructed to simultaneously uniaxially stimulate various scaffolds. The chamber's sides were wider compared to LigaGen's [180]. This allowed for larger grips to accommodate bigger scaffolds and hold more samples. To ensure an airtight seal between the acrylic lid and the chamber body, effectively isolating the interior environment from the exterior, we added an intrusion at the top of the chamber. The isolating ring, which achieved this separation, was fabricated from PDMS due to its resistance to chemicals, autoclavable nature, and flexibility. The imprinted intrusion at the top of the chamber was 10 mm shorter than the height of the PDMS ring. To securely fasten the lid to the chamber, four screw holes were incorporated on the outer parts of

the sides, as depicted in Figure 7.3. The chamber was 3D printed to ensure there would be no leakage at the chamber's boundaries. To maintain sterility while still allowing gas diffusion in and out of the chamber, the lid featured one hole for a 0.22 μm filter.

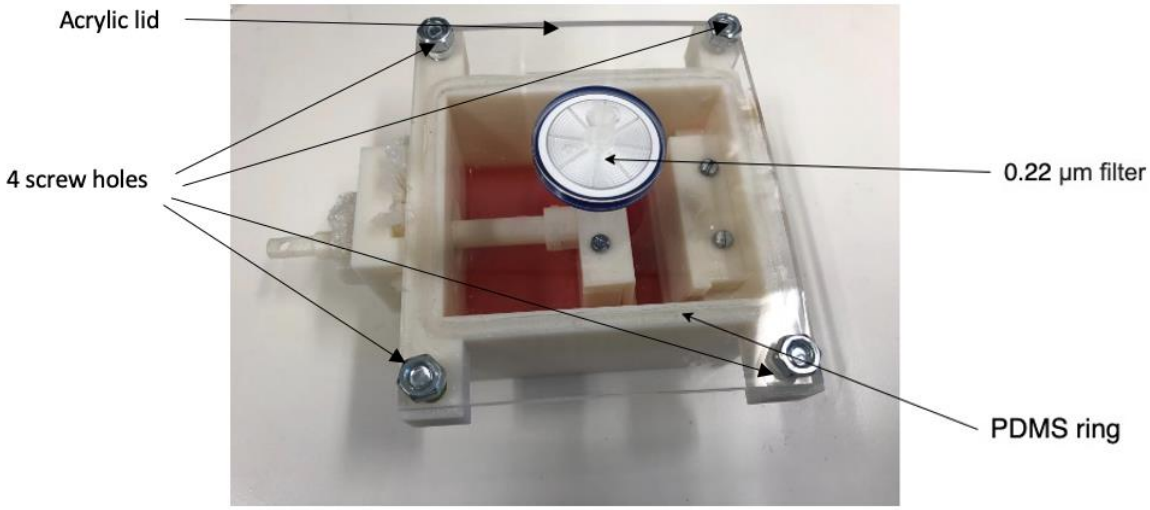

Figure 7.3 - A chamber of a robotic bioreactor with the major components.

7.1.1.2 Gripping mechanism

The clamping system is essential for ensuring that force is transferred efficiently to the samples. The samples must be held tightly by the grips, with limited room for movement. In this research, the grips were continually refined to fit this purpose. The initial design of the handle was inspired by the wider grips found on the Ebers TC-3 bioreactor. A rough surface on the gripping mechanism supplied the friction necessary for a secure hold on the scaffolding. However, this was subsequently changed to a tweezer-like device for ease of use and sterilising. Each grip featured a single screw hole for adjusting the clamping mechanism. Both grips were detachable from the chamber and actuator, allowing them to be cleaned without difficulty. Unfortunately, this version was difficult to operate with tweezers and a screwdriver in a class-II biological safety cabinet. Thus, a

version with a lock and key mechanism was designed as the final product. As shown in Figure 7.4, the top portion of the grip has a 1 mm extrusion that was matched by a 1 mm intrusion at the bottom portion of the grip. The purpose of these extrusion and intrusion was to increase the efficiency of the grips and decrease the setup time, as the lock would be in place as soon as the two grips components were joined. This ensures scaffolds were immediately and securely grabbed while allowing the user to simply tighten the screws. There are two screws between each set of grips to provide contact between them. For sterilising purposes, the grips were again able to be detached from the chamber.

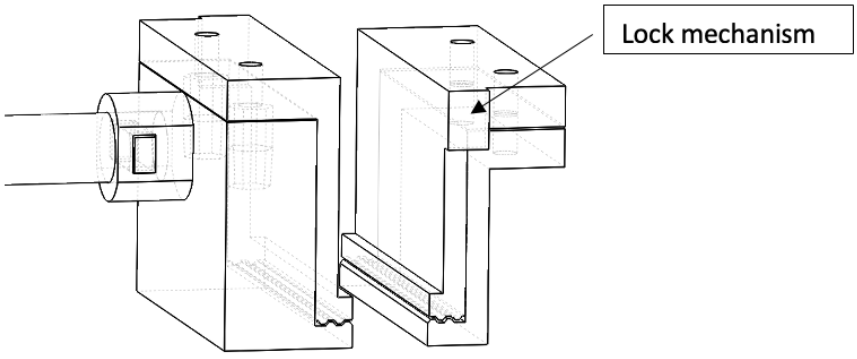

Figure 7.4 - the image of the recent version of grips, with the lock mechanism.

7.1.1.3 Membrane and filtering mechanism

The inside environment was separated from the atmosphere using parafilm. This membrane was attached to the actuator and positioned on the chamber's side. According to Figure 7.5, a 3D-printed screw was used to secure the membrane to the chamber in order to seal off the chamber's environment from the outside world. The only component

that passed through the membrane and was sealed on the other end by a screw was the rod connected to the grip.

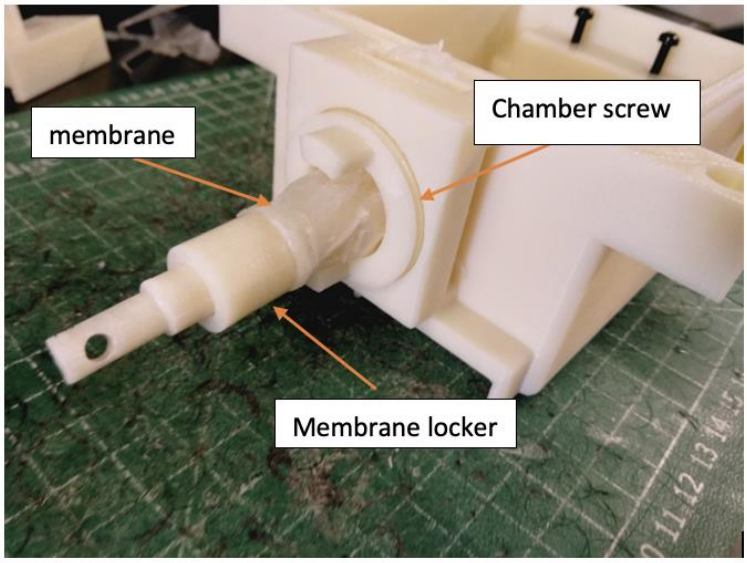

Figure 7.5 - The membrane locking mechanism and its components.

7.1.1.4 Force sensor and its housing

For a precise stiffness calculation, a force sensor (Honeywell FSS005WNGT) must be as close as possible to the scaffolds. Unfortunately, because the sensor cannot be disinfected or in contact with moisture, it cannot be put at the point where the rod is attached to the samples. As seen in Figure 7.6, one rod exited the chamber via parafilm. This rod required sterilisation. Afterwards, it was connected to the connector at the other end. This connector provided space for a force sensor, which was also attached to the actuator at the opposite end. Once the actuator retracted the rods, force data were collected.

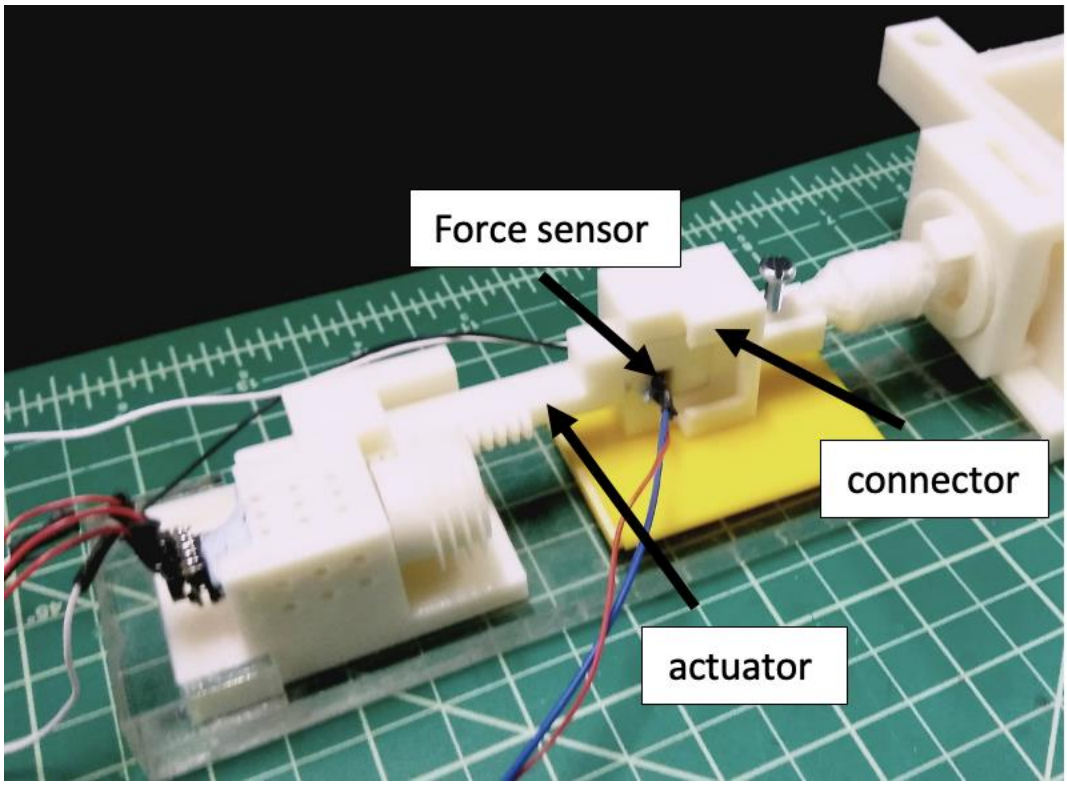

Figure 7.6 - the image represents the actuator that connected to the connector. At the point where two parts connected, it was the place where a force sensor was located.

7.1.1.5 Distance sensor, motor, and their housing

As illustrated in Figure 7.7, the actuator was coupled to the motor (12 V DC Pololu) via a worm gear. A distance sensor, often known as an encoder, was mounted to the back of a motor to control its movement. A worm gear, a motor, and a distance sensor were housed within a 3D-printed housing in order to record the displacement. The details of the system is published in the paper from ICRA 2021 conference by Abigail Smith[186]

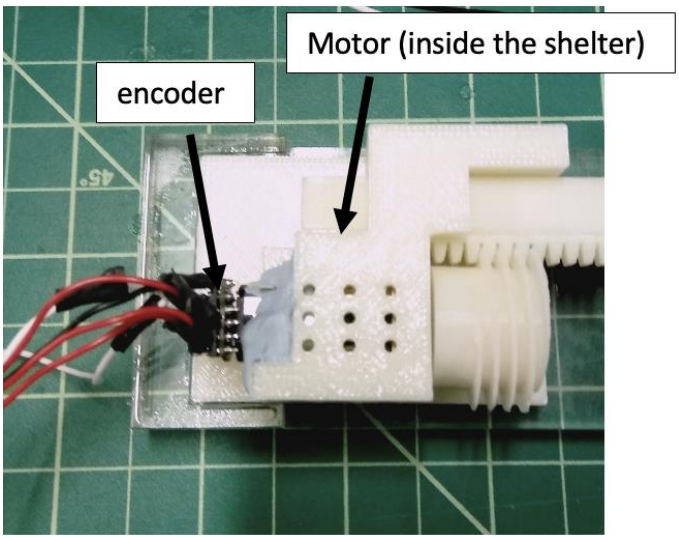

Figure 7.7 - the picture of a motor inside an ABS shelter and an encoder which attached at the end of a motor.

7.1.1.6 Components sterilisation

The bioreactor underwent initial sterilization using an autoclave. The intention was to use Ultem1010 due to its durability, high-temperature resistance, chemical resistance, and biocompatibility [187]. However, considering the high cost of Ultem1010, we opted for ABS P430, which was readily available and compatible with the Mojo 3D printer. Consequently, the sterilization method was modified to employ 70% isopropyl alcohol.

Due to the printer's limited resolution setting, there were gaps between the layers of the printed components, leading to leakage in the chamber. To address this issue, acetone was applied for ten seconds to clean the surface of each component requiring sterilization. This procedure effectively sealed the gaps and was necessary only once after the initial printing. Following this acetone treatment to eliminate the gaps, the components became ready for use.

7.1.1.7 Force sensor calibration

To assess the accuracy of the force sensor in the initial prototype, a comparison was made between the stiffness values calculated by the robotic bioreactor and those calculated using force data from the Bose machine. Figure 7.8 presents the differences in stiffness between the Bose machine and the robotic bioreactor, along with the mean stiffness values obtained from both devices. The linear trend line on the graph indicated a bias of -0.05264, which was consistent between both devices. This finding confirmed that the force sensor operated accurately with the PGS-M scaffolds.

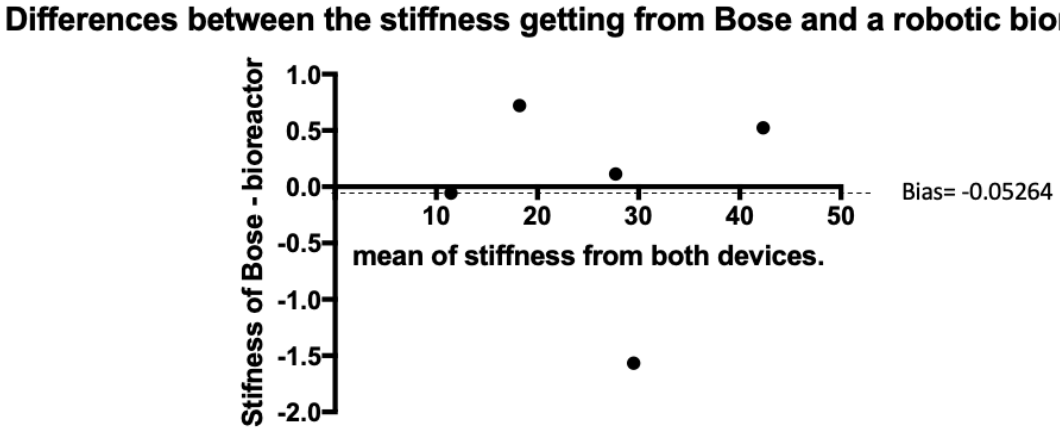

Figure 7.8 - The graph showing the differences in stiffness obtained from the Bose machine and a bioreactor and the mean stiffness from both machines. The bias value of two devices' stiffness was represented by the trend line.

7.1.1.8 Movement controlling and Data transferring

In this section, the responsibility lay in identifying and designing the experimental components. Theo Le Signor handled the programming and design of the graphical user interface (GUI).

To control the stimulation regime, the user can modify the frequency of the push and pull motion, the travel distance over which the sample is stretched, and the sample's length

within the first screen. Also, the force sensor, encoder, and all parameters can be reset before the actual experiment begins. Prior to indicate 0 mm, the grips must be positioned closely together. Once the adjustment has been made, the encoder instructs the motor to drive the rod backwards to the input position. In accordance with the environment, stimulation then commences.

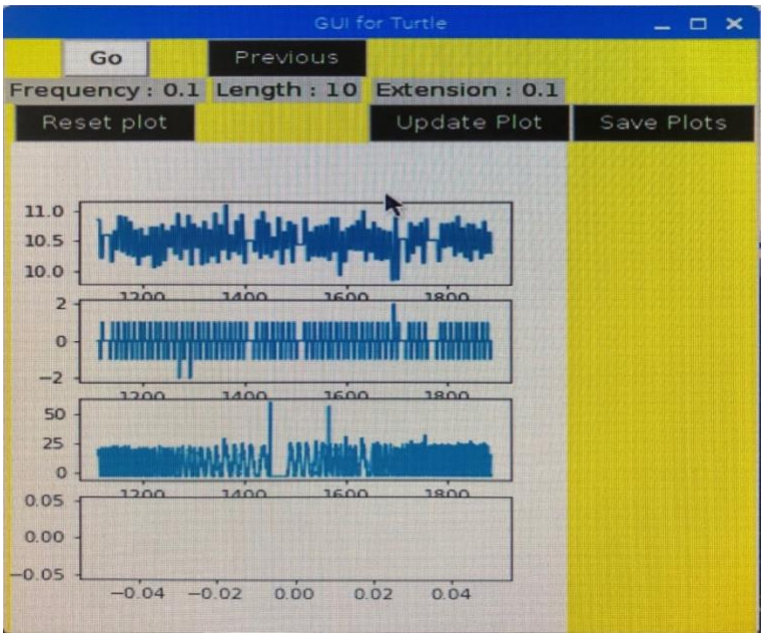

Figure 7.9 - the graphic user interface of the robotic bioreactor.

A Raspberry Pi controls the motion of the robotic bioreactor. Via Arduino UNO, this Raspberry Pi gathers data from the force sensor and distance sensor. After collecting force and travel distance data from sensors, the Raspberry Pi calculates the stiffness, recalculates the journey distance if the actuator moves erroneously, and stores the data in Excel for later research. In addition, since the Raspberry Pi is the system's CPU, it is connected to the monitor so that the user can observe the experiment. In addition, the trip distance from an encoder, the speed input that the Arduino UNO instructed to the motor,

the force data from the force sensor, and the stiffness measurement were displayed on the graphical user interface (Figure 7.9).

7.2 Setting up the experiments

Figure 7.10 illustrates the prototype's smaller size compared to the Eber TC-3, connected with an acrylic plate. In an initial test, the machine performed well. The experiment was conducted alongside the Eber TC-3 bioreactor to compare cell metabolic rate and collagen production after seven days. Nevertheless, moisture damage occurred to the encoder and wires due to the experiment being conducted overnight in a humid atmosphere (with a water tray inside the Ebers TC-3).

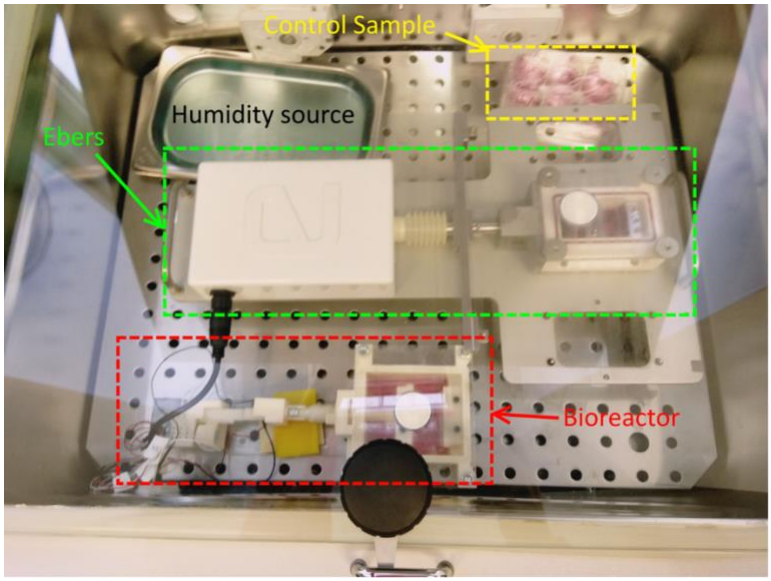

Figure 7.10 - the setup of the trial using both the robotic bioreactor and the Ebers TC-3.

Not only were the cables damaged but also the CO_2 and temperature sensors failed, making it impossible to conduct the experiment as described in chapter 6. After developing several solutions to these issues, the entire setup was relocated to a separate

incubator. The Ebers TC-3 base, containing the actuator, was installed on the upper level of the incubator, as illustrated in Figure 7.11. In order to provide both bioreactors with the same environment, the robotic bioreactor was installed on the lower level of the incubator. Wires and sensors were encased in the plastic bag to prevent them from being harmed by humidity.

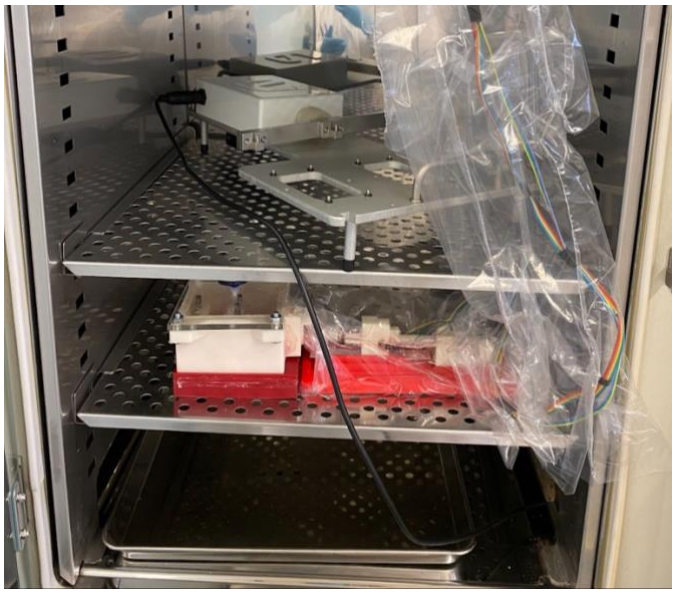

Figure 7.11 –The set up the Eber TC-3 and robotic bioreactor inside an incubator.

7.3 in vitro experiments

After seeding the PGS-M scaffolds with HDFs overnight, three seeded scaffolds were loaded into Ebers chamber. To monitor the operation of the force sensor, one scaffold was inserted into the robotic bioreactor. Before employing the tweezers and screwdrivers within the chambers, they were disinfected with 70% IMS.

Initial in vitro testing of this robotic bioreactor did not incorporate mechanical stimulation. The objective of this experiment was to examine the metabolic rate of seeded PGS-M scaffolds in the bioreactor under static conditions for one week and compare them to a

sample incubated in a TCP well plate over the same period. In both cases the data was normalized against the 2D control in which cells were seeded directly on the TCP surface. As indicated in Figure 7.12, there was no significant difference between the findings collected from the two materials. This shows that after a week of incubation, the robotic bioreactor did not release a chemical toxic to the cells.

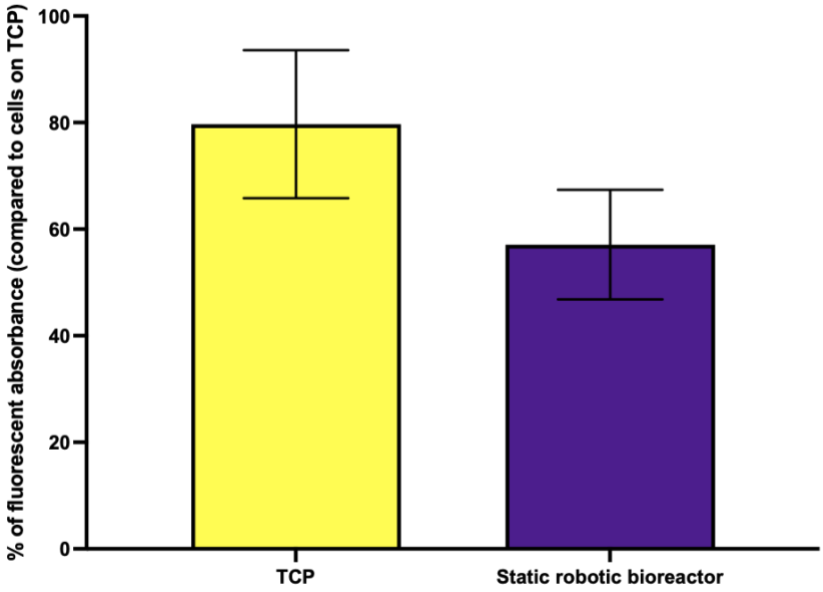

Figure 7.12 – The metabolic rate of seeded PGS-M scaffold collected from TCP well plate and the robotic bioreactor (N=1, n=3).

Once it was confirmed that the cells could survive and maintain metabolic activity inside the chamber, the first mechanical stimulation was initiated. The mechanical regime was set at a 5% travel distance and 1 Hz frequency, with continuous stimulation of the cells throughout the week. The 3D control consisted of seeded PGS-M scaffolds in a static environment, incubated in a TCP well plate. As previously mentioned, only one sample was loaded into the robotic bioreactor. Figure 7.13 shows that the metabolic rate of the stimulated cells was significantly lower than that of the unstimulated cells incubated in the well plate.

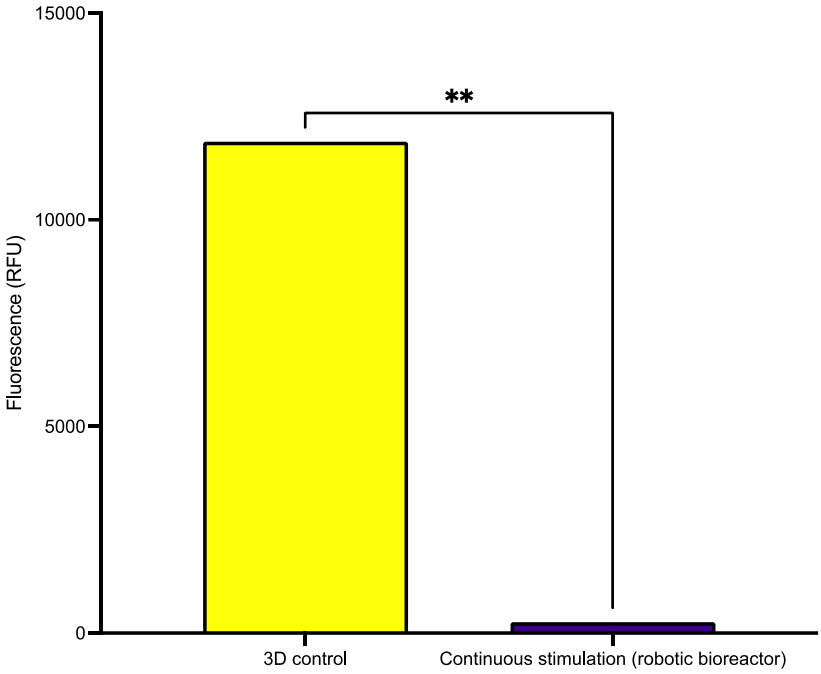

Figure 7.13 – The metabolic rate after being stimulated of seeded PGS-M scaffold collected from TCP well plate and the robotic bioreactor. The mechanical stimulation used in this experiment was 5% elongation continuous regime. The stimulation was applied for one week before evaluation (N=1, n=1).

The significantly lower of the metabolic rate shown in Figure 7.13 was not due to the cell metabolism. Further investigation showed that an issue occurred during the weekend when no one was able to observe the experiment. Although a parafilm membrane was used to divide the interior environment from the exterior environment, the membrane itself served as a reservoir during the experiment. The medium was drawn into a reservoir created by the membrane during uniaxial stimulation. As a result, the cell-seeded scaffold was left in the chamber without any medium. Hence, this result did not reflect the actual metabolic rate from the HDFs seeded on the scaffold inside the robotic bioreactor. The cells were already inactive before the test due to no medium and nutrition over long period. Since the problem arose during the weekend (day 6 and 7 of the experiment), the cells were stimulated properly during the weekday and should still be examine for the collagen

production. The hypothesis was that although the cells were left without any medium for 2 days, the ECM in which was formed before then should still be present in the scaffold. Information regarding collagen was extracted using picrosirius red. The results of the collagen production from the 3D control scaffold and the stimulated scaffold are displayed in Figure 7.14. The outcome revealed that there was no discernible difference between unstimulated and stimulated scaffolds. In addition, this demonstrated that the cells had been alive for the majority of the culture period and were capable of producing collagen. This matched the hypothesis as the collagen was still intact after the absent of the medium.

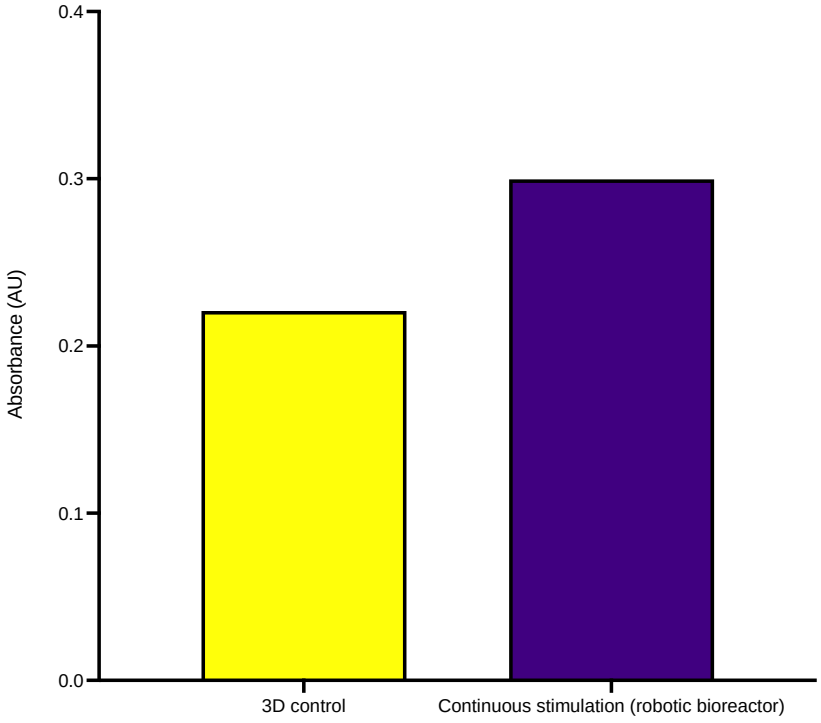

Figure 7.14 –The total collagen content after being stimulated of seeded PGS-M scaffold collected from TCP well plate and the robotic bioreactor. The mechanical stimulation used in this experiment was 5% elongation continuous regime. The stimulation was applied for one week before evaluation (N=1, n=1).

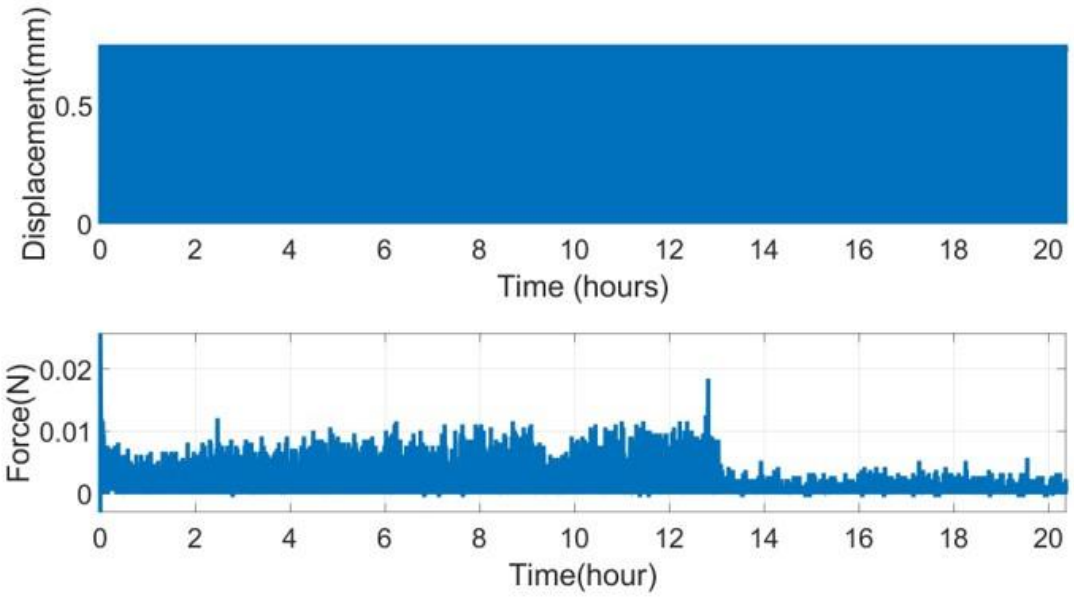

Figure 7.15 –image depicts the displacement (mm) and force (N) collected from the force sensor in the first day of stimulation.

Figure 7.15 shows the displacement (in mm) and force (in Newton or N) from the first 20 h of the experiment. This information indicates that the force sensor still functioned during the first day of the experiment. The user was able to track the change in displacement and force throughout the experiment.

According to the data presented in Figures 7.13 and 7.14, the robotic bioreactor could serve as a model for mechanical stimulation. Despite the fact that several publications [83, 87, 188] have shown the favourable effects of continuous stimulation on cell proliferation and collagen formation; however, the collected data for this experiment revealed no statistically significant difference. This could be due to the short duration of experiment. In addition, as demonstrated in my MSc report, continuous regime did not increase the metabolic rate of cells. This was merely a pilot study to determine whether this robotic bioreactor can be used to conduct in vitro research under different mechanical regimes. The membrane functioning as a reservoir was addressed and repaired after this

experiment. The membrane was reduced to ensure that any liquid drawn out as the rod was moved out of the chamber was transferred back into the chamber as the rod was pushed back into the chamber.

This robotic bioreactor was demonstrated to be a novel model of bioreactor with force sensing capabilities in real time. This also allowed the cells to develop without generating any toxins [186] that could be harmful to the cells. Unfortunately, further work on the bioreactor was halted during Covid-19, and there were also issues restarting the project afterwards. For further research of this robotic bioreactor, one of the potential things to work with is the stability of the system and compare the experiment with commercial bioreactor. The bioreactor itself is already reported to have no toxicity and it works properly on the bench top, developing it to be able to withstand the humidity and temperature will allow us to test the bioreactor and its functions.

Chapter 8 – Key Findings and Future Works

8.1 Key findings

8.1.1 Optimisation of PGS-M scaffolds

1. Resazurin assay; 1:50 (v/v) 10mM resazurin stock in fresh Complete medium. Incubate the 3D cell culture on a rocker inside an incubator (5% CO_2 at 37°C) for 4 hours.
2. Picogreen assay; lysing the cells with the freeze and thaw technique for 5 cycles by using 1x TE buffer in dH_2O with 1% Triton-x. Leave the sample at room temperature for 30 minutes each cycle before putting back in -80 freezer.
3. Picrosirius red assay; wash the samples with 0.2M NaOH until there is no excess stain.
4. Fabrication method: 80% PGS-M scaffold with emulsion technique
5. Disinfection method: 10 minutes of O_2 plasma treatment on the freeze dried PGS-M scaffold.

8.1.2 Decellularisation protocol for PGS-M scaffold

The most appropriate decellularisation for the PGS-M scaffolds is by using the freeze and thaw technique for 6 cycles, leave the samples at room temperature for 30 minutes for defrosting before putting them back into -80 freezer.

8.1.3 Mechanical stimulation

1. The most appropriate regime for cell proliferation; shorter percentage of travel distance with shorter resting period.
2. The most appropriate regime for collagen production; longer percentage of travel distance with longer resting period.

Extend the length of the experiments to understand in more detail regarding the cell proliferation and ECM production. This is to understand whether these profiles change with the longer period or not, and to summarise how long should the experiment run.

8.2 Future works

8.2.1 Hybrid scaffold

It has already been reported that the PGSM-80 E scaffold with O_2 plasma treatment works well as a template for cell culture and is able to withstand the mechanical stimulation for two weeks. The further research that can be continued for this aspect are as below.

1. Alter the mechanical stimulation regimens to explore the effect of the percentage of displacement, the increasing of the amplitude and the frequency on cell proliferation profile, degradation rate of the scaffold and the ECM production.
2. Extend the length of the experiments to understand in more detail regarding the cell proliferation and ECM production. This is to understand whether these

profiles change with the longer period or not, and to summarise how long should the experiment run.

3. The finding shows that the regimes that are able to increase the cell proliferation or and the collagen production are different. The hypothesis regarding the most effective way to enhance the total collagen production is firstly applying the regime that increase the cell proliferation, then follow by the regime that enhance the collagen production.
4. Decellularisation methods can be explored wider. The effects on the cells, its immunogenic components, and the ECM structure from various decellularisation methods can be observed to be able to come up with the most appropriate approach for lysing the cells.
5. The in vivo experiments can be carried out to test the hybrid scaffold.

8.2.2 Robotic bioreactor

The novel robotic bioreactor is invented since the adaptive force sensing and real-time displacement monitoring application are considered as important functions. The force and displacement sensors are already calibrated on the bench; however, in vitro experiment up to the same level is still in need. The possible further research for this topic will be:

1. Invent the system that will allow the electrical circuits (including the force and displacement sensor) to be able to work in an incubator (humid environment).
2. Run the experiment and compare with commercial bioreactors.

3. Invent the system that is able to accurately track the displacement and the force in multiple scaffolds. This will allow the user to stimulate more than one scaffold at one time.

References

[1] N. I. o. B. I. a. Bioengineering. "Tissue Engineering and Regenerative Medicine." National Institutes of Health. https://www.nibib.nih.gov/science-education/science-topics/tissue-engineering-and-regenerative-medicine (accessed.

[2] K. Rogers, "Tissue engineering," in *Biology*, ed: Encyclopedia Britannica.

[3] Y. Ikada, "Challenges in tissue engineering," (in eng), *J R Soc Interface,* vol. 3, no. 10, pp. 589-601, Oct 2006, doi: 10.1098/rsif.2006.0124.

[4] R. Samsudin, "Stem cell and tissue engineering - the challenge of imitating nature," (in eng), *Malays J Med Sci,* vol. 10, no. 2, pp. 1-3, Jul 2003.

[5] M. D. Grounds, "Obstacles and challenges for tissue engineering and regenerative medicine: Australian nuances," (in eng), *Clin Exp Pharmacol Physiol,* vol. 45, no. 4, pp. 390-400, Apr 2018, doi: 10.1111/1440-1681.12899.

[6] "Tissue Engineering and Regenerative Medicine." National Institutes of Health. https://www.nibib.nih.gov/science-education/science-topics/tissue-engineering-and-regenerative-medicine (accessed.

[7] F. J. O'Brien, "Biomaterials & scaffolds for tissue engineering," *Materials Today,* vol. 14, no. 3, pp. 88-95, 2011/03/01/ 2011, doi: https://doi.org/10.1016/S1369-7021(11)70058-X.

[8] M. Brovold *et al.*, "Naturally-derived biomaterials for tissue engineering applications," *Novel biomaterials for regenerative medicine,* pp. 421-449, 2018.

[9] H. Tran Le Bao, Q. To Minh, V. Doan Nguyen, and S. Do Minh, "Naturally Derived Biomaterials: Preparation and Application," in *Regenerative Medicine and Tissue Engineering*, A. A. Jose Ed. Rijeka: IntechOpen, 2013, p. Ch. 11.

[10] M. Casarin *et al.*, "Porcine Small Intestinal Submucosa (SIS) as a Suitable scaffold for the creation of a tissue-engineered urinary conduit: Decellularization, biomechanical and biocompatibility characterization using new approaches," *International Journal of Molecular Sciences,* vol. 23, no. 5, p. 2826, 2022.

[11] R. R. Betz, "Limitations of autograft and allograft: new synthetic solutions," *Orthopedics,* vol. 25, no. 5, pp. S561-S570, 2002.

[12] K. M. Malloy and A. S. Hilibrand, "Autograft versus allograft in degenerative cervical disease," *Clinical Orthopaedics and Related Research®,* vol. 394, pp. 27-38, 2002.

[13] J. Jung, H. S. Seol, and S. Chang, "The generation and application of patient-derived xenograft model for cancer research," *Cancer research and treatment: official journal of Korean Cancer Association,* vol. 50, no. 1, pp. 1-10, 2018.

[14] F. J. Maksoud *et al.*, "Porous biomaterials for tissue engineering: a review," *Journal of Materials Chemistry B,* 2022.

[15] M. T. Wolf, C. L. Dearth, S. B. Sonnenberg, E. G. Loboa, and S. F. Badylak, "Naturally derived and synthetic scaffolds for skeletal muscle reconstruction," (in eng), *Adv Drug Deliv Rev,* vol. 84, pp. 208-21, Apr 2015, doi: 10.1016/j.addr.2014.08.011.

[16] A. Huczko, "Template-based synthesis of nanomaterials," *Applied Physics A,* vol. 70, no. 4, pp. 365-376, 2000/04/01 2000, doi: 10.1007/s003390051050.
[17] K. Prasad *et al.*, "Metallic Biomaterials: Current Challenges and Opportunities," *Materials,* vol. 10, no. 8, p. 884, 2017.
[18] S. K. Chowdhury, V. Nagarjuna, and B. Bhaskar, "Metallic Biomaterials in Tissue Engineering: Retrospect and Prospects," in *Biomaterials in Tissue Engineering and Regenerative Medicine: From Basic Concepts to State of the Art Approaches*, B. Bhaskar, P. Sreenivasa Rao, N. Kasoju, V. Nagarjuna, and R. R. Baadhe Eds. Singapore: Springer Singapore, 2021, pp. 19-60.
[19] J. Huang and S. M. Best, "Chapter 1 - Ceramic biomaterials for tissue engineering," in *Tissue Engineering Using Ceramics and Polymers (Third Edition)*, A. R. Boccaccini, P. X. Ma, and L. Liverani Eds.: Woodhead Publishing, 2022, pp. 3-40.
[20] T. M. Hamdy, "Polymers and ceramics biomaterials in orthopedics and dentistry: a review article," *Egyptian Journal of Chemistry,* vol. 61, no. 4, pp. 723-730, 2018.
[21] S. Punj, J. Singh, and K. Singh, "Ceramic biomaterials: Properties, state of the art and future prospectives," *Ceramics International,* vol. 47, no. 20, pp. 28059-28074, 2021/10/15/ 2021, doi: https://doi.org/10.1016/j.ceramint.2021.06.238.
[22] H. Davis and J. Leach, "Hybrid and composite biomaterials in tissue engineering," *Topics in multifunctional biomaterials and devices,* vol. 10, pp. 1-26, 2008.
[23] A. R. Boccaccini, J. A. Roelher, L. L. Hench, V. Maquet, and R. Jérŏme, "A Composites Approach to Tissue Engineering," in *26th Annual Conference on Composites, Advanced Ceramics, Materials, and Structures: B: Ceramic Engineering and Science Proceedings*, 2002, pp. 805-816.
[24] G. Khang, S. J. Lee, M. S. Kim, and H. B. Lee, "Biomaterials: tissue engineering and scaffolds," *Encyclopedia of Medical devices and instrumentation,* vol. 2, pp. 366-83, 2006.
[25] A. A. Chaudhari *et al.*, "Future Prospects for Scaffolding Methods and Biomaterials in Skin Tissue Engineering: A Review," *International Journal of Molecular Sciences,* vol. 17, no. 12, p. 1974, 2016.
[26] F. J. O'Brien, "Biomaterials & scaffolds for tissue engineering," *Materials Today,* vol. 14, no. 3, pp. 88 - 95, 2011, doi: https://doi.org/10.1016/S1369-7021(11)70058-X.
[27] D. S. Kohane and R. Langer, "Polymeric Biomaterials in Tissue Engineering," *Pediatric Research,* vol. 63, no. 5, pp. 487-491, 2008/05/01 2008, doi: 10.1203/01.pdr.0000305937.26105.e7.
[28] X. Tang *et al.*, "Polymeric biomaterials in tissue engineering and regenerative medicine," *Natural and synthetic biomedical polymers,* pp. 351-371, 2014.
[29] Y. Wang, G. A. Ameer, B. J. Sheppard, and R. Langer, "A tough biodegradable elastomer," (in eng), *Nat Biotechnol,* vol. 20, no. 6, pp. 602-6, Jun 2002, doi: 10.1038/nbt0602-602.
[30] X. J. Loh, A. Abdul Karim, and C. Owh, "Poly(glycerol sebacate) biomaterial: synthesis and biomedical applications," *Journal of Materials Chemistry B,* 10.1039/C5TB01048A vol. 3, no. 39, pp. 7641-7652, 2015, doi: 10.1039/C5TB01048A.
[31] R. Rai, M. Tallawi, A. Grigore, and A. R. Boccaccini, "Synthesis, properties and biomedical applications of poly(glycerol sebacate) (PGS): A review," *Progress in Polymer Science,* vol.

37, no. 8, pp. 1051-1078, 2012/08/01/ 2012, doi: https://doi.org/10.1016/j.progpolymsci.2012.02.001.
[32] J. M. Kemppainen and S. J. Hollister, "Tailoring the mechanical properties of 3D-designed poly(glycerol sebacate) scaffolds for cartilage applications," (in eng), *J Biomed Mater Res A,* vol. 94, no. 1, pp. 9-18, Jul 2010, doi: 10.1002/jbm.a.32653.
[33] C. G. Jeong and S. J. Hollister, "A comparison of the influence of material on in vitro cartilage tissue engineering with PCL, PGS, and POC 3D scaffold architecture seeded with chondrocytes," (in eng), *Biomaterials,* vol. 31, no. 15, pp. 4304-12, May 2010, doi: 10.1016/j.biomaterials.2010.01.145.
[34] Q. Z. Chen *et al.*, "An elastomeric patch derived from poly(glycerol sebacate) for delivery of embryonic stem cells to the heart," (in eng), *Biomaterials,* vol. 31, no. 14, pp. 3885-93, May 2010, doi: 10.1016/j.biomaterials.2010.01.108.
[35] C. A. Sundback *et al.*, "Biocompatibility analysis of poly(glycerol sebacate) as a nerve guide material," (in eng), *Biomaterials,* vol. 26, no. 27, pp. 5454-64, Sep 2005, doi: 10.1016/j.biomaterials.2005.02.004.
[36] Z. J. Sun *et al.*, "The application of poly (glycerol-sebacate) as biodegradable drug carrier," (in eng), *Biomaterials,* vol. 30, no. 28, pp. 5209-14, Oct 2009, doi: 10.1016/j.biomaterials.2009.06.007.
[37] C. Zhu, S. R. Kustra, and C. J. Bettinger, "Photocrosslinkable biodegradable elastomers based on cinnamate-functionalized polyesters," (in eng), *Acta Biomater,* vol. 9, no. 7, pp. 7362-70, Jul 2013, doi: 10.1016/j.actbio.2013.03.041.
[38] S. Pashneh-Tala, R. Owen, H. Bahmaee, S. Rekštytė, M. Malinauskas, and F. Claeyssens, "Synthesis, Characterization and 3D Micro-Structuring via 2-Photon Polymerization of Poly(glycerol sebacate)-Methacrylate–An Elastomeric Degradable Polymer," (in English), *Frontiers in Physics,* Original Research vol. 6, no. 41, 2018-May-08 2018, doi: 10.3389/fphy.2018.00041.
[39] J. Thanarak, H. Mohammed, S. Pashneh-Tala, F. Claeyssens, and N. Green, "Enhanced Collagen Production from Human Dermal Fibroblasts on Poly(glycerol sebacate)-methacrylate Scaffolds," pp. 1-4, 2018, doi: 10.1109/BMEiCON.2018.8609928.
[40] S. Pashneh-Tala, R. Moorehead, and F. Claeyssens, "Hybrid manufacturing strategies for tissue engineering scaffolds using methacrylate functionalised poly(glycerol sebacate)," *Journal of Biomaterials Applications,* vol. 34, no. 8, pp. 1114-1130, 2020, doi: 10.1177/0885328219898385.
[41] J. H. Kim, S. B. Lee, S. J. Kim, and Y. M. Lee, "Rapid temperature/pH response of porous alginate-g-poly (N-isopropylacrylamide) hydrogels," *Polymer,* vol. 43, no. 26, pp. 7549-7558, 2002.
[42] J. Armstrong, M. Burke, B. Carter, S. Davis, and A. Perriman, "3D Bioprinting Using a Templated Porous Bioink," *Advanced Healthcare Materials,* vol. 5, pp. 1681-1681, 2016, doi: 10.1002/adhm.201600022.
[43] A. Jakus, N. Geisendorfer, P. Lewis, and R. Shah, "3D-printing porosity: a new approach to creating elevated porosity materials and structures," *Acta biomaterialia,* vol. 72, pp. 94-109, 2018.
[44] G. L. Ying *et al.*, "Aqueous Two-Phase Emulsion Bioink-Enabled 3D Bioprinting of Porous Hydrogels," *Advanced Materials,* vol. 30, 2018, doi: 10.1002/adma.201805460.

[45] B. Aldemir Dikici, S. Dikici, G. Reilly, S. Macneil, and F. Claeyssens, "A Novel Bilayer Polycaprolactone Membrane for Guided Bone Regeneration: Combining Electrospinning and Emulsion Templating," *Materials,* vol. 12, p. 2643, 2019, doi: 10.3390/ma12162643.
[46] H. Chen, Y. Peng, S. Wu, and L. P. Tan, "Electrospun 3D fibrous scaffolds for chronic wound repair," *Materials,* vol. 9, no. 4, p. 272, 2016.
[47] S. I. Jeong, N. A. Burns, C. A. Bonino, I. K. Kwon, S. A. Khan, and E. Alsberg, "Improved cell infiltration of highly porous 3D nanofibrous scaffolds formed by combined fiber–fiber charge repulsions and ultra-sonication," *Journal of Materials Chemistry B,* vol. 2, no. 46, pp. 8116-8122, 2014.
[48] Y. Wu *et al.*, "The regeneration of macro-porous electrospun poly (ε-caprolactone) vascular graft during long-term in situ implantation," *Journal of Biomedical Materials Research Part B: Applied Biomaterials,* vol. 106, no. 4, pp. 1618-1627, 2018.
[49] P. S. Gungor-Ozkerim, I. Inci, Y. S. Zhang, A. Khademhosseini, and M. R. Dokmeci, "Bioinks for 3D bioprinting: an overview," *Biomaterials science,* vol. 6, no. 5, pp. 915-946, 2018.
[50] D. Zindani, K. Kumar, and J. Paulo Davim, "4 - Metallic biomaterials—A review," in *Mechanical Behaviour of Biomaterials*, J. P. Davim Ed.: Woodhead Publishing, 2019, pp. 83-99.
[51] E. Davoodi *et al.*, "Additively manufactured metallic biomaterials," *Bioactive Materials,* vol. 15, pp. 214-249, 2022/09/01/ 2022, doi: https://doi.org/10.1016/j.bioactmat.2021.12.027.
[52] W. Billotte, "Ceramic biomaterials," in *Biomaterials*: CRC Press, 2007, pp. 2-1-2-34.
[53] M. Abraham, D. V. Claudio, S. Stefano, A. Alidad, and D. J. W., "Contact angles and wettability: towards common and accurate terminology," *Surface Innovations,* vol. 5, no. 1, pp. 3-8, 2017, doi: 10.1680/jsuin.17.00002.
[54] K. L. Menzies and L. Jones, "The Impact of Contact Angle on the Biocompatibility of Biomaterials," *Optometry and Vision Science,* vol. 87, no. 6, 2010.
[55] B. Ratner, "Correlation, surfaces and biomaterials science," *Biomaterials science: an introduction to materials in medicine,* vol. 2, pp. 765-71, 2004.
[56] Y. Arima and H. Iwata, "Effect of wettability and surface functional groups on protein adsorption and cell adhesion using well-defined mixed self-assembled monolayers," *Biomaterials,* vol. 28, no. 20, pp. 3074-3082, 2007/07/01/ 2007, doi: https://doi.org/10.1016/j.biomaterials.2007.03.013.
[57] S. R. Kim, "Surface modification of poly(tetrafluoroethylene) film by chemical etching, plasma, and ion beam treatments," *Journal of Applied Polymer Science,* vol. 77, no. 9, pp. 1913-1920, 2000, doi: https://doi.org/10.1002/1097-4628(20000829)77:9<1913::AID-APP7>3.0.CO;2-#.
[58] J. Lai *et al.*, "Study on hydrophilicity of polymer surfaces improved by plasma treatment," *Applied Surface Science,* vol. 252, no. 10, pp. 3375 - 3379, 2006, doi: https://doi.org/10.1016/j.apsusc.2005.05.038.
[59] D. Hegemann, H. Brunner, and C. Oehr, "Plasma treatment of polymers for surface and adhesion improvement," *Nuclear Instruments and Methods in Physics Research Section B: Beam Interactions with Materials and Atoms,* vol. 208, pp. 281-286, 2003/08/01/ 2003, doi: https://doi.org/10.1016/S0168-583X(03)00644-X.

[60] Y. Tamada and Y. Ikada, "Cell adhesion to plasma-treated polymer surfaces," *Polymer,* vol. 34, no. 10, pp. 2208 - 2212, 1993, doi: https://doi.org/10.1016/0032-3861(93)90752-V.
[61] H.-Y. Yu, Y.-j. Xie, M.-X. Hu, J.-L. Wang, S.-Y. Wang, and Z.-K. Xu, "Surface modification of polypropylene microporous membrane to improve its antifouling property in MBR: CO2 plasma treatment," *Journal of Membrane Science,* vol. 254, no. 1, pp. 219 - 227, 2005, doi: https://doi.org/10.1016/j.memsci.2005.01.010.
[62] J. Yip, K. Chan, K. M. Sin, and K. S. Lau, "Low temperature plasma-treated nylon fabrics," *Journal of Materials Processing Technology,* vol. 123, no. 1, pp. 5-12, 2002/04/10/ 2002, doi: https://doi.org/10.1016/S0924-0136(02)00024-9.
[63] M. L. Steen, L. Hymas, E. D. Havey, N. E. Capps, D. G. Castner, and E. R. Fisher, "Low temperature plasma treatment of asymmetric polysulfone membranes for permanent hydrophilic surface modification," *Journal of Membrane Science,* vol. 188, no. 1, pp. 97 - 114, 2001, doi: https://doi.org/10.1016/S0376-7388(01)00375-1.
[64] N. Farr *et al.*, "Understanding Surface Modifications Induced via Argon Plasma Treatment through Secondary Electron Hyperspectral Imaging," *Advanced Science,* vol. n/a, no. n/a, p. 2003762, doi: https://doi.org/10.1002/advs.202003762.
[65] S. Pal, "Mechanical properties of biological materials," *Design of Artificial Human Joints & Organs,* pp. 23-40, 2014.
[66] M. Capurro and F. Barberis, "9 - Evaluating the mechanical properties of biomaterials," in *Biomaterials for Bone Regeneration*, P. Dubruel and S. Van Vlierberghe Eds.: Woodhead Publishing, 2014, pp. 270-323.
[67] M. A. Meyers, P.-Y. Chen, A. Y.-M. Lin, and Y. Seki, "Biological materials: structure and mechanical properties," *Progress in materials science,* vol. 53, no. 1, pp. 1-206, 2008.
[68] H. Sano, B. Ciucchi, W. Matthews, and D. H. Pashley, "Tensile properties of mineralized and demineralized human and bovine dentin," *Journal of dental research,* vol. 73, no. 6, pp. 1205-1211, 1994.
[69] "Ultimate Tensile Strength (UTS)." Corrosionpedia. https://www.corrosionpedia.com/definition/1126/ultimate-tensile-strength-uts (accessed.
[70] Ashish. "What Is Ultimate Tensile Strength?" ScienceABC. https://www.scienceabc.com/pure-sciences/what-is-ultimate-tensile-strength.html (accessed.
[71] B. M. Alberts *et al.* "cell." https://www.britannica.com/science/cell-biology (accessed.
[72] K. S. Saladine, C. A. Gan, and H. N. Cushman, *Anatomy & Physiology*. McGraw-Hill.
[73] "14 Types of Cells in the Human Body & their Functions." study read. https://www.studyread.com/types-cells-human-body/ (accessed.
[74] A. Mandal. "What are Fibroblasts?" https://www.news-medical.net/health/What-are-Fibroblasts.aspx (accessed 03/03, 2018).
[75] K. Rogers. "Fibroblasts." https://www.britannica.com/science/fibroblast (accessed 03/03, 2018).
[76] M. V. Plikus *et al.*, "Fibroblasts: Origins, definitions, and functions in health and disease," *Cell,* vol. 184, no. 15, pp. 3852-3872, 2021.

[77] E. S. White, "Lung extracellular matrix and fibroblast function," *Annals of the American Thoracic Society,* vol. 12, no. Supplement 1, pp. S30-S33, 2015.
[78] L. E. Tracy, R. A. Minasian, and E. Caterson, "Extracellular matrix and dermal fibroblast function in the healing wound," *Advances in wound care,* vol. 5, no. 3, pp. 119-136, 2016.
[79] W. Sun, X. Gao, H. Lei, W. Wang, and Y. Sun, "Biophysical Approaches for Applying and Measuring Biological Forces," *Advanced Science,* vol. 9, p. 2105254, 02/14 2022, doi: 10.1002/advs.202105254.
[80] J. H.-C. Wang, B. P. Thampatty, J.-S. Lin, and H.-J. Im, "Mechanoregulation of gene expression in fibroblasts," *Gene,* vol. 391, no. 1-2, pp. 1-15, 2007.
[81] B. Kuehlmann, C. A. Bonham, I. Zucal, L. Prantl, and G. C. Gurtner, "Mechanotransduction in wound healing and fibrosis," *Journal of clinical medicine,* vol. 9, no. 5, p. 1423, 2020.
[82] J. Thanarak, "Mechanical effects on fibroblasts for collagen production," The University of Sheffield, Master's dissertation, 2018.
[83] J. B. Schmidt, K. Chen, and R. T. Tranquillo, "Effects of Intermittent and Incremental Cyclic Stretch on ERK Signaling and Collagen Production in Engineered Tissue," *Cellular and Molecular Bioengineering,* vol. 9, no. 1, pp. 55-64, Mar 2016, doi: 10.1007/s12195-015-0415-6.
[84] R. Roskoski, "Roskoski R Jr.ERK1/2 MAP kinases: structure, function, and regulation. Pharmacol Res 66:105-143," *Pharmacological research : the official journal of the Italian Pharmacological Society,* vol. 66, pp. 105-43, 04/27 2012, doi: 10.1016/j.phrs.2012.04.005.
[85] R. Buscà, J. Pouysségur, and P. Lenormand, "ERK1 and ERK2 Map Kinases: Specific Roles or Functional Redundancy?," (in English), *Frontiers in Cell and Developmental Biology,* Review vol. 4, no. 53, 2016-June-08 2016, doi: 10.3389/fcell.2016.00053.
[86] J. S. Weinbaum, J. B. Schmidt, and R. T. Tranquillo, "Combating Adaptation to Cyclic Stretching by Prolonging Activation of Extracellular Signal-Regulated Kinase," *Cellular and Molecular Bioengineering,* vol. 6, no. 3, pp. 279-286, 2013/09/01 2013, doi: 10.1007/s12195-013-0289-4.
[87] G. S. Ugolini, A. Pavesi, M. Rasponi, G. B. Fiore, R. Kamm, and M. Soncini, "Human cardiac fibroblasts adaptive responses to controlled combined mechanical strain and oxygen changes in vitro," *Elife,* vol. 6, Mar 2017, Art no. e22847, doi: 10.7554/eLife.22847.
[88] G. S. Ugolini *et al.*, "On-chip assessment of human primary cardiac fibroblasts proliferative responses to uniaxial cyclic mechanical strain," *Biotechnology and Bioengineering,* vol. 113, no. 4, pp. 859-869, Apr 2016, doi: 10.1002/bit.25847.
[89] W. Manuyakorn *et al.*, "Mechanical Strain Causes Adaptive Change in Bronchial Fibroblasts Enhancing Profibrotic and Inflammatory Responses," *Plos One,* vol. 11, no. 4, Apr 2016, Art no. e0153926, doi: 10.1371/journal.pone.0153926.
[90] M. E. Blaauboer, T. H. Smit, R. Hanemaaijer, R. Stoop, and V. Everts, "Cyclic mechanical stretch reduces myofibroblast differentiation of primary lung fibroblasts," *Biochemical and Biophysical Research Communications,* vol. 404, no. 1, pp. 23-27, Jan 2011, doi: 10.1016/j.bbrc.2010.11.033.

[91] M. Eastwood, V. C. Mudera, D. A. McGrouther, and R. A. Brown, "Effect of precise mechanical loading on fibroblast populated collagen lattices: Morphological changes," *Cell Motility and the Cytoskeleton,* vol. 40, no. 1, pp. 13-21, 1998, doi: 10.1002/(sici)1097-0169(1998)40:1<13::aid-cm2>3.0.co;2-g.

[92] Z. H. Syedain, L. A. Meier, J. W. Bjork, A. Lee, and R. T. Tranquillo, "Implantable arterial grafts from human fibroblasts and fibrin using a multi-graft pulsed flow-stretch bioreactor with noninvasive strength monitoring," *Biomaterials,* vol. 32, no. 3, pp. 714-722, Jan 2011, doi: 10.1016/j.biomaterials.2010.09.019.

[93] B. Lohberger, H. Kaltenegger, N. Stuendl, B. Rinner, A. Leithner, and P. Sadoghi, "Impact of cyclic mechanical stimulation on the expression of extracellular matrix proteins in human primary rotator cuff fibroblasts," vol. 24, 2015.

[94] M. Brunelli, C. M. Perrault, and D. Lacroix, "Short bursts of cyclic mechanical compression modulate tissue formation in a 3D hybrid scaffold," *Journal of the Mechanical Behavior of Biomedical Materials,* vol. 71, pp. 165-174, 2017/07/01/ 2017, doi: https://doi.org/10.1016/j.jmbbm.2017.03.008.

[95] H. Lu, T. Hoshiba, N. Kawazoe, and G. Chen, "Comparison of decellularization techniques for preparation of extracellular matrix scaffolds derived from three-dimensional cell culture," *Journal of Biomedical Materials Research Part A,* vol. 100A, no. 9, pp. 2507-2516, 2012, doi: https://doi.org/10.1002/jbm.a.34150.

[96] F. Franks, "Freeze-drying of bioproducts: putting principles into practice," *European Journal of Pharmaceutics and Biopharmaceutics,* vol. 45, no. 3, pp. 221-229, 1998/05/01/ 1998, doi: https://doi.org/10.1016/S0939-6411(98)00004-6.

[97] D. Singh, A. J. Harding, E. Albadawi, F. M. Boissonade, J. W. Haycock, and F. Claeyssens, "Additive manufactured biodegradable poly(glycerol sebacate methacrylate) nerve guidance conduits," *Acta Biomaterialia,* vol. 78, pp. 48-63, 2018/09/15/ 2018, doi: https://doi.org/10.1016/j.actbio.2018.07.055.

[98] Z. Dai, J. Ronholm, Y. Tian, B. Sethi, and X. Cao, "Sterilization techniques for biodegradable scaffolds in tissue engineering applications," (in eng), *Journal of tissue engineering,* vol. 7, pp. 2041731416648810-2041731416648810, 2016, doi: 10.1177/2041731416648810.

[99] "Sterilization for Medical Devices." U.S. Food and Drug Administration. https://www.fda.gov/medical-devices/general-hospital-devices-and-supplies/sterilization-medical-devices#:~:text=Medical%20devices%20are%20sterilized%20in,acid%2C%20and%20nitrogen%20dioxide (accessed 2023).

[100] "ISO 17665 Steam Sterilization." Life Science Outsoucing. https://lso-inc.com/services/sterilization-validation/standards/iso-17665-steam-sterilization/ (accessed.

[101] S. Lerouge, M. R. Wertheimer, and L. H. Yahia, "Plasma Sterilization: A Review of Parameters, Mechanisms, and Limitations," *Plasmas and Polymers,* vol. 6, no. 3, pp. 175-188, 2001/09/01 2001, doi: 10.1023/A:1013196629791.

[102] T. Jacobs, R. Morent, N. De Geyter, P. Dubruel, and C. Leys, "Plasma Surface Modification of Biomedical Polymers: Influence on Cell-Material Interaction," *Plasma Chemistry and*

Plasma Processing, vol. 32, no. 5, pp. 1039-1073, 2012/10/01 2012, doi: 10.1007/s11090-012-9394-8.

[103] P. K. Chu, J. Y. Chen, L. P. Wang, and N. Huang, "Plasma-surface modification of biomaterials," *Materials Science and Engineering: R: Reports,* vol. 36, no. 5, pp. 143-206, 2002/03/29/ 2002, doi: https://doi.org/10.1016/S0927-796X(02)00004-9.

[104] I. H. Jaafar, M. M. Ammar, S. S. Jedlicka, R. A. Pearson, and J. P. Coulter, "Spectroscopic evaluation, thermal, and thermomechanical characterization of poly(glycerol-sebacate) with variations in curing temperatures and durations," *Journal of Materials Science,* vol. 45, no. 9, pp. 2525-2529, 2010/05/01 2010, doi: 10.1007/s10853-010-4259-0.

[105] Q.-Z. Chen *et al.*, "Characterisation of a soft elastomer poly(glycerol sebacate) designed to match the mechanical properties of myocardial tissue," *Biomaterials,* vol. 29, no. 1, pp. 47-57, 2008/01/01/ 2008, doi: https://doi.org/10.1016/j.biomaterials.2007.09.010.

[106] P. Heydari, S. Parham, A. Z. Kharazi, S. H. Javanmard, and S. Asgary, "In Vitro Comparison Study of Plasma Treated Bilayer PGS/PCL and PGS/PLA Scaffolds for Vascular Tissue Engineering," *Fibers and Polymers,* vol. 23, no. 9, pp. 2384-2393, 2022/09/01 2022, doi: 10.1007/s12221-022-0228-x.

[107] M. Sarikanat, Y. Seki, K. Sever, E. Bozaci, A. Demir, and E. Ozdogan, "The effect of argon and air plasma treatment of flax fiber on mechanical properties of reinforced polyester composite," *Journal of Industrial Textiles,* vol. 45, no. 6, pp. 1252-1267, 2016, doi: 10.1177/1528083714557057.

[108] M. O. H. Cioffi, H. J. C. Voorwald, L. R. O. Hein, and L. Ambrosio, "Effect of cold plasma treatment on mechanical properties of PET/PMMA composites," *Composites Part A: Applied Science and Manufacturing,* vol. 36, no. 5, pp. 615-623, 2005/05/01/ 2005, doi: https://doi.org/10.1016/j.compositesa.2004.08.006.

[109] M. Griffin, A. Ibrahim, A. Seifalian, P. Butler, D. Kalaskar, and P. Ferretti, "Argon plasma modification promotes adipose derived stem cells osteogenic and chondrogenic differentiation on nanocomposite polyurethane scaffolds; implications for skeletal tissue engineering," *Materials Science and Engineering: C,* vol. 105, p. 110085, 08/01 2019, doi: 10.1016/j.msec.2019.110085.

[110] T. Huhtamäki, X. Tian, J. T. Korhonen, and R. H. A. Ras, "Surface-wetting characterization using contact-angle measurements," *Nature Protocols,* vol. 13, no. 7, pp. 1521-1538, 2018/07/01 2018, doi: 10.1038/s41596-018-0003-z.

[111] J. L. Ifkovits, R. F. Padera, and J. A. Burdick, "Biodegradable and radically polymerized elastomers with enhanced processing capabilities," (in eng), *Biomed Mater,* vol. 3, no. 3, p. 034104, Sep 2008, doi: 10.1088/1748-6041/3/3/034104.

[112] C. L. Nijst *et al.*, "Synthesis and characterization of photocurable elastomers from poly(glycerol-co-sebacate)," (in eng), *Biomacromolecules,* vol. 8, no. 10, pp. 3067-73, Oct 2007, doi: 10.1021/bm070423u.

[113] J. L. Ifkovits, J. J. Devlin, G. Eng, T. P. Martens, G. Vunjak-Novakovic, and J. A. Burdick, "Biodegradable fibrous scaffolds with tunable properties formed from photo-cross-linkable poly(glycerol sebacate)," (in eng), *ACS Appl Mater Interfaces,* vol. 1, no. 9, pp. 1878-86, Sep 2009, doi: 10.1021/am900403k.

[114] A. Kumar, J. K. Placone, and A. J. Engler, "Understanding the extracellular forces that determine cell fate and maintenance," (in eng), *Development,* vol. 144, no. 23, pp. 4261-4270, Dec 1 2017, doi: 10.1242/dev.158469.

[115] M. Griffin *et al.*, "Evaluation of Sterilisation Techniques for Regenerative Medicine Scaffolds Fabricated with Polyurethane Nonbiodegradable and Bioabsorbable Nanocomposite Materials," *International Journal of Biomaterials,* vol. 2018, pp. 1-14, 10/03 2018, doi: 10.1155/2018/6565783.

[116] S. Technologies. "Resazurin (Sodium Salt)." https://www.myendnoteweb.com/EndNoteWeb.html?func=new& (accessed.

[117] E. M. Czekanska, "Assessment of Cell Proliferation with Resazurin-Based Fluorescent Dye," in *Mammalian Cell Viability: Methods and Protocols*, M. J. Stoddart Ed. Totowa, NJ: Humana Press, 2011, pp. 27-32.

[118] G. Cox, E. Kable, A. Jones, I. Fraser, F. Manconi, and M. D. Gorrell, "3-dimensional imaging of collagen using second harmonic generation," (in eng), *J Struct Biol,* vol. 141, no. 1, pp. 53-62, Jan 2003.

[119] J. Gao, A. E. Ensley, R. M. Nerem, and Y. Wang, "Poly(glycerol sebacate) supports the proliferation and phenotypic protein expression of primary baboon vascular cells," *Journal of Biomedical Materials Research Part A,* vol. 83A, no. 4, pp. 1070-1075, 2007, doi: https://doi.org/10.1002/jbm.a.31434.

[120] A. Ovsianikov *et al.*, "Laser Fabrication of 3D Gelatin Scaffolds for the Generation of Bioartificial Tissues," (in eng), *Materials (Basel),* vol. 4, no. 1, pp. 288-299, Jan 19 2011, doi: 10.3390/ma4010288.

[121] P. Tayalia, C. R. Mendonca, T. Baldacchini, D. J. Mooney, and E. Mazur, "3D Cell-Migration Studies using Two-Photon Engineered Polymer Scaffolds," *Advanced Materials,* vol. 20, no. 23, pp. 4494-4498, 2008, doi: https://doi.org/10.1002/adma.200801319.

[122] M. T. Raimondi, S. M. Eaton, M. M. Nava, M. Laganà, G. Cerullo, and R. Osellame, "Two-photon laser polymerization: from fundamentals to biomedical application in tissue engineering and regenerative medicine," (in eng), *J Appl Biomater Funct Mater,* vol. 10, no. 1, pp. 55-65, Jun 26 2012, doi: 10.5301/jabfm.2012.9278.

[123] D. P. Dowling, I. S. Miller, M. Ardhaoui, and W. M. Gallagher, "Effect of Surface Wettability and Topography on the Adhesion of Osteosarcoma Cells on Plasma-modified Polystyrene," *Journal of Biomaterials Applications,* vol. 26, no. 3, pp. 327-347, 2011, doi: 10.1177/0885328210372148.

[124] J. H. Lee, J. W. Park, and H. B. Lee, "Cell adhesion and growth on polymer surfaces with hydroxyl groups prepared by water vapour plasma treatment," *Biomaterials,* vol. 12, no. 5, pp. 443 - 448, 1991, doi: https://doi.org/10.1016/0142-9612(91)90140-6.

[125] J. van Meerloo, G. J. L. Kaspers, and J. Cloos, "Cell Sensitivity Assays: The MTT Assay," in *Cancer Cell Culture: Methods and Protocols*, I. A. Cree Ed. Totowa, NJ: Humana Press, 2011, pp. 237-245.

[126] J. Xiao, Y. Zhang, J. Wang, W. Yu, W. Wang, and X. Ma, "Monitoring of Cell Viability and Proliferation in Hydrogel-Encapsulated System by Resazurin Assay," *Applied Biochemistry and Biotechnology,* journal article vol. 162, no. 7, pp. 1996-2007, November 01 2010, doi: 10.1007/s12010-010-8975-3.

[127] E. Magnani and E. Bettini, "Resazurin detection of energy metabolism changes in serum-starved PC12 cells and of neuroprotective agent effect," *Brain Research Protocols,* vol. 5, no. 3, pp. 266 - 272, 2000, doi: https://doi.org/10.1016/S1385-299X(00)00022-2.
[128] R. W. Forsey and J. B. Chaudhuri, "Validity of DNA analysis to determine cell numbers in tissue engineering scaffolds," *Biotechnology Letters,* journal article vol. 31, no. 6, pp. 819-823, June 01 2009, doi: 10.1007/s10529-009-9940-5.
[129] Y. Chen, M. Sonnaert, S. J. Roberts, F. P. Luyten, and J. Schrooten, "Validation of a PicoGreen-Based DNA Quantification Integrated in an RNA Extraction Method for Two-Dimensional and Three-Dimensional Cell Cultures," *Tissue Engineering Part C: Methods,* vol. 18, no. 6, pp. 444-452, 2012, doi: 10.1089/ten.tec.2011.0304.
[130] R. Lattouf *et al.*, "Picrosirius Red Staining:A Useful Tool to Appraise Collagen Networks in Normal and Pathological Tissues," *Journal of Histochemistry & Cytochemistry,* vol. 62, no. 10, pp. 751-758, 2014, doi: 10.1369/0022155414545787.
[131] D. Taskiran, E. Taşkiran, H. Yercan, and F. Kutay, "Quantification of Total Collagen in Rabbit Tendon by the Sirius Red Method," *Turkish Journal of Medical Sciences,* vol. 29, pp. 7-9, 1999.
[132] I. Caputo, M. Lepretti, C. Scarabino, C. Esposito, and A. Proto, "An acetic acid-based extraction method to obtain high quality collagen from archeological bone remains," *Analytical Biochemistry,* vol. 421, no. 1, pp. 92 - 96, 2012, doi: https://doi.org/10.1016/j.ab.2011.10.024.
[133] Q. Xing, K. Yates, M. Tahtinen, E. Shearier, Z. Qian, and F. Zhao, "Decellularization of Fibroblast Cell Sheets for Natural Extracellular Matrix Scaffold Preparation," *Tissue Engineering Part C: Methods,* vol. 21, no. 1, pp. 77-87, 2015/01/01 2014, doi: 10.1089/ten.tec.2013.0666.
[134] P. N. Nonaka *et al.*, "Effects of freezing/thawing on the mechanical properties of decellularized lungs," *Journal of Biomedical Materials Research Part A,* https://doi.org/10.1002/jbm.a.34708 vol. 102, no. 2, pp. 413-419, 2014/02/01 2014, doi: https://doi.org/10.1002/jbm.a.34708.
[135] T. Hoshiba, H. Lu, N. Kawazoe, and G. Chen, "Decellularized matrices for tissue engineering," *Expert Opinion on Biological Therapy,* vol. 10, no. 12, pp. 1717-1728, 2010/12/01 2010, doi: 10.1517/14712598.2010.534079.
[136] L.-C. Wu *et al.*, "Optimized decellularization protocol including α-Gal epitope reduction for fabrication of an acellular porcine annulus fibrosus scaffold," *Cell and Tissue Banking,* vol. 18, no. 3, pp. 383-396, 2017/09/01 2017, doi: 10.1007/s10561-017-9619-4.
[137] T. W. Gilbert, T. L. Sellaro, and S. F. Badylak, "Decellularization of tissues and organs," *Biomaterials,* vol. 27, no. 19, pp. 3675-3683, 2006/07/01/ 2006, doi: https://doi.org/10.1016/j.biomaterials.2006.02.014.
[138] Q. Yao, Y.-W. Zheng, Q.-H. Lan, L. Kou, H.-L. Xu, and Y.-Z. Zhao, "Recent development and biomedical applications of decellularized extracellular matrix biomaterials," *Materials Science and Engineering: C,* vol. 104, p. 109942, 2019/11/01/ 2019, doi: https://doi.org/10.1016/j.msec.2019.109942.
[139] D. Choudhury, M. Yee, Z. L. J. Sheng, A. Amirul, and M. W. Naing, "Decellularization systems and devices: State-of-the-art," *Acta Biomaterialia,* vol. 115, pp. 51-59, 2020/10/01/ 2020, doi: https://doi.org/10.1016/j.actbio.2020.07.060.

[140] Q. Wang *et al.*, "The preparation and comparison of decellularized nerve scaffold of tissue engineering," *Journal of Biomedical Materials Research Part A,* https://doi.org/10.1002/jbm.a.35103 vol. 102, no. 12, pp. 4301-4308, 2014/12/01 2014, doi: https://doi.org/10.1002/jbm.a.35103.

[141] A. H. Fischer, K. A. Jacobson, J. Rose, and R. Zeller, "Hematoxylin and eosin staining of tissue and cell sections," *Cold spring harbor protocols,* vol. 2008, no. 5, p. pdb. prot4986, 2008.

[142] A. T. Feldman and D. Wolfe, "Tissue processing and hematoxylin and eosin staining," *Histopathology: Methods and Protocols,* pp. 31-43, 2014.

[143] Y. Li *et al.*, "Hematoxylin and eosin staining of intact tissues via delipidation and ultrasound," *Scientific Reports,* vol. 8, no. 1, p. 12259, 2018/08/16 2018, doi: 10.1038/s41598-018-30755-5.

[144] K. Percival and Z. Radi, "A modified Verhoeff-van Gieson elastin histochemical stain to enable pulmonary arterial hypertension model characterization," *European journal of histochemistry: EJH,* vol. 60, no. 1, 2016.

[145] V. Kazlouskaya, S. Malhotra, J. Lambe, M. H. Idriss, D. Elston, and C. Andres, "The utility of elastic Verhoeff-Van Gieson staining in dermatopathology," *Journal of Cutaneous Pathology,* https://doi.org/10.1111/cup.12036 vol. 40, no. 2, pp. 211-225, 2013/02/01 2013, doi: https://doi.org/10.1111/cup.12036.

[146] W. Garvey, C. Jimenez, and B. Carpenter, "A modified Verhoeff elastic-van Gieson stain," *Journal of Histotechnology,* vol. 14, no. 2, pp. 113-115, 1991.

[147] K.-S. Park, E.-G. Lee, and Y. Son, "Uniaxial cyclic strain stimulates cell proliferation and secretion of interleukin-6 and vascular endothelial growth factor of human dermal fibroblasts seeded on chitosan scaffolds," *Journal of Biomedical Materials Research Part A,* https://doi.org/10.1002/jbm.a.34881 vol. 102, no. 7, pp. 2268-2276, 2014/07/01 2014, doi: https://doi.org/10.1002/jbm.a.34881.

[148] S. S. Menon, C. Guruvayoorappan, K. M. Sakthivel, and R. R. Rasmi, "Ki-67 protein as a tumour proliferation marker," *Clinica Chimica Acta,* vol. 491, pp. 39-45, 2019/04/01/ 2019, doi: https://doi.org/10.1016/j.cca.2019.01.011.

[149] A. Chalkidou, D. B. Landau, E. W. Odell, V. R. Cornelius, M. J. O'Doherty, and P. K. Marsden, "Correlation between Ki-67 immunohistochemistry and 18F-Fluorothymidine uptake in patients with cancer: A systematic review and meta-analysis," *European Journal of Cancer,* vol. 48, no. 18, pp. 3499-3513, 2012/12/01/ 2012, doi: https://doi.org/10.1016/j.ejca.2012.05.001.

[150] S. Hamada and S. Fujita, "DAPI staining improved for quantitative cytofluorometry," *Histochemistry,* vol. 79, no. 2, pp. 219-226, 1983/06/01 1983, doi: 10.1007/BF00489783.

[151] A. A. Appel, M. A. Anastasio, J. C. Larson, and E. M. Brey, "Imaging challenges in biomaterials and tissue engineering," *Biomaterials,* vol. 34, no. 28, pp. 6615-6630, 2013/09/01/ 2013, doi: https://doi.org/10.1016/j.biomaterials.2013.05.033.

[152] H. Al.Turkistani, F. Tashkandi, and Z. Mohammedsaleh, "Histological Stains: A Literature Review and Case Study," *Global Journal of Health Science,* vol. 8, 06/25 2015, doi: 10.5539/gjhs.v8n3p72.

[153] M. N. Gurcan, L. E. Boucheron, A. Can, A. Madabhushi, N. M. Rajpoot, and B. Yener, "Histopathological Image Analysis: A Review," *IEEE Reviews in Biomedical Engineering,* vol. 2, pp. 147-171, 2009, doi: 10.1109/RBME.2009.2034865.
[154] K. D. Vernon-Parry, "Scanning electron microscopy: an introduction," *III-Vs Review,* vol. 13, no. 4, pp. 40-44, 2000/07/01/ 2000, doi: https://doi.org/10.1016/S0961-1290(00)80006-X.
[155] A. Abdullah and A. Mohammed, *Scanning Electron Microscopy (SEM): A Review*. 2019.
[156] A. Gilpin and Y. Yang, "Decellularization strategies for regenerative medicine: from processing techniques to applications," *BioMed research international,* vol. 2017, 2017.
[157] S. Zia, M. Mozafari, G. Natasha, A. Tan, Z. Cui, and A. M. Seifalian, "Hearts beating through decellularized scaffolds: whole-organ engineering for cardiac regeneration and transplantation," *Critical Reviews in Biotechnology,* vol. 36, no. 4, pp. 705-715, 2016/07/03 2016, doi: 10.3109/07388551.2015.1007495.
[158] Y. Ding, W. Zhang, B. Sun, X. Mo, and J. Wu, "Cyclic freeze–thaw grinding to decellularize meniscus for fabricating porous, elastic scaffolds," *Journal of Biomedical Materials Research Part A,* vol. 110, no. 11, pp. 1824-1839, 2022, doi: https://doi.org/10.1002/jbm.a.37435.
[159] L.-J. Ning *et al.*, "Fabrication and characterization of a decellularized bovine tendon sheet for tendon reconstruction," *Journal of Biomedical Materials Research Part A,* vol. 105, no. 8, pp. 2299-2311, 2017, doi: https://doi.org/10.1002/jbm.a.36083.
[160] V. Telis, K. Wolf, and P. Sobral, "Characterizations of Collagen Fibers for Biodegradable Films Production," p. 929, 2006.
[161] P. Smeriglio, J. Lee, and N. Bhutani, "Soluble Collagen VI treatment enhances mesenchymal stem cells expansion for engineering cartilage," *Bioengineering & Translational Medicine,* vol. 2, no. 3, pp. 278-284, 2017, doi: https://doi.org/10.1002/btm2.10078.
[162] M. Rühl *et al.*, "Soluble Collagen VI Induces Tyrosine Phosphorylation of Paxillin and Focal Adhesion Kinase and Activates the MAP Kinase Erk2 in Fibroblasts," *Experimental Cell Research,* vol. 250, no. 2, pp. 548-557, 1999/08/01/ 1999, doi: https://doi.org/10.1006/excr.1999.4540.
[163] A. Hatamochi, M. Aumailley, C. Mauch, M. Chu, R. Timpl, and T. Krieg, "Regulation of Collagen VI Expression in Fibroblasts," *Journal of Biological Chemistry,* vol. 264, pp. 3494-3499, 02/01 1989, doi: 10.1016/S0021-9258(18)94093-7.
[164] H. Eagle, "Buffer Combinations for Mammalian Cell Culture," *Science,* vol. 174, no. 4008, pp. 500-503, 1971, doi: doi:10.1126/science.174.4008.500.
[165] S. Naddaf Dezfuli, Z. Huan, J. M. C. Mol, M. A. Leeflang, J. Chang, and J. Zhou, "Influence of HEPES buffer on the local pH and formation of surface layer during in vitro degradation tests of magnesium in DMEM," *Progress in Natural Science: Materials International,* vol. 24, no. 5, pp. 531-538, 2014/10/01/ 2014, doi: https://doi.org/10.1016/j.pnsc.2014.08.009.
[166] S. C. Baicu and M. J. Taylor, "Acid–base buffering in organ preservation solutions as a function of temperature: new parameters for comparing buffer capacity and efficiency," *Cryobiology,* vol. 45, no. 1, pp. 33-48, 2002/08/01/ 2002, doi: https://doi.org/10.1016/S0011-2240(02)00104-9.

[167] R. Depping and K. Seeger, "1H-NMR spectroscopy shows cellular uptake of HEPES buffer by human cell lines—an effect to be considered in cell culture experiments," *Analytical and Bioanalytical Chemistry,* vol. 411, no. 4, pp. 797-802, 2019/02/01 2019, doi: 10.1007/s00216-018-1518-4.
[168] A. Itagaki and G. Kimura, "TES and HEPES buffers in mammalian cell cultures and viral studies: Problem of carbon dioxide requirement," *Experimental Cell Research,* vol. 83, no. 2, pp. 351-361, 1974/02/01/ 1974, doi: https://doi.org/10.1016/0014-4827(74)90349-8.
[169] S. D. Joshi and K. Webb, "Variation of cyclic strain parameters regulates development of elastic modulus in fibroblast/substrate constructs," *Journal of Orthopaedic Research,* https://doi.org/10.1002/jor.20626 vol. 26, no. 8, pp. 1105-1113, 2008/08/01 2008, doi: https://doi.org/10.1002/jor.20626.
[170] G. Yang, R. C. Crawford, and J. H. C. Wang, "Proliferation and collagen production of human patellar tendon fibroblasts in response to cyclic uniaxial stretching in serum-free conditions," *Journal of Biomechanics,* vol. 37, no. 10, pp. 1543-1550, 2004/10/01/ 2004, doi: https://doi.org/10.1016/j.jbiomech.2004.01.005.
[171] S. J. Coeyman, Y. Zhang, C. F. Baicu, M. R. Zile, A. D. Bradshaw, and W. J. Richardson, "In vitro bioreactor for mechanical control and characterization of tissue constructs," *Journal of Biomechanics,* vol. 147, p. 111458, 2023/01/01/ 2023, doi: https://doi.org/10.1016/j.jbiomech.2023.111458.
[172] R. S. Kenett and S. Zacks, *Modern industrial statistics: With applications in R, MINITAB, and JMP*. John Wiley & Sons, 2021.
[173] H. I. Okagbue, P. E. Oguntunde, E. C. M. Obasi, and E. M. Akhmetshin, "Trends and usage pattern of SPSS and Minitab Software in Scientific research," *Journal of Physics: Conference Series,* vol. 1734, no. 1, p. 012017, 2021/01/01 2021, doi: 10.1088/1742-6596/1734/1/012017.
[174] B. F. Ryan, B. L. Joiner, and J. D. Cryer, *MINITAB handbook: update for release*. Cengage Learning, 2012.
[175] J. A. Asenjo and J. C. Merchuk, *Bioreactor System Design*. 1994.
[176] G. Najafpour, "Bioreactor Design," 2007, pp. 142-169.
[177] R. Pörtner, S. Nagel-Heyer, C. Goepfert, P. Adamietz, and N. M. Meenen, "Bioreactor design for tissue engineering," *Journal of Bioscience and Bioengineering,* vol. 100, no. 3, pp. 235-245, 2005/09/01/ 2005, doi: https://doi.org/10.1263/jbb.100.235.
[178] "Biotense | perfusion bioreactor." ADMET, Inc. https://www.admet.com/products/micro-testers/biotense-bioreactor/ (accessed.
[179] B. a. T. G. T. (TGT), "CartiGen: Mechanical Compression Bioreactor Systems," ed: Bangalore Integrated System Solutions (P) ltd.
[180] B. a. T. G. T. (TGT). "LigaGen: Tension Bioreactor Systems." Bangalore Integrated System Solutions (P) ltd. http://www.tissuegrowth.com/prod_ligament.cfm (accessed.
[181] T. Instruments. "BioDynamic 5200." TA Instruments. https://www.tainstruments.com/5200-products/ (accessed.
[182] "TC-3 bioreactor." Ebers. http://www.ebersmedical.com/tissue-engineering/bioreactors/load-culture/tc-3 (accessed.

[183] E. Boaden, D. Gold, M. Khader-Lindon, C. X. Lee, H. Williams, and J. Wilson, "The robotic bioreactor," The University of Sheffield, Undergraduate's Interim report, 2017.
[184] I. Martin, D. Wendt, and M. Heberer, "The role of bioreactors in tissue engineering," *Trends in Biotechnology,* vol. 22, no. 2, pp. 80-86, 2004/02/01/ 2004, doi: https://doi.org/10.1016/j.tibtech.2003.12.001.
[185] T. Robinson and P. Nigam, "Bioreactor design for protein enrichment of agricultural residues by solid state fermentation," *Biochemical Engineering Journal,* vol. 13, no. 2, pp. 197-203, 2003/03/01/ 2003, doi: https://doi.org/10.1016/S1369-703X(02)00132-8.
[186] A. F. Smith, J. Thanarak, M. Pontin, N. H. Green, and D. D. Damian, "Design and Development of a Robotic Bioreactor for In Vitro Tissue Engineering," in *2021 IEEE International Conference on Robotics and Automation (ICRA)*, 30 May-5 June 2021 2021, pp. 12428-12434, doi: 10.1109/ICRA48506.2021.9560728.
[187] "ULTEM 1010 Resin." Stratasys Inc. https://www.rnd-tech.com/media/fdm-pdfs/spec-sheets/ultem1010materialspecsheeten1014.pdf (accessed.
[188] K. T. S. Palomares *et al.*, "Mechanical Stimulation Alters Tissue Differentiation and Molecular Expression during Bone Healing," *Journal of Orthopaedic Research,* vol. 27, no. 9, pp. 1123-1132, Sep 2009, doi: 10.1002/jor.20863.